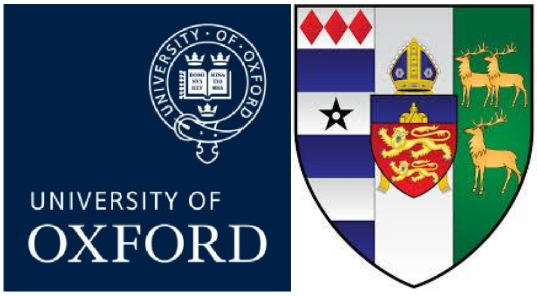
Microwave-initiated Catalytic Dehydrogenation of Fossil Fuels for the Facile Production and Safe Storage of Hydrogen



Xiangyu Jie

Lincoln College, University of Oxford

Supervisors

Prof. Peter P. Edwards FRS ML

Prof. Richard G. Compton FRSC MAE

A thesis submitted to the Department of Chemistry, University of Oxford for the Degree of *Doctor of Philosophy in Inorganic Chemistry*

2019

Microwave-initiated Catalytic Dehydrogenation of Fossil Fuels for the Facile Production and Safe Storage of Hydrogen

Xiangyu Jie, Lincoln College

A thesis submitted to the Department of Chemistry, University of Oxford for the Degree of Doctor of Philosophy in Inorganic Chemistry

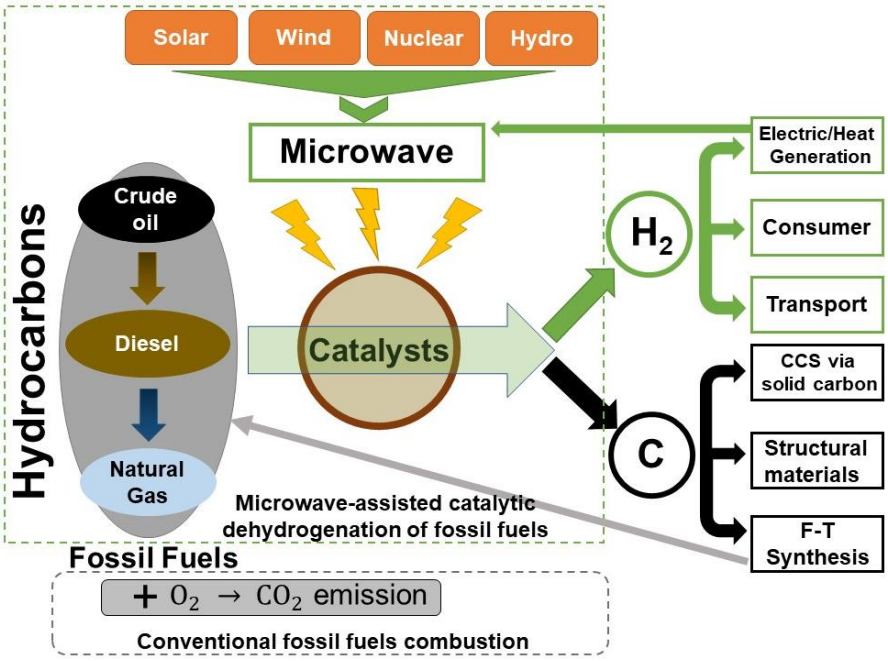
Abstract

Hydrogen offers the prospect of a highly effective fuel for future sustainable energy, not only because of its intensive energy density per unit-mass but also because its combustion produces no environmentally damaging CO_2 at its point-of-use. Hydrogen is presently manufactured on an industrial scale by steam reforming or partial oxidation of methane and to a lesser degree by gasification of coal. However, these processes also generate significant quantities of CO_2, with obvious attendant environmental problems. The utilisation of solar energy now yields increasing amounts of hydrogen by the splitting of water, as does the harnessing of other sources of natural energy. But even if the photocatalytic or electrolytic breakdown of water could be greatly improved to produce the necessary huge quantities of hydrogen, the resulting challenge of its safe storage and rapid release for immediate use in fuel cells, for example, is problematic. An alternative platform is to utilise the high intrinsic hydrogen content of fossil fuel hydrocarbons but in such a way as to rapidly release only their constituent hydrogen *without any CO_2 production*. Such CO_2-free hydrogen production from hydrocarbons has been advanced through pioneering studies on the catalytic thermolysis of methane and petroleum-range hydrocarbons. My doctoral research work centres on a method of rapidly liberating high-purity hydrogen from hydrocarbons without CO_2 emission. An innovative system combining microwave technology and heterogeneous catalysis is thus proposed. As a result, a H_2 production selectivity from all evolved gases of some 98%, is achieved with less than a fraction of a percent of adventitious CO and CO_2 through the *microwave-initiated catalytic dehydrogenation* of liquid alkanes using Fe and Ni particles supported on silicon carbide.

In this doctoral work, the complex interaction between the heterogeneous catalyst system and the induced microwave electric field was carefully studied by scanning a variety of metals and supports. Consequently, the optimised catalyst system was developed in effectively response to the microwave irradiation. Another enthusiastic and exciting part of the work is that a variety of actual, real petroleum products, ranging from heavy crude oil, crude oil through diesel, petrol to natural gas (methane) have been demonstrated that can be the vehicle for high-purity hydrogen production through the *microwave-initiated catalytic dehydrogenation.*

Based on this work, we showed that the undoubted attractive attributes of fossil fuels - relatively inexpensive, widely available and readily adaptable to applications large and small, simple and complex, - can significantly assist in the staged transition to a hydrogen-based, sustainable hydrogen energy economy. A new scientific and technological era of "*Fossil fuel decarbonisation*'' can arise where we will not destroy naturally-occurring fossil fuels by combustion – with the attendant CO_2 emissions, but rather utilise them to produce clean

hydrogen. Carbonaceous fossil fuels are thereby transformed from carbon-rich to hydrogen-rich fuels for future energy.



Microwave-initiated catalytic dehydrogenation of naturally occurring petroleum for the facile production and safe storage of hydrogen

Acknowledgements

Looking back through these 4 years study and research in chemistry at Oxford, I felt very much satisfied. Not only about what I have achieved, but more on what I have learned and experienced in this world-leading university, and thus making up my mind for my future career.

I would like to express my sincerest gratitude to my supervisor, Professor Peter Edwards for his guidance, encouragement and support in my DPhil research. His full support has really allowed me the freedom to choose my research topics and design and develop the whole experiment work. This has given me the opportunity to grow and learn in a way to be an independent young scientist, and I hope that I have lived up to his trust.

My deepest appreciation and thanks extended to Dr. Tiancun Xiao for his generous advice and full support both in my research work and out-of-lab activities and paternal care. His experience and encouragement have really opened my mind and learned the way to transfer a laboratory technique to application.

I would like to thank my second supervisor, Prof. Richard Compton who have always offered the strongest support and given me the opportunity to broad my research horizon.

To all my friends and colleagues in PPE group, I am most grateful to all your kind help, discussion and advice. Specifically, I would like to thank Dr. Sergio Gonzalez-Cortes and Dr. Benzhen Yao for all your generous offer and all the times and discussions in the lab. And I must give my special thanks to Ms. Linda Webb who had made everything well organised and happened in the group.

Special thanks also go to Sir Prof. John Meurig Thomas, Prof. Jon Dilworth and Dr. Danial Slocombe for all the discussions and insightful comments that had really made my work to a higher level.

And I would like to thank China Scholarship Council for an invaluable financial support, without which I couldn't be fully focus on my research work and the life in Oxford should be much harder.

To all my friends in Oxford, the life would have been so boring without you. Zhaoxi and Jin, for hosting us for several wonderful barbecue parties, Yiwen, Lun, Di, Ming and Hugh for organising so many relaxing game nights, and Jingyuan and Peimei for having so many holidays together travelling around Europe. These last 4 years couldn't be so colourful and enjoyable without you.

Finally, to my beloved parents Jun Jie and Ning Lv, there is never enough thanks that can be said for all your support and distance companionship. Your love and faith in me have always brought myself power and ensure my completion of this degree. And to my wife Bingling your love and company has brought me so much happiness and joy at home and kept the loneliness away from me for these nearly 10 years study in Japan and UK. I am most grateful for your wholeheartedly support in my career decisions and your contribution to this work is priceless.

Last and not least, I would like to dedicate this work to my supervisor, mentor Prof Peter Edwards on the occasion of his 70th birthday.

− Xiangyu Jie

August 2019, Oxford, UK

Publications

Xiangyu Jie, Sergio Gonzalez-Cortes, Tiancun Xiao, Benzhen Yao, Jiale Wang, Daniel R. Slocombe, Yiwen Fang, Noah Miller, Hamid A. Al-Megren, Jonathan R. Dilworth, John M. Thomas, and Peter P. Edwards. *"The decarbonization of petroleum and other fossil hydrocarbon fuels for the facile production and safe storage of hydrogen."* Energy & Environmental Science (2019), 12(1), 238-249.

Changzhen Wang, Xiangyu Jie, Yuan Qiu, Yongxiang Zhao, Hamid A. Al-Megren, Saeed Alshihri, Peter P. Edwards, and Tiancun Xiao. "The importance of inner cavity space within Ni@ SiO2 nanocapsule catalysts for excellent coking resistance in the high-space-velocity dry reforming of methane." *Applied Catalysis B: Environmental* (2019), 259, 118019.

Xiangyu Jie, Tiancun Xiao, Benzhen Yao, Sergio Gonzalez-Cortes, Jiale Wang, Yiwen Fang, Hamid A. Al-Megren, Jonathan R. Dilworth, and Peter P. Edwards. *"On the performance optimization of Fe catalysts in the microwave – assisted H_2 production by the dehydrogenation of hexadecane"* Catalysis Today (2018), 317, 29-35.

Benzhen Yao, Tiancun Xiao, Xiangyu Jie, Sergio Gonzalez-Cortes and Peter P. Edwards. *" H_2 rich gas production from leaves "* Catalysis Today (2018), 317, 43-49.

Xiangyu Jie, Sergio Gonzalez-Cortes, Tiancun Xiao, Jiale Wang, Benzhen Yao, Daniel R. Slocombe, Hamid A. Al-Megren, Jonathan R. Dilworth, John M. Thomas, and Peter P. Edwards. *"Rapid Production of High-Purity Hydrogen Fuel through Microwave-Promoted Deep Catalytic Dehydrogenation of Liquid Alkanes with Abundant Metals."* Angewandte Chemie International Edition (2017), 56(34), 10170-10173.

Patents

Xiangyu JIE, Tiancun Xiao, Peter P. Edwards, Oxford University Innovation Limited, ‘‘Process for producing hydrogen’’, **WO 2018/104712 A1**.

Xiangyu JIE, Tiancun Xiao, Peter P. Edwards, Oxford University Innovation Limited, ‘‘Hydrogen from plastics via microwave-initiated catalytic dehydrogenation’’, **1809199.1, PCT GB2019/061541** 5th June 2019.

Xiangyu JIE, Tiancun Xiao, Peter P. Edwards, Oxford University Innovation Limited, ‘‘Plastics to Monomers’’, **1901784.7**, 8th February 2019.

Xiangyu JIE, Tiancun Xiao, Peter P. Edwards, Oxford University Innovation Limited, ‘‘Process for methane to hydrogen’’, July 2019.

Contents

Abstract i

Acknowledgements iii

Publications v

Patents vi

Contents vii

List of Figures xiv

List of Tables xxiii

1 Introduction 1

1.1 Overview of fossil fuels as primary energy sources 2

1.2 Hydrogen Economy 7

1.3 Methods of producing hydrogen 8

1.3.1 Use of Renewable Energy to Produce Hydrogen 10

1.3.2 Coal gasification 11

1.3.3 Fossil fuel reforming 12

1.3.4 Pyrolysis 14

1.3.5 Other methods 15

1.4 CO_2-free hydrogen production from hydrocarbons 16

1.5 Catalysts overview for hydrogen production systems 19

1.6 Fossil fuels as hydrogen storage materials 21

1.7 Hydrogen production involving microwave-initiated catalysis 24

1.7.1 Introduction to microwave chemistry and application 24

1.7.2 Fundamental principle of microwave science 27

1.7.3 Microwave Heating Phenomena 32

1.7.4 Hydrogen Production through Microwave-initiated Catalysis 34

1.8 Thesis objective and research summary 39

2 Experimental methods 52

2.1 Experimental set-up 52

2.1.1 Microwave system 52

2.1.2 Temperature control and measurements 56

2.2 Catalysts preparation 56

2.3 Evaluation of catalytic performance 57

2.4 Products analysis 58

2.4.1 Gas Chromatography (GC) 58

2.4.2 Gas Chromatography-Mass Spectrometry (GC-MS) 60

2.5 Techniques used for characterisation of catalysts 61

2.5.1 X-ray Diffraction (XRD) 61

2.5.2 Scanning Electron Microscopy and Energy-dispersive X-ray spectroscopy (SEM-EDS) 63

2.5.3 Transmission Electron Microscopy (TEM) 65

2.5.4 Thermogravimetric Analysis (TGA) 67

2.5.5 Laser- Raman Spectroscopy 68

2.5.6 Microwave Cavity Perturbation Measurements 70

3 Microwave-initiated Dehydrogenation of Hexadecane for High-purity Hydrogen Production 76

3.1 Introduction....76

3.2 Experimental....77

3.3 Results and discussion 78

3.3.1 Microwave-initiated catalytic dehydrogenation of hexadecane 78

3.3.2 Microwave heating vs. conventional thermal heating 80

3.3.3 Dielectric properties of prepared catalysts 84

3.3.4 Pre- and post- reaction analysis of catalysts....87

3.3.4.1 X-ray diffraction (XRD) 87

3.3.4.2 Scanning electron microscopy (SEM) 89

3.3.4.3 High resolution transmission electron microscopy (HRTEM) 91

3.3.4.4 Energy-dispersive X-ray spectroscopy (EDS)....94

3.3.5 Possible mechanisms for the microwave-initiated deep dehydrogenation using iron catalysts....95

3.4 Conclusion 97

4 Optimisation of Catalyst Performance 101

4.1 Introduction....101

4.2 Experimental....103

4.2.1 Preparation of catalysts....103

4.2.2 Characterisation of catalysts 103
4.2.3 Evaluation of catalysts' performance 104
4.3 Results and discussion 106
4.3.1 Studies on different metal catalysts supported by SiC 106
4.3.2 Study of the effect of support materials 109
4.3.3 Fe/SiC catalysts with various Fe loading 112
4.3.4 Power absorption and temperature considerations 118
4.3.5 Dielectric properties of investigated catalysts 119
4.3.6 Summary of catalyst characterisation 122
4.3.6.1 X-ray diffraction (XRD) 122
4.3.6.2 Scanning electron microscopy (SEM) 123
4.3.6.3 Raman spectroscopy 125
4.4 Conclusion 126

5 The Decarbonisation of Petroleum and Other Fossil Hydrocarbon Fuels for the Facile Production and Safe Storage of Hydrogen 131

5.1 Introduction 131
5.2 Experimental 133
5.2.1 Preparation of catalysts 133
5.2.2 Characterisation of catalysts 133
5.2.3 Microwave initiated dehydrogenation process 133
5.2.4 Conventional thermal dehydrogenation process 134
5.2.5 Compositional analysis of petroleum samples 134

5.3 Results and discussion 135

5.3.1 Model fluid *n*-alkanes and aromatics.....135

5.3.2 Hydrogen production characteristics from petroleum and fossil hydrocarbons.....138

5.3.3 Parametric studies of the microwave-initiated dehydrogenation of diesel fuel 141

5.3.4 Post- reaction analysis of catalysts 145

5.3.4.1 High resolution transmission electron microscopy (HRTEM) 145

5.3.4.2 X-ray diffraction (XRD), Raman spectroscopy, thermogravimetric analysis (TGA) and scanning electron microscopy (SEM) 146

5.3.5 Fossil fuels as hydrogen storage materials 149

5.3.6 Net Energy Balance (NEB) considerations 151

5.3.6.1 Thermodynamic analysis 151

5.3.6.2 NEB comparison of microwave and conventional thermal methods in lab scale 153

5.3.7 The regeneration of metal catalysts and carbon by-product conversion 156

5.3.8 The storage and possible utilisation of carbon by-product residues.....157

5.4 Conclusions.....159

6 Study of Carbonaceous Materials for Their Catalytic Performance under Microwave Irradiation 163

6.1 Introduction.....163

6.2 Experimental.....165

6.2.1 Preparation of catalysts.....165

6.2.2 Apparatus and method used for catalytic activity evaluation 165

6.2.3 Characterisation of catalysts 166

6.3 Results and discussion 166

6.3.1 Successive cycles of hexadecane dehydrogenation using Fe/SiC catalysts.. 166

6.3.2 Catalytic activity of model carbons for microwave-initiated dehydrogenation of hexadecane 169

6.3.3 Reaction temperature and absorption power 171

6.3.4 Characterisation of carbon residues and comparison with model carbon materials 173

6.3.4.1 Thermogravimetric analysis (TGA).....173

6.3.4.2 Scanning electron microscopy (SEM), Transmission electron microscopy (TEM) and Energy-dispersive x-ray spectroscopy (EDS) 177

6.3.4.3 Raman spectroscopy, x-ray diffraction (XRD) and BET analysis..180

6.3.4.4 Microwave cavity perturbation measurements 185

6.3.5 Evolved carbon deposition and the proposed deactivation Mechanisms190

6.4 Conclusion 192

7 Conclusion, Challenges and Perspectives 195

7.1 Concluding remarks 195

7.2 The challenges and future works 196

7.3 Perspectives 199

Appendix A: The detailed composition analysis of petroleum samples **203**

Appendix B: The detailed composition analysis of product distribution by GC **207**

Appendix C: Theoretical and Experimental Hydrogen Density of Hydrocarbons **211**

Appendix D: Theoretical and Experimental Hydrogen Density of Hydrocarbons **213**

Appendix E: Representative Profiles of Microwave Absorption and Temperature during the Reactions **216**

Appendix F: Acknowledgement and copyright **220**

List of Figures

Figure 1.1. A comment from Professor Peter Edwards on Oxford Magazine.....2

Figure 1.2. Pathway of petroleum utilisation from crude oil to petroleum derived fuels.....4

Figure 1.3. Global energy-related CO_2 emissions, 2000-2017; World CO_2 emissions from fuel combustion by sector, 2015.....6

Figure 1.4. Photocatalytic system of water splitting. (a) Light absorption, (b) charge transfer, (c) redox reactions, (d) adsorption, desorption, and mass diffusion of chemical species, and (e) charge recombination 11

Figure 1.5. Product distribution of cyclohexane decomposition over (4.5 wt.% Fe–0.5 wt.% Pd)/Al_2O_3 catalyst vs. temperature 17

Figure 1.6. Hydrogen production with a Ni-Bi molten catalyst 18

Figure 1.7. Hydrogen storage materials and options with their gravimetric and volumetric density 22

Figure 1.8. Fields of applications with microwave chemistry.....25

Figure 1.9. The dipole rotation of a polar molecule, showing the fluctuation in the dipole moment in a particular direction.....28

Figure 1.10. Loss tangent vector diagram 29

Figure 1.11. Debye relaxation of water at 30°C.....31

Figure 1.12. Total electromagnetic absorption in non-magnetic particles as a function of conductivity and mean particle radius, for peak applied electric field 1 V m^{-1}, satisfying the relationship $E_0 = \eta_0 H_0$ oscillating at a frequency of 2.45 GHz.....32

Figure 1.13. Effect of the reaction temperature on methane conversion, under microwave heating or conventional heating.....36

Figure 1.14. Product distribution of paraffin wax ($C_{26}H_{54}$) decomposition over 5 wt.% Ru/AC catalyst for absorbed power between 80 and 60W.....38

Figure 1.15. Comparisons of microwave and thermal treatment on the resulting evolved gas mixture composition 39
Figure 2.1. Reaction system configuration 53
Figure 2.2. The reflected power measurement system 54
Figure 2.3. The purpose built TM010 mode aluminium cavity 55
Figure 2.4. A conventional thermal system configuration, heating by an electric furnace. 58
Figure 2.5. Schematic diagram of Bragg's law. 62
Figure 2.6. Scanning electron microscope column 64
Figure 2.7. Transmission electron microscope column 66
Figure 2.8. A representative TGA-DSC curve of activated carbon oxidation under air atmosphere 68
Figure 2.9. Principles of Raman spectroscopy 69
Figure 2.10. Microwave cavity perturbation measurement set up 71
Figure 2.11. Example of microwave cavity perturbation measurement. 72
Figure 3.1. Evolved gas composition of representative catalysts for microwave-promoted dehydrogenation of hexadecane ($C_{16}H_{34}$) 78
Figure 3.2. A representative experiment with 0.5 mL hexadecane @ 5 wt.% Fe/SiC catalyst for "time-on-stream" evaluation 79
Figure 3.3. Recharging catalytic cycles for 0.5 mL hexadecane @ 5 wt.% Fe/SiC catalyst. 0.5 mL hexadecane was added for each successive cycle (30 min irradiation) 80
Figure 3.4. Comparison of microwave and thermal system. (a) conventional thermal system (b) microwave system. 81
Figure 3.5. Comparison of microwave and conventional thermal method 82
Figure 3.6. Microwave cavity perturbation measurement curve of pre- and post- reaction 5 wt.% Fe/SiC catalysts 85
Figure 3.7. High-temperature microwave cavity perturbation measurement 86

Figure 3.8. XRD pattern comparison of 5 wt.% Fe/SiC, 5 wt.% Ni/SiC, and 5 wt.%-Fe, 1 wt.%-Ni Fe-Ni/SiC catalysts before the microwave-initiated catalytic dehydrogenation of hexadecane, 2θ= 40°-50° 88
Figure 3.9. XRD pattern comparison of 5 wt.% Fe/SiC, 5 wt.% Ni/SiC, and 5 wt.%-Fe, 1 wt.%-Ni Fe-Ni/SiC catalysts before and after the microwave-promoted catalytic decomposition of hexadecane, 2θ= 40°-50°.....88
Figure 3.10. The scanning electron microscopy (SEM) images of (a, b) 5 wt.% Fe/SiC catalyst, (c, d) 5 wt.% Ni/SiC, (e, f) 5 wt.%-Fe, 5 wt.%-Ni Fe-Ni/SiC catalysts before and after the microwave-initiated catalytic dehydrogenation of hexadecane.....90
Figure 3.11. The scanning electron microscopy (SEM) images of (a) fresh Fe particle catalysts on SiC of 5 wt.% Fe/SiC catalyst; (b) fresh Fe-Ni alloy particle catalysts on SiC of 5 wt.%-Fe, 5 wt.%-Ni Fe-Ni/SiC catalysts; (c, d) resulting carbon residues observed after the dehydrogenation of hexadecane under microwave irradiation.....91
Figure 3.12. High Resolution Transmission Electron Microscopy (HRTEM) images of 5 wt.% Fe/SiC before (a, b) and after (c, d) microwave-initiated catalytic dehydrogenation of hexadecane 92
Figure 3.13. High Resolution Transmission Electron Microscopy (HRTEM) images of 5 wt.%-Fe, 1 wt.%-Ni FeNi/SiC before (a, b) and after (c, d) microwave-initiated catalytic dehydrogenation of hexadecane 93
Figure 3.14. Low magnification Transmission Electron Microscopy (TEM) images of Ni/SiC (a) before and (b) after microwave treatment.....94
Figure 3.15. Scanning electron microscope (SEM) and Energy-dispersive X-ray spectroscopy (EDS) mapping of the elemental species on the surface of 5 wt.% Fe/SiC catalysts before microwave initiation.....95
Figure 3.16. Proposed reaction pathways and selective C-H bond cleavage mechanisms for high-purity hydrogen production through microwave-initiated iron catalysed dehydrogenation of fossil fuels 96

Figure 4.1. Comparison of different metals operating under same conditions of one cycle of substrate and products analysed after 10 minutes 106
Figure 4.2. Evolved gas composition of iron based bimetallic metal (Fe-X/SiC, X = Ni, Co, Cu and Ru) through microwave-initiated dehydrogenation of hexadecane 108
Figure 4.3. Evolved gas composition for catalysts on different support materials in the microwave–assisted dehydrogenation of hexadecane 110
Figure 4.4. Evolved gas composition for Fe/SiC catalysts at different Fe loadings under microwave–initiated dehydrogenation of hexadecane 113
Figure 4.5. X-Ray Diffraction patterns of Fe/SiC with various Fe loadings. (a) Before; and (b) After microwave-initiated catalytic dehydrogenation of hexadecane 115
Figure 4.6. Raman spectra of Fe/SiC catalysts with various Fe loading after the microwave-initiated dehydrogenation of hexadecane 116
Figure 4.7. Thermogravimetric analysis (TGA) of Fe/SiC catalysts with various Fe loading through microwave-initiated dehydrogenation of hexadecane.....116
Figure 4.8. Scanning electron microscopy (SEM) of Fe/SiC catalysts with various Fe loading, (a, c and e) before and (b, d and f) after microwave-initiated catalytic hexadecane dehydrogenation 117
Figure 4.9. The changes of microwave absorption power (Watts) and temperature (°C) for 5 wt. % Fe/SiC catalyst under 750 W microwave power (a) with and without hexadecane fuel during exposure of the system to microwaves (b) Comparison of fresh and spent sample without fuel.....118
Figure 4.10. Dielectric properties of catalysts, (a, b and c) before and (d, e and f) after microwave-initiated catalytic dehydrogenation of hexadecane.....120
Figure 4.11. The plots summarised the relation between dielectric properties of catalysts and hydrogen selectivity 121
Figure 4.12. XRD patterns of various metal catalysts and metal alloys before and after the microwave-initiated catalytic dehydrogenation of hexadecane, 2θ= 20°-80.....123

Figure 4.13. The scanning electron microscopy (SEM) images of (a) Fe particle obtained by hydro-reduction from iron nitrate, (b) 5 wt.% Fe/AC catalyst, (c) 5 wt.% Fe/SiO_2 catalyst, (c) 5 wt.% Fe/Al_2O_3 catalyst.....124
Figure 4.14. The scanning electron microscopy (SEM) images of (a) 5 wt.% Fe/SiC catalyst, (b) 5 wt.% Ni/SiC catalyst, (c, d) 5 wt.% Pt /SiC catalysts, (e) 5 wt.% Ru/SiC catalyst and (f) 5 wt.% Cu/SiC catalyst.....125
Figure 4.15. Raman spectra of spent catalysts from hexadecane dehydrogenation under microwave treatment.....126
Figure 5.1. Gas chromatography-mass spectrometry (GCMS) analysis on extra-heavy crude oil, crude oil and diesel.....135
Figure 5.2. Microwave initiated dehydrogenation of saturated alkanes (C_7 to C_{17}) and aromatics over 5 wt.% Fe/SiC catalysts under 750W microwave irradiation. (a) Selectivity of H_2 and small alkanes; (b) Comparison on theoretical and experimental H_2 density of these aliphatics via microwave initiated heterogenous catalysis.....136
Figure 5.3. Comparison of microwave-initiated dehydrogenation of selective aliphatics and aromatics using a 5 wt.% Fe/SiC catalyst. (a) Selectivity of H_2 and small alkanes; (b) Evolved gas volume obtained through aromatics dehydrogenation.....137
Figure 5.4. Cumulative evolved H_2 volume through the microwave-initiated iron catalysed dehydrogenation of fossil fuels.....139
Figure 5.5. Evolved gas composition of various fossil fuel feedstocks over iron catalysts on silicon carbide (SiC) and activated carbon (AC) under microwave initiation.....139
Figure 5.6. Methane conversion and hydrogen selectivity over 5 wt.% Fe/SiC catalysts under microwave.....140
Figure 5.7. H_2 production per volumetric and gravimetric fuel consumption.....141
Figure 5.8. Study of hydrogen production from diesel over 5 wt.% Fe/SiC catalyst under microwave initiation. (a) Cumulative evolved H_2 volume determined by 'time on stream' with different absorbed power. (b) The effect of absorbed power on the gas distribution and (c) reaction rate of hydrogen production with different absorbed power.....142

Figure 5.9. Comparison of product distribution from diesel @ 5 wt.% Fe/SiC sample under (a) microwave initiation and (b, c) thermal reactions 143
Figure 5.10. Characterisation of 5 wt.% Fe/SiC catalyst before and after microwave-initiated dehydrogenation of diesel. HRTEM images of (a) unreacted catalyst recorded along a <011> zone axis of a Fe_3O_4 particle and (b) spent catalyst recorded along a <120> zone axis of a Fe_3C particle (c) Low magnification TEM images of produced carbon nanotubes and iron carbide particles in a spent sample 146
Figure 5.11. Pre- and Post- reaction characterisation of 5 wt.% Fe/SiC catalyst. (a) X-ray diffraction (XRD) patterns and (b) Raman spectra of 5 wt.% Fe/SiC catalyst. before and after microwave-initiated dehydrogenation of diesel; (c) Thermogravimetric analysis (TGA) of spent sample after microwave treatment, the sample was first characterised under nitrogen, and followed by a temperature programmed oxidation; (d) Derivative plots of temperature programmed oxidation of spent sample reference to the model carbons 147
Figure 5.12. The scanning electron microscope (SEM) of 5 wt.% Fe/SiC catalyst, (a), (b) before and (c), (d) and (e) after microwave-initiated dehydrogenation of diesel 149
Figure 5.13. Comparison of theoretical hydrogen density of fossil hydrocarbons with the experimental hydrogen density obtained via microwave-initiated catalytic dehydrogenation of diesel and petrol over 5 wt.% Fe/SiC catalyst 150
Figure 5.14. Energy input of *n*-hexadecane cracking in atmospheric pressure 153
Figure 5.15. Comparison of microwave process and conventional thermal process for diesel dehydrogenation over 5 wt.% Fe/SiC catalyst.....154
Figure 5.16. Energy balance evaluation between microwave process and conventional thermal processes.....156
Figure 5.17. Successive tests on diesel dehydrogenation under microwave irradiation over 5 wt.% Fe/SiC catalysts 157
Figure 5.18. Representative storage and various utilisation routes for elemental carbon produced from fossil fuel dehydrogenation, where the hydrogen component of fossil fuels is

used as a clean fuel and the remaining solid carbon ends up as either stored underground or other uses 159

Figure 6.1. Hexadecane dehydrogenation over 5 wt. % Fe/SiC catalyst. (a) $C_{16}H_{34}$ dehydrogenation rate; (b) evolved gas composition in the exit gas.....167

Figure 6.2. The effect of carbon residue removal and regeneration of Fe_2O_3/SiC sample for hexadecane dehydrogenation. (a) $C_{16}H_{34}$ dehydrogenation rate; (b) evolved gas composition in the exit gas.....168

Figure 6.3. Hexadecane dehydrogenation over model carbon materials, of activated carbons (ACs), carbon black (CB), mesoporous carbon (MC), graphene nanoplatelets, multi-wall carbon nanotubes (MWCNT), carbon nanofibers (CNF), graphite, and glassy carbon. (a) $C_{16}H_{34}$ dehydrogenation rate; (b) evolved gas composition in the exit gas.....170

Figure 6.4. Absorbed (dissipated) power as a function of time. (a) model carbon materials. (b) Fe/SiC, Fe_2O_3/SiC, SiC, and Fe.....172

Figure 6.5. Reaction temperature recorded as a function of time. (a) model carbon materials. (b) Fe/SiC, Fe_2O_3/SiC, SiC, and Fe.....173

Figure 6.6. Thermogravimetric analysis (TGA).....174

Figure 6.7. Derivative plots of temperature programmed oxidation (TPO) of spent Fe/SiC sample reference to the model carbons 175

Figure 6.8. Reaction rate (a) and Evolved gas composition (b) as a function of the weight of carbon deposition 176

Figure 6.9. The Scanning Electron Microscope (SEM) of Fe/SiC samples through successive cycles of hexadecane dehydrogenation under microwave 178

Figure 6.10. The Scanning Electron Microscope (SEM) of model carbon materials.....179

Figure 6.11. Transmission electron microscopy (TEM) and Energy-dispersive X-ray spectroscopy (EDS) mapping on spent Fe/SiC samples.....180

Figure 6.12. EDS mapping of needle-liked fibres that observed on the surface of SiC 180

Figure 6.13. Raman Spectrum. (a) samples of Fe/SiC through 10 successive cycles of catalytic reaction. (b) samples of different model carbon materials 182

Figure 6.14. XRD patterns. (a) The change of the XRD pattern of 5 wt.% Fe/SiC sample during the successive cycles of hexadecane dehydrogenation under microwaves. (b) The XRD pattern of model carbon materials. (c) XRD pattern comparison of fresh Fe/SiC sample and after 1, 5, and 10 cycles, 2θ= 5°-80°, and (d) 2θ= 40°-50°.....183
Figure 6.15. Dielectric constant and Loss tangent of 9 different kinds of model carbon materials 186
Figure 6.16. Microwave cavity perturbation measurement of activated carbon and graphene nanoplatelets, before and after catalytic reactions under microwave irradiation. (a) Dielectric constant and (b) Loss tangent.....187
Figure 6.17. (a) Dielectric constant and (b) Loss tangent of 5 wt.% Fe/SiC sample measured at different temperature, before and after successive cycles of catalytic reactions.....188
Figure 6.18. (a) The change of dielectric constant and loss tangent of 5 wt.% Fe/SiC samples through successive cycles of catalytic reactions under microwave activation. (b) Dielectric constant and Loss tangent of 5 wt.% Fe/SiC samples as a function of the weight of carbon residues.....189
Figure 6.19. A representative diagram of carbon deposition and transformation through microwave-initiated hexadecane dehydrogenation over Fe/SiC catalysts.....191
Figure 7.1. Schematic representation of one approach to mitigate CO_2 emission in transportation.....201
Figure E1. Microwave-initiated dehydrogenation of diesel on 5 wt.% Fe/SiC catalysts. (a) Original microwave input power and absorbed power (delivery power); (b) Record reaction temperature and absorbed power (delivery power).....206
Figure E2. Microwave-initiated dehydrogenation of petrol on 5 wt.% Fe/SiC catalysts. (a) Original microwave input power and absorbed power (delivery power); (b) Record reaction temperature and absorbed power (delivery power).....207
Figure E3. Microwave-initiated dehydrogenation of diesel on 5 wt.% Fe/AC catalysts. (a) Original microwave input power and absorbed power (delivery power); (b) Record reaction temperature and absorbed power (delivery power).....208

Figure E4. Microwave-initiated dehydrogenation of crude oil on 5 wt.% Fe/AC catalysts. (a) Original microwave input power and absorbed power (delivery power); (b) Record reaction temperature and absorbed power (delivery power) 209

List of Tables

Table 1.1: Overview of hydrogen production methods 9

Table 1.2: Summary of fossil fuel reforming technologies 12

Table 1.3: A representative summary for CO_2-free hydrogen production 17

Table 3.1: Dielectric properties of catalysts 85

Table 4.1: Summary of H_2 conversion and yields of different metal catalysts supported by SiC through microwave-initiated dehydrogenation of hexadecane 107

Table 4.2. Summary of H_2 conversion and yields of various iron-based bimetallic metal alloy catalysts supported by SiC through microwave-initiated dehydrogenation of hexadecane ...109

Table 4.3: Summary of H_2 conversion and yields of Fe catalysts on different support materials under microwave-initiated dehydrogenation of hexadecane 111

Table 4.4: Summary of H_2 conversion and yields of Fe catalysts with various Fe loadings in the microwave-initiated dehydrogenation of hexadecane 113

Table 5.1: Comparison of the energy balance of microwave and conventional thermal methods 155

Table 6.1: Oxidation temperatures of Model Carbon Materials and Fe/SiC sample.....175

Table 6.2: BET Surface and Porosity of Model Carbon Materials and Fe/SiC sample 184

Table A1. The composition of diesel determined by GCMS 203

Table A2. The composition of petrol determined by GCMS 204

Table A3. The chemical compounds analysis on extra-heavy crude oil. 206

Table A4. The chemical compounds analysis on crude oil. 206

Table B1. Evolved gas composition of the prepared catalysts assessed by GC analysis 207

Table B2. Evolved gas composition of 5 wt.% Fe/SiC assessed by GC analysis from various liquid alkanes and aromatics 209

Table B3. Evolved gas composition of 5 wt.%-Fe, 5 wt.%-Ni FeNi/SiC assessed by GC analysis from various liquid alkanes and aromatics 210

Table C1: Theoretical hydrogen densities of various hydrogen storage materials.....211

Table C2: Experimental hydrogen densities of diesel, petrol and hexadecane obtained over 5 wt.% Fe/SiC catalysts.....212

Table D1: The energy requirement and energy output for the combustion of H_2 produced via the diesel cracking.....213

Table D2: The energy requirement and energy output for the combustion of H_2 produced via the diesel cracking.....214

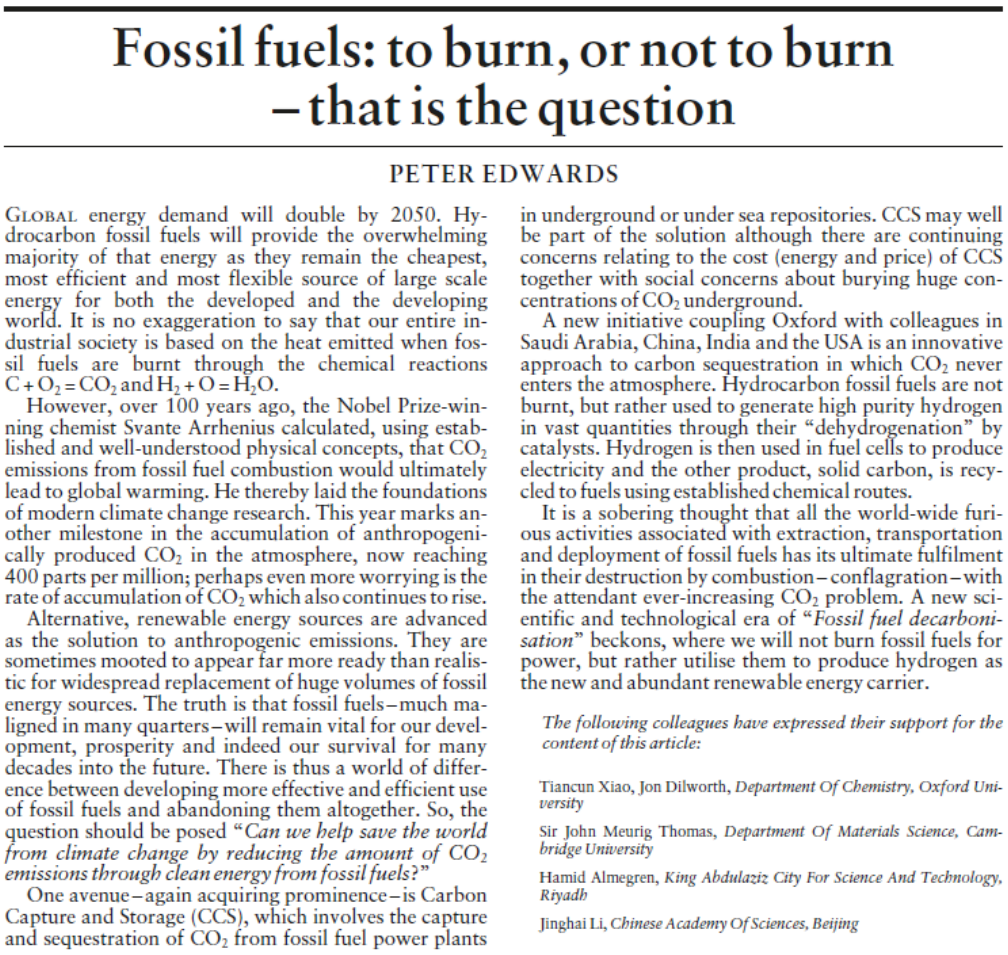
Chapter 1

Introduction

No doubt, another century dominated by the combustion of fossil fuels is disastrous. Renewable energy is widely acknowledged as the long-term potential of the replacement of fossil energy. However, the truth is that the world energy supply will be still dominated by fossil fuels in the near and mid- term future. It is no exaggeration to say that our entire industrial society is based on the heat emitted from fossil fuels burnt. Therefore, compared to depletion threat, the CO_2 emissions caused by fossil fuel combustion is the major problem for fossil fuels utilisation in the foreseeable future.

The Paris Agreement has set the warming limit target for 1.5 °C. But with current technologies of Carbon Capture and Storage (CCS) and renewables, the decarbonisation is not compatible with continued increase of energy demand and population growth. Moreover, so far, existing policies are not likely to fix the gap. While we are still in the carbon economy, the development of new scientific and technological CO_2-free routes for fossil fuels utilisation may be the best or the only environmentally safe alternative to CO_2 sequestration. In another word, the future of fossil fuels is not to be burnt, but rather to be utilised in the way to produce hydrogen as the new and abundant renewable energy carrier[1].

If the energy provided by the combustion of hydrocarbons is divided into C and H contributions, the H part is 'clean' energy and the energy via C combustion is 'dirty', i.e., producing greenhouse gas. There is therefore, the fundament of the new scientific and technological era of '*Fossil fuels decarbonisation*' is based on the simple idea of extracting only hydrogen compound from fossil fuels to produce high purity hydrogen fuel with recovery of solid carbon product to be utilised on various applications, rather than burning carbon.



Fossil fuels: to burn, or not to burn – that is the question

PETER EDWARDS

GLOBAL energy demand will double by 2050. Hydrocarbon fossil fuels will provide the overwhelming majority of that energy as they remain the cheapest, most efficient and most flexible source of large scale energy for both the developed and the developing world. It is no exaggeration to say that our entire industrial society is based on the heat emitted when fossil fuels are burnt through the chemical reactions $C + O_2 = CO_2$ and $H_2 + O = H_2O$.

However, over 100 years ago, the Nobel Prize-winning chemist Svante Arrhenius calculated, using established and well-understood physical concepts, that CO_2 emissions from fossil fuel combustion would ultimately lead to global warming. He thereby laid the foundations of modern climate change research. This year marks another milestone in the accumulation of anthropogenically produced CO_2 in the atmosphere, now reaching 400 parts per million; perhaps even more worrying is the rate of accumulation of CO_2 which also continues to rise.

Alternative, renewable energy sources are advanced as the solution to anthropogenic emissions. They are sometimes mooted to appear far more ready than realistic for widespread replacement of huge volumes of fossil energy sources. The truth is that fossil fuels – much maligned in many quarters – will remain vital for our development, prosperity and indeed our survival for many decades into the future. There is thus a world of difference between developing more effective and efficient use of fossil fuels and abandoning them altogether. So, the question should be posed "*Can we help save the world from climate change by reducing the amount of CO_2 emissions through clean energy from fossil fuels?*"

One avenue – again acquiring prominence – is Carbon Capture and Storage (CCS), which involves the capture and sequestration of CO_2 from fossil fuel power plants in underground or under sea repositories. CCS may well be part of the solution although there are continuing concerns relating to the cost (energy and price) of CCS together with social concerns about burying huge concentrations of CO_2 underground.

A new initiative coupling Oxford with colleagues in Saudi Arabia, China, India and the USA is an innovative approach to carbon sequestration in which CO_2 never enters the atmosphere. Hydrocarbon fossil fuels are not burnt, but rather used to generate high purity hydrogen in vast quantities through their "dehydrogenation" by catalysts. Hydrogen is then used in fuel cells to produce electricity and the other product, solid carbon, is recycled to fuels using established chemical routes.

It is a sobering thought that all the world-wide furious activities associated with extraction, transportation and deployment of fossil fuels has its ultimate fulfilment in their destruction by combustion – conflagration – with the attendant ever-increasing CO_2 problem. A new scientific and technological era of "*Fossil fuel decarbonisation*" beckons, where we will not burn fossil fuels for power, but rather utilise them to produce hydrogen as the new and abundant renewable energy carrier.

The following colleagues have expressed their support for the content of this article:

Tiancun Xiao, Jon Dilworth, *Department Of Chemistry, Oxford University*

Sir John Meurig Thomas, *Department Of Materials Science, Cambridge University*

Hamid Almegren, *King Abdulaziz City For Science And Technology, Riyadh*

Jinghai Li, *Chinese Academy Of Sciences, Beijing*

Figure 1.1. A comment from Professor Peter Edwards on Oxford Magazine. (Adapted from Ref 1).

1.1 Overview of fossil fuels as primary energy sources

Fossil fuels have been used as energy sources that drive the development of whole society for several decades[2, 3]. The fossil fuels are commonly known as coal, petroleum and natural gas. Other fossil fuels, such as shale oil, shale gas and tar sands are not yet in large-scale commercial use.

Generally, fossil fuels refer to the substances that are derived from the remains of animals or plants from past millions of years ago and can be burned to generate heat. They consist principally of carbon (C) and hydrogen (H), and other important constituents are oxygen (O), nitrogen (N) and sulfur (S)[4]. They are naturally found as solids, liquids or gases – coal is a

brown or black solid, petroleum is a yellowish to black liquid, and natural gas (methane) is a colourless gas.

Since James Watt discovered the steam engine in 1796, coal had powered Britain's great economic growth and launched the industrial revolution. For the first time machines powered by coal, could carry out work formerly done by humans and animals. This revolution speeded up manufacturing and reduced the costs of operate, and subsequently boosted the economic growth. Later in the 1880s, coal was first been used to generate electricity for industry and domestic use. The coal fired power plants continue to be used to provide electricity and accounts for around 40% of the world electricity[5]. However, in 2016, the demand for coal fell by 231 million tons of oil equivalent (mtoe)[6] as many countries switched away from coal generation to natural gas or renewables. This is because the burning of coal releases many pollutants, such as oxides of nitrogen (NO_x) and sulfur (SO_x) and particulate matter etc., and a large amount of CO_2 emission.

Unlike coal, which is a widespread resource and has been mined for over a 1000 years in China and Britain, petroleum and gas are geographically concentrated, mainly in reserves in the Middle East[7]. After World War II when cheap oil became available, the petroleum rapidly revolutionised the way we live. Petroleum is often referred to as 'black gold', and drove many of the dramatic changes in the twentieth century which is probably best characterised as the century of oil[7].

Petroleum is a fluid with the composition of 83 – 87% carbon, 11 – 16% hydrogen, 0 – 4% of oxygen and nitrogen, and 0 – 4% of sulfur[8]. Compared to coal, petroleum is much less variable and most of them contain more hydrogen. Despite the thousands of compounds present in petroleum, generally, they contain the hydrocarbons consisting of 5 to about 40 carbon atoms. The hydrocarbon molecules found are either straight or branched and are called paraffins. The paraffins are saturated hydrocarbons which every carbon atom is surrounded by hydrogen atoms and they can be depicted as the molecular formula of C_nH_{2n+2}. Another type of hydrocarbons found in petroleum are the aromatic compounds, which they have a ring structure such as benzene (C_6H_6).

Unlike coal and gas for which little processing or no processing is required before use, the petroleum cannot be simply utilised when they are extracted from Earth, and a complex petroleum refinery process is required to separate different compounds for the best use. Thus, the common petroleum - derived commodities of petrol (gasoline) and diesel fuels etc., are the products from petroleum refinery. Figure 1.2 illustrates the schematic representative pathway for petroleum utilisation through refinery process. In principal, approximately 40% of refinery products goes to petrol and diesel fuels, and other fuels (jet fuel, fuel oil etc.), gases and solid residuals are also produced and used in a variety of industrial areas.

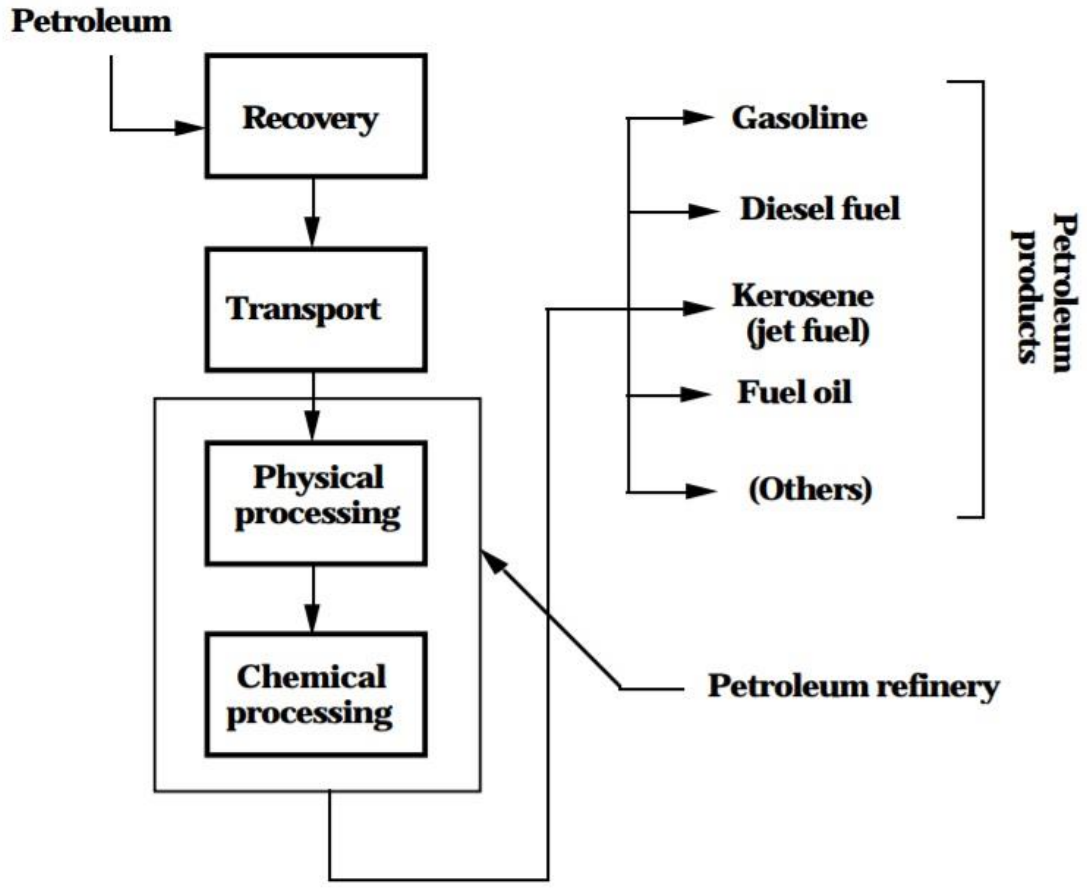


Figure 1.2. Pathway of petroleum utilisation from crude oil to petroleum derived fuels. (Adapted from Ref 6).

Turning to natural gas, its lower carbon emission compared to coal and oil suggests it will play a significant role in the transition to a cleaner energy future[9]. Therefore, natural gas is the only fossil fuel whose share of the primary energy mix is expected to grow. Currently, natural

gas is the third most widely used fuel in global primary energy and the second energy source in power generation. These numbers may potentially grow in the future due to the recent technological breakthroughs in shale gas production. Nearly 60 % of the increase in natural gas supplies comes from shale gas production and it is predicted that the shale gas will account for around a quarter of total gas production by 2035[10].

In summary, today the world's ever-increasing energy demand is still based almost exclusively on fossil fuels, not only because of their unrivalled energy-carrying properties but also because of the demands of the world-wide energy infrastructure developed over the past century. Despite the highest growth rate of renewables was recorded in 2017, fossil fuels still account for over 85% of the global primary energy demand and are expected to remain the dominant in 2035 with more than 75% of total energy supplies. Thus, it is no exaggerated to say that our society is largely powered by the combustion of fossil fuels[10].

Over decades, fossil fuels are linked with two major problems of depletion threat[11] and CO_2 emission. A peak for oil extraction has often been predicted[11, 12], but it has continued to increase remarkably due to subsequent oil discoveries. The most famous prediction of oil peak is credited to geologist M. King Hubbert who successfully predicted the US peak oil production in 1970[13]. However, his prediction that global oil production would peak near the year 2000 is now proved incorrect. Although the academic debate on the depletion threat of fossil fuels remain, the energy supply will still be dominated by fossil fuels in the near- and mid- term future[11, 14]. Thus, compared to the depletion threat, the CO_2 emissions caused by fossil fuel combustion is the critical problem for fossil fuels utilisation in the foreseeable future.

Over 100 years ago, the Nobel Prize-winning chemist Svante Arrhenius laid the foundations of modern climate change research[1]. The atmospheric concentration of CO_2 has increased from 280 ppm in the pre-industrial age to more than 400 ppm now and is expected to be above 500 ppm by the end of this century. In 2017, the global energy related CO_2 emissions reached a historic high of 32.5 Gt with an increase of 460 million tonnes (Mt) compared to 2016 [15]. The combustion of fossil fuels accounts for approximately 90% of annual global CO_2 emissions[16].

Moreover, electricity and heat generation and transportation accounted for nearly two-thirds of global CO_2 emissions in 2015[16].

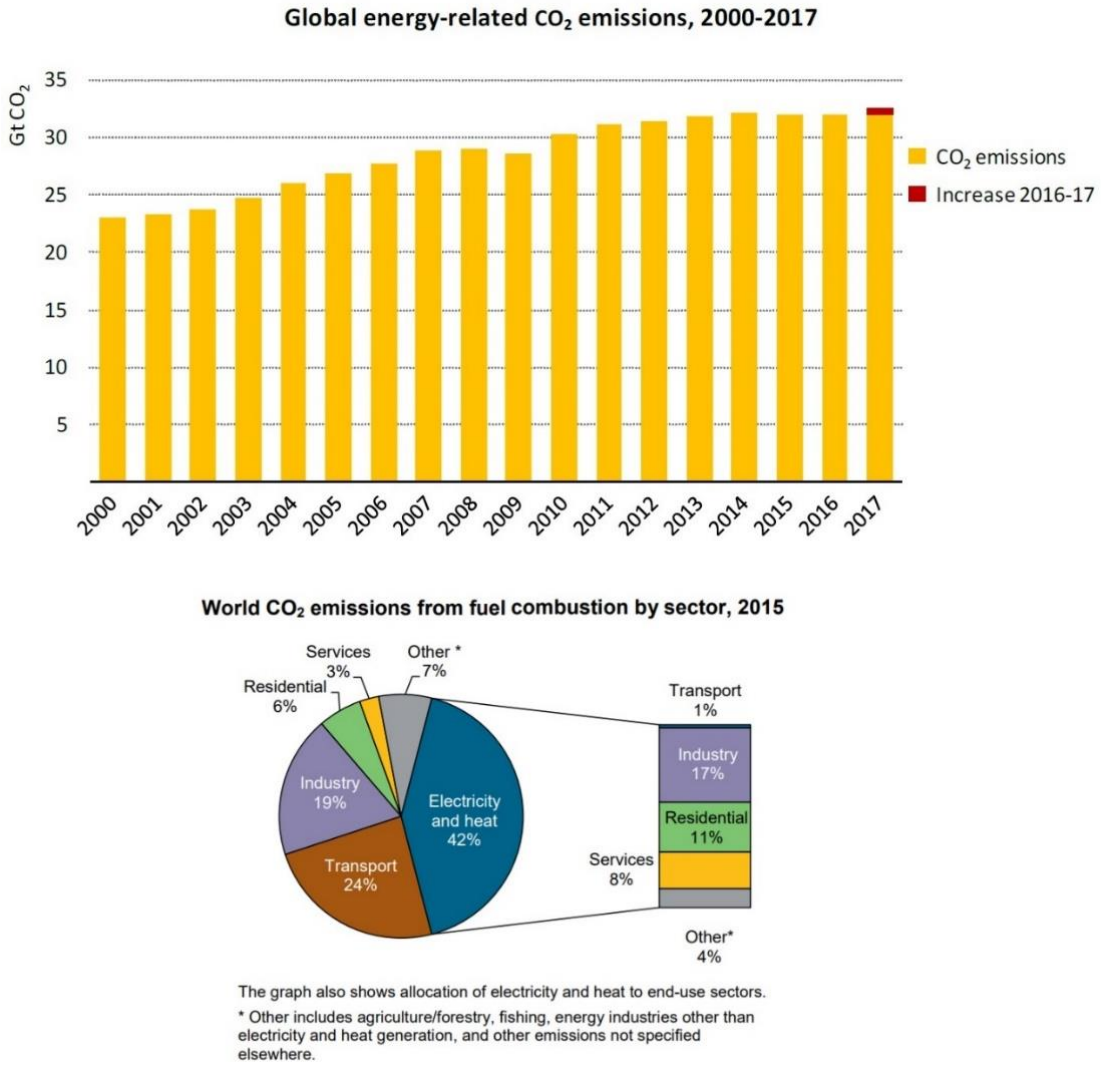


Figure 1.3. Global energy-related CO_2 emissions, 2000-2017. (Adapted from Ref 15; IEA, *Global Energy & CO_2 Status Report*); World CO_2 emissions from fuel combustion by sector, 2015. (Adapted from Ref 16; IEA, *CO_2 emissions form fuel combustions*)

Thus, in order to develop a low-carbon world the historic Paris Agreement was signed in 2015 and now has 195 countries in one agreement aiming to keep the increase in global average temperature to below 1.5 ºC above pre-industrial levels. In addition to the Paris Agreement, previous climate treaties such as the Kyoto Protocol, the Copenhagen Accord and the Cancun Agreements also aim to limit the global CO_2 emissions. Efforts need to be made by cross

policymakers and scientists throughout all fields to achieve the goal set by Paris Agreement. Considering the fossil fuels account for majority of our primary energy supplies and will still dominant the upcoming decades, we believe in the near- and mid- future, the scientific and technological goal is set: *''fossil fuels decarbonisation''*.

1.2 Hydrogen Economy

To solve the environmental problem caused by utilising hydrocarbon fuels (carbon economy), the concept of the ''hydrogen economy'' was advanced which advocated hydrogen as a potential fuel applies to the energetic, ecological, and economic aspects [17]. In 1972, a paper entitled ''A Hydrogen Economy''[17] was published in Science by John Bockris, which listed the advantages of a hydrogen economy. Firstly, water which is abundant and generously distributed throughout the world could be a source of hydrogen[18]. Hydrogen can also be produced from diverse other resources, both renewable (hydro, wind, solar, biomass, geothermal) and non-renewable (coal, natural gas, nuclear). Second and importantly, through the combustion or oxidation reaction of hydrogen, energy is explosively released in heat and water is the only by-product. Furthermore, the hydrogen would contribute to the transportations[17], by means of fuel cell-battery combinations and electric motors, which would be not only non-polluting but also silent and cheaper because of the greater efficiency of fuel cells. Meanwhile, the use of hydrogen and fuel cells in transportation, heat generation and stationary electricity, could eventually eliminate CO_2 and harmful gas emissions (such as NO_x, unsaturated hydrocarbons and particular matters (PM) etc.) from the energy sector.

However, one of the principal reasons why progress towards the hydrogen economy[19-26] has been so slow, is that there is no readily available massive source of "natural" hydrogen. Furthermore, to date, no reliable means exists for storing hydrogen in such a manner that it can be rapidly released on demand for the appropriate fuel cell application. There are therefore, significant scientific, technological and socioeconomic barriers such as the cost of hydrogen

production and delivery, hydrogen storage systems, and the cost of hydrogen utilisation systems need to be overcome in order to achieve a successful transition from a carbon-based economy to a hydrogen economy[19 27, 28].

1.3 Methods of producing hydrogen

Hydrogen as an abundant element, which can be naturally found in the substances such as fossil fuels, water and biomass etc. In order to produce hydrogen fuel, several methods have been designed and developed to extract hydrogen from these feedstocks using either thermal, electrical, photonic, or biochemical energy. The potential methods of hydrogen production using renewable and non-renewable sources have been previously reviewed by various authors[29-33].

Table 1.1 presents an overview and brief description of hydrogen production methods along with their primary energy input and substance sources[29]. In the early 1800s, based on the work of Volta and Davy, electrolysis of water was used to produce hydrogen, which is a method still in wide use (but still relatively inefficient). More esoteric methods of generating hydrogen were subsequently discovered, e.g., enzymatic decomposition of sugars and the reforming in aqueous solution of the components[34] of biomass[35]**.** The thermal decomposition of appropriate inorganic compounds was also used, and the method gained popularity when solar furnaces (capable of reaching very elevated temperatures) became available. Thermolysis of alkanes has also been quite an effective method[36]. Nowadays, most of the industrial hydrogen production is based on the steam methane reforming (SMR) process, but thanks to the burgeoning use of renewable sources of energy –solar, wind, hydro and geothermal- an increasing quantity of hydrogen is generated by photoelectrochemical, electrocatalytic and photocatalytic means.

Table 1.1: Overview of hydrogen production methods. (Modified from Ref. 29)

Method		Energy Input	Hydrogen Resource	Brief description
Electrolysis		Electrical	Water	Direct current is used to split water into $O_2$and H_2(electrochemical reaction)
Plasma arc decomposition			Fossil fuels	Cleaned natural gas is passed through plasma arc to generate H_2 and carbon soot
Microwave			Hydrocarbons	High purity hydrogen was produced from hydrocarbons with assistance of microwave.
Thermolysis		Thermal	Water	Thermal decomposition of water (steam) at temperatures over 2500 K
Thermochemical processes	**Water splitting**			Cyclical chemical reactions (net reaction: water splitting into H_2)
	Biomass conversion		Biomass	Thermocatalytic conversion
	Gasification			Conversion of biomass into syngas
	Reforming			Conversion of liquid biomass (biofuels) into H_2
PV electrolysis		Photonic	Water	PV panels are used to generate electricity
Photocatalysis				Water is split into H_2 by using the electron-hole pair generated by the photocatalyst
Photoelectrochemical method				A hybrid cell simultaneously produces current and voltage upon absorption of light
Dark fermentation		Biochemical	Biomass	Biological systems are used to generate H_2 in the absence of light
High temperature electrolysis		Electrical + Thermal	Water	Electrical and thermal energy are used together to drive water splitting at high temperatures
Hybrid thermochemical cycles				Electrical and thermal energy are used together to drive cyclical chemical reactions
Coal gasification				Conversion of coal into syngas
Fossil fuel reforming				Fossil fuels are converted to H_2 and CO_2
Biophotolysis		Photonic + Biochemical	Biomass + Water	Biological systems (microbes, bacteria, etc.) are used to generate H_2
Photofermentation				Fermentation process activated by exposure to light
Artificial photosynthesis				Chemically engineered systems mimic photosynthesis to generate H_2
Photoelectrolysis		Electrical + Photonic	Water	Photoelectrodes and external electricity are used to drive water electrolysis

1.3.1 Use of Renewable Energy to Produce Hydrogen

Extensive work involving principally solar radiation (as well as wind and other natural sources) has been done to produce hydrogen by splitting water either via a photo-assisted manner or by electrolysis[37-42]. It is relevant to recall that, in May 2014, a hydrogen fuelling facility (HRS) was established in California State College, Los Angeles, and the hydrogen was produced from a renewable energy source by electrolysis[34, 43]. Most of these processes, irrespective of whether or not they utilize photovoltaics, photocatalysis, photoelectrochemistry (or by electrolysis) to produce hydrogen are rather inefficient[34].

Generally, in straightforward photocatalytic systems, an electrochemically appropriate inorganic photocatalyst (e.g. $SrTiO_3$ or modified TiO_2) is dispersed as a powder in aqueous solution, and hydrogen and oxygen are produced simultaneously[34]. When a photon hits the photocatalyst, electrons and holes are generated inside semiconductor photocatalyst particles by band-gap excitation. Photoexcited carriers are transferred to surface active sites and subsequently consumed by surface redox reactions[44]. The photoreduction and photo oxidation reactions can be generalised as follows[29]:

$$Photo - reduction: 2H_2O + 2e^- \overset{hv}{\rightarrow} H_2 + 2OH^- \quad (1.1)$$

$$Photo - oxidation: 2H_2O \overset{hv}{\rightarrow} O_2 + 4H^+ + 4e^- \quad (1.2)$$

Since hydrogen and oxygen are simultaneously generated through photocatalytic water splitting, such arrangements require elaborate methods for separating these gases[34]. Thus, a novel photocatalytic system, called the Z-scheme, which mimics the well-known Z mechanism in natural photosynthesis of green plants, has been developed by Abe *et al.*, [45] to generate hydrogen and oxygen simultaneously. The Z-scheme consists of a hydrogen photocatalyst and an oxygen photocatalyst to perform water splitting. Despite the huge progress has been made in photocatalytic water splitting over recent years, photocatalytic splitting is still at a very low technological readiness and has several challenges to overcome. Moreover, whilst the cost of hydrogen production from renewable energy has been continuously decreasing, the cost of these methods is still about 25 times higher than that of fossil fuel alternatives[29, 34].

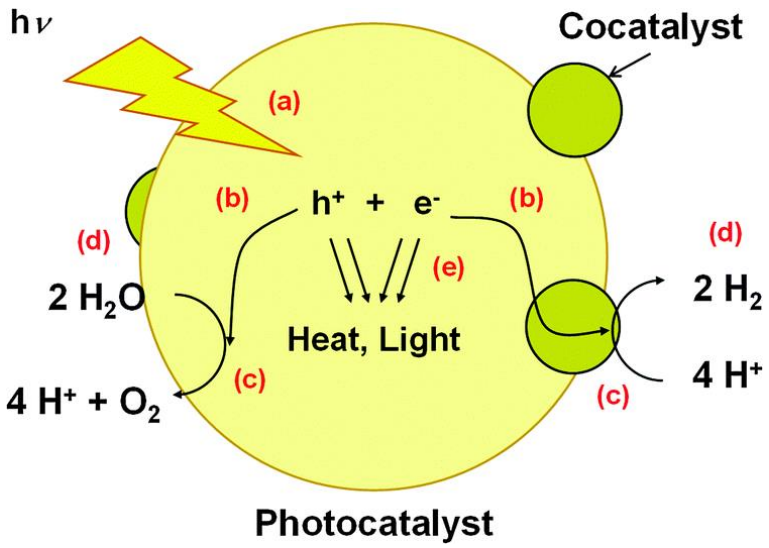


Figure 1.4. Photocatalytic system of water splitting. (a) Light absorption, (b) charge transfer, (c) redox reactions, (d) adsorption, desorption, and mass diffusion of chemical species, and (e) charge recombination. (Adapt from Ref. 44)

1.3.2 Coal gasification

The gasification of coal is a general option to produce hydrogen in large scale plants considering the current state of technology and worldwide coal reserves[29]. The gasification of coal is generally represented by the following two steps of reactions:

$$C + H_2O \rightarrow CO + H_2 \cdots Step\ 1 \quad (1.3)$$

$$CO + H_20 \rightarrow CO_2 + H_2 \cdots Step\ 2 \quad (1.4)$$

In the first step of gasification, coal (elemental carbon) is reacted with steam which is partially oxidized to produce syngas in a high-temperature and high-pressure reactor. The second step in the process consists of a water gas shift (WGS) reaction, in which the CO reacts with steam to generate more H_2 together with CO_2 production. Finally, the H_2 gas will be separated and cleaned by removing unwanted CO_2 and other impurities such as sulfuric impurities etc.

At present, the cost of hydrogen production from coal gasification is slightly higher than that of methane steam reforming. The major concern of using coal gasification is massive CO_2 emissions from

the process. Moreover, despite the lower unit price of raw material (coal), the unit capital costs are higher for coal gasification plants[29].

1.3.3 Fossil fuel reforming

Almost all the hydrogen that is produced worldwide nowadays for industrial purposes comes from the steam reforming of natural gas and, to a less degree, from the gasification of coal. In the fossil fuel reforming, three main techniques are used: steam reforming, partial oxidation (POX), and autothermal reforming (ATR)[29, 32, 33, 36]. The advantages and challenges of each of these processes are listed in Table 1.2. In general, the related hydrocarbons reforming reactions are given below[33]:

Table 1.2: Summary of fossil fuel reforming technologies. (Modified from Ref. 29 and 33)

Technology	Advantages	Disadvantages
Steam reforming	· Most extensive industrial experience · No oxygen requirement · Lowest process temperature · Best H_2/CO ratio	· Highest CO_2 emissions
Partial oxidation	· Decreased desulfurization requirement · No catalyst required · Low methane slip	· Low H_2/CO ratio · High processing temperatures · Soot formation · Complex handling process
Autothermal reforming	· Lower process temperature than partial oxidation · Low methane slip	· Limited commercial experience · Requires air or oxygen

Steam reforming

$$C_mH_n + mH_2O = mCO + \left(m + \frac{1}{2}n\right)H_2 \qquad (1.5)$$

$$\cdots \Delta H = \ hydrocarbon\ dependent, endothermic$$

Partial oxidation

$$C_mH_n + \frac{1}{2}mO_2 = mCO + \frac{1}{2}H_2 \ \cdots \ \Delta H = hydrocarbon\ dependent, exothermic \qquad (1.6)$$

Autothermal reforming

$$C_mH_n + \frac{1}{2}mH_2O + \frac{1}{4}mO_2 = mCO + \left(\frac{1}{2}m + \frac{1}{2}n\right)H_2 \quad (1.7)$$

$$\cdots \Delta H = hydrocarbon\ dependent, thermally\ neutral$$

Water-gas-shift (WGS)

$$CO + H_2O = CO_2 + H_2 \ \cdots \Delta H = -41.1\ kJ/mol \quad (1.8)$$

Reverse Water-gas-shift (RWGS)

$$CO_2 + H_2 = CO + H_2O \ \cdots \Delta H = 41.1\ kJ/mol \quad (1.9)$$

Carbon (coke) formation

$$C_mH_n = xC + C_{m-x}H_{n-2x} + xH_2 \ \cdots \Delta H = hydrocarbon\ dependent \quad (1.10)$$

Through steam reforming hydrocarbons are partially oxidized via steam with external heat sources. No oxygen is required for the steam reforming and the process can be operated at a lower temperature than POX and ATR[46, 47], with higher H_2/CO ratio of ca. 3:1 which is beneficial for hydrogen production. Although steam reforming is commonly used in industry for the production of hydrogen from methane and achieves up to approximately 85% thermal efficiencies based on its higher heating values[33], it does produce the highest CO_2 emissions among these three processes.

In partial oxidation, hydrocarbons are converted to hydrogen by partially oxidizing (combusting) with oxygen. There is no catalyst requirement in partial oxidation, and it has minimal methane slip and is more sulfur tolerant than the other processes. Due to the exothermic reactions of partial oxidation (combustion) reactions, partial oxidation does not need an external heat source. Typically, the partial oxidation occurs at the temperature of 1300 – 1500 ºC to ensure completion of the reactions and to reduce the formation of carbon and soot[33]. Thus, catalysts can be introduced to the process as catalytic partial oxidation (CPOX) to lower the operating temperature. At the beginning, partial oxidation and catalytic partial oxidation of hydrocarbons were proposed for use in hydrogen production for

automobile fuel cells[48-50]. However, it is hard to control the temperature of both processes because the exothermic nature of the reactions contributes to the coke and hot spot formation[48, 51]. In term of the thermal efficiencies of POX, the 60 -75% efficiencies are achieved with methane, based on the higher heating values[33].

Autothermal reforming, on the other hand, combines the partial oxidation and steam reforming which result in a thermally neutral process[52-55]. The POX or CPOX (thermal zone) generates the heat needed to drive the steam reforming reactions (catalytic zone). A sharp rise of temperature is a characteristic of the thermal zone, followed by the temperature steadily decreasing in the catalytic zone[33, 56, 57]. The heat generated from POX simplifies the system and decreases the start-up time which significantly improves the steam reforming process, and enables a rapid start and stop operating while producing a large quantity of hydrogen. However, they require an expensive and complex oxygen separation unit in order to feed pure oxygen to the reactor and the product gas is diluted with nitrogen[33].

Generally, significant amounts of carbon monoxides, about 5% or more[33, 46], are produced during the reforming process. Therefore, the product gas is additionally treated through the water-gas-shift (WGS) reaction to decrease the carbon monoxide content whilst increasing the amount of hydrogen. Also, the carbon dioxide can react with the hydrogen via reverse water-gas-shift (RWGS), so it is important to carefully control the reaction conditions in order to minimize unnecessary consumption of hydrogen.

Whilst the large-scale hydrogen production is through these methods from fossil fuels and substantial improvements have been made to these technologies[32] the problem is a vast amount of carbon dioxide emitted. This means that it cannot contribute sustainably to the long-term hydrogen economy, even with development of technologies such carbon capture and storage (CCS) and/or carbon capture and utilisation (CCU). Thus, alternatively, the methods for CO_2-free hydrogen production is necessary.

1.3.4 Pyrolysis

Pyrolysis as a CO_2-free hydrogen producing technology is to decompose hydrocarbon (without water or oxygen present) into hydrogen and carbon[33, 36, 58, 59]. The reactions of pyrolysis can be written as follow:

$$C_nH_m \rightarrow nC + \frac{1}{2}mH_2 \quad \cdots \Delta H = hydrocarbon\ dependent \qquad (1.11)$$

The pyrolysis is simple, and no carbon oxides are formed during the process, eliminating the need for secondary reactions such as WGS etc., which subsequently reduce the CO_2 emissions compared to reforming processes. Generally, the pyrolysis process is fuel flexible and can be carried out with any organic materials. Oxygen is presented in the materials such as biomass, from which CO_2 and CO can be also produced via pyrolysis[32, 60, 61].

One of the challenges with pyrolysis is the carbon formation during the process which will poison any catalysts used. However, it is claimed that this can be minimized by appropriate design or utilisation of clean carbon by-product directly. Since no CO_2 and CO are formed during the pyrolysis of hydrocarbons, it has high potential to provide a suitable method for CO_2-free hydrogen production. In addition, since solid carbon can be easily captured and much more easily sequestered than gaseous CO_2[33, 59, 62, 63], pyrolysis may play a significant role in the future.

1.3.5 Other methods

Other methods such as plasma arc decomposition, microwave pyrolysis, water thermolysis etc., are also designed for generation hydrogen production in order to underpin the development of the hydrogen economy. Regarding the hydrogen production for fuel cells, there is one method so-called Hot Spot Technology that merits mention[34].

The Hot Spot Technology was invented by the Johnson Matthey Company[64-66] and uses methanol as hydrogen carrier. In essence, the Hot Spot technology entails, first, the use of a base metal that dehydrogenates methanol:

$$CH_3OH \rightarrow CO + 2H_2 \qquad \Delta H^\theta = +306\ kcal/mol \qquad (1.12)$$

This is an endothermic process, but the liberated carbon monoxide is then oxidized in air, catalysed by a noble metal, and this is an exothermic process:

$$CO + \frac{1}{2}O_2 \rightarrow CO_2 \qquad \Delta H^\theta = -67.6\ kcal/mol \qquad (1.13)$$

The heat released in this oxidation then sustains the production of hydrogen by dehydrogenating methanol. The advantages of the Hot Spot technology are, it requests no power to initiate its action, it needs no water and it is capable of rapid "stand up", and it is ideally suited to feed hydrogen into a typical solid polymer type fuel cell (SPFC)[34]. However, it does produce CO_2.

1.4 CO_2-free hydrogen production from hydrocarbons

Since the large-scale hydrogen production technology of steam reforming currently emits large quantities of CO_2, one of the greatest challenges for any future hydrogen economy is the necessity for large scale hydrogen production without involving concurrent CO_2 production. The CO_2-free hydrogen production from hydrocarbons via thermal, catalytic decomposition has been developed in pioneering work by Steinberg[67, 68], Muradov[59, 69-71] and co-workers. This was also achieved more recently through the use of microwave heterogeneous catalysis[72-74], plasma processing [75, 76] and the use of catalytic molten metals for the direct conversion of methane to hydrogen and separable carbon[58, 77] . Such methods for CO_2-free hydrogen production from various hydrocarbon feedstocks has previously been reviewed by Muradov *et al.* [78] and Ahmed *et al.* [36] in general, thermo-catalytic methane cracking has been extensively studied. Table 1.3 summarised a literature review on previous studies on CO_2-free hydrogen production from different hydrocarbons.

Muradov *et al.* [85] investigated several routes to hydrogen production from natural gas (or methane) with carbon-based catalysts and several technological approaches were discussed based on thermocatalytic decomposition (or pyrolysis) of methane into hydrogen gas and elemental carbon. Huffman *et al.* [101] addressed the catalytic decomposition of cyclohexane using the (4.5 wt.% Fe–0.5 wt.% Pd)/Al_2O_3 catalyst. It was shown that H_2, benzene, and un-reacted cyclohexane are the primary products obtained in the exit gas flow below 450 °C, but only H_2, CH_4, and carbon nanotubes (CNTs) above 500 °C (see Figure 1.5).

Table 1.3: A representative summary for CO_2-free hydrogen production.

Hydrocarbon	Method and Technology	References
Methane (CH_4)	•Pyrolysis •Thermocatalytic cracking •Microwave •Plasma	[68], [79], [70] [80], [81], [82], [62], [83], [84], [85], [86], [87], [88], [89], [90], [91], [92] [73] [75], [76], [93], [94], [95], [96], [97], [98]
Ethane (C_2H_6)	•Thermocatalytic cracking	[99], [100]
Propane (C_3H_8)	•Thermocatalytic cracking •Plasma	[62], [100], [101] [93]
Hexane (C_6H_{14})	•Pyrolysis •Thermocatalytic cracking	[79] [100], [101], [102], [103]
Diesel	•Pyrolysis •Thermocatalytic cracking •Plasma	[79] [49] [98]
Gasoline	•Pyrolysis •Thermocatalytic cracking •Plasma	[79], [70] [62] [98], [104], [105]
Kerosene	•Thermocatalytic cracking •Plasma	[106], [107] [98]
Wax	•Microwave	[133]

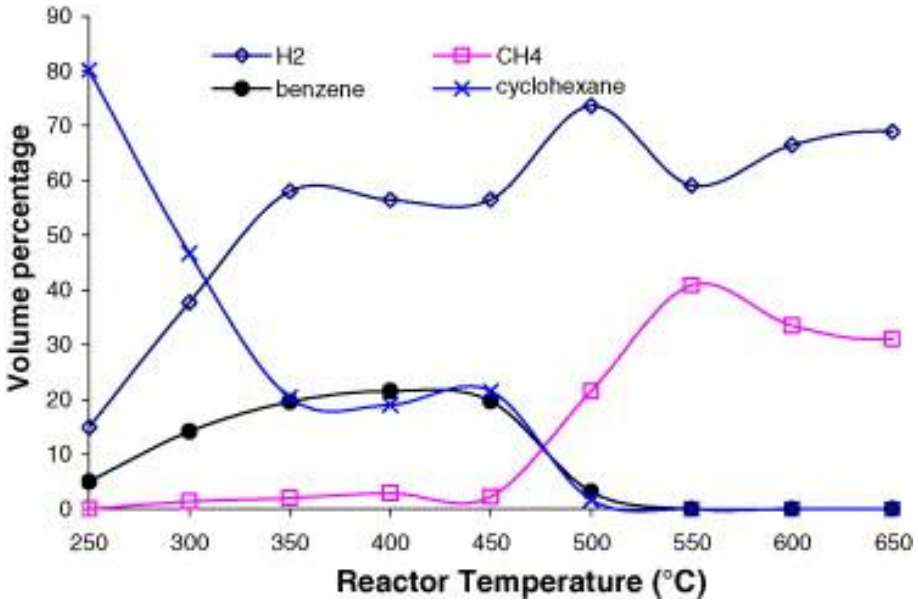


Figure 1.5. Product distribution of cyclohexane decomposition over (4.5 wt.% Fe–0.5 wt.% Pd)/Al_2O_3 catalyst vs. temperature. (Adapted from Ref. 101).

Recently, Upham *et al.* [77] reported a catalytic pyrolysis of methane to hydrogen and separable carbon using molten metals. A molten metal alloy of 27% Ni- 73% Bi catalyst achieved 95% methane conversion at 1064 ºC and produced pure hydrogen with insoluble carbon floats to the surface which

can be skimmed off (see Figure 1.6). This offers potential practical use for direct CH_4 pyrolysis with a practical process for carbon removal, because the carbon poisoning is the well acknowledged problem for direct CH_4 pyrolysis.

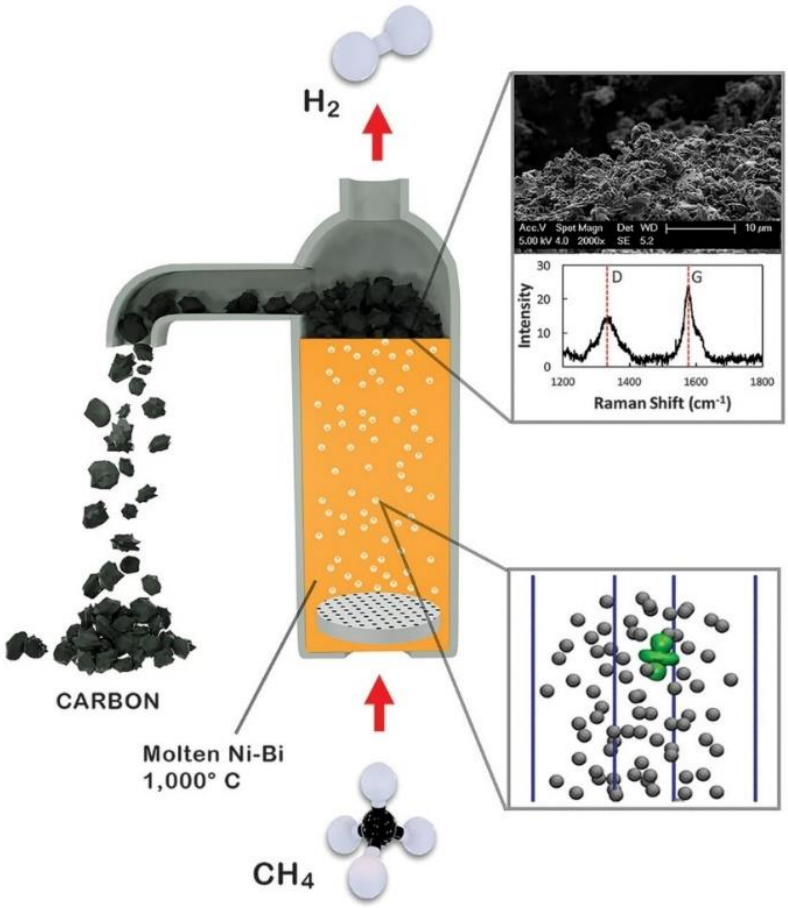


Figure 1.6. Hydrogen production with a Ni-Bi molten catalyst. (Adapted from Ref. 77).

As for the dehydrogenation of heavier hydrocarbons, one scenario for fossil fuels decarbonisation would be achieved if hydrogen can be rapidly released from these heavier hydrocarbons. And this would subsequently facilitate the smooth transition from the current carbon economy to a hydrogen economy.

1.5 Catalysts overview for hydrogen production systems

Irrespective of the hydrogen supply resources and hydrogen production systems applied, high-efficiency, low-cost, and robust catalyst systems are critically needed. To develop efficient and robust catalysts, the design most occurs in accordance with the catalytic reaction and mechanism.

In the steam methane reforming process (SMR), nickel catalysts are used almost universally in industry, although many researches have shown that noble metal-based catalysts, particularly Rh [33, 108], exhibit much higher specific activities than nickel catalysts[32, 33]. Similarly, the catalysts containing group 8, 9 and 10 metals (Ni, Co, Ru, Pt, Pd, Rh, etc.) are preferred for the steam reforming of liquid hydrocarbons [31]. To minimise the coke formation during steam reforming, the tetra- and pentavalent p metals (Ge, Sn, and Pb or As, Sb, and Bi) are studied as dopants because the similar electronic structure of carbon[32, 109]. Trimm[109] reported the dopant of tin (Sn) at a low level below 1.75%, significantly reducing the coke formation without any influence on the catalytic rate of steam reforming[31]. Moreover, modification of Ni catalysts by other metals such as Co, Mo, W, Re and Sr revealed a high resistance for coking[32, 110, 111]. Several supports have also been studied, such as the magnesia-supported and silica-supported nickel catalysts where it was proposed that the enhanced adsorption of surface hydroxyl groups on the support surface react with the CH_x fragments adsorbed on the nickel surface leading to improved catalytic lifetime[112].

For the catalytic partial oxidation (CPOX) and autothermal reforming (ATR), the active catalysts used are very similar to the steam reforming[31] where the supported metals, generally the group 8, 9 and 10 metals (Ni, Co, Ru, Pt, Pd, Rh, etc.) are used. In general, nickel, cobalt, and other noble metals (Ru, Rh, Pt) have been most studied for CPOX. Since the catalysts with a high thermal stability are required for ATR process when operating at the high temperature, a low level nickel containing catalyst supported on alumina (α-Al_2O_3) and magnesium alumina spinel ($MgAl_2O_4$) are preferred for ATR[31]. Other catalysts system such as bimetallic Ni-Pt catalysts also revealed an increased catalytic activity during methane ATR[113].

The water-gas-shift (WGS) reaction (Eq. 1.8) as an important step in steam reforming can enhance the hydrogen yield of the process. Also, the WGS reaction is a key step in fuel processing to generate

hydrogen and one of the oldest catalytic processes[32] that applied in various chemical industries for ammonia synthesis and methanol production etc. Conventional catalysts used for the WGS reaction are Fe_2O_3-Cr_2O_3 and Cu-ZnO-Al_2O_3. However, the low activity of these catalysts at high temperature makes them unsuitable for use in small-scale re-formers[32]. Thus, the promoted Cu-ZnO catalyst systems with alkali are designed to overcome the limitation of former catalysts with better activity and durability[32]. Other catalyst systems such as cobalt-vanadium binary oxides[32] and molybdenum carbide[114] were discovered and displayed specific activities higher than that of Cu-ZnO catalyst systems. Other than non-precious metal catalysts which are found suitable for WGS reaction due to their low cost, new WGS catalysts were designed using Pt group metals or Au[115] when activity and cost are balanced[32]. CeO_2 supported Pt group metals have been reported to be more active and non-pyrophoric than conventional WGS catalysts and operate at mild reaction temperatures[116]. Due to the high oxygen storage capability of ceria, ceria-supported Pt, Pd, Rh, Ni, Fe and Co metals have been established for WGS reaction and showed a high catalytic activity[32, 117]. Besides, TiO_2-supported catalyst systems[118] and gold catalysts[119] supported by CeO_2[120], TiO_2[121] and Fe_2O_3[122] also display good performance in WGS reaction.

The catalysts used for CO_2-free hydrogen production reactions are generally metal catalysts such as Ni, Co, Fe and Pt etc., which cleave C – H bonds of the hydrocarbon molecules and sustain a high activity for a long time[32]. Among many of the transition metal catalysts, nickel and iron- based catalysts have been the most studied for methane decomposition as well as the catalytic decomposition of other hydrocarbons[59, 88, 123-127]. Because the CO_2-free hydrogen production reactions generate only hydrogen and carbon, various carbon materials were investigated as possible catalysts for catalytic methane decomposition[73, 83, 128, 129]. Muradov *et al.* investigated the element carbon for thermal cracking of methane, which suggested the disordered forms of carbon (e.g. activated carbon and carbon black) are more catalytically active than the ordered carbon of graphite and diamond powder [128]. One of primary issues hindering the commercial application of catalytic methane decomposition (CMD) as well as CO_2-free hydrogen production from various hydrocarbons is the carbon poisoning on catalysts. To address the carbon deposition problem of CMD, a new method using molten metals is proposed to easily separate carbon when insoluble carbon floats to the surface which can be skimmed off after cooling

down. In this process, low-melting-temperature metals such as In, Bi, Sn, Ga and Pb etc. were used as metal ‘‘solvents’’. Due to less catalytically activity is observed over these metals, the active metals like Ni and Pt etc. are added in the solvent. In a recent advance, Upham *et al.* [77] reported a molten metal alloy of 27% Ni- 73% Bi catalyst achieving high conversion of methane of 95% at 1064 ºC.

In most cases of hydrogen production using renewable energy, noble metals (Pt, Pd, Ru, Rh etc.) are widely used. In the photocatalytic water-splitting hydrogen production, noble metals including Pt, Au, Pd, Rh, Ni, Cu and Ag, have been reported to be very effective for photocatalytic water-splitting when loaded on TiO_2 catalysts[130]. With the noble metals, the possibility of electron-hole recombination is significantly reduced because the low Fermi levels of noble metals enables the photo-excited electrons transferred from conduction band (CB) to metal particles, while photo-generated valence band (VB) holes remain on the TiO_2[130, 131]. In the area of PEM fuel cells, use of Pt-based catalysts is still dominant which is largely responsible for the high price of PEM fuel cells. Although a variety of catalysts are being investigated to reduce the use of Pt, the catalysts used for PEM fuel cell are still Pt/C and Pt-modified or alloyed catalysts. This is mainly because the low overpotential and high catalytic activity of Pt for the hydrogen oxidation reaction (HOR) and the oxygen reduction reaction (ORR)[132]. More importantly, Pt is rather stable in the harsh acidic environment inside a PEM fuel cell[132].

There is thus, it is not simply the question of cost that impels academics and industries these days to seek alternatives for platinum group metals (PGM) as catalysts, it is also because, given the expected future demands for fuel cells that the hydrogen economy requires, it is unlikely that there will be sufficient PMG, to satisfy future needs. Again, it is platitudinous to point out that there is a pressing need to replace PGM catalysts with more abundant but comparably effective ores. For the indefinite future, in the drive to arrive at the hydrogen economy, it is abundantly clear that inexpensive earth – abundant – heterogeneous catalyst will be in increasing demand.

1.6 Fossil fuels as hydrogen storage materials

Another crucial scientific and technological barrier to the widespread use of hydrogen is that there are no suitable hydrogen storage materials and methods that can be used for commercialisation in the

applications of transportation, portable power and stationary power[18, 19, 27, 133]. This is mainly because the hydrogen has a very low energy density value per unit volume, despite having the highest energy density per mass compared to other substances. To meet the critical requirement for commercialisation, the US department of Energy (U.S DoE) has set the targets of H_2 gravimetric and volumetric densities of 7.5 kg-H_2/ kg and 70 kg-H_2/ m^3, respectively[134, 135]. There are a variety of hydrogen storage methods proposed, where hydrogen can be physically stored as either a gas or liquid, or chemically stored in materials such as metal hydride and liquid organic etc. (Figure 1.7).

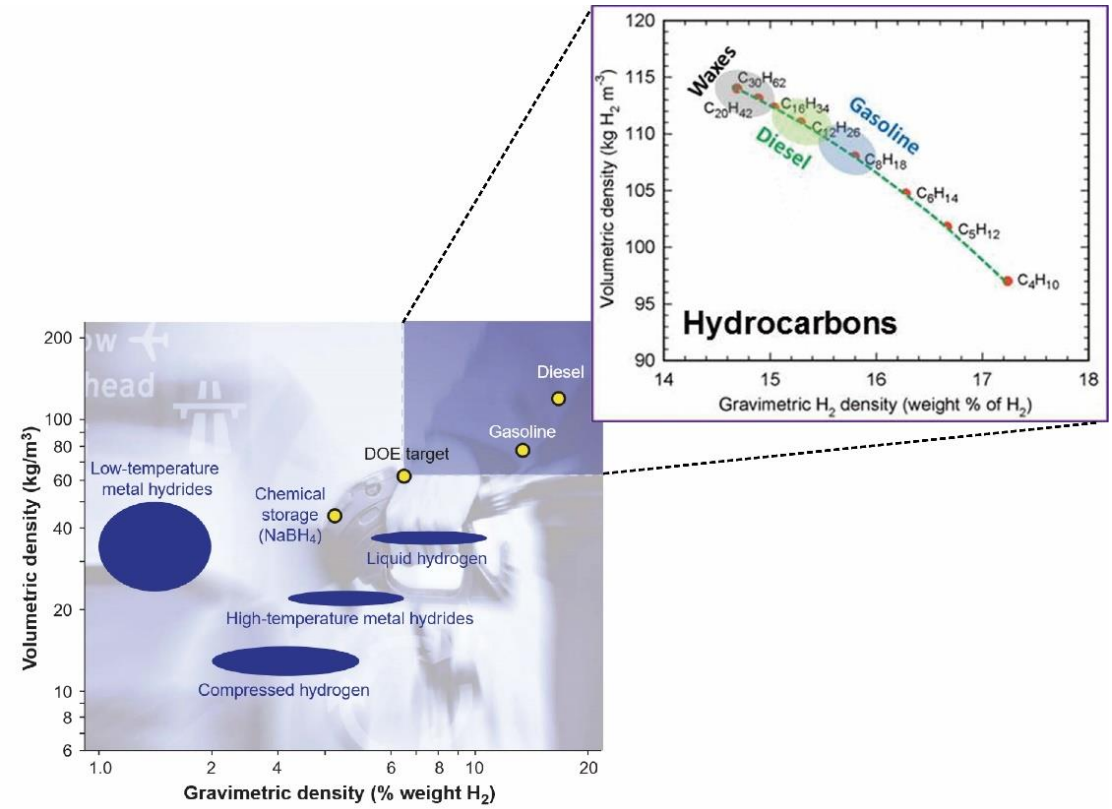


Figure 1.7. Hydrogen storage materials and options with their gravimetric and volumetric density. (Modified from Ref. 136).

Present hydrogen options for fuel cell vehicles involve the use of high-pressure (up to 700 bar) gas containers which a pressure of 70 MPa is required in operating[137]. Unfortunately, compressed hydrogen has a rather low gravimetric and volumetric hydrogen density that will never reach the performance targets required by the DoE. Another physical solution for hydrogen storage is cryogenically cooled liquid hydrogen. Despite the higher gravimetric and volumetric hydrogen density which are obtained

when hydrogen is liquified, the challenges are in its filling and transport requiring temperatures below -252.8 ºC. Hydrogen can be also physically stored on high surface solids (by adsorption) or within solids such as carbon nanotubes, metal-organic frameworks (MOFs) and other nanostructured materials[27, 135, 138, 139].

In terms of chemical solutions, hydrogen can be stored either in hydride storage systems or liquid hydrogen carriers. Generally, metal hydride materials are interstitial compounds formed by hydrogen with metals. Remarkably, there are several classes of metal hydrides (for example, $NaBH_4$) with higher energy densities than liquid hydrogen[19, 134, 140]. However, the danger in their use and the cost and time involved in their hydrogen absorption/desorption are too high, thus more research and development are required[19]. Liquid organic hydrogen carriers such as toluene, methanol and ethanol etc. are another option for storing hydrogen chemically. Similar to other methods of hydrogen storage, it is still in development.

The possibility of using ammonia as a hydrogen carrier merits a mention as such technologies have drawn a great deal of attention due to the high hydrogen density of ammonia. The advantages of using ammonia are that the technologies for production and transportation are well developed and already in widespread use on an industrial scale[141]. Moreover, there is no CO_2 emission at the end user. However, the toxic nature of ammonia and the unfavourable reaction conditions for the several imide and amide systems explored make it disfavoured[141].

It is worth noting that fossil fuels are themselves excellent hydrogen storage materials since they themselves exceed the targets of H_2 gravimetric and volumetric densities set by the U.S DoE[134, 135]. Generally, hydrogen and carbon are the two major compounds that compose fossil fuels. As the result of combustion, hydrogen is transformed to water while carbon is converted to CO_2 through the chemical reactions $2H_2 + O_2 = 2H_2O$ and $C + O_2 = CO_2$ [14]. Thus, instead of burning carbon, extracting only hydrogen gas from fossil fuels to produce high purity hydrogen with recovery of solid carbon product, will provide a new scientific and technological era of '*Fossil fuels decarbonisation*' and the hydrogen economy.

Recently, we have developed a method of rapidly liberating high purity hydrogen from various hydrocarbons as well as naturally occurring fossil fuels with the assistance of microwave technology

using metal catalysts[133, 142]. With the well-established distribution and transportation infrastructure for fossil fuels utilisation, we believe the fossil fuels are potentially ideal hydrogen carriers for fuel cell vehicles and may play a significant role for both the production and storage of hydrogen in the future.

1.7 Hydrogen production involving microwave-initiated catalysis

As briefly mentioned above, my DPhil research focuses on CO_2-free hydrogen production from fossil fuels (hydrocarbons) via microwave-initiated heterogeneous catalysis. In this section, the basic of microwave catalysis as well as the previous work on microwave-initiated hydrogen production will be reviewed.

1.7.1 Introduction to microwave chemistry and application

The microwave radiation comprises electromagnetic waves which have no mass, move at the speed of light and possess significant energy. Microwave radiation falls between radio waves and infrared waves on the frequencies between 30 GHz and 300 MHz, and this corresponds to wavelengths of 1m to 1cm. In general, microwaves are widely used in communications and especially in heating process for food processing. Since the domestic microwave oven was first designed in the 1970s by Japanese scientists, microwave chemistry has been widely investigated in different fields for its applications such as sterilization and pasteurization, different drying processes, rubber vulcanization, polymerization or curing of resins and polymers by elimination of polar solvents, etc. [143-145]. Microwave heating by high-frequency electromagnetic radiation waves could interact with charged particles (catalysts, reactants or solvent) and cause these compounds heat up in the electric field of electromagnetic radiation. This selective heating can subsequently lead to less by-products and/or decomposition products[146].

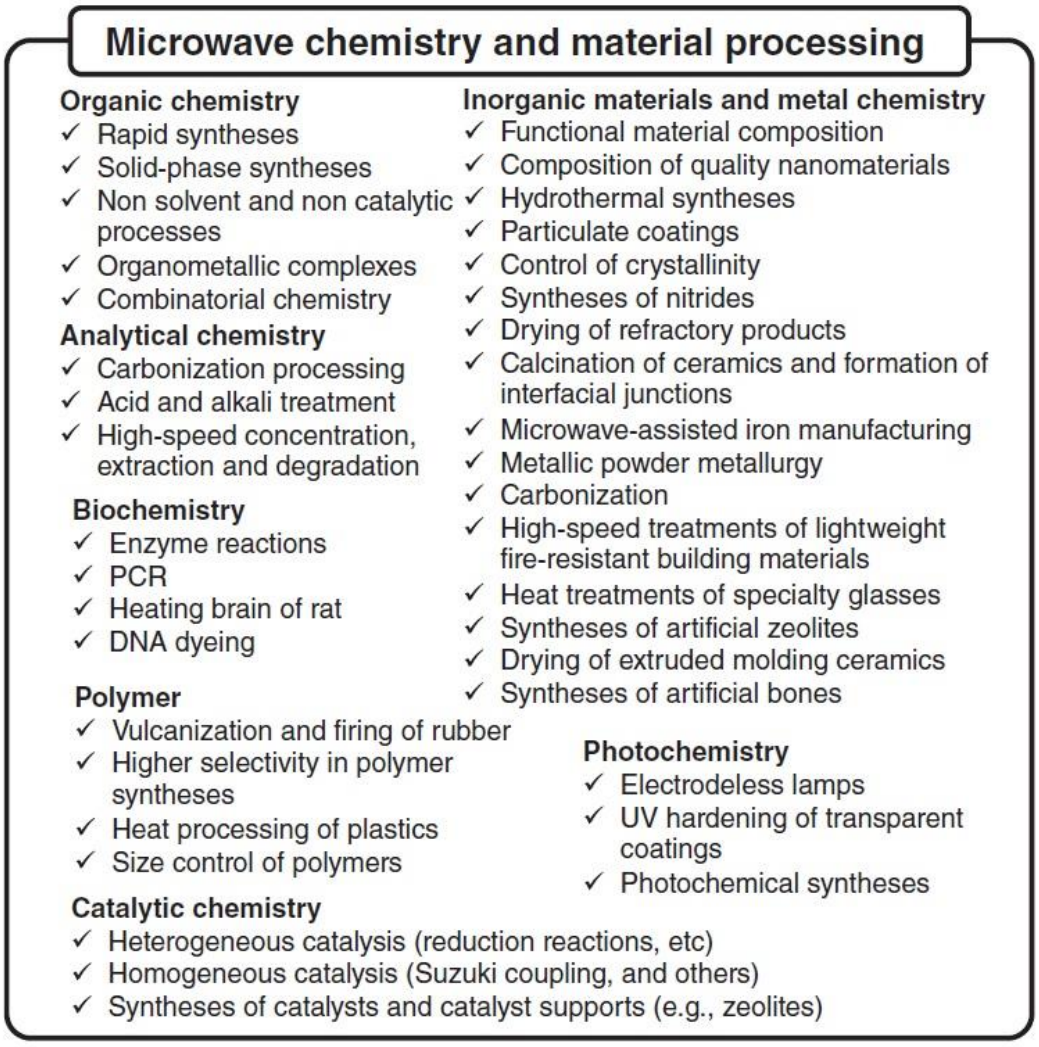


Figure 1.8. Fields of applications with microwave chemistry. (Reproduced from Ref. 147).

One example where microwaves are used in organic synthesis is the Suzuki-Miyaura cross coupling reaction[148, 149], where the reaction times are significantly reduced from days and hours to minutes and seconds when microwave heating is applied. This acceleration effect of microwave rapid heating in organic transformations has also been proven and reported in several other different organic reactions including selective Heck coupling[150] and asymmetric substitutions etc.[151]. The use of microwaves in chemical synthesis is particularly attractive in the field of Green Chemistry in order to meet the increasing demand for environmentally benign chemical processes. Through the extensive research into such applications of microwave organic synthesis, microwave heating has now been able to move from the academic laboratory to the industrial level.

Another important application of microwave is materials synthesis. Specifically, recent studies have reported the calcination and sintering of ceramics, fabricating zeolites, mixed oxide and mesoporous molecular sieves by using microwave heating. The effective sintering of ceramic materials was developed via the fact that ceramics could be self-heated under microwave irradiation. Compared to the conventional sintering where the heat transfers by conduction, convection and radiation, the use of microwave enables the sintering to be carryied out at low temperature for a short time because the sample itself can generate heat under microwave irradiation[152, 153]. The microwave synthesis of zeolites has also been widely investigated and reported over the last decade[154]. It has also been claimed that the microwave synthesis of zeolites could provide relatively small crystals with higher rates of formation. Other synthesis of new materials, such as manganese oxides, nanoporous octahedral molecular sieves, mesoporous molecular sieves, perovskite and other nanoporous materials etc. have also shown that microwave heating can lead to faster preparations[154].

Recently, microwave pyrolysis of lignocellulosic biomass generates great interest in renewable biofuels and green materials[60]. Lignocellulosic biomass, which is derived from plant cell wall components comprised of mainly cellulose (30-50%), hemicelluloses (10-30%), and lignin (10-35%), is the most abundant renewable organic resource on the earth[60]. Microwave pyrolysis of different biomass feedstocks such as corn stover, rice straw, sugarcane bagasse, coffee grounds and bamboo etc. have been widely studied[155]. In general, a mixture of gas (syngas), liquid (bio-oil) and solid (bio-char) can be generated via microwave pyrolysis of biomass. The yields of the different phases of products are highly dependent on operating conditions such as temperature, processing time and microwave power levels. Compared with conventional pyrolysis, microwave pyrolysis is faster, and requires less energy. This is more substantial at lower temperatures because the occurring of a hot spot on the sample itself under microwave irradiation can enhance the energy efficiency of the whole pyrolysis process. However, like conventional pyrolysis of biomass, to upgrade the product quality particular a bio-oil, is a great challenge. Therefore, combining catalysis with microwave pyrolysis may make an important breakthrough for the next generation of bio-fuel production.

When microwave is used in activating/initiating the heterogeneous catalysts for chemical reactions, the fundamental difference of microwave heating and traditional heating should be taken into account.

Unlike traditional heating where a wide spectrum of active centres can be generated on the catalysts' surface, leading to various side reactions, the microwave heating selectively activates charged catalysts, and this is of the great importance to increase the activity and selectivity of catalytic processes. There is thus, a section of the basic principle of microwave as well as the phenomena of microwaves interaction with catalysts as described in the following section.

1.7.2 Fundamental principle of microwave science

The microwave radiation as describe above, is electromagnetic radiation spanning the frequency range from 0.3 – 300 GHz. In general, an operating frequency of 2.45 GHz is used in domestic microwaves corresponding to a wavelength of 12.24 cm and an energy of 1.02×10^{-5} eV. In industrial application, a frequency of 915 MHz is usually used in industrial microwave because it can provide up to 100 kW in larger scale heating applications[147]. It should be noted that only some specific frequencies in the range of microwave can be employed for the industrial, scientific, and medical (ISM) purposes to avoid any electromagnetic interference and disruption to radio communications. And the ISM bands which has been reserved globally are 2.45, 5.8 and 24 GHz, with other frequencies are established by each respective country[147].

Since atoms are made of a positively charged nucleus and negatively charged electrons, polarization phenomena are generated when an electric field is applied. This is also called the electric and atomic polarization and generally occurs at high frequencies, but for many dry solids, this is also the dominant polarization mechanisms at microwave frequencies[156]. Regardless of the polar or nonpolar nature of matter, the polarization always occurs. However, in terms of orientation polarization/alignment polarization, it occurs only when those polar molecules are affected by the oscillating electric field. In a microwave electric field, the electric field (E field) will exercise a torque (T) on the electric field (Figure 1.9), and the dipoles will rotate and re-align themselves with the oscillating electric field thus causing orientation polarization to occur. When the direction of the microwave electric field changes, the torque will also change in direction and result in the rotation and rearrangement of dipoles. However, the fast microwaves vibration (2450000000 times/s for general domestic microwave at the frequency of 2.45 GHz) will cause a time difference between the oscillating microwave electric field and the dipole

of molecules because a molecular cluster cannot follow this microwave vibration. This delay subsequently converts to heat energy (kinetic energy) as loss of the electromagnetic wave energy and the dipole rotation also contributes to the dielectric losses based upon the friction[147].

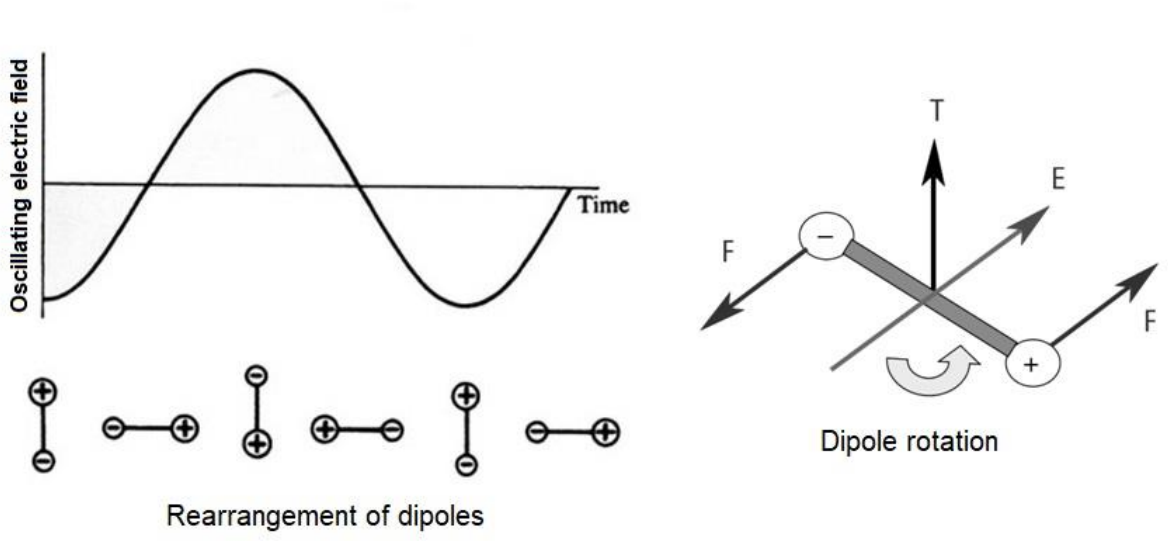


Figure 1.9. The dipole rotation of a polar molecule, showing the fluctuation in the dipole moment in a particular direction. (Modified from Ref. 156 and 157).

In ionic materials (e.g. NaCl), the ionic polarisation is dominant when an electric field is applied. When a field acts, the anion and cation are displaced further in opposite direction and their inter ionic separation increases until bonding force stops the process thus increasing the dipole moment[156]. It should be noted that ionic crystal in general is natural dipoles with exactly zero polarization, and these dipoles cannot rotate because their direction is fixed. The applied microwave electric field induces a net dipole moment, and this causes the heating as a result of electric resistance.

In metals, the conductivity arises from movement of free electrons on the presence of an electric field. The collections of free electrons on the metal's surface cause a high concentration of electric field on the surface whereas 0 electric field is inside of the metal particles. These localised high fields could cause the formation of 'hot spot' which has been always acknowledged in microwave chemistry and linked to the enhanced selectivity and energy efficiency. The produced hotspot on metal particles is also considered as an important factor of the hydrocarbon conversion process selectivity enhancement towards the products of interest (hydrogen) in this thesis.

In essence, a material may have several dielectric mechanisms or polarization effects that contribute to its overall permittivity. The permittivity or dielectric constant of a material, by definition, is a non-dimensional real quantity which is an important measure of the extent to which the electric charge distribution in the material can be distorted or polarized by application of an electric field[156]. The complex dielectric constant or dielectric permittivity (ε*) is given in Eq. 1.14 which consists of a real part ε' and an imaginary part ε". The real part of ε' represents the ability of materials to store electromagnetic energy and the imaginary part of ε'' represents the loss which determines the efficiency of converting electromagnetic energy to heat[147].

$$\varepsilon^* = \varepsilon' + \varepsilon'' \tag{1.14}$$

When complex permittivity is drawn as a simple vector diagram (Figure 1.10), the real and imaginary components are 90° out of phase. The vector sum forms an angle δ with the real axis (ε') [147, 156]. Thus, the loss tangent (tanδ) is given by Eq. 1.15, which is defined as the ratio of the imaginary part of the permittivity to the real part. The loss tangent of a material represents the ratio of the energy lost to the energy stored which importantly determines the ability of the materials to convert electromagnetic energy to heat. A material with high loss tangent enables the efficient conversion of microwave energy to thermal energy. The Q denoting quality factor which is also called as the 'Q-factor', is the reciprocal of the loss tangent.

$$\tan\delta = \frac{\varepsilon''}{\varepsilon'} = \frac{1}{Q} \tag{1.15}$$

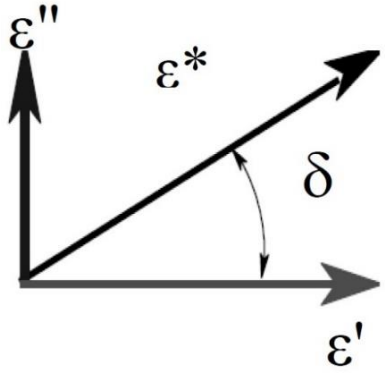


Figure 1.10. Loss tangent vector diagram. (Reproduced from Ref. 156).

Other essential properties need to be considered for any materials when interacting with microwave irradiation are the relaxation time and the penetration depth of microwave. Relaxation time (τ) is a measure of the mobility of the molecules (dipoles) that exist in a material. In the absence of an external electric field, the electrons in substance move in random directions, and these electrons acquire a constant resultant velocity in the opposite direction to the applied electric field when an external electric field is applied. Thus, the relaxation time determines the time required for a displaced system aligned in an electric field to return to $1/e$ of its random equilibrium value when the external electric field is turned off, or the time required for dipoles to approach the final state of orientation polarization in an electric field. Materials that exhibit a single relaxation time constant (τ) can be modelled by the Debye relation (Eq. 1.16) which appears a characteristic response in permittivity as a function of relaxation frequency, where the relaxation frequency (f_c) is inversely related to relaxation time constant (τ) (Eq. 1.17) [156].

$$\varepsilon * (\omega) = \varepsilon_\infty + \frac{\varepsilon_s - \varepsilon_\infty}{1 + i\omega\tau} \tag{1.16}$$

where,

ε_∞ is the permittivity at infinite frequency, or is the optical permittivity

ε_s is the measured permittivity at low frequency, or is the static permittivity

$$\tau = \frac{1}{2\pi f_c} \tag{1.17}$$

At frequencies below the relaxation (f_c), the field variation is slow enough so that the dipoles can keep pace with the oscillating electric field, thus causing polarization to be fully developed. However, when the frequencies lie above the relaxation (f_c), the orientation polarization disappears because the alternating electric field is too fast to enforce the dipole rotation. Take water as an example in Figure 1.11, the dielectric constant (ε ') is above and below the relaxation with the transition occurring near the relaxation frequency (22 GHz). And for the dielectric loss (ε "), it peaks in the transition region at the relaxation frequency[156].

The penetration depth (D_p) is the depth from the surface of material at which microwaves pervade into the material and the power level reduced to $1/e$ (≈ 37%) of its surface value. And the D_p can be estimated as follow (Eq. 1.18) [147, 158],

$$D_p = \frac{\lambda}{2\sqrt{2}\pi}\left[\varepsilon'\left(\sqrt{1+(\varepsilon''/\varepsilon')^2}-1\right)\right]^{-1/2} \quad (1.18)$$

Where, λ is the wavelength of the radiation ($\lambda_{(2.45\ \mathrm{GHz})}$ = 12.24 cm). As the dielectric constant and the dielectric loss are incorporated in this equation, the penetration depth depends on the applied frequency and temperature. For example, the penetration depth of water at 25 °C is about 1.8cm and it changes to 3.1cm and 5.4 cm at the temperature of 50 °C and 90 °C, respectively[147]. However, the penetration depth of water becomes remarkably shallow and negligibly small to the temperature changes when ions are contained. Unlike polar materials, the penetration depth of nonpolar material is very deep and could be fully transparent for the materials such as plastics etc. Therefore, it is necessary to examine the penetration depth of microwaves into a substance to achieve high efficiency.

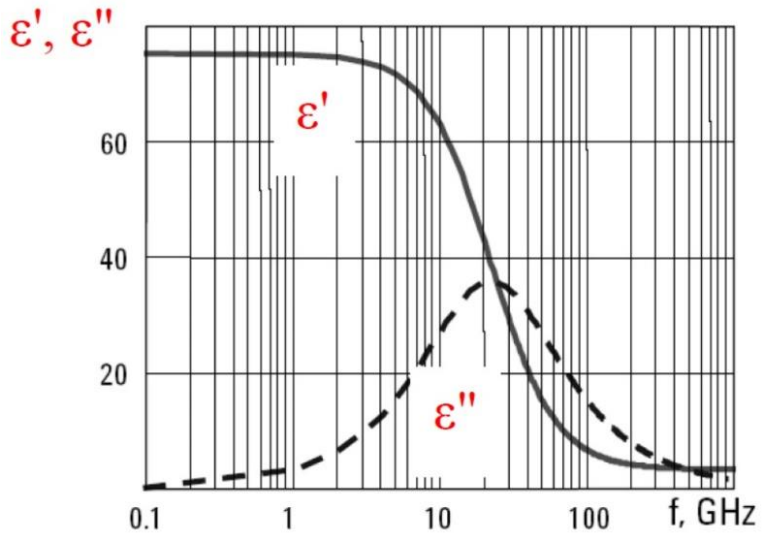


Figure 1.11. Debye relaxation of water at 30°C. (Reproduced from Ref. 156).

For microwave penetration in powders of small conducting particles (such as metals), the "skin depth" (δ) is in general used to describe the distance at which the microwave power decreases to 1/*e* of its power value at the surface. The skin depth is related to the electrical conductivity and the microwave frequency is defined as follow (Eq. 1.19)[158],

$$\delta = \frac{1}{(\upsilon\pi\mu\sigma)^{1/2}} \quad (1.19)$$

where, υ is the microwave frequency and σ is the electrical conductivity. In response of the size dependency on microwave absorption, Porch *et al.*[159] calculated the electromagnetic absorption within

small conducting particles in microwave fields for a range of practical values of particle size and conductivity. As a result, the electromagnetic absorption is predominantly driven by a microwave electric field for particles of low conductivity, and for highly conducting particles, magnetic dipole absorption is dominant regardless of the particle radii, from <10nm to >1mm. As observed in Figure 1.12, there are the regions of dominant electric (E-field) absorption and magnetic (H-field) absorption, with the optimal (size independent) electric absorption, given by $\sigma \approx 3\omega\varepsilon_0$, and the optimal magnetic absorption, given by $a = 2.41\delta$.[159] Also, a region of low electromagnetic absorption shown in blue is given, where sub-micron sized, conducting particles will heat poorly. Therefore, they concluded that for a metal of any given conductivity at a particular frequency, maximum magnetic absorption can be assured by simple selection of the mean particle radius[159].

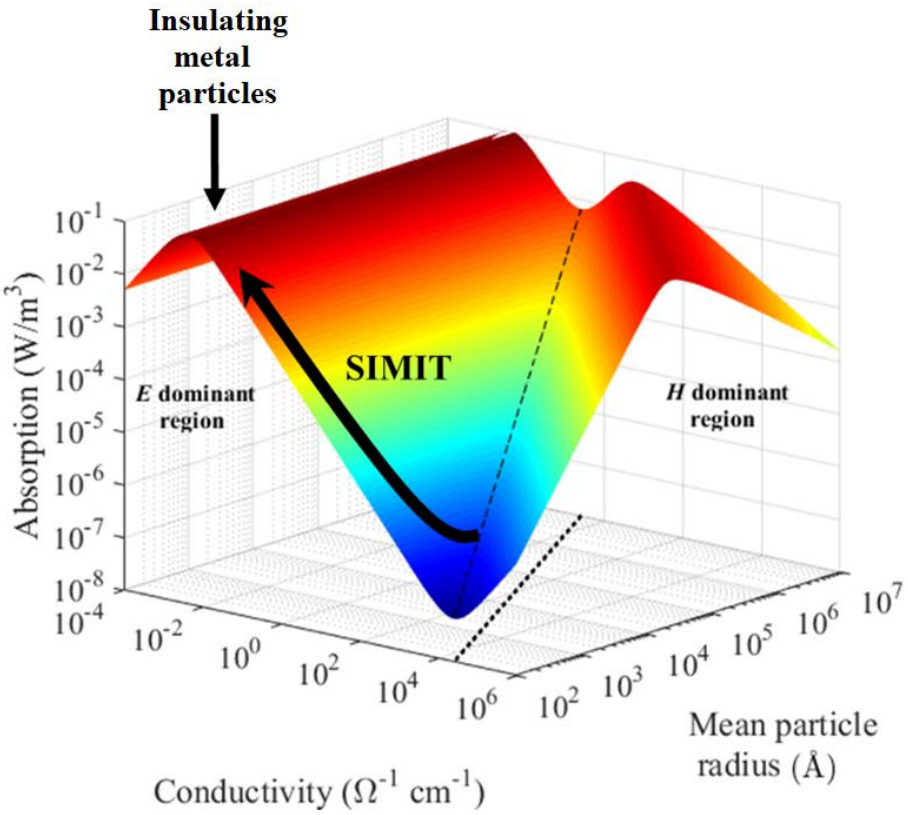


Figure 1.12. Total electromagnetic absorption in non-magnetic particles as a function of conductivity and mean particle radius, for peak applied electric field 1 V m^{-1}, satisfying the relationship $E_0 = \eta_0 H_0$ oscillating at a frequency of 2.45 GHz. Optimal electric absorption and optimal magnetic absorption are marked in red. (Reproduced from Ref. 159).

1.7.3 Microwave Heating Phenomena

There are three types of important heating phenomena caused by microwaves based upon the substances: conduction loss heating, dielectric loss heating and magnetic heating. As such the thermal energy *P* produced per unit volume originating from microwave radiation can be expressed by Eq. 1.20[147]:

$$P = \frac{1}{2}\sigma|E|^2 + \pi f \varepsilon_0 \varepsilon_r''|E|^2 + \pi f \mu_0 \mu_r''|H|^2 \quad (1.20)$$

In this equation, E and H denote the strength of the electric and magnetic fields of the microwaves respectively; σ refers to electrical conductivity; *f* is the frequency of the microwaves; ε_0 refers to the vacuum permittivity and ε'' is the relative dielectric loss factor; μ_0 is the magnetic permeability in a vacuum and μ'' is the relative magnetic loss[147]. There are thus, the three important heating phenomena: the conduction loss (first term), dielectric loss (second term) and magnetic loss (third term) identified in this equation. Therefore, the electrical, dielectric and magnetic properties of materials are rather decisive for microwave heating, hence the change of electric or magnetic fields can affect the materials in response to the microwave irradiation.

Conduction loss heating (the first term in Eq. 1.20), also known as Eddy current loss and Joule loss, occurs when the material contains mobile charge carriers such as electrons and fast ion conductors, and is dipolar characteristics. According to Faraday's laws of induction, the oscillating microwave field gives rise to currents travelling in phase and the energy will dissipate in the form of heat by resistance. It is also worth to note that in solid materials like carbon black powder, conduction losses could be enhanced by defects in materials because these sharply reduce the energy needed to generate electrons and holes in the conduction and valence bands[147]. Such material is thus usually used as additive to solids with poor dielectric losses.

Dielectric loss heating on the other hand, can heat nonconductive materials through the molecular rotation under the alternating microwave electric field. The molecular dipoles intend to re-align themselves with the changes of the electric field, and thereby generating heat as a result of friction between molecules. For polar compounds which possess a permanent dipole moment, microwave

heating is governed mostly by dielectric loss heating because the dipole rotation lags behind the field variation, thus result in the heating of the irradiated material[147].

Unlike Eddy current losses which are induced by domain wall and electron spin resonance, magnetic loss heating occurs in magnetic materials such as transition metal oxides (e.g., iron, nickel, and cobalt oxides) in the microwave region. Compared to non-magnetic materials, microwave heating is dramatically enhanced by magnetic losses within the magnetic materials because they have a lossy part to their complex permeability. For example, the magnetite (Fe_3O_4) can be rapidly heated in a microwaves magnetic field, whereas induction heating cannot occur on hematite (Fe_2O_3) because it is not a magnetic material[147].

It is worth to point out the microwave heating phenomena for small metal particles, where there is a common misconception that metals are heated when exposed to a microwave electric field. As with the simple physical explanation by Porch *et. al.* [159], the highly conducting particles is highly screened when exposed to a microwave electric field. There is therefore, the truth is the metal particles are not itself heated, rather there is a high concentration of electric field outside (on the surface of the metal particles) that can heat surrounding region (if filled with a lossy material), or could form a local plasma that will then drive heat into all of its surroundings via thermal conduction. Therefore, we could predict heating based on the microwave power absorbed by the sample and its heat capacity.

$$P = C \cdot \frac{\Delta T}{\Delta t}$$

where *P* is the microwave power delivered to the sample, *C* is the heat capacity of the material, T is the temperature and t is the time.

1.7.4 Hydrogen Production through Microwave-initiated Catalysis

Microwave heating has a number of advantages over conventional heating including non-contact and selective heating, rapid heating and quick start-up and shutdown etc. In addition, microwave can heat the interior of the catalysts bodies without heating the surrounding substances, and the energy can be transported from the source through a transparent quartz or a hollow, non-magnetic metal tube[160]. However, microwave heating effects on solid state compounds are complex and still not fully

understood. There are thus, only few prior works[72-74, 161, 162] have reported using microwave for hydrogen production. And among the different hydrocarbons which have been used as feedstocks, methane is mostly investigated, because it is the simplest hydrocarbon with the highest H/C ratio.

In recent years, the so-called microwave plasma has also been investigated since a very high reaction temperature can be achieved by plasma technology. By means, microwave plasma is generated using a microwave frequency which has been reported for diamond vapor deposition and IC manufacturing etc. The advantages of microwave plasma are easy operation, an electrodeless reactor, high plasma density and high electron mean energy[160]. Accordingly, the microwave plasma at atmospheric pressure can provide the electron temperature of 4000 – 10000 K, and the heavy particle temperature of 2000-6000 K[163]. Jasinski *et al.* reported that microwave plasma is attractive for hydrogen production by methane decomposition because of the facts of high hydrogen production rate, low cost and effective[164]. However, the thermal plasma-assisted methane decomposition process requires intensive electric energy consumption which has been reported operating at temperatures in excess of 5000 °C. In comparison, the catalytic methane decomposition can be accomplished at temperatures comparable to that of the conventional SMR process, i.e., 850–900 °C, a temperature range about 400–500 °C lower than that for non-catalytic methane decomposition. Muradov *et al.* showed that non-thermal plasma-assisted methane decomposition can be achieved over catalytically active carbon aerosol particles at near-ambient conditions[165].

Therefore, it appears to be of great importance to choose the catalyst for microwave-initiated catalytic hydrogen production process as it must meet some specific requirements in addition to the common demands of high activity, selectivity and stability. Such a catalyst must be a good microwave absorber/receptor and able to retain its structure and properties under intense microwave irradiation[160, 166]. In general, metal- and carbon-based catalysts have been developed for microwave-initiated CO_2-free hydrogen production from hydrocarbons decomposition (mostly methane decomposition). The main problem of using metal-based catalysts is due to the carbon deposition that causes the deactivation of the catalysts by the blockage of catalytic active sites. The use of carbon-based catalysts offers certain advantages over metal catalysts due to their high durability and low cost[165]. Most importantly, the

carbon materials are the excellent microwave absorber/accepter which can efficiently convert the electromagnetic energy to heat.

Domínguez *et al.* reported microwave-initiated decomposition of methane on activated carbon and illustrated a higher selectivity to H_2 with higher conversions compared to electric heating (conventional heating)[73] (Figure 1.13). This is considered due to the formation of hot spots inside the catalyst bed which favours CH_4 decomposition. Through the reactions of hydrocarbons dehydrogenation, carbon-forming processes involve chemisorption of different kinds of carbons or condensed hydrocarbons some of which may be active towards the catalytic reactions and others may act as catalyst poisons. Later study by Menéndez *et al.* have reviewed the microwave heating processes involving carbon materials[167]. In general, carbon materials are used as microwave acceptors/receptors to heat other materials indirectly, or directly act as a catalyst in different heterogeneous reactions due to their excellent ability to absorb microwaves. There is thus, a variety of carbon materials, such as activated carbons, metallurgical cokes, chars or anthracite, used for several microwave-enhanced heterogeneous catalytic reactions, in which carbons acted as catalyst and microwave receptor[167].

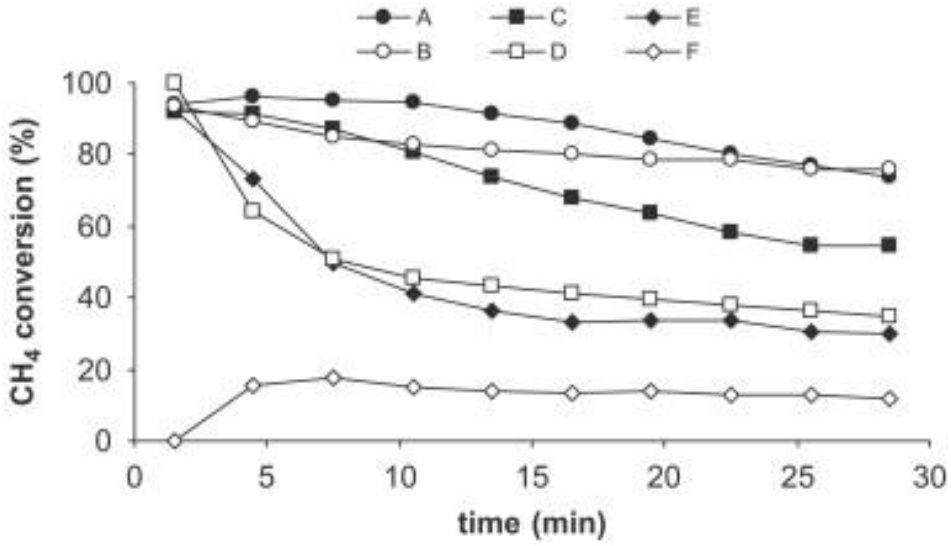


Figure 1.13. Effect of the reaction temperature on methane conversion, under microwave heating (solid symbol) or conventional heating (empty symbol). Runs A and B: 900 °C; runs C and D: 800 °C; and runs E and F: 700 °C. VHSV=0.160L/g h. (Reproduced from Ref. 73).

Unlike methane decomposition, few works have been done on heavy hydrocarbons for hydrogen production via microwave-initiated catalytic processes[72, 133, 162]. Tanner *et al.* reported the microwave-

initiated catalytic reactions of a variety of liquid hydrocarbons (straight chain, branched, aromatic, and functionalized) using millimetre-sized chars. Accordingly, a vigorous emission of sparks was generated over chars under microwave irradiation and result in molecular hydrogen, gaseous hydrocarbons (CH_4, C_2H_2, C_2H_4, C_2H_6, C_3H_6, C_4H_8, C_4H_6), and a range of liquid olefins have been observed as products[72, 168]. Especially for hexadecane pyrolysis, the researchers presented that microwave heating gave mainly hydrogen, ethylene and α-olefins in the liquid products, in which the content of α-olefins was more than an order of magnitude greater than the content of other products (mostly alkanes). They attributed the high α-olefins selectivity to the spark discharge arising on the carbon surface upon microwave irradiation, which caused C – C or C – H bond cleavage to form alkyl radicals and hydrogen atoms in a short reaction time[72]. However, Udalov *et al.* argued that the exclusive selectivity of hexadecane pyrolysis to hydrogen, ethylene and α-olefins might also be a consequence of the catalytic action of a variety of naturally occurring metals contained in the carbons because the metallic catalyst under microwave irradiation have been proposed to involve hot spots which promote the thermal reactions of methane, leading to the formation of gas-phase methyl radicals and hydrogen atoms[162]. There is thus, an expanding range of catalysts including Fe_2O_3 magnetic microspheres (coal combustion ash, 92.5% mass % Fe_2O_3 with major impurities: 4.9% CaO, 1.3% MgO, 1.3% SiO_2), glass fibre supported palladium catalysts, metal-ceramic Al_2O_3/Al catalysts, ZSM-12 zeolite catalysts, and 70% ZSM-5/Al_2O_3 (0.2-1.0 mm fraction) were investigated for microwave-initiated hexadecane pyrolysis. As a result, methane, ethylene, and propylene were found predominated in the gaseous reaction products, and similarly α-olefins were mostly observed in the liquid products of hexadecane pyrolysis on magnetic microspheres and metal-ceramics contain[162]. These again indicate the great importance to choose the catalyst for microwave-initiated catalysis in different heterogeneous catalysis.

Prior work in the group by Gonzalez-Cortes *et al.*[133] have proposed using the long chain alkanes - paraffin wax (> C_{20} alkanes), as a benign hydrogen storage material with a demonstration of rapid liberating hydrogen from paraffin wax by microwave-initiated catalytic process. An activated carbon supported ruthenium (Ru/AC) catalyst was prepared and used for hydrogen production by paraffin wax ($C_{26}H_{54}$) decomposition. And a hydrogen concentration of 60 – 80 mol.% was obtained in the exit gas stream over Ru/AC catalysts (Figure 1.14). In contrast, only about 40 mol.% of hydrogen was produced

for microwave irradiation in only activated carbon (in the absence of ruthenium metal catalyst) (Figure 1.15). This is presumably as a consequence of the large availability of surfaces of activated ruthenium metal nanoparticles[133].

In comparison of microwave heating and conventional heating, it was found that the average temperature for the system under dielectric heating (ca. 723 K) was significantly lower than that used in the thermal-treated sample (823 K). Despite of the temperature differences, compared to conventional heating, the gas composition of the 50 wt. % paraffin wax @ 5 wt. % Ru/AC under dielectric heating showed a slightly increase of the hydrogen production while the methane concentration was reduced (Figure 1.15). This finding highlights the remarkable effect of the selective heating of the microwave irradiation and hence the dual effect of the hot and cold spots over the overall gas distribution.

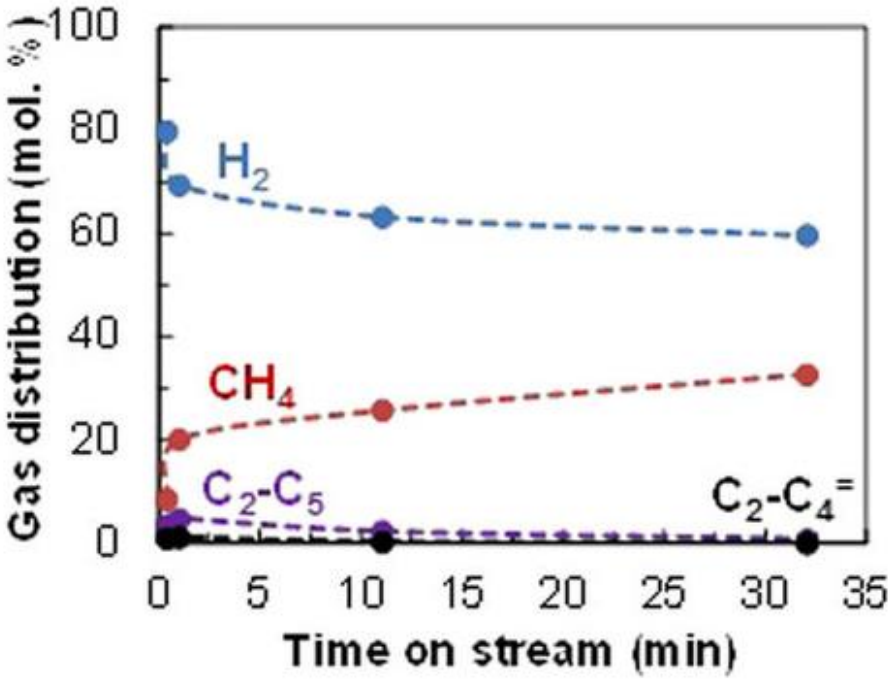


Figure 1.14. Product distribution of paraffin wax ($C_{26}H_{54}$) decomposition over 5 wt.% Ru/AC catalyst for absorbed power between 80 and 60W. (Adapted from Ref. 133).

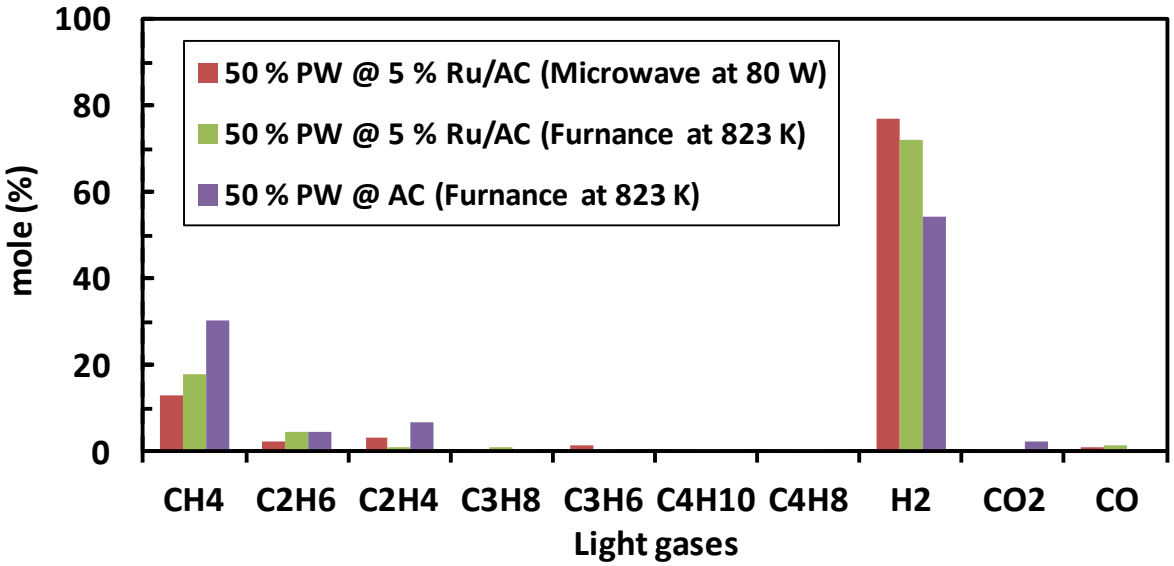


Figure 1.15. Comparisons of microwave and thermal treatment on the resulting evolved gas mixture composition. (Adapted from Ref. 133).

Besides the linear alkanes, the aromatic hydrocarbons can be also used for hydrogen production through microwave heating and these features have been proposed as possible carriers of hydrogen[147]. Horikoshi and co-workers have reported the dehydrogenation of decalin and tetralin in gas-phase on Pt and activated carbon supported Pt catalysts[74, 169]. As a result, the tetralin conversion was significantly enhanced from 31% in conventional thermal heating to 56% under microwave conditions. The enhancement was explained by the heating ability of Pt/carbon particles causing a large-temperature gradient between the catalyst and the tetralin solution under microwave conditions. However, the naphthalene produced from tetralin and decalin dehydrogenation, has a melting point of 80 °C and are easily to solidify, thereby clogging the reactor or the pipes[147]. Therefore, the methylcyclohexane to toluene cycle was proposed by the same researchers, where the dehydrogenation of the organic hydride MCH (methylcyclohexane) was carried out in a continues flow over an activated carbon supported palladium (Pd/AC) catalyst with the assistance of microwave[170]. The advantages of microwave over conventional heating are observed in both MCH conversion (94%) and a considerable energy saving (ca. 75%) as the microwave heating led to hydrogen evolution in much shorter times.

In a brief summary, pioneering researches have shown the possibility using microwave for hydrogen production from a variety of hydrogen containing feedstocks. And several demonstration works have

been done in comparison of microwave and conventional heating process. Although the advantages of microwave versus conventional heating are listed, there are still many challenges across the fundamental differences and the future applications for microwave, especially when it is combined with heterogeneous catalysis. In the study of microwave-initiated catalytic hydrogen production, it is still in its very early stage and more efforts are needed in both scientific and engineering aspects to achieve the real breakthrough on microwave towards high-purity hydrogen production.

1.8 Thesis objective and research summary

Hydrogen as an energy carrier promises a sustainable energy revolution. However, one of the greatest challenges for any future hydrogen economy is the necessity for large scale hydrogen production *not involving concurrent CO_2 production*. The intrinsically high hydrogen content of liquid-range alkane hydrocarbons offers a potential route to CO_2-free hydrogen production through their catalytic deep dehydrogenation. Pioneering work by Steinberg[67, 68] and Muradov[59, 69] has led to CO_2-free hydrogen production from hydrocarbons, predominantly methane, via thermal pyrolysis. Hydrogen production through this route has then been studied through the use of microwaves[72, 73, 133, 171], plasma's[75, 76] and molten metals [58, 77]. My DPhil research work centres on a method of rapidly liberating high-purity hydrogen from hydrocarbons without CO_2 emission. There is thus, an innovative system combining microwave technology and heterogeneous catalysis proposed. As a result, a H_2 production selectivity from all evolved gases of some 98%, is achieved with less than a fraction of a percent of adventitious CO and CO_2 through the *microwave-initiated catalytic dehydrogenation* of liquid alkanes using Fe and Ni particles supported on silicon carbide.

The first part of my doctoral research explores the suitable catalyst systems for the proposed process. The challenge for this new developed catalytic system is to examine the catalyst materials interaction with microwave irradiation. Therefore, I conducted a series of catalyst preparation, characterization and evaluation for the CO_2-free hydrogen production from prototype hydrocarbons through microwave-initiated dehydrogenation. Consequently, I was able to develop the most effective catalysts system for rapid high-purity hydrogen fuel production from hydrocarbons under microwave irradiation.

A second strand of this work deals with a variety of actual, real petroleum products, ranging from heavy crude oil, crude oil through diesel, petrol to natural gas (methane). The enthusiasm and excitement at this part of work is that I demonstrated that real hydrocarbon fossil fuels (even crude oil) can be the vehicle for high-purity hydrogen production, so that we did not spell out solely for a single, model hydrocarbon; but from a variety of actual carbonaceous and petroleum products. Therefore, the undoubted attractive attributes of fossil fuels - relatively inexpensive, widely available and readily adaptable to applications large and small, simple and complex, - can significantly assist in the staged transition to a hydrogen-based, sustainable hydrogen energy economy. Based on these works, one patent has been filed and three papers[142, 172, 173] are published.

In addition, to get a better understanding of this new developed technique system and make it more efficient in order to provide the economic impetus for its uptake, the expanding work has been carried out continually and will last in my future research. Apart from the demonstration on the rapid and effective process of microwave-initiated fossil hydrocarbons dehydrogenation for high-purity hydrogen production, I have also showed that a very large positive net energy balance can, in principle, be obtained in microwave conditions, given high selectivity in this dehydrogenation process. Moreover, I have demonstrated that the microwave –initiated process is more energy efficient than conventional thermal catalytic processes in a small-scale experimental laboratory configuration.

Another important study on by-product of solid carbon has also been carried out in my doctoral work which has partially done but not yet optimised. I have tested and characterised the resulting carbon residues for their morphologies and physical properties etc. In addition to the overall process of hydrogen production from fossil fuels dehydrogenation, several potential applications and recycle routes for the residual pure by-products, elemental solid carbon, are proposed.

Therefore, in my DPhil study and research, I believe that a new scientific and technological era of "*Fossil fuel decarbonisation*'' can arise where we will not destroy naturally-occurring fossil fuels by combustion – fire - conflagration[174] – with the attendant CO_2 emissions, but rather utilise them to produce clean hydrogen. Carbonaceous fossil fuels are thereby transformed from carbon - rich to hydrogen-rich fuels for future energy.

Bibliography:

1. P. P. Edwards, *Oxford Magzine*, 2017, EIGHTH WEEK, HILARY TERM, 11.
2. D. Helm, *Oxford Review of Economic Policy*, 2016, 32, 191-205.
3. M. K. Hubbert, *Science*, 1949, 109, 103-109.
4. M. Spence, *Fossil fuels*, Gloucester Press, London, 1993.
5. World Coal Association, Coal & Electricity, available at https://www.worldcoal.org/coal/uses-coal/coal-electricity.
6. World Energy Council, *World Energy Resources 2016*, 2016.
7. L. R. Radovic, *Energy and fuels in society*, Primis, 1998.
8. L. R. Radovic and H. H. Schobert, *Energy and fuels in society*, McGraw-Hill, 1992.
9. World Energy Council, *Natural Gas*, 2016.
10. BP, *BP Energy Outlook 2017*, 2017.
11. R. L. Hirsch, R. M. Bezdek and R. M. Wendling, *Peaking of world oil production: impacts, mitigation, & risk management*, National Energy Technology Laboratory (NETL), Pittsburgh, PA, Morgantown, WV, and Albany, OR, 2005.
12. R. G. Miller and S. R. Sorrell, *Philosophical Transactions of the Royal Society A: Mathematical, Physical and Engineering Sciences*, 2014, 372.
13. K. S. Deffeyes and M. P. Silverman, *Hubbert's peak: the impending world oil shortage*, 2004, 126-127.
14. S. Sorrell, J. Speirs, R. Bentley, R. Miller and E. Thompson, *Energy*, 2012, 37, 709-724.
15. International Energy Agency (IEA), *Global Energy & CO_2 Status Report*, 2017.
16. International Energy Agency (IEA), *CO_2 emission from fuel combustion*, 2017.
17. J. O. Bockris, *Science*, 1972, 176, 1323.
18. G. W. Crabtree, M. S. Dresselhaus and M. V. Buchanan, *Physics Today*, 2004, 57, 39-44.
19. P. P. Edwards, V. L. Kuznetsov, W. I. F. David and N. P. Brandon, *Energy Policy*, 2008, 36, 4356-4362.

20. S. A. Wells, A. Sartbaeva, V. L. Kuznetsov and P. P. Edwards, *Encyclopedia of Inorganic and Bioinorganic Chemistry*, 2010, 309-332.

21. R. H. Crabtree, *Energy & Environmental Science*, 2008, 1, 134-138

22. J. A. Turner, *Science*, 2004, 305, 972-974.

23. U. Eberle, B. Müller and R. Von Helmolt, *Energy & Environmental Science*, 2012, 5, 8780-8798.

24. K. Hirose, *Philosophical Transactions of the Royal Society of London A: Mathematical, Physical and Engineering Sciences*, 2010, 368, 3365-3377.

25. L. Barreto, A. Makihira and K. Riahi, *International Journal of Hydrogen Energy*, 2003, 28, 267-284.

26. J. Barber, *Sustainable Energy & Fuels*, 2018, 927-935.

27. L. Schlapbach and A. Zuettel, *Nature* , 2001, 414, 353-358.

28. M. L. Wald, *Scientific American.*, 2004, 290, 66-73.

29. I. Dincer and C. Acar, *International Journal of hydrogen energy*, 2015, 40, 11094-11111.

30. S. Dutta, *Journal of Industrial and Engineering Chemistry*, 2014, 20, 1148-1156.

31. K. Christopher and R. Dimitrios, *Energy & Environmental Science*, 2012, 5, 6640-6651.

32. R. M. Navarro, M. A. Pena and J. L. G. Fierro, *Chemical Review*, 2007, 107, 3952-3991.

33. J. D. Holladay, J. Hu, D. L. King and Y. Wang, *Catalysis Today*, 2009, 139, 244-260.

34. X. Jie, P. P. Edwards and J. M. Thomas, unpublished work.

35. R. D. Cortright, R. Davda and J. A. Dumesic, *Nature*, 2002, 418, 964-967.

36. S. Ahmed, A. Aitani, F. Rahman, A. Al-Dawood and F. Al-Muhaish, *Applied Catalysis A: General*, 2009, 359, 1-24.

37. H. B. Gray, *Nature Chemistry*, 2009, 1, 7-7.

38. D. G. Nocera, *Accounts of Chemical Research*, 2012, 45, 767-776.

39. S. Bensaid, G. Centi, E. Garrone, S. Perathoner and G. Saracco, *ChemSusChem*, 2012, 5, 500-521.

40. C. Genovese, C. Ampelli, S. Perathoner and G. Centi, *Journal of Catalysis*, 2013, 308, 237-249.

41. J. M. Thomas, *ChemSusChem*, 2014, 7, 1801-1832.

42. N. S. Lewis, *MRS Bull*, 2007, 32, 808-820.

43. Cal State HRS, *Cal State LA Hydrogen Research and Fueling Facility*, 2014.

44. T. Hisatomi, J. Kubota and K. Domen, *Chemical Society Reviews*, 2014, 43, 7520-7535.

45. K. Sayama, R. Yoshida, H. Kusama, K. Okabe, Y. Abe and H. Arakawa, *Chemical Physics Letters*, 1997, 277, 387-391.

46. C. Song, *Catalysis Today*, 2002, 77, 17-49.

47. R. Farrauto, S. Hwang, L. Shore, W. Ruettinger, J. Lampert, T. Giroux, Y. Liu and O. Ilinich, *Annual Review of Materials Research*, 2003, 33, 1-27.

48. K. Hohn and L. Schmidt, *Applied Catalysis A: General*, 2001, 211, 53-68.

49. J. J. Krummenacher, K. N. West and L. D. Schmidt, *Journal of Catalysis.*, 2003, 215, 332-343.

50. L. Pino, V. Recupero, S. Beninati, A. K. Shukla, M. S. Hegde and P. Bera, *Applied Catalysis A: General*, 2002, 225, 63-75.

51. D. L. Trimm and Z. I. Önsan, *Catalysis Reviews*, 2001, 43, 31-84.

52. I. Dybkjær, *Fuel Processing Technology*, 1995, 42, 85-107.

53. T. Christensen and I. Primdahl, *Hydrocarbon Processing*, 1994, 73.

54. K. Takehira, T. Shishido, P. Wang, T. Kosaka and K. Takaki, *Journal of Catalysis*, 2004, 221, 43-54.

55. S. Ayabe, H. Omoto, T. Utaka, R. Kikuchi, K. Sasaki, Y. Teraoka and K. Eguchi, *Applied Catalysis A: General*, 2003, 241, 261-269.

56. R. Bellows, *Technical challenges for hydrocarbon fuel reforming, Conference Proceedings*, 1999, 6-8.

57. F. Joensen and J. R. Rostrup-Nielsen, *Journal of Power Sources*, 2002, 105, 195-201.

58. T. Geißler, A. Abánades, A. Heinzel, K. Mehravaran, G. Müller, R. K. Rathnam, C. Rubbia, D. Salmieri, L. Stoppel, S. Stückrad, A. Weisenburger, H. Wenninger and T. Wetzel, *Chemical Engineering Journal*, 2016, 299, 192-200.

59. N. Z. Muradov, *Energy Fuels*, 1998, 12, 41-48.

60. T. Kan, V. Strezov and T. J. Evans, *Renewable and Sustainable Energy Reviews*, 2016, 57, 1126-1140.

61. A. Tanksale, J. N. Beltramini and G. M. Lu, *Renewable and Sustainable Energy Reviews*, 2010, 14, 166-182.

62. N. Z. Muradov, *Journal of Power Sources*, 2003, 118, 320-324.

63. N. Z. Muradov and T. N. Veziroğlu, *International Journal of Hydrogen Energy*, 2005, 30, 225-237.

64. J. Jenkins and E. Shutt, *Platinum Metals Review*, 1989, 33, 118-127.

65. N. Edwards, S. R. Ellis, J. C. Frost, S. E. Golunski, A. N. J. van Keulen, N. G. Lindewald and J. G. Reinkingh, *Journal of Power Sources*, 1998, 71, 123-128.

66. S. Golunski, *Platinum Metals Review*, 1998, 42, 2-7.

67. M. Steinberg and H. C. Cheng, *International Journal of Hydrogen Energy*, 1989, 14, 797-820.

68. M. Steinberg, *International Journal of Hydrogen Energy*, 1999, 24, 771-777.

69. N. Z. Muradov, *International Journal of Hydrogen Energy*, 1993, 18, 211-215.

70. N. Z. Muradov, *Proceedings 2001 U.S. DOE Hydrogen Program Review*, 2001, 271-296.

71. N. Z. Muradov, *International Journal of Hydrogen Energy*, 2017, 42(20), 14058-14088.

72. D. D. Tanner, P. Kandanarachchi, Q. Ding, H. Shao, D. Vizitiu and J. A. Franz, *Energy & fuels*, 2001, 15, 197-204.

73. A. Domínguez, B. Fidalgo, Y. Fernández, J. Pis and J. Menéndez, *International Journal of Hydrogen Energy*, 2007, 32, 4792-4799.

74. Y. Suttisawat, S. Horikoshi, H. Sakai and M. Abe, *International Journal of Hydrogen Energy*, 2010, 35, 6179-6183.

75. O. Mutaf-yardimci, A. V. Saveliev, A. A. Fridman and L. A. Kennedy, *International Journal of Hydrogen Energy*, 1998, 23, 1109-1111.

76. H. L. Chen, H. M. Lee, S. H. Chen, Y. Chao and M. B. Chang, *Applied Catalysis B: Environmental*, 2008, 85, 1-9.

77. D. C. Upham, V. Agarwal, A. Khechfe, Z. R. Snodgrass, M. J. Gordon, H. Metiu and E. W. McFarland, *Science*, 2017, 358, 917-921.

78. N. Z. Muradov and T. N. Veziroğlu, *International Journal of Hydrogen Energy*, 2008, 33, 6804-6839.

79. N. Z. Muradov, *Energy & Fuels*, 1998, 12, 41-48.

80. T. V. Choudhary, C. Sivadinarayana, C. C. Chusuei, A. Klinghoffer and D. W. Goodman, *Journal of Catalysis*, 2001, 199, 9-18.

81. B. Gaudernack and S. Lynum, *International Journal of Hydrogen Energy*, 1998, 23, 1087-1093.

82. N. Z. Muradov, Z. Chen and F. Smith, *International Journal of Hydrogen Energy*, 2005, 30, 1149-1158.

83. E. K. Lee, S. Y. Lee, G. Y. Han, B. K. Lee, T.-J. Lee, J. H. Jun and K. J. Yoon, *Carbon*, 2004, 42, 2641-2648.

84. J. W. Halloran, *International Journal of Hydrogen Energy*, 2008, 33, 2218-2224.

85. N. Z. Muradov, F. Smith, C. Huang and T. Ali, *Catalysis today*, 2006, 116, 281-288.

86. O. Bautista, F. Méndez and C. Trevino, *International Journal of Hydrogen Energy*, 2008, 33, 7419-7426.

87. J. Ashok, M. Subrahmanyam and A. Venugopal, *Catalysis Surveys from Asia*, 2008, 12, 229.

88. Y. Li, B. Zhang, X. Xie, J. Liu, Y. Xu and W. Shen, *Journal of Catalysis*, 2006, 238, 412-424.

89. U. Ashik, W. W. Daud and H. F. Abbas, *Renewable and Sustainable Energy Reviews*, 2015, 44, 221-256.

90. A. E. Awadallah, A. A. Aboul-Enein and A. K. Aboul-Gheit, *Energy Conversion and Management*, 2014, 77, 143-151.

91. D. Torres, J. Pinilla, M. Lázaro, R. Moliner and I. Suelves, *International Journal of Hydrogen Energy*, 2014, 39, 3698-3709.

92. S. Abanades, H. Kimura and H. Otsuka, *Fuel Processing Technology*, 2014, 122, 153-162.

93. Y. Nishida, C.-Z. Cheng and K. Iwasaki, *IEEE Transactions on Plasma Science*, 2014, 42, 3674-3680.

94. L. Bromberg, D. R. Cohn, A. Rabinovich, N. Alexeev, A. Samokhin, R. Ramprasad and S. Tamhankar, *International Journal of Hydrogen Energy*, 2000, 25, 1157-1161.

95. M. S. Benilov and G. V. Naidis, *International Journal of Hydrogen Energy*, 2006, 31, 769-774.

96. L. Bromberg, D. Cohn, A. Rabinovich and N. Alexeev, *International Journal of Hydrogen Energy*, 1999, 24, 1131-1137.

97. O. Khalifeh, A. Mosallanejad, H. Taghvaei, M. R. Rahimpour and A. Shariati, *Applied Energy*, 2016, 169, 585-596.

98. M. A. Malik, D. Hughes, A. Malik, S. Xiao and K. H. Schoenbach, *Plasma Chemistry and Plasma Processing*, 2013, 33, 271-279.

99. S. Y. Chin, Y.-H. Chin and M. D. Amiridis, *Applied Catalysis A: General*, 2006, 300, 8-13.

100. K. Otsuka, Y. Shigeta and S. Takenaka, *International Journal of Hydrogen Energy*, 2002, 27, 11-18.

101. Y. Wang, N. Shah and G. P. Huffman, *Catalysis Today*, 2005, 99, 359-364.

102. K. Otsuka, Y. Abe, N. Kanai, Y. Kobayashi, S. Takenaka and E. Tanabe, *Carbon*, 2004, 42, 727-736.

103. Y. Wang, N. Shah and G. P. Huffman, *Energy & Fuels*, 2004, 18, 1429-1433.

104. T. Paulmier and L. Fulcheri, *Chemical Engineering Journal*, 2005, 106, 59-71.

105. M. G. Sobacchi, A. V. Saveliev, A. A. Fridman, L. A. Kennedy, S. Ahmed and T. Krause, *International Journal of Hydrogen Energy*, 2002, 27, 635-642.

106. S. Takenaka, Y. Kobayashi and K. Otsuka, *Energy & Fuels*, 2004, 18, 1775-1783.

107. S. Takenaka, K. Kawashima, H. Matsune and M. Kishida, *Applied Catalysis A: General*, 2007, 321, 165-174.

108. Y. Wang, Y.-H. Chin, R. T. Rozmiarek, B. R. Johnson, Y. Gao, J. Watson, A. Tonkovich and D. P. Vander Wiel, *Catalysis Today*, 2004, 98, 575-581.

109. D. L. Trimm, *Catalysis Today*, 1999, 49, 3-10.

110. T. Borowiecki, G. Giecko and M. Panczyk, *Applied Catalysis A: General*, 2002, 230, 85-97.

111. L. Wang, K. Murata, Y. Matsumura and M. Inaba, *Energy & Fuels*, 2006, 20, 1377-1381.

112. M. C. J. Bradford and M. A. Vannice, *Applied Catalysis A: General*, 1996, 142, 97-122.

113. J. A. Dias and J. M. Assaf, *Journal of Power Sources*, 2004, 130, 106-110.

114. J. Patt, D. J. Moon, C. Phillips and L. Thompson, *Catalysis Letters*, 2000, 65, 193-195.

115. Q. Fu, H. Saltsburg and M. Flytzani-Stephanopoulos, *Science*, 2003, 301, 935-938.

116. T. Bunluesin, R. Gorte and G. Graham, *Applied Catalysis B: Environmental*, 1998, 15, 107-114.

117. W. Ruettinger, O. Ilinich and R. J. Farrauto, *Journal of Power Sources*, 2003, 118, 61-65.

118. H. Iida, K. Tahara, H. Higashi and A. Igarashi, *Advances in Technlogy of Materials and Materials Processing Journal*, 2002, 4, 62-65.

119. G. C. Bond, *Catalysis Today*, 2002, 72, 5-9.

120. D. Andreeva, V. Idakiev, T. Tabakova, L. Ilieva, P. Falaras, A. Bourlinos and A. Travlos, *Catalysis Today*, 2002, 72, 51-57.

121. F. Boccuzzi, A. Chiorino, M. Manzoli, D. Andreeva, T. Tabakova, L. Ilieva and V. Iadakiev, *Catalysis Today*, 2002, 75, 169-175.

122. D. Andreeva, T. Tabakova, V. Idakiev, P. Christov and R. Giovanoli, *Applied Catalysis A: General*, 1998, 169, 9-14.

123. L. Zhou, L. R. Enakonda, M. Harb, Y. Saih, A. Aguilar-Tapia, S. Ould-Chikh, J.-l. Hazemann, J. Li, N. Wei and D. Gary, *Applied Catalysis B: Environmental*, 2017, 208, 44-59.

124. L. Zhou, L. R. Enakonda, Y. Saih, S. Loptain, D. Gary, P. Del-Gallo and J. M. Basset, *ChemSusChem*, 2016, 9, 1243-1248.

125. M. Pudukudy and Z. Yaakob, *Chemical Engineering Journal*, 2015, 262, 1009-1021.

126. A. A. Ibrahim, A. H. Fakeeha, A. S. Al-Fatesh, A. E. Abasaeed and W. U. Khan, *International Journal of Hydrogen Energy*, 2015, 40, 7593-7600.

127. T. V. Reshetenko, L. B. Avdeeva, V. A. Ushakov, E. M. Moroz, A. N. Shmakov, V. V. Kriventsov, D. I. Kochubey, Y. T. Pavlyukhin, A. L. Chuvilin and Z. R. Ismagilov, *Applied Catalysis A: General*, 2004, 270, 87-99.

128. N. Z. Muradov, *Catalysis Communications*, 2001, 2, 89-94.

129. M. Lázaro, J. Pinilla, I. Suelves and R. Moliner, *International Journal of Hydrogen Energy*, 2008, 33, 4104-4111.

130. M. Ni, M. K. H. Leung, D. Y. C. Leung and K. Sumathy, *Renewable and Sustainable Energy Reviews*, 2007, 11, 401-425.

131. M. Matsuoka, M. Kitano, M. Takeuchi, K. Tsujimaru, M. Anpo and J. M. Thomas, *Catalysis Today*, 2007, 122, 51-61.

132. S. Zhang, X.-Z. Yuan, J. N. C. Hin, H. Wang, K. A. Friedrich and M. Schulze, *Journal of Power Sources*, 2009, 194, 588-600.

133. S. Gonzalez-Cortes, D. Slocombe, T. Xiao, A. Aldawsari, B. Yao, V. Kuznetsov, E. Liberti, A. Kirkland, M. Alkinani and H. Al-Megren, J. M Thomas, P. P. Edwards, *Scientific Reports*, 2016, 6, 35315.

134. W. Grochala and P. P. Edwards, *Chemical Review*, 2004, 104, 1283-1315.

135. S. Satyapal, J. Petrovic, C. Read, G. Thomas and G. Ordaz, *Catalysis Today*, 2007, 120, 246-256.

136. R. F. Service, *Science*, 2004, 305, 958-961.

137. D. Mori and K. Hirose, *International Journal of Hydrogen Energy*, 2009, 34, 4569-4574.

138. U. Eberle, M. Felderhoff and F. Schueth, *Angewandte Chemie International Edition*, 2009, 48, 6608-6630.

139. F. L. Darkrim, P. Malbrunot and G. Tartaglia, *International Journal of Hydrogen Energy*, 2002, 27, 193-202.

140. B. Sakintuna, F. Lamari-Darkrim and M. Hirscher, *International Journal of Hydrogen Energy*, 2007, 32, 1121-1140.

141. A. Klerke, C. H. Christensen, J. K. Nørskov and T. Vegge, *Journal of Materials Chemistry*, 2008, 18, 2304-2310.

142. X. Jie, S. Gonzalez-Cortes, T. Xiao, J. Wang, B. Yao, D. R. Slocombe, H. A. Al-Megren, J. R. Dilworth, J. M. Thomas and P. P. Edwards, *Angewandte Chemie International Edition*, 2017, 56, 10170-10173.

143. S. Horikoshi and N. Serpone, *Catalysis Science & Technology*, 2014, 4, 1197-1210.

144. S. A. Galema, *Chemical Sociaty Review*, 1997, 26, 233-238.

145. F. Langa, P. De La Cruz, A. De La Hoz, A. Diaz-Ortiz and E. Diez-Barra, *Contemporary Organic Synthesis*, 1997, 4, 373-386.

146. P. Lidstrom, J. Tierney, B. Wathey and J. Westman, *Tetrahedron*, 2001, 57, 10229.

147. S. Horikoshi and N. Serpone, *Microwaves in Catalysis: Methodology and Applications*.

148. V. V. Namboodiri and R. S. Varma, *Green Chemistry*, 2001, 3, 146-148.

149. M. Larhed, G. Lindeberg and A. Hallberg, *Tetrahedron letters*, 1996, 37, 8219-8222.

150. K. M. Dawood, *Tetrahedron*, 2007, 63, 9642-9651.

151. M. Larhed, C. Moberg and A. Hallberg, *Accounts of chemical research*, 2002, 35, 717-727.

152. J. D. Katz, *Annual Review Material Science*, 1992, 22, 153-170.

153. D. K. Agrawal, *Current Opinion in Solid State and Materials Science*, 1998, 3, 480-485.

154. G. A. Tompsett, W. C. Conner and K. S. Yngvesson, *Chemphyschem: a European Journal of Chemical Physics and Physical Chemistry*, 2006, 7, 296-319.

155. Y.-F. Huang, P.-T. Chiueh, W.-H. Kuan and S.-L. Lo, *Energy*, 2016, 100, 137-144.

156. A. Ward, *Dielectric Materials for Advanced Applications*, 2016.

157. K. Gibson, Microwave Spectroscopy Rotational Spectroscopy, available at https://slideplayer.com/slide/6169345/.

158. A. M. Aldawsari, *Dielectric measurements and catalytic cracking of heavy oils using advanced microwave technologies*, Thesis, 2017.

159. A. Porch, D. Slocombe and P. P. Edwards, *Physical Chemistry Chemical Physics*, 2013, 15, 2757-2763.

160. H. F. Abbas and W. M. A. Wan Daud, *International Journal of Hydrogen Energy*, 2010, 35, 1160-1190.

161. B. Fidalgo, Y. Fernández, A. Domínguez, J. Pis and J. Menéndez, *Journal of Analytical and Applied Pyrolysis*, 2008, 82, 158-162.

162. E. Udalov, V. Bolotov, Y. Y. Tanashev, Y. D. Chernousov and V. Parmon, *Theoretical and Experimental Chemistry*, 2011, 46, 384-392.

163. M. Jasiński, M. Dors and J. Mizeraczyk, *The European Physical Journal D*, 2009, 54, 179-183.

164. M. Jasiński, M. Dors and J. Mizeraczyk, *Journal of Power Sources*, 2008, 181, 41-45.

165. N. Z. Muradov, F. Smith, G. Bockerman and K. Scammon, *Applied Catalysis A: General*, 2009, 365, 292-300.

166. Y. Y. Tanashev, V. I. Fedoseev, Y. I. Aristov, V. V. Pushkarev, L. B. Avdeeva, V. I. Zaikovskii and V. N. Parmon, *Catalysis today*, 1998, 42, 333-336.

167. J. A. Menéndez, A. Arenillas, B. Fidalgo, Y. Fernández, L. Zubizarreta, E. G. Calvo and J. M. Bermúdez, *Fuel Processing Technology*, 2010, 91, 1-8.

168. D. D. Tanner and W. Richland, *ACS Fuels,* 1999, 1.

169. Y. Suttisawat, H. Sakai, M. Abe, P. Rangsunvigit and S. Horikoshi, *International Journal of Hydrogen Energy*, 2012, 37, 3242-3250.

170. S. Horikoshi, M. Kamata, T. Sumi and N. Serpone, *International Journal of Hydrogen Energy*, 2016, 41, 12029-12037.

171. X. Jie, S. Gonzalez-Cortes, T. Xiao, J. Wang, B. Yao, D. R. Slocombe, H. A. Al-Megren, J. R. Dilworth, J. M. Thomas and P. P. Edwards, *Angewandte Chemie International Edition*, 2017, *56*, 10170-10173.

172. X. Jie, T. Xiao, B. Yao, S. Gonzalez-Cortes, J. Wang, Y. Fang, N. Miller, H. AlMegren, J. Dilworth and P.P. Edwards, *Catalysis Today*, 2018, *317*, 29-35.

173. X. Jie, S. Gonzalez-Cortes, T. Xiao, B. Yao, J. Wang, D. R. Slocombe, Y. Fang, N. Miller, H. A. Al-Megren and J. R. Dilworth, J. M. Thomas and P. P. Edwards, *Energy & Environmental Science*, 2018, *12*(1), 238-249.

174. J. C. Macrae, *An Introduction to the Study of Fuel*, Elsevier, 1966.

Chapter 2

Experimental methods

This chapter summarises the experimental techniques and procedures applied in this thesis. The design of microwave system, catalysts preparation and the evaluation of catalytic performance are described by sections. Moreover, a variety of characterisation techniques used in this work are also introduced.

2.1 Experimental set-up

Figure 2.1 shows the experimental setup used in this work. A microwave system which consists of a microwave generation system, a purpose-built microwave cavity and a control system is presented. The generated gases are collected by metrical cylinders with controlled valves, so that can separate the gases in different times for the study on a 'time on stream' basis. The collected gases are then analysed by Gas Chromatography (GC) using a Perkin-Elmer, Clarus 580 GC. The liquid products and/or the 'escaped' feedstocks are trapped using two cold traps and the liquids are collected and analysed by Gas Chromatograph Mass Spectrometer (GC-MS) using a SHIMADZU, GCMS-QP2010 SE.

2.1.1 Microwave system

The microwave heating system chain prior to the applicator (cylindrical cavity) consisted of a power generator, microwave head, microwave circulator, dummy load, microwave power meters and tuneable waveguide sections which was designed and supplied by the French company Sairem Ltd. The system was computer controlled using the Labview software. The applicator section was fabricated in the Inorganic Chemistry Laboratory at the University of Oxford.

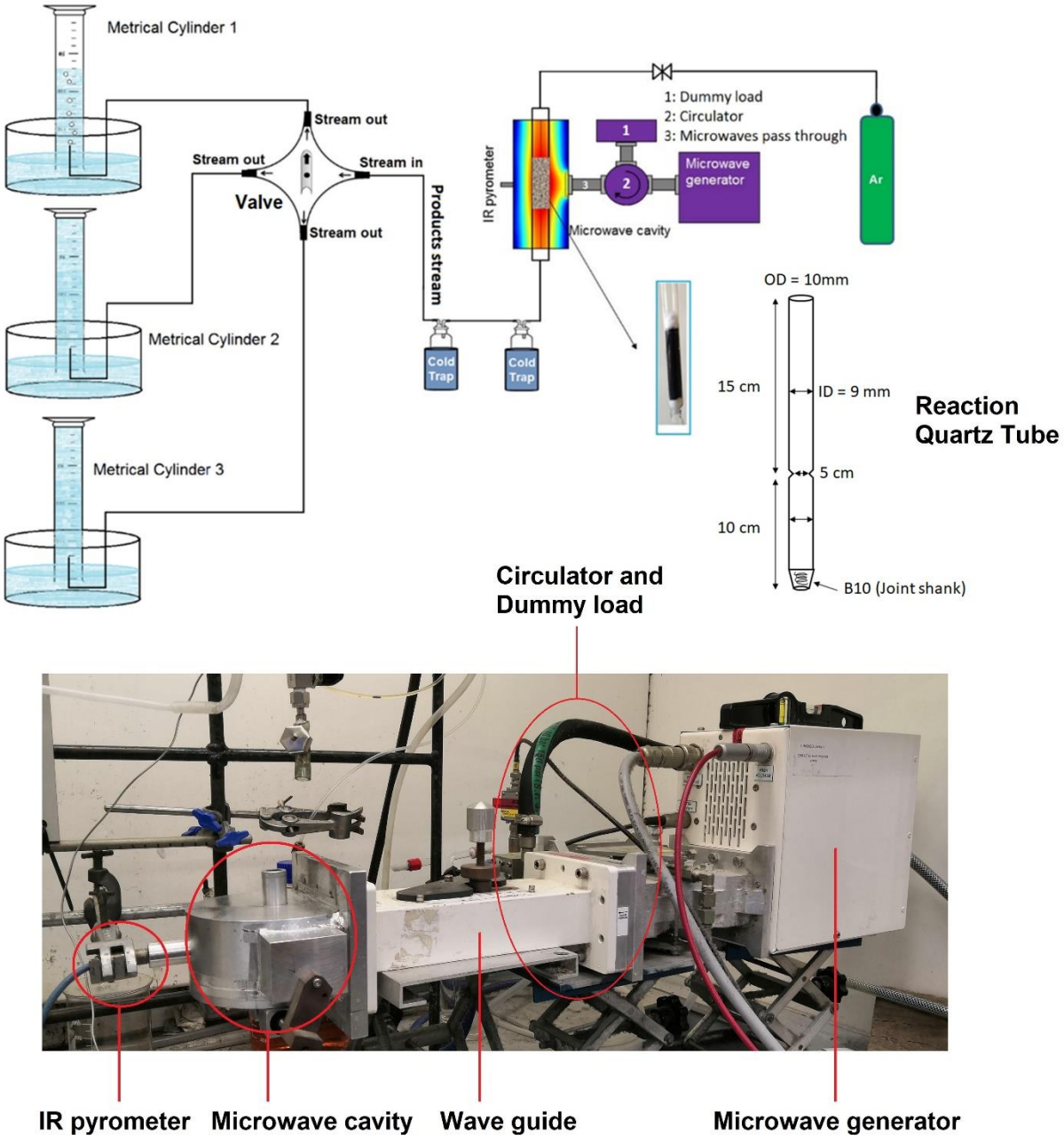


Figure 2.1. Reaction system configuration.

The power generator is equipped with a magnetron as microwave source with a ripple rate of < 1% RMS from 10% to 100%. The operating frequency of the microwave system was 2450 MHz (± 25 MHz) from 10% to 100% of nominal power. The maximum output power was 2000 W with 1% stability from 10% to 100% of maximum power after thirty minutes on. The power rise time is about 100 μs and the microwave output is via WR 340 waveguides. The power generator is a resonant switching converter with frequencies of 30 kHz up to 80 kHz and an efficiency of 93% at nominal power[1, 2]. The power

supply and microwave head are both water and air cooled. The cooling system requires a minimum water flow rate of 5L/min with a differential pressure of 1.9 bar. The power generator will automatically shut down when the water flow rate below 3L/min and 0.7 bar[3]. And the generator is controlled remotely via an RS232 MODBUS gateway using the Labview software.

A rectangular waveguide is constructed to guide the microwave to the cavity. And a circulator and dummy load are equipped in the middle of the waveguide to protect the power generator from the damage by the reflected power which hasn't been absorbed by either the samples or the system. To detect and calculate the amount of reflected energy, a reflected power measurement system which consists of a crystal detector, isolator load and level adapter box is also equipped in the microwave system (Figure 2.2). The reflected power R, was measured by a crystal detector mounted onto the isolator load, from which the power absorbed by the sample, P is determined. If the power transmitted to the applicator is W, then $P = W - R - X$, where X is the microwave power lost in the cavity walls and by minor applicator leakages. The applicator used in this work is a TM_{010} resonant cavity to enable a well-characterized field distribution and high nominal field strength[1, 2]. Thus, in this work electric field driven processes, with a high electric energy density in the sample region is investigated.

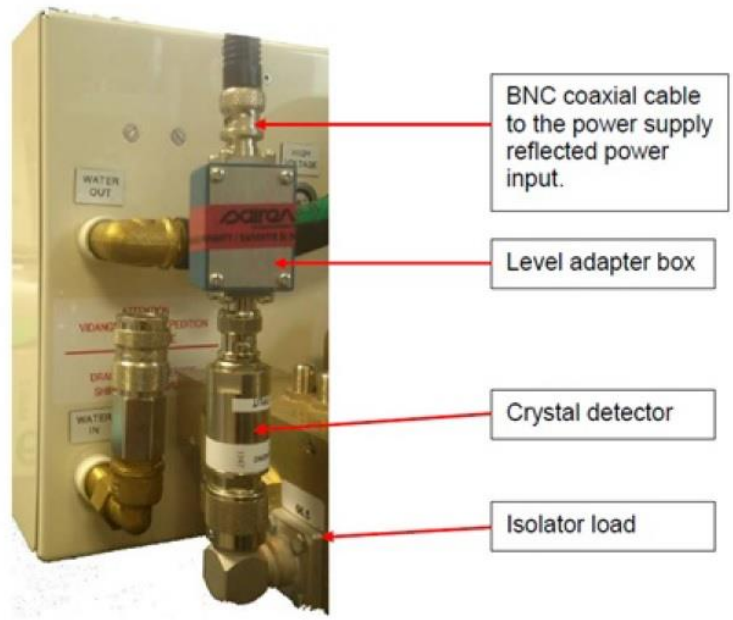


Figure 2.2. The reflected power measurement system. (Reproduced from Ref.3)

The applicator designed for this work is a single-mode cavity which built up by aluminium, and only one possible field is created by the standing wave between the walls of the cylindrical cavity. The TM_{010} mode used in this work is therefore, created as only a uniform electric field is presented in the centre of the cylindrical cavity. The cylindrical cavity is 18 cm in diameter and 10 cm in height. Two holes of 1 cm in diameter are made in the centre of cavity on and under, so that a sample tube can be inserted and fully exposed to the microwave electric field (Figure 2.3). It should be noted that the holes have to be small enough to (a) avoid disturbing the electromagnetic fields and affecting the field distribution, and (b) avoid causing propagation of the microwaves through the holes and reduce the escape of microwaves. [3] A square with sides of length 4 cm on the back of the cavity is connected to the waveguide. Opposite on the cavity wall, a viewing hole is made for the temperature measurement by IR pyrometer.

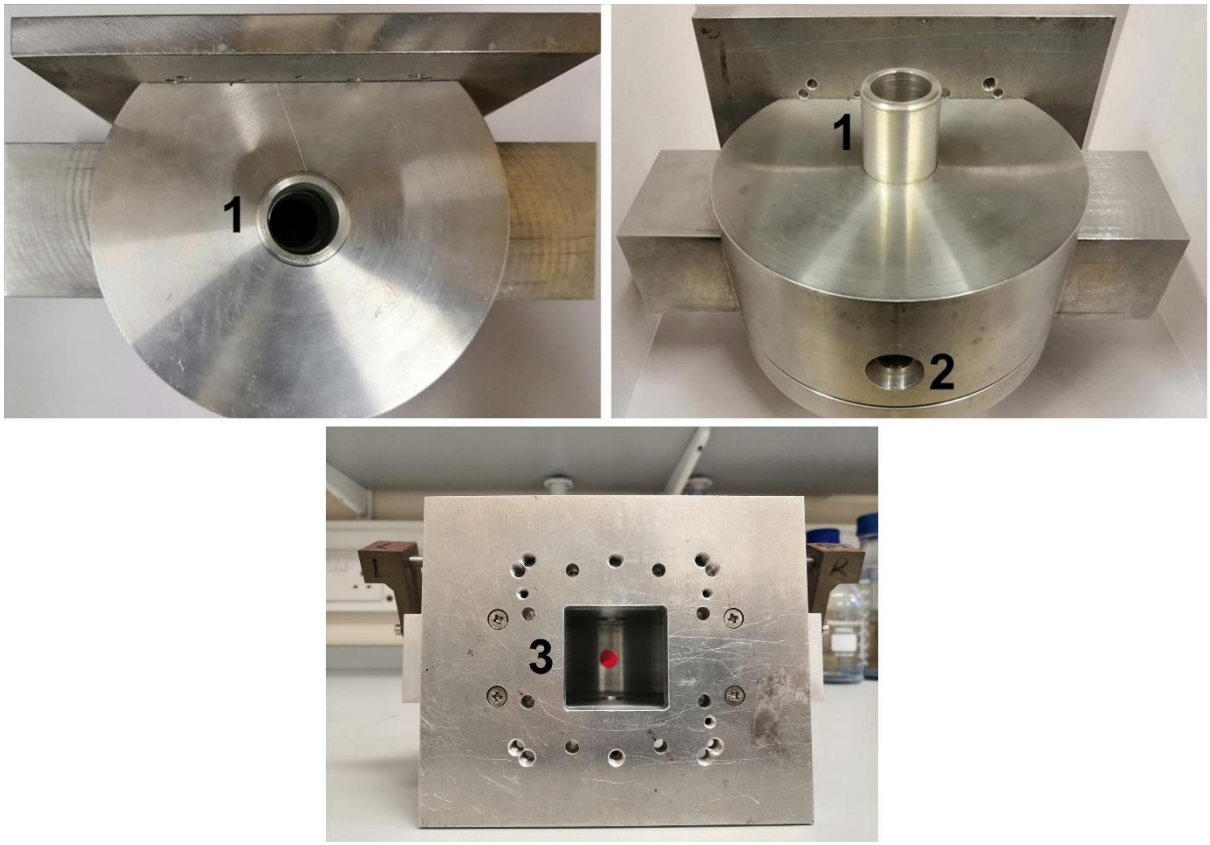


Figure 2.3. The purpose built TM010 mode aluminium cavity. 1) The central hole where samples are inserted along the axis of the microwave electric field. 2) The viewing port for temperature measurement by IR pyrometer. 3) Rectangular connection to the wave guide.

A quartz tube is used as the reactor because quartz is highly transparent to the induced microwave irradiation and can reduce exclusion of microwave samples from the field[3]. Sample are packed in the

quartz tube using quartz wools that seals both sides of the tube. Then it is placed into the cavity along the axis at the point of high field intensity. The height of the sample bed is usually 3.5 - 4 cm that ensure the sample is exposed to the axially polarised (TM_{010}) uniform electric fields (Figure 2.1).

Although, there are other modes operating in the cavity can vary the distribution fields, thereby affect the samples. In this design, we want to separate the magnetic fields and determine the heating phenomena caused by only the electric fields. It should be also noted that the presence of the sample in the microwave fields can also modify the field distribution, thus it is very important to take into account of the sample's size, configuration, and permittivity when design the applicator in order to guarantee the fully-loaded cavity is still operating in the required field distribution[3].

2.1.2 Temperature control and measurements

The sample temperature is measuring using an infrared (IR) pyrometer, which was also used to control the power to the generator. The pyrometer was positioned horizontally to face a side hole in the microwave cavity (Figure 2.3)[1]. Since the common temperature measurement techniques such as thermocouple or other sensing devices are not applicable to a microwave system, the IR thermometer is chosen to detect the temperature through the viewing port. However, the IR thermometer can only measure the external surface temperature of the catalyst and cannot detect the regions' temperature. It is thus, difficult to precisely measure the exact temperatures occurring throughout the samples[1, 3]. Adjusting the input microwave power has been developed to control the process temperature and a Labview software is linked to control the microwave system. During the microwave experiment a temperature (T) versus time (t) of reaction profile was recorded via the Labview program and this method has been proved to be a reliable for this work.

2.2 Catalysts preparation

The catalysts used in this study are prepared using the so-called incipient wetness impregnation method. Metal nitrates, for example $Fe(NO_3)_3 \cdot 9H_2O$ (Iron (III) nitrate nonahydrate, Sigma-Aldrich) and $Ni(NO_3)_2 \cdot 6H_2O$ (Nickel (II) nitrate hexahydrate, Sigma-Aldrich) etc. are used as metal precursor.

Support material used for the catalyst preparation are SiC (silicon carbide, Fisher Scientific), AC (activated carbon, Sigma-Aldrich) and other types of carbons, SiO_2 (silica mesoporous, Sigma-Aldrich) and Al_2O_3 (aluminium oxide, Sigma-Aldrich) etc.

The powders of support material are first mixed with an aqueous solution of metal nitrate, which was calculated to produce a desired content of metal on the support and stirred at 150°C on a magnetic hot plate in a fume hood for 3h until it became a slurry. The slurry then is moved into the drying oven, for drying overnight. The resulting solid mixtures are calcined in a furnace at 350 °C for 3 h. Finally, the active catalysts were obtained by a reduction process in 10% H_2 /Argon gases at 800 °C for 6h.

Catalysts of various metal supported by different supports are prepared by the same method. For the preparation of binary metal catalyst, the supports were mixed with the aqueous solution of two or more metal nitrate precursors. Moreover, the catalysts with various metal loading ranging from 5 – 100 wt.% are synthesised using the same method.

2.3 Evaluation of catalytic performance

The catalyst is firstly placed in a quartz tube (inner diameter 6mm, outer diameter 9mm) because the quartz reduces exclusion of microwave from the field. The height of the catalyst bed exposed to the axially polarised (TM_{010}) uniform electric fields is 4cm, with typically about 1.13 cm^3 of catalysts. 0.5 mL (or 30-50 wt.% of catalysts equivalent) liquid hydrocarbons (feedstocks), are then injected into tube and waiting 5-10 minutes until the aqueous hydrocarbon was well dispersed into catalysts bed. Then, the filled tube was placed axially in the centre of the TM_{010} microwave cavity in order to minimise depolarisation effects under microwave radiation. Before starting microwave irradiation, the samples were purged with an Ar flow rate of 1.67 mL $\cdot$ s^{-1} for a period of 15 minutes. Then, the sample was irradiated with microwaves for 30 min at microwave irradiation (typically 750 W is used). The microwave system is not impedance matched, thus the energy delivered to the sample cavity and the microwave power to which the sample was exposed significantly less than this value. The generated gases are collected and analysed by gas chromatography (GC) using a Perkin-Elmer, Clarus 580 GC.

The “escaped” hydrocarbon was analysed by gas chromatograph mass spectrometer (GC-MS) using a SHIMADZU, GCMS-QP2010 SE.

For comparison purpose, the conventional thermal experiments are also carried out in an electric furnace. The experimental setup is shown in Figure 2.4. The heating rate of electric furnace used in these experiments were 10 °C/min.

The conventional thermal process is in general carried out through two different procedures. For one thermal procedure, a hydrocarbons pre-loaded sample is subjected to a pre-heated furnace (550 °C), while in another procedure, the catalyst (without fuel) was pre-heated in the furnace to 550 °C and the diesel was then carefully introduced to the hot catalyst bed by a syringe.

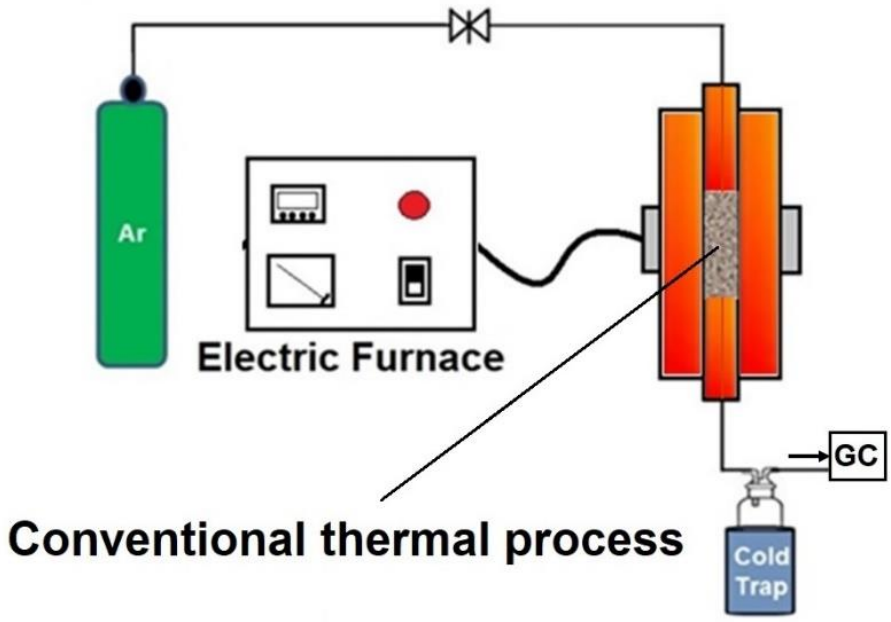


Figure 2.4. A conventional thermal system configuration, heating by an electric furnace.

2.4 Products analysis

2.4.1 Gas Chromatography (GC)

Gas chromatography (GC) is a common analytic technique for separation and identification of compounds in a mixture. The technique allows for the detection of each compounds in a mixture qualitatively and quantitatively, and it enables to detect a compound with a very small quantity.

There are two basic phenomena for the chromatographic separation process: the separation of the substances and the broadening of the substance bands. The separation process is based on the distinct migration rates of the components caused by the different interactions with the stationary phase. During the transportation of a mixture through the column, each compound in the mixture is superimposed with mixing processes (dispersion), thus causing a broadening of the substance bands and counteract the separation[4]. Consequently, for detecting the different components, appropriate column dimensions and operating parameters is chosen to achieve the maximum of the differences in migration rates of the components[4]. The migration rate of a compound is the time that pass through the column or known as the retention time in the stationary phase, and each compound has a specific retention time. Thus, with a successful separation process of injected gas mixture, each component is detected and qualitatively and quantitatively analysed by detectors at the end of the separation column, therefore produces peaks at different times in a chromatogram.

In this thesis, a Perkin-Elmer, Clarus 580 GC which equipped with two types of detectors is used. A flame ionization detector (FID) is commonly used to detect hydrocarbons such as methane, ethane, ethylene etc. and many carbon containing compounds. FID has several advantages including low noise level, linear response over a very wide range, high sensitivity and little affected by the operating factors such as detector temperature, flow rates of gas and other parameters, which make it the most widely and successfully used gas chromatographic detector[5, 6]. The FID passes sample and carrier gas from the column through a hydrogen-air flame and works by burning of carbon compounds to produce ions. When these ions pass between electrodes placed near the flame they are collected, and a current is produced which is proportional to the amount of compound being burned. This current is then sensed by an electrometer and gives a recordable digital signal[5, 6].

Another detector used in this thesis is the thermal conductivity detector (TCD) which can detect hydrogen, carbon monoxide, carbon dioxide, nitrogen, air, inorganic gases and other compounds. The TCD works based on the principle of comparing the thermal conductivities between pure carrier gas (the reference gas) and carrier gas plus sample components. A filament in detector is heated electrically and kept constant while reference flow and effluent flow (sample components in carrier gas) pass over it. There is thus, the difference in thermal conductivity between reference flow and effluent flow is

generated as a result of different power requirement for keeping the filament temperature constant changes. This difference produces a voltage signal which is proportional to the concentration of the sample components, thus a detectable signal is produced[6, 7].

For the Perkin-Elmer, Clarus 580 GC used in this thesis, a 50 m long GC column with 320 μm in diameter is equipped. The operating temperature of the oven is 200 °C with a heating rate of 25 °C /min from 80 °C to 200 °C. The carrier gas used for TCD is helium with a flow rate set as 40 mL/min, and the operating temperature is 200 °C. For FID, the flow rates of H_2 and air are set to be 45 mL/min and 450 mL/min, respectively and the running temperature is 250 °C[3]. The GC was carefully calibrated using standard gases and the error given is $\pm 0.01 - 0.1\%$.

2.4.2 Gas Chromatography-Mass Spectrometry (GC-MS)

Gas Chromatography-Mass Spectrometry (GC-MS) is an apparatus that successfully combined gas chromatography (GC) and mass spectrometry (MS) techniques. The advantages of GC-MS are that GC can effectively separate volatile and semi-volatile mixture compounds into various components and MS provides specific detection on each component, whereas GC alone is not always able to selectively detect the compounds and MS is suffering on separation of mixtures. Therefore, GC-MS is widely used for qualitative and quantitative determination of volatile and semi-volatile organic compounds in a variety of fields[8].

In a GC-MS analyte process, a mixture will firstly separate into various components in GC and these heated gases pass through the column in carrier gas (normally helium) and then flow into the MS. MS works based on the principle of breaking the specimen molecules into charged fragments by electrically charging the specimen molecules, accelerating them through a magnetic field. Then, each compound is identified by detecting the difference in charges of fragments and the mass of each fragment is displayed via a spectral plot. Consequently, using these fragment masses together can give the mass of the original molecule and thus a compound's mass spectrum enables for qualitative identification[9].

In this thesis, GC/MS analysis for liquid products is carried out using a SHIMADZU, GCMS-QP2010 SE. A capillary column (SHIM-5MS) of 30 m in length and 0.25 mm in diameter is equipped. The

helium is used as carrier gas. The temperature of oven in GC is 50 °C and the injection temperature is set to be 250 °C. The ion source temperature of MS is 200 °C, with an interface temperature is set 250 °C.

2.5 Techniques used for characterisation of catalysts

The catalysts are carefully characterised before and after experiments by powder X-ray diffraction (XRD, PANalytical X'Pert PRO diffractometer), scanning electron microscope (SEM, JEOL 840F and ZEISS EVO), energy-dispersive X-ray spectroscopy (EDS, ZEISS EVO), high-resolution transmission electron microscopy (HRTEM, JEM-3000F 300 kV), thermogravimetric analysis (TGA, TA Instrument, SDT Q-600), Laser-Raman spectroscopy (PerkinElmer RamanStation^{TM} 400F spectrometer) and microwave cavity perturbation measurements.

2.5.1 X-ray Diffraction (XRD)

Diffraction occurs when the incident beams which generated by an electron gun, interacts with the periodic array of molecules in a crystal[10]. Among these, x-ray diffraction (XRD) is most widely used in solid state chemistry to identify the crystalline structure of a material, with other properties such as particle size etc. can also be measured.

When a x-ray beam hits atom in a crystal, the scattering of x-rays from atoms produces constructive interference at specific angles, thereby producing a diffraction pattern which contains information about the atomic arrangement within the crystal[11]. The Bragg's Law (Eq. 2.1) is used to determine constructive interference from x-ray scattered by parallel planes of atoms and calculate the angle (the position of the diffraction peaks) by the distance between parallel planes of atoms.

$$n\lambda = 2d \sin \theta \tag{2.1}$$

where the variable d is the distance between atomic layers in a crystal, and θ is the certain angles of incidence by reflected x-ray beams. λ is the wavelength of the incident x-ray and n in the equation is an integer.

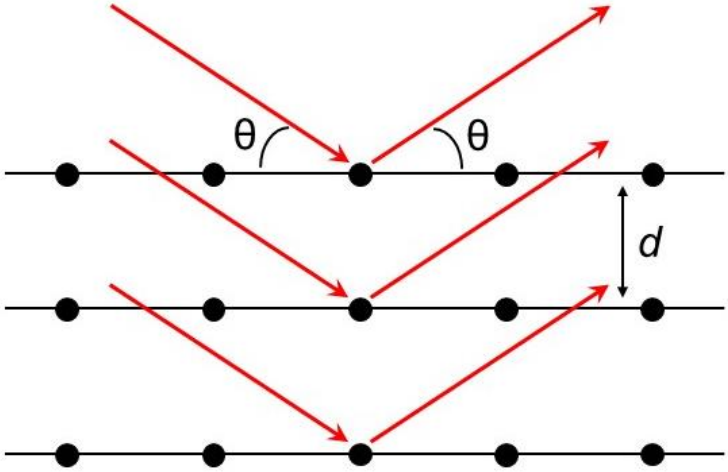


Figure 2.5. Schematic diagram of Bragg's law.

Theoretically, different kinds of crystal have their unique diffraction patterns and even with tiny changes of the crystal structure can lead to the change of XRD patterns which appeared by the shift of diffraction peak position. Furthermore, the size of particles can be estimated through Sherrer Equation (Eq. 2.2) by measuring the full width at half maximum (FWHM) of diffraction peaks in XRD patterns[11, 12].

$$\tau = \frac{K\lambda}{\beta COS\theta} \tag{2.2}$$

In this equation (Eq.2.2), τ is the mean size of the ordered (crystalline) domains with a unit in *nm*. This could be smaller or equal to the grain size of the sample. λ is the wavelength of the incident x-ray and K is a dimensionless shape factor with a value close to unity and typically has a value of ca. 0.9. β is the width at half the maximum intensity (FWHM) and the θ is the angle of incidence.

In this thesis, the catalysts are characterised by powder X-ray diffraction (XRD) using a Cu Kα X-ray source (45 kV, 40 mA, 0.15418nm) on a PANalytical X'Pert PRO diffractometer. The specimen is prepared by filling a purpose-built sample holder with fine powders and make the surface of sample remain smooth and flat. In this study, the sample is in general scanning in a range (in 2θ) of 10° to 80°.

2.5.2 Scanning Electron Microscopy and Energy-dispersive X-ray spectroscopy (SEM-EDS)

Scanning electron microscopy (SEM) is a powerful and mature technique that has been applied widely in many scientific applications for the examination of materials. A normal scanning electron microscope consists of electron gun, condenser lenses, apertures, scanning system and specimen chamber (Figure 2.6)[13, 14]. The electron gun is located at the top of the electron column and generates the electron beam under a high vacuum. Typically, a tungsten filament is used to generate the free electrons by thermionic emission at ca. 2700K. The electron beam is then accelerated toward an anode through an adjustable high voltage from 200V to 30 kV, and pass through condenser lenses and a system of apertures to produce a convergent electron beam which is focused down to 1000 times its original size. Hence, the condenser lenses are primarily responsible for determining the intensity of the electron beam while the function of apertures is to reduce and exclude extraneous electrons in the lenses[14]. The images are finally formed by the beam scanning the surface of the specimen where electrons are emitted from the specimen by the action of the scanning beam and collected by a suitably-positioned detector[13]. The specimen chamber is located at the lower portion of the column where the secondary electron detector is mounted above the specimen stage and controls. The stage can be controlled by a goniometer which allows for x-y-z movement, 360 rotation and 90 tilt.

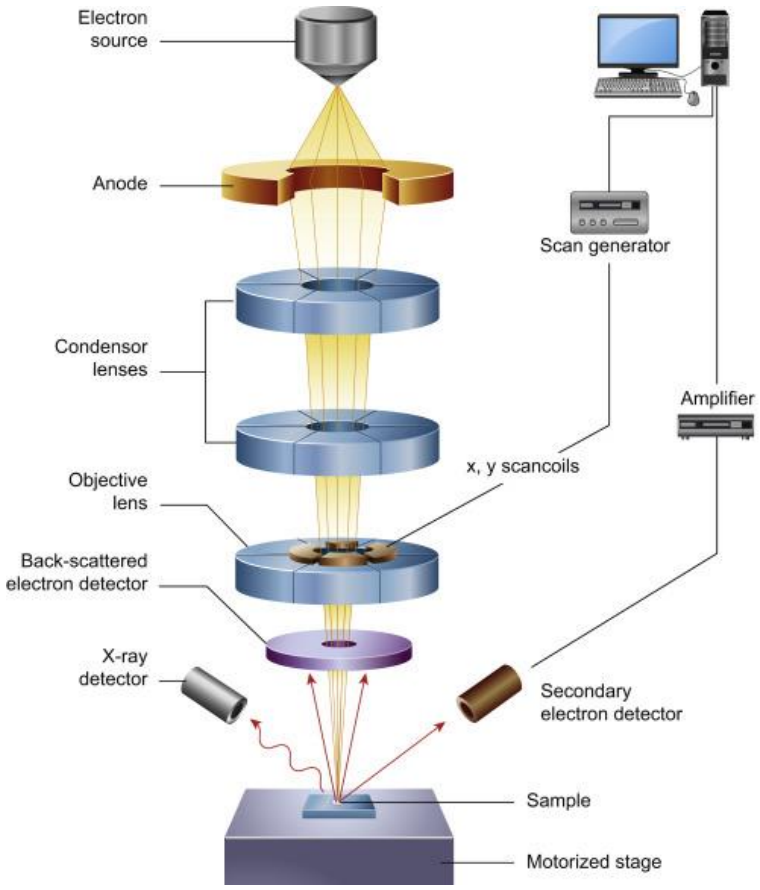


Figure 2.6. Scanning electron microscope column. (Reproduced from Ref. 13)

Scanning electron microscopy utilise two types of signals by which secondary and backscattered electrons to visually inspect the surface of a specimen. Secondary and backscattered electrons are generated as a result of two separate types of interaction between the specimen and electron beam. The secondary electrons come from the inelastic collision and scattering of incident electrons with electrons around atoms in specimen. This signal is used to reveal the surface structure of a material with a resolution of about 10 nm or better[14]. With backscattered electrons which are a result of an elastic collision and scattering event between incident electrons and specimen nuclei or electrons[14], we are able to resolve topographical contrast and atomic number contrast further from the surface of the material with a resolution of >1 μm. Besides, an x-ray detector is mounted on the column to receive the x-ray signal that is generated from a specimen under an electron beam. The x-ray signal which is generated by the recombination interactions between free electrons and positive electron holes within the material,

allows for determination of elemental composition of the specimen through energy dispersive x-ray spectroscopy (EDS) analysis.

EDS analysis can in principle detect all elements from atomic number 4 (Be) to 92 (U). And quantitative analysis is also possible to determine the concentration of the elements in the specimen sample surface. In a detector, x-ray photons cause ionization, thereby producing an electrical charge which is then amplified by a sensitive preamplifier. Based upon the energy characteristic of the elements, EDS employ pulse height analysis, by which an output pulses given by a detector is proportional in height to the x-ray photon energy and this is in conjunction with a pulse height analyser[15].

In this thesis, the scanning electron microscope (SEM-EDS, ZEISS EVO) is in general used to characterise the surface morphology of the catalysts before and after the reactions, and the surface elemental analysis is carried out with the equipped Energy-dispersive X-ray spectroscopy. Another scanning electron microscope (SEM-EDS, ZEISS MERLIN) is also proportional employed for some characterization.

2.5.3 Transmission Electron Microscopy (TEM)

Like scanning electron microscopy (SEM), transmission electron microscopy (TEM) is an electron microscopy which can be performed on chemical analysis, studying the growth of layers and the composition and defects in materials. A TEM can divided to several different forms such as high resolution transmission electron microscope (HRTEM), scanning transmission electron microscope (STEM) and analytical electron microscope (AEM). A HRTEM can be used to analyse the quality, shape, size and density of quantum wells, quires and dots. Unlike SEM, only thin samples which allow a fraction of the incident electron beam to go through the sample can be studied using TEM technique[16]. Figure 2.7 illustrates the electron column of the TEM which consists of the illumination system, the objective lens/stage, and the imaging system operating in vacuum.

The role of the illumination system is to accelerate the electrons from the electron gun and transfer them to the specimen. Through set of condenser lenses, an electron beam of the accelerated electrons (with an energy in the range 20 – 1000 keV) is produced with a desired diameter. The electron beams

then impinge upon the specimen on the stage which is placed in front of the objective lens. The objective lens forms an image of the electron density distribution at the exit surface of the specimen based on the electron optical principles[16]. The creation of the various images and diffraction pattern are subsequently formed and magnified by the diffraction, projection, and intermediate lenses below the objective lens in the imaging system. These lenses magnify either the diffraction pattern or the image onto a fluorescent screen, which converts the electrons into visible light signal for viewing and recording via a detector such as CCD or TV camera.

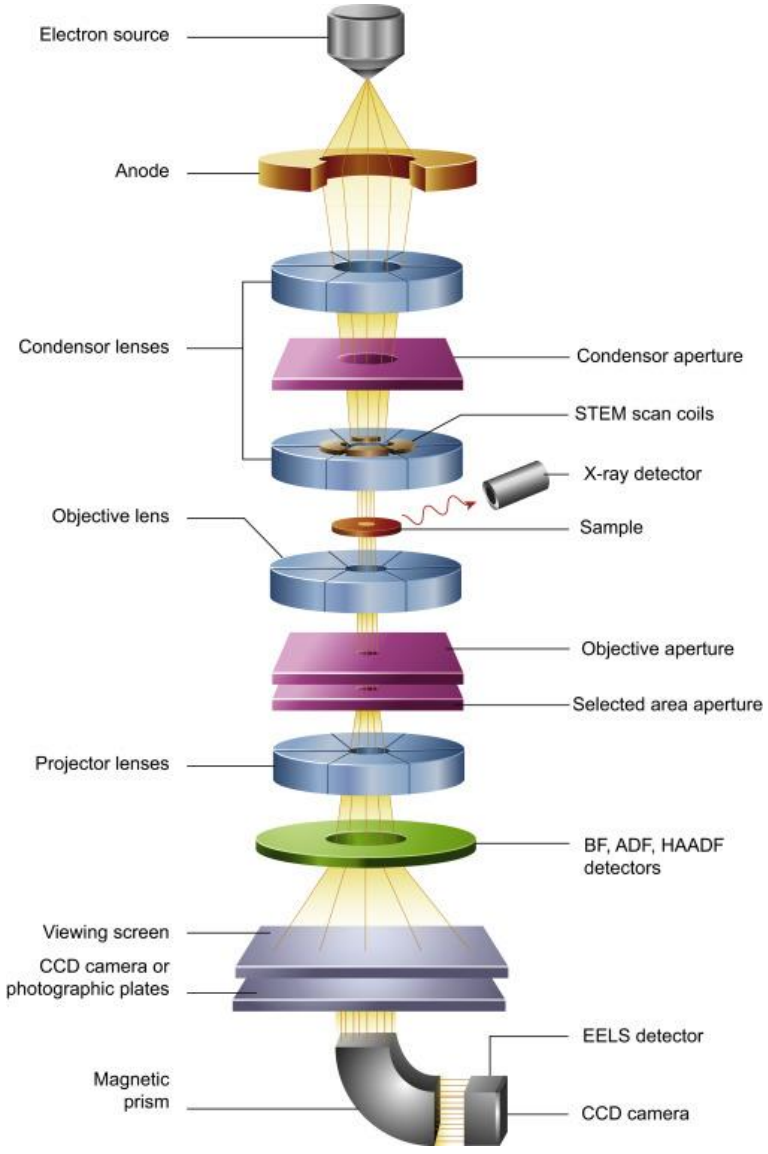


Figure 2.7. Transmission electron microscope column. (Reproduced from Ref. 13)

A variety of interactions that take place during the collision of the electron beam and the sample, including directly transmitted electrons, backscattered electrons, secondary electrons, coherent elastic scattered electrons, incoherent inelastic electrons, incoherent elastic forward scattered electrons, characteristic, and continuum x-rays, Auger electrons, long-wavelength radiation in the visible, ultraviolet, and infrared regions of the spectrum, lattice vibrations (phonons), electron oscillations in metals (plasmons), electron-hole pair generation, electrical current, in principle can be used to derive information on the nature of the specimen[16].

In this thesis, the catalysts are examined by high-resolution transmission electron microscopy (HRTEM) before and after microwave treatment using JEM-3000F microscope (300 kV). The specimen is prepared by dispersing the catalyst powder in ethanol in an ultra-sonic bath for 15 min. The solution is then drop cast onto a 300-mesh copper TEM holey carbon grid on a filter paper and allowed to evaporate. An oriented gold crystal grid is used to calibrate scale bars for all the TEM images.

I would like to thank Dr Jiale Wang from Oxford Materials for helping conduct the HRTEM analysis for this work.

2.5.4 Thermogravimetric Analysis (TGA)

Thermogravimetric Analysis (TGA) is primarily used to determine the thermal properties of materials and to estimate the composition of materials. The technique can measure the weight change and the rate of weight change as a function of temperature in a certain open atmosphere[17]. The weight loss of a sample is corresponding to decomposition, evaporation, reduction (reducing atmosphere) or desorption while the weight gain is a result of oxidation (oxidizing atmosphere) or absorption. There is thus, a so-called TGA curve produced by the measurement can tell the thermal stability and oxidative stability of materials, the composition of multi-component systems, decomposition kinetics of materials, moisture and volatiles content of materials and the effect of reactive or corrosive atmospheres on materials.

In addition, a differential scanning calorimetry (DSC) analyser is usually incorporated with TGA to measure the energy changes that occur as a sample is heated, cooled or held isothermally[17]. The energy changes enable to find and measure the transitions that occur in the materials quantitatively, and to note the temperature where they occur, so that to characterise a material for melting processes and to

determine the chemical reactions of endothermic or exothermic. The heat flow is measured by DSC which the energy into or out of the materials is shown in a heat flow curve in units of mW (TGA-DSC curve on the right *y*-axis, Figure 2.8) as a function of temperature[17].

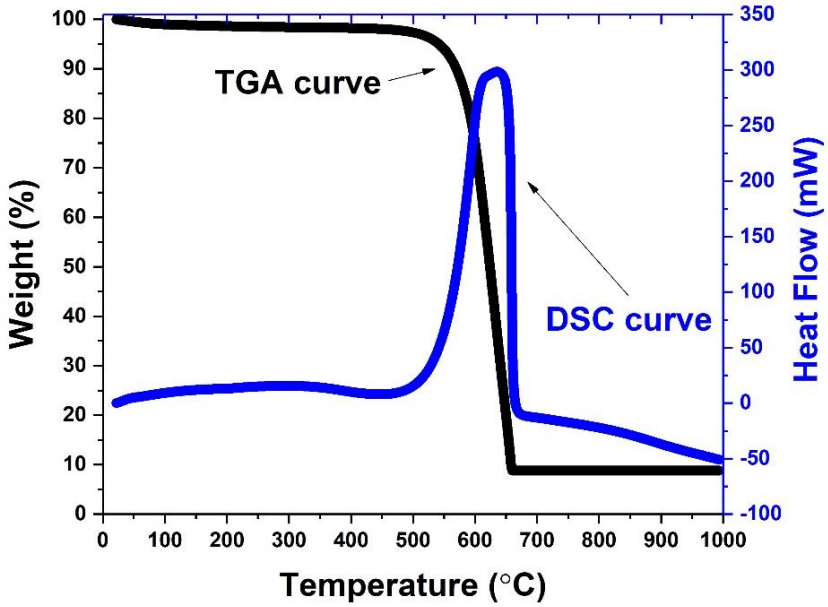


Figure 2.8. A representative TGA-DSC curve of activated carbon oxidation under air atmosphere.

In this thesis, a TA Instrument, SDT Q-600 is employed for TGA-DSC measurement. The technique is mainly used to characterise the liquid hydrocarbons (feedstocks) left in spent samples and to determine the amount and types of resulting carbon residues. Therefore, a program is set up to measure the remaining fuels and the produced carbons, as which the first ramp of TGA on spent catalysts are heated under N_2 atmosphere with a heating rate of 10 °C/min to 1000 °C, then followed by a continues ramp when the sample cooled down to room temperature by switching the atmosphere to air, and again heat the sample to 1000 °C at a heating rate of 10 °C/min.

2.5.5 Laser- Raman Spectroscopy

Raman spectroscopy is a scattering technique based on inelastic scattering of monochromatic light which is produced by a laser source. When sample is interacted with a monochromatic laser beam, photons of the laser are absorbed by the sample and then reemitted (scattered radiation). Among these scattered radiations, much of them have a same frequency with the incident radiation which forms

Rayleigh scattering. Hence, a small fraction of these scattered radiations has a frequency different from that of incident light and therefore constitutes Raman scattering which is used to construct a Raman spectrum. In Raman spectrum, Stokes lines depict the scattered radiation which has a lower frequency than that of incident radiation, and anti-Stokes lines appear in Raman spectrum when the frequency of scattered radiation is higher than the frequency of incident radiation[18].

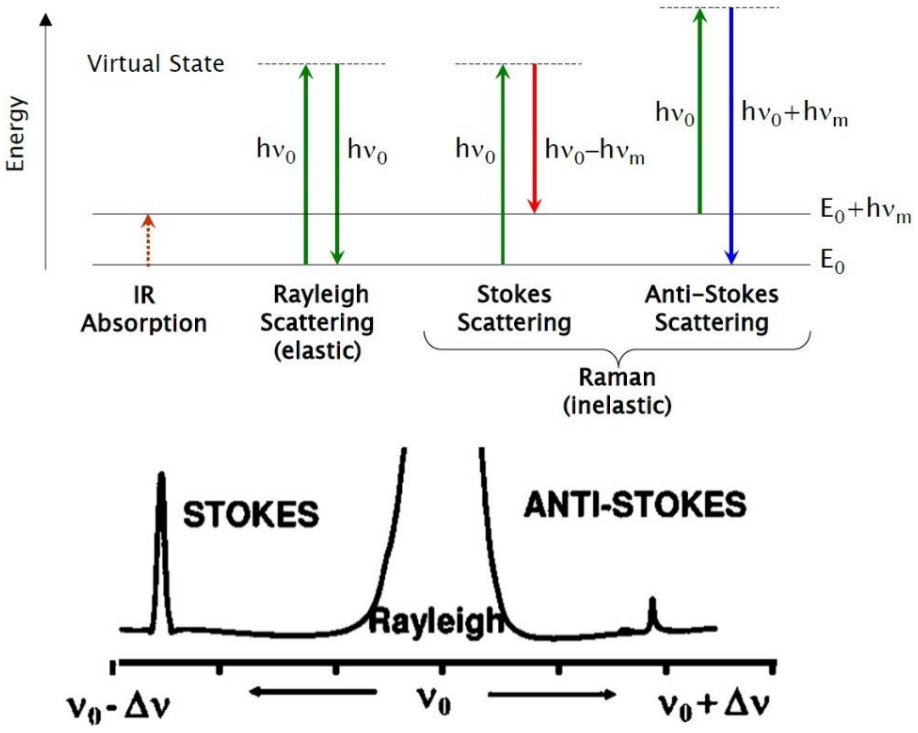


Figure 2.9. Principles of Raman spectroscopy. (Modified from Ref. 19)

Raman spectroscopy has a wide variety of applications in chemistry, biology, medicine, geology and mineralogy[20]. And it has been historically used in the study and characterisation of graphitic materials, being widely used over the last four decades to characterize pyrolytic graphite, carbon fibers, glassy carbon, carbon nanotubes, and graphene etc.[21, 22]. In this study, Raman spectroscopy plays an important role in investigation and determination of main by-product residue carbons.

From a Raman spectrum of sp^2 nanocarbons such as graphene and carbon nanotubes, a variety of information such as crystallite size, clustering of the sp^2 phase, the presence of sp^2–sp^3 hybridization and the introduction of chemical impurities etc. is given[21]. The disorder-induced D-band at position of about 1345 cm^{-1} in a Raman spectrum indicates disorder in sp^2-hybridized carbon systems. The presence

of disorder leads to rich and intriguing phenomena in their resonance Raman spectrum, thus making Raman spectroscopy enable to identify disorder in the sp^2 network of different carbon structures, such as diamond-like carbon, amorphous carbon, nanostructured carbon, as well as carbon nanofibers and nanotubes[21].

The so-called G-band Raman feature at the position of about 1582 cm^{-1} is commonly observed to all sp^2 carbon system which is given rise by the stretching of the C-C bond in graphitic materials. Due to the high sensitivity to strain effects in sp^2 carbons, the G-band in a Raman spectrum can be ued to probe any modification to the flat geometric structure of graphene[21]. Together with the G-band, another G'-band which appears in the rage 2500-2800 cm^{-1} indicates a Raman-allowed mode for sp^2 carbons. The G'-band is a second-order two-phonon process and, it exhibits a strong frequency dependence on the excitation laser energy E_{laser}[21].

In this thesis, the characterisation of resulting carbon residues via Raman spectroscopy is operated on a PerkinElmer RamanStation^{TM} 400F spectrometer, with laser excitation at 785nm. For comparison purpose, a variety of model carbon materials which is mainly sp^2 bonded carbons such as activated carbons (ACs), carbon black (CB), graphite, and multi-wall carbon nanotubes (MWCNTs) etc., is investigated by Raman spectroscopy.

2.5.6 Microwave Cavity Perturbation Measurements

The cavity perturbation measurements are usually used to characterise the materials' complex permittivity and permeability. The advantages of cavity perturbation technique are simple, accurate and easy for data interpreting. Measuring dielectric properties of a material using perturbation technique is based on the change of frequency curve of the resonance and the Q factor of the cavity[3, 23].

The perturbation cavity (shown in Figure 2.10) used in this thesis uses the Transverse Magnetic TM_{010} mode. The TM_{010} mode within a waveguide has a highly uniform electric field that only varies radially within the cavity. The microwaves are coupled to the cavity using coaxial cables placed at Port 1 and Port 2 and terminated with an open circuit extended centre conductor oriented to provide capacitive coupling to the electric fields of the TM_{010} mode at radial positions 3 cm from the axis. A quartz tube (inner diameter 2mm, outer diameter 4mm) is used as a container due to its high microwave

transparency. And the sample is placed into the quartz tube and placed in the centre of the cavity, at the maximum of a standing wave. All microwave measurements are performed using an Agilent E5071B network analyser. Measurements are performed of the transmitted microwave power $|S_{21}|^2$ in the frequency domain. The effects of cavity couplings are removed by converting the loaded quality factor Q_L into the unloaded quality factor Q in each case. The cavity couplings are adjusted so that they are equal (i.e., symmetric) and so the conversion is made using the simple formula $Q = Q_L(1 - 10^{-IL/20})$, where IL is the insertion loss (i.e., transmitted power) at resonance, measured in dB [1, 24, 25].

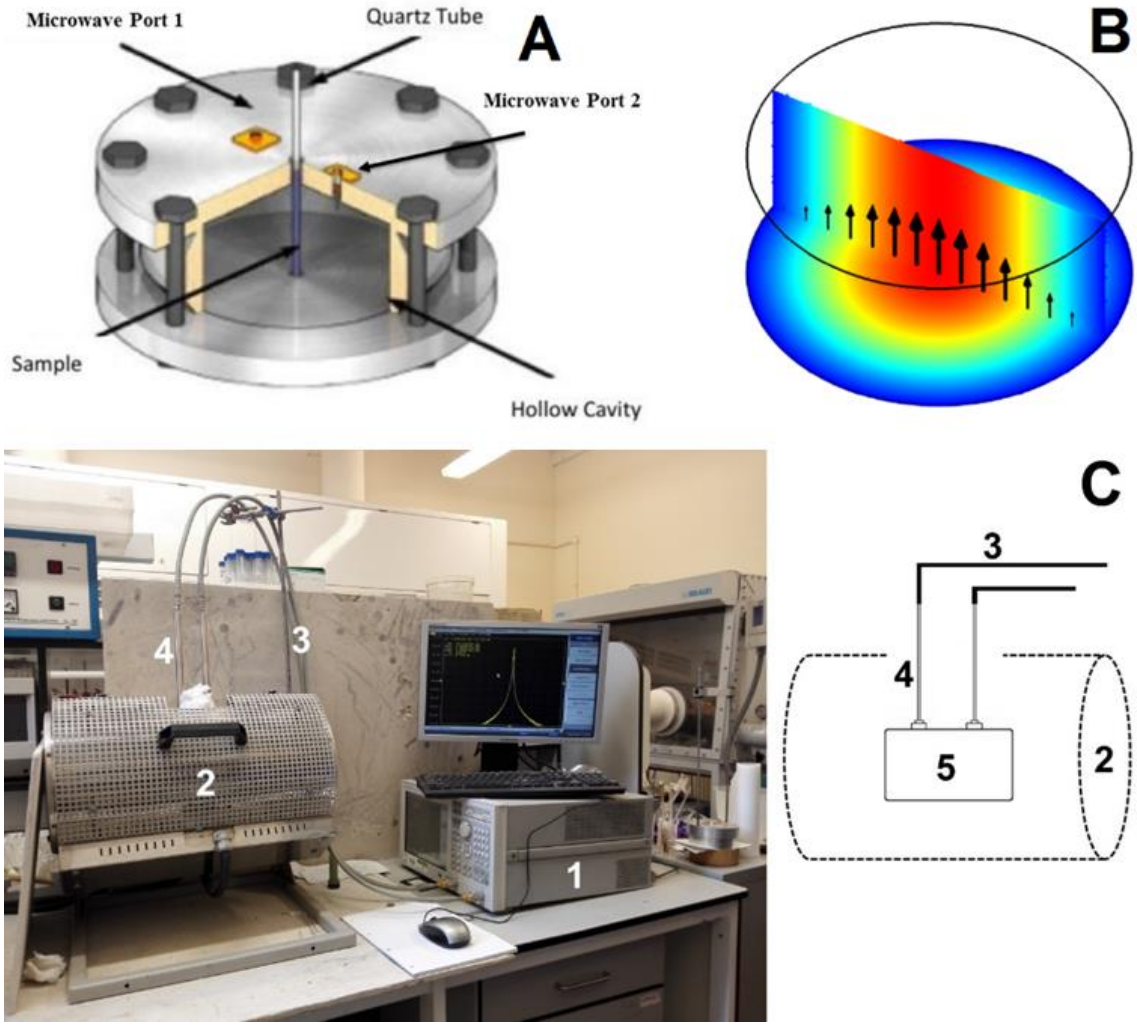


Figure 2.10. Microwave cavity perturbation measurement set up A) Quarter section of a perturbation cavity, cut to show the location of the sample tube. B) Finite element model of TM_{010} electric field distribution in the cylindrical cavity. High fields are shown in red. C) Experimental setup for high temperature dielectric measurement: (1) Agilent E5071B network analyser, (2) Tubular furnace, (3) Coaxial cables, (4) Stainless steel rigid coaxial cables, and (5) Copper TM_{010} cavity. (Adapt from Ref. 1 and 25).

In this thesis, two TM_{010} cavities which made of aluminium and copper respectively are used for the measurement. The measurement at room temperature is carried out in the aluminium TM_{010} cavity. For the measurement at higher temperature, a copper TM_{010} cavity is applied due to the limitation of the aluminium TM_{010} cavity. The copper TM_{010} cavity was set up in a tubular furnace and carefully calibrated before the measurement. In order to avoid the temperature gradient during the measurement, the sample is pre-heat to the due temperature in another tubular furnace. The measurement is carried out in a similar approach at both room temperature and high temperature conditions which the filled quartz tube is placed in the centre of the cavity and measured using an Agilent E5071B network analyser[1].

The calibration had been carried out by measuring the permittivity of model basic n-alkanes including hexane, octane, dodecane and hexadecane with which their permittivity is well-known. The maximum error obtained is less than 5% [3].

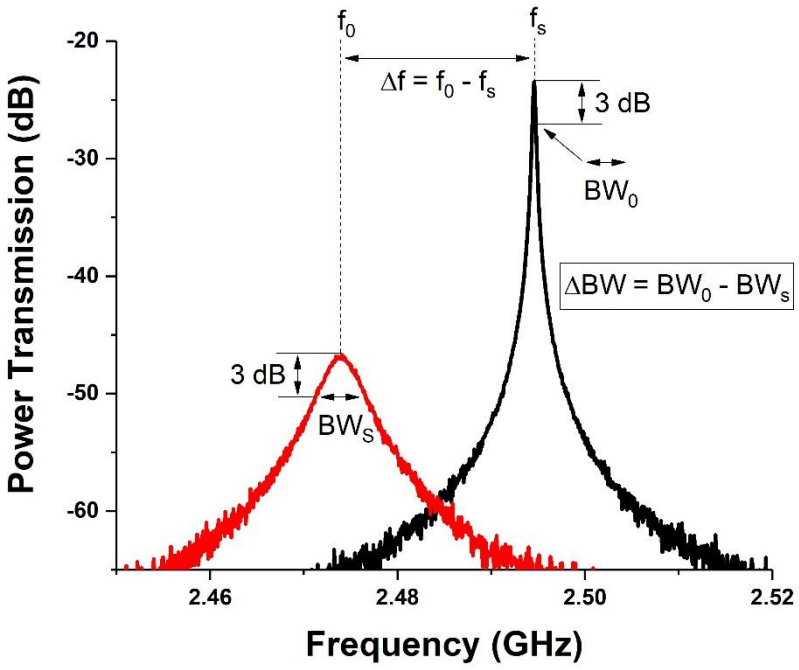


Figure 2.11. Example of microwave cavity perturbation measurement.

Figure 2.11 illustrates the example of microwave cavity perturbation measurement. When a material is placed inside the resonator, both resonant frequency and bandwidth shift according to the intrinsic dielectric properties of the sample. In the cavity perturbation measurement, the bandwidth is defined as

the correct 3 dB bandwidth as labelled in Figure 2.11. The dielectric property of the sample then can be calculated from the change in the resonant frequency Δf and bandwidth ΔBW by Eq. 2.3 and Eq. 2.4, respectively [26, 27]. The dielectric constant (ε') in Eq. 2.3 represents the ability of the catalysts to store electrical potential energy under the microwave irradiation. The dielectric loss (ε'') quantifies the efficiency with which the absorbed energy is converted into heat. The loss tangent ($\tan\delta$) defines the ability of the catalysts to convert electromagnetic energy into heat energy at a given frequency and temperature, which expressed as an equation in Eq. 2.5 [1, 28, 29].

$$\frac{\Delta f}{f_0} = (\varepsilon' - 1)AV_S \tag{2.3}$$

$$\frac{\Delta BW}{f_0} = 2\varepsilon'' AV_S \tag{2.4}$$

$$\tan\delta = \varepsilon''/\varepsilon' \tag{2.5}$$

where A is a constant determined by the size and geometry of the cavity and V_s is the effective volume of the sample in the cavity. Here in this thesis, the value of A is approximately 7.554×10^{-3} and V_s is about 0.12564 cm^3 for the measurement carried out in the aluminium cavity and for the measurement carried out in the copper cavity, the value of A is approximately 7.114×10^{-3} and V_s is about 0.0314 cm^3 for the measurement[1].

Bibliography:

1. X. Jie, S. Gonzalez-Cortes, T. Xiao, J. Wang, B. Yao, D. R. Slocombe, H. A. Al-Megren, J. R. Dilworth, J. M. Thomas and P. P. Edwards, *Angewandte Chemie International Edition*, 2017, 56, 10170-10173.
2. S. Gonzalez-Cortes, D. Slocombe, T. Xiao, A. Aldawsari, B. Yao, V. Kuznetsov, E. Liberti, A. Kirkland, M. Alkinani and H. Al-Megren, J. M. Thomas and P. P. Edwards, *Scientific Reports*, 2016, 6, 35315.
3. A. M. Aldawsari, *Dielectric measurements and catalytic cracking of heavy oils using advanced microwave technologies*, Thesis, 2017.
4. W. Engewald and K. Dettmer-Wilde, *Theory of Gas Chromatography*, Springer-Verlag Berlin Heidelberg, 2014.
5. T. Holm, *Journal of Chromatography A*, 1999, 842, 221-227.
6. J. G. Sevcik, *Detectors in gas chromatography*, Elsevier, 2011.
7. The Thermal Conductivity Detector, available at http://www.ecs.umass.edu/eve/facilities/equipment/Agilent6890/The%20Thermal%20Conductivity%20Detector.pdf.
8. J. Sneddon, S. Masuram and J. Richert, *Analytical Letters*, 2007, 40, 1003-1012.
9. F. Douglas, GC/MS Analysis, (http://www.scientific.org/tutorials/articles/gcms.html).
10. Y. Waseda, E. Matsubara and K. Shinoda, *X-ray diffraction crystallography: introduction, examples and solved problems*, Springer Science & Business Media, 2011.
11. M. M. Woolfson and M. M. Woolfson, *An introduction to X-ray crystallography*, Cambridge University Press, 1997.
12. X. Du, *Catalysis for CO_2 activation reactions with light alkanes*, Thesis, 2016.
13. B. J. Inkson, G. Hübschen, I. Altpeter, R. Tschuncky and H.-G. Herrmann, *Materials Characterization Using Nondestructive Evaluation (NDE) Methods*, Woodhead Publishing, 2016, pp. 17-43.

14. B. Cheney, *Introduction to scanning electron microscopy*, Materials Engineering department San Jose State University, 2007.

15. J. C. Russ, *Fundamentals of Energy Dispersive X-Ray Analysis: Butterworths Monographs in Materials*, Butterworth-Heinemann, 2013.

16. D. B. Williams and C. B. Carter, in *Transmission electron microscopy*, Springer, 1996, pp. 3-17.

17. P. Gabbott, *Principles and applications of thermal analysis*, John Wiley & Sons, 2008.

18. G. S. Bumbrah and R. M. Sharma, *Egyptian Journal of Forensic Sciences*, 2016, 6, 209-215.

19. Theory of Raman scattering, available at http://bwtek.com/raman-theory-of-raman-scattering/.

20. B. Schrader, *Infrared and Raman spectroscopy: methods and applications*, John Wiley & Sons, 2008.

21. M. S. Dresselhaus, A. Jorio, M. Hofmann, G. Dresselhaus and R. Saito, *Nano Letters*, 2010, 10, 751-758.

22. A. C. Ferrari and J. Robertson, *Philosophical Transactions of the Royal Society of London A: Mathematical, Physical and Engineering Sciences*, 2004, 362, 2477-2512.

23. Agilent Technologies, *Agilent Basics of Measuring the Dielectric Properties of Materia*, 2006.

24. D. Slocombe, A. Porch, E. Bustarret and O. A. Williams, *Applied Physics Letters*, 2013, 102, 244102-244104.

25. J. A. Cuenca, E. Thomas, S. Mandal, O. Williams and A. Porch, *Carbon*, 2015, 81, 174-178.

26. A. Porch, D. Slocombe, J. Beutler, P. P. Edwards, A. Aldawsari, T. Xiao, V. Kuznetsov, H. Almegren, S. Aldrees and N. Almaqati, *Applied Petrochemical Researc*h, 2012, 2, 37-44.

27. S. Li, C. Akyel and R. G. Bosisio, *IEEE Trans. Microwave Theory Technology*, 1981, MTT-29, 1041-1048.

28. P. Lidstrom, J. Tierney, B. Wathey and J. Westman, *Tetrahedron*, 2001, 57, 10229.

29. S. A. Galema, *Chemical Sociaty Review*, 1997, 26, 233-238.

Chapter 3

Microwave-initiated Dehydrogenation of Hexadecane for High-purity Hydrogen Production

Overview

This chapter[1] describes the discovery of using microwave-initiated catalysis for high-purity hydrogen production through hexadecane ($C_{16}H_{34}$) dehydrogenation[1]. An earth abundant Fe and Ni catalyst supported on silicon carbide was designed for this process. As a result, a H_2 production selectivity from all evolved gases of some 98%, is achieved with less than a fraction of a percent of adventitious CO and CO_2. The major co-product is solid, elemental carbon.

3.1 Introduction

It is important to remark that there is a presumed need to phase out fossil-derived fuels and equally to phase-in low carbon energy sources, including hydrogen[2-10]. One of the principal reasons why progress towards the hydrogen economy[3, 11, 12] has been so slow is due to the fact that there is no readily available large scale source of "natural" hydrogen. Furthermore, to date, no reliable means exists for storing hydrogen so that it can be rapidly released on demand for a fuel cell application.

Almost all the hydrogen that is produced nowadays worldwide, for industrial purposes comes from the steam reforming, partial oxidation and autothermal reforming of natural gas and, to a lesser degree, from the gasification of coal. All generate a vast amount of carbon dioxide[13-18] in the technological

[1] The work described in this chapter is reproduced and modified from my publications in 2017, in *Angewandte Chemie* entitled ''Rapid Production of High-Purity Hydrogen Fuel through Microwave-Promoted Catalytic Dehydrogenation of Liquid Alkanes with Abundant Metals''; and in 2018, in *Energy & Environmental Science* entitled ''The decarbonisation of petroleum and fossil hydrocarbon fuels for the production and storage of hydrogen''.

chain of the process. In relation to so-called green hydrogen production methods, extensive work involving principally solar radiation (as well as wind and other natural renewable energy sources) has been carried out to produce hydrogen by splitting water either via photo-assisted processes or by electrolysis[19-22], Unfortunately, these important methods suffer from relatively low efficiency and durability as compared to, say, the steam reforming of methane[23, 24]. These are, therefore, inhibiting grand challenges central to the decarbonization basis of future hydrogen energy economy.

CO_2-free hydrogen production from hydrocarbons via thermal, catalytic decomposition has been developed in pioneering work by Steinberg[13, 14] and Muradov[15, 16]and co-workers. More recently, this was also achieved through the use of microwave pyrolysis[25-27], plasma processing [28, 29] and the use of catalytic molten metals[30, 31] for the direct conversion of methane to hydrogen and separable carbon. Here, we demonstrate that microwave–initiated deep dehydrogenation of hexadecane ($C_{16}H_{34}$) using the earth-abundant, inexpensive metal catalysts iron or nickel, on alloys of these metals, supported on silicon carbide, provides a highly effective and rapid route to the production of high-purity hydrogen.

3.2 Experimental

The catalysts used in this study were based on iron and nickel as the cheap and earth abundant materials and are more likely to meet economic and environmental constraints. The catalyst was prepared by an incipient wetness impregnation method, where $Fe(NO_3)_3{\cdot}9H_2O$ (Iron (III) nitrate nonahydrate, Sigma-Aldrich) and $Ni(NO_3)_2{\cdot}6H_2O$ (Nickel (II) nitrate hexahydrate, Sigma-Aldrich) were used as metal precursor and SiC (Silicon Carbide, Fisher Scientific) was used as the support material. Catalysts with 5 wt.% metal content were prepared.

The microwave-initiated catalytic dehydrogenation of hexadecane was investigated using a purpose-built microwave cavity system embedded within a trickle-column reactor containing the supported metal catalysts. The resulting products were analysed quantitatively by gas chromatography (GC).

The pre- and post- reaction catalysts were carefully characterised via a variety of techniques including x-ray diffraction (XRD), scanning electron microscopy (SEM) and high-resolution transmission electron microscopy (HRTEM). The dielectric properties of prepared iron and nickel catalysts

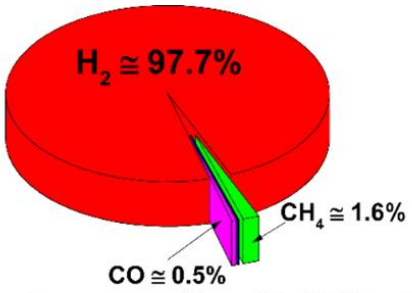
supported on SiC were measured in both room temperature and high temperature via microwave cavity perturbation measurements.

The complete experimental process is outlined in Chapter 2 in details.

3.3 Results and discussion

3.3.1 Microwave-initiated catalytic dehydrogenation of hexadecane

Upon exposure to microwaves, the liquid hexadecane feedstock was rapidly and deeply dehydrogenated to H_2, solid carbon and minor products (Figure 3.1). The results were described in terms of the volume % (or selectivity) of the product composition in the exit gases. We selected hexadecane ($C_{16}H_{34}$) as the prototypical alkane for our detailed study, because of its close similarity to hydrocarbon components of diesel. A high purity H_2 stream was obtained for the microwave initiated Fe catalysed dehydrogenation of hexadecane. Using Ni catalysts or an alloy of Fe and Ni showed even higher H_2 selectivity. The highest H_2 selectivity was observed with a Fe-Ni alloy catalyst, reaching levels of ca. 98 vol.%. Near zero levels of CO_x were produced (detected by GC at only ca. 0.5 vol.%).



$$C_nH_{2n+2} \xrightarrow[MW]{[Catalyst]} nC + (n+1)H_2$$

Evolved gas composition of Fe-Ni/SiC catalyts

Catalyst	H_2 [Vol%]	Methane [Vol%]	Ethylene [Vol%]	Small Alkanes (C_2-C_5) [Vol%]	CO_2 [Vol%]	CO [Vol%]
Fe/SiC (5)	93.1	2.2	0.7	0.6	0.2	3.2
Ni/SiC (5)	96.6	1.4	0.1	0.1	0.1	1.7
Fe-Ni/SiC (5,5)	97.7	1.6	0.1	0.1	0.0	0.5

Figure 3.1. Evolved gas composition of representative catalysts for microwave-promoted dehydrogenation of hexadecane ($C_{16}H_{34}$). The results showed three catalysts of 5 wt.% Fe/SiC, 5 wt.% Ni/SiC and 5 wt.%-Fe, 5 wt.%-Ni FeNi/SiC. The catalyst was mixed with 0.5 mL of hexadecane and the sample was subjected to microwave irradiation for 30 minutes.

The data for a representative 'time-on-stream' experiment for Fe/SiC catalyst mixed with hexadecane are illustrated in Figure 3.2. High-purity hydrogen was rapidly evolved from the onset of the microwave–initiated catalytic dehydrogenation. The hydrogen concentration rapidly increased over a period of ca. 90 seconds to reach 96 vol. % in the evolved gases. Such a rapid evolution of hydrogen could help solve the challenge of slow start-up found for on-board steam reforming or partial oxidation of methane, for example, and enable an instant H_2 supply for fuel cell vehicles. We note that although, the reactions were immediately taken place from the start of microwave, it still took few minutes to reach the optimal conditions (over 95 vol% hydrogen selectivity) due to the heated up of catalyst (microwave receptors) in interaction with induced microwave electric field.

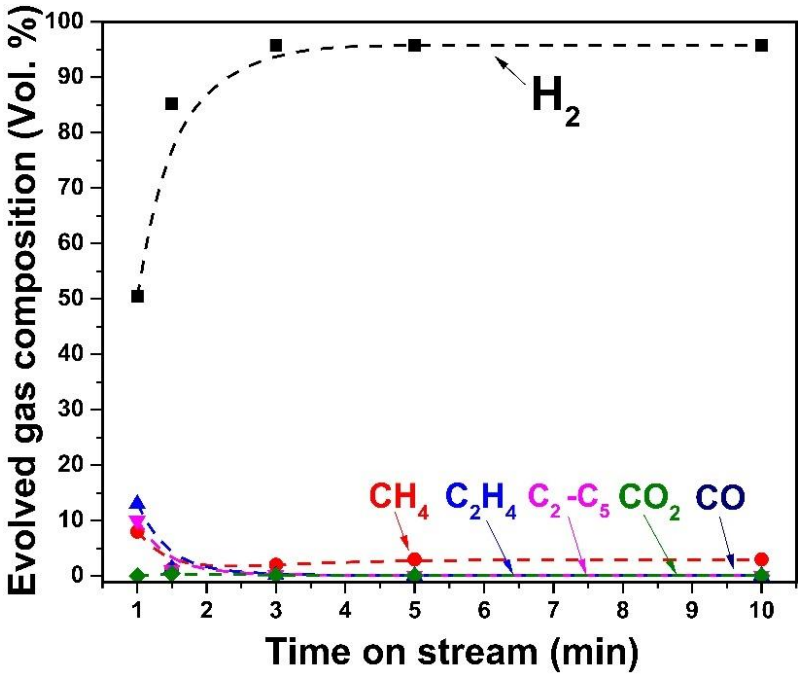


Figure 3.2. A representative experiment with 0.5 mL hexadecane @ 5 wt.% Fe/SiC catalyst for 'time-on-stream' evaluation. Each microwave irradiation experiment was carried out for 30 minutes and the gaseous products were collected and analysed after 1, 1.5, 3, 5 and 10 minutes.

Importantly, the catalyst system can also function efficiently in the deep dehydrogenation of hexadecane for several catalytic cycles through successive additions of fresh aliquots of substrate to the reactor system; a typical sequence is shown in Figure 3.3. Through successive cycles of the catalytic reaction, both the amount of evolved hydrogen and its selectivity gradually decreased, whilst corresponding methane and ethylene concentrations gradually increased. We attribute this to advancing

carbon deposition on the metal catalyst active sites, as will be evident in our electron microscopy studies. Importantly, although less hydrogen was produced in the later cycles, the catalyst still remained active through the 5 cycles of substrate additions.

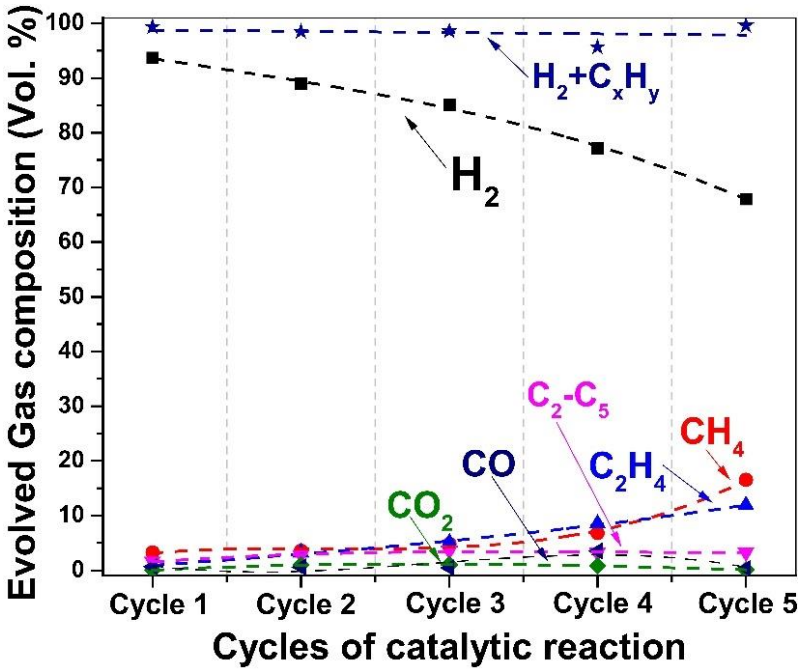


Figure 3.3. Recharging catalytic cycles for 0.5 mL hexadecane @ 5 wt.% Fe/SiC catalyst. 0.5 mL hexadecane was added for each successive cycle (30 min irradiation)

3.3.2 Microwave heating vs. conventional thermal heating

At the outset it is important to establish the key differences between conventional and microwave (MW) heating. In a conventional heating process, thermal energy is transferred through convection, conduction and radiation of heat from the outer surfaces of a container and into the material itself, in the present case, hexadecane. In contrast, microwave energy is delivered directly to the (microwave) absorbing component through molecular and in the case of metallic catalyst particles – conduction electron interactions with the electromagnetic field. In heat transfer, energy is transferred due to thermal gradients by conventional heating. However, in microwave heating, electromagnetic energy is transferred, and heat is instead generated within the sample by electromagnetic coupling through a variety of charge-dynamical processes. This fundamental and difference results in important advantages in using microwaves to initiate the catalytic dehydrogenation of hydrocarbon fuels.

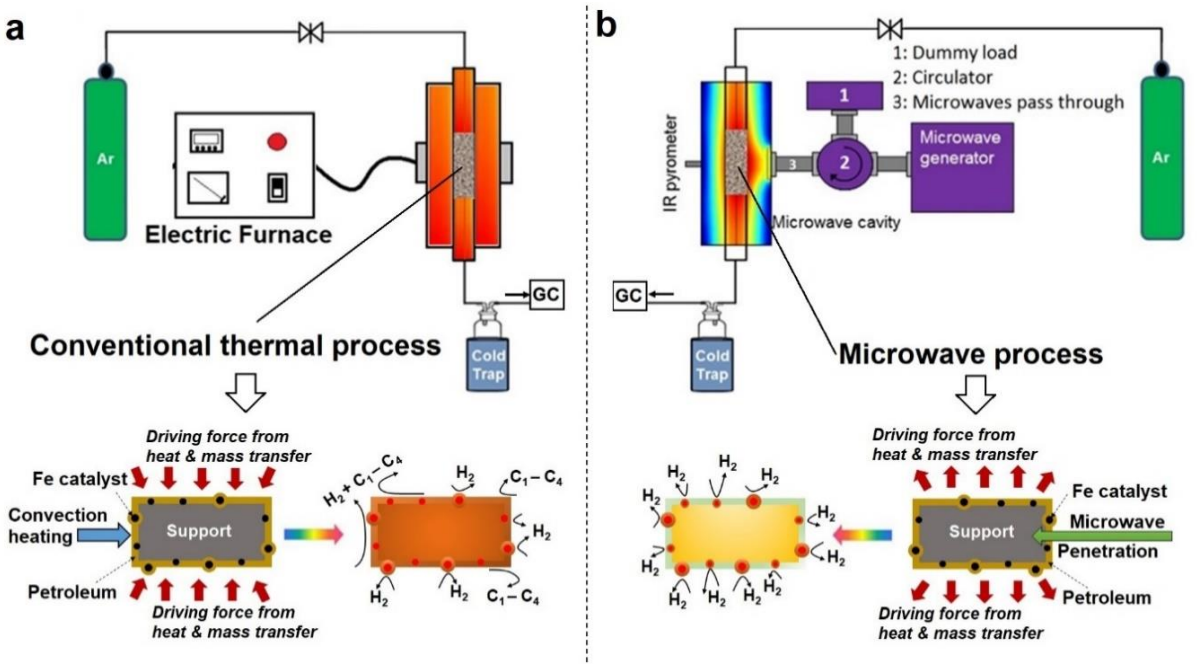


Figure 3.4. Comparison of microwave and thermal system. **(a)** conventional thermal system **(b)** microwave system.

Compared to the conventional heating process in which the iron catalyst is gradually heated up by convection heating, the microwave irradiation interacts directly with the iron catalysts without significantly heating up the bulk of the hydrocarbon feedstock (Figure 3.4). This causes a rapid heating of the catalyst particles and potentially increases the resulting product selectivity. In addition, the applied microwave field can induce a temperature gradient over the metal catalyst's surface that enhances molecular diffusion and improves the transport of the active species in a reaction system[32, 33], which subsequently changes the overall reaction rate under microwave conditions as compared with conventional heating.

The difference in the microwave and thermal heating process is also evident in heat transfer[33]. Under microwave irradiation, the iron catalyst particle heats rapidly and transfers such heat from the iron catalyst itself to the surrounding support and substances. In contrast, in a conventional thermal process, the heat transfer is initiated from the surroundings then ultimately to the metal catalyst based purely on convection heating. This heat transfer through the medium finally raises the temperature of an iron catalyst particle above that of its surroundings to the appropriate catalytic reaction temperature. Under MW irradiation, it will be demonstrated that this initiation process minimises the catalytic side reactions

whilst increasing the hydrogen selectivity. In contrast, under classical convection heating, the temperature of the surroundings is higher than the catalyst as the process begins. Thus, the host substance (here the hydrocarbon) could either self-decompose or decompose over the catalyst/ support and leads to different products. This important aspect was demonstrated by comparing microwave method and conventional thermal method for hexadecane dehydrogenation (Figure 3.5).

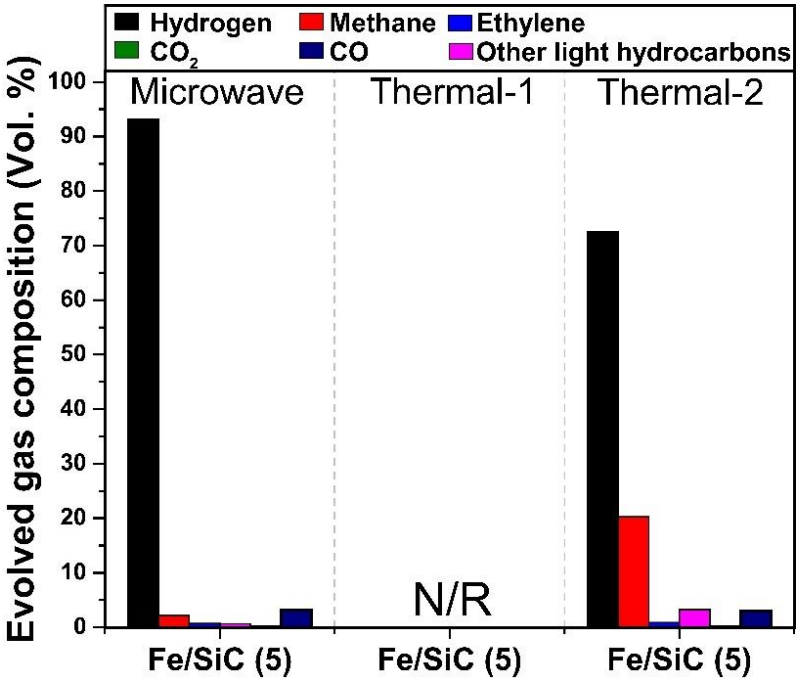


Figure 3.5. Comparison of microwave and conventional thermal method. For the microwave method, the average and the highest temperature recorded were 462 °C and 617 °C, respectively. For the thermal-1 method, A hexadecane pre-loaded Fe/SiC sample was subjected to a pre-heated furnace (550 °C), while in the thermal-2 method, the Fe/SiC catalyst (without fuel) was pre-heated in the furnace to 550 °C and the liquid hexadecane was then carefully introduced to the hot catalyst bed by a syringe. 'N/R' means no reaction was observed under these conditions. The number in parentheses after catalyst shows the iron content, wt. %.

Compared to the microwave-initiated catalytic dehydrogenation of hexadecane experiments, a set of thermal dehydrogenation reactions were investigated through two different procedures (Figure 3.5). Labelled Thermal-1, an hexadecane pre-loaded Fe/SiC sample was subjected to a pre-heated furnace (550 °C), while in the Thermal-2 procedure, the Fe/SiC catalyst (without fuel) was pre-heated in the furnace to 550 °C and the hexadecane was then carefully introduced to the hot catalyst bed by a syringe. The lack of H_2 formation over the hexadecane pre-loaded Fe/SiC catalyst under conventional thermal reaction conditions (Thermal-1), but very high yield of H_2 under microwave irradiation illustrates that

the high H_2 selectivity obtained over metal/SiC catalyst is strongly dependent on the use of microwaves. The reactions may be catalysed by microwaves at the temperature below the (bulk) boiling point of the fuel, while the thermal process necessarily gives rise to fuel vaporization before any dehydrogenation on the catalyst surface. A second hypothesis could be that the rapid heating of microwave energy converts part of the hydrocarbons before losing the liquid by vaporisation, suggesting that two main processes are taking place simultaneously: vaporization and chemical reactions. Vaporization predominates in the thermal experiment because of slow heating of the catalyst particle, whilst the microwave-promoted catalysis proceeds rapidly, probably as a consequence of the rapid heating of the particles by microwave radiation. Although, the Fe/SiC catalyst can clearly catalyse the dehydrogenation of hexadecane when pre-heated (Thermal-2), the hydrogen selectivity is noticeably different. However, it should be noted also that the temperature of 'hot spots' formed on catalysts' surface could be much higher than 550 °C and products distribution could be varied with higher temperature in conventional thermal conditions. Future studies that take into account the thermal heating at different higher temperature are planned in order to make a more realistic comparison with microwave and especially for the local temperatures over 'hot spots'.

Unlike conventional thermal Fluid Catalytic Cracking (FCC), the results show that the cleavage of C-H bonds is preferred upon microwave irradiation or promotion. Our previous studies suggested that the scission of C-H bonds during dehydrogenation could take place through a consecutive mechanism[34]. Dehydrogenation steps occur on the metal catalyst surface to give adsorbed intermediates before the cleavage of C-H. Adsorbed species with metal-C bonds and subsequent cleavage of C-H leads to the formation of H_2 and carbon. Meanwhile, the minor products of small hydrocarbons may be generated through the hydrogenation of developing carbon residues or directly via a cracking process[35, 36]. Clearly, further studies are needed to ascertain the precise catalytic processes.

The presence of high frequency electromagnetic fields makes microwave systems more complex and challenging to understand[37]. It is considered that the extremely high hydrogen selectivity obtained in these studies may be a direct result of the intrinsic response of the metal catalysts under microwave irradiation. Furthermore, the applied microwave electric field causes highly non-uniform field distributions in the catalyst bed, leading to regions of high electric field on the surfaces of metal particles

on the SiC, consequently, both an (induced) electron-rich and strong polar medium can be created that could enhance the polarisation of, for example, a C-H bond and subsequently the hydrogen formation. The complete cleavage of C-H via two mechanisms of oxidative addition and electrophilic substitution are accelerated by microwave irradiation which leads to the high hydrogen selectivity [38]. The high thermal conductivity and mechanical strength of SiC, together with a clearly reduced tendency to yield oxygenated products, are also considered important. These factors contribute by restricting the formation of by-products under microwave irradiation by avoiding any thermal degradation to the support during the reactions and quickly achieving a thermal balance in the system [39].

3.3.3 Dielectric properties of prepared catalysts

The intrinsic dielectric properties of individual metal particle catalysts are clearly a critical factor affecting its response to incident microwave irradiation. These properties have been carefully characterised by cavity perturbation measurements under both room temperature and high temperature conditions (Table 3.1 and Figure 3.7).

In the study, the measurements were carried out in TM_{010} mode at 2.494 GHz (in practice)[40]. An aluminium cavity was used for measurement performed at room temperature while a copper cavity was built for high temperature measurements. The measurements of each catalyst sample before and after reactions were tested and recorded for a minimum of five times and the average values were presented.

Figure 3.6 illustrates the resulting curve obtained via microwave cavity perturbation measurement of pre- and post- reaction 5 wt.% Fe/SiC catalysts. When the sample is applied into the cavity, the shift in resonant frequency and the change of bandwidth were observed as compared to the empty sample tube (reference). The dielectric constant (ε'), dielectric loss (ε'') and loss tangent (tan δ) of the catalyst can be then calculated based on the following Eq. 3.1-3.3[41-44]:

$$\frac{\Delta f}{f_0} = (\varepsilon' - 1)AV_S \tag{3.1}$$

$$\frac{\Delta BW}{f_0} = 2\varepsilon'' AV_S \tag{3.2}$$

$$\tan\delta = \varepsilon''/\varepsilon' \tag{3.3}$$

where A is a constant determined by the size and geometry of the cavity and V_s is the effective volume of the sample in the cavity. Here, the value of A is approximately 7.554×10^{-3} and V_s is about 0.12564 cm^3 for the measurement carried out in the aluminium cavity and for the measurement carried out in the copper cavity, the value of A is approximately 7.114×10^{-3} and V_s is about 0.0314 cm^3 for the measurement.

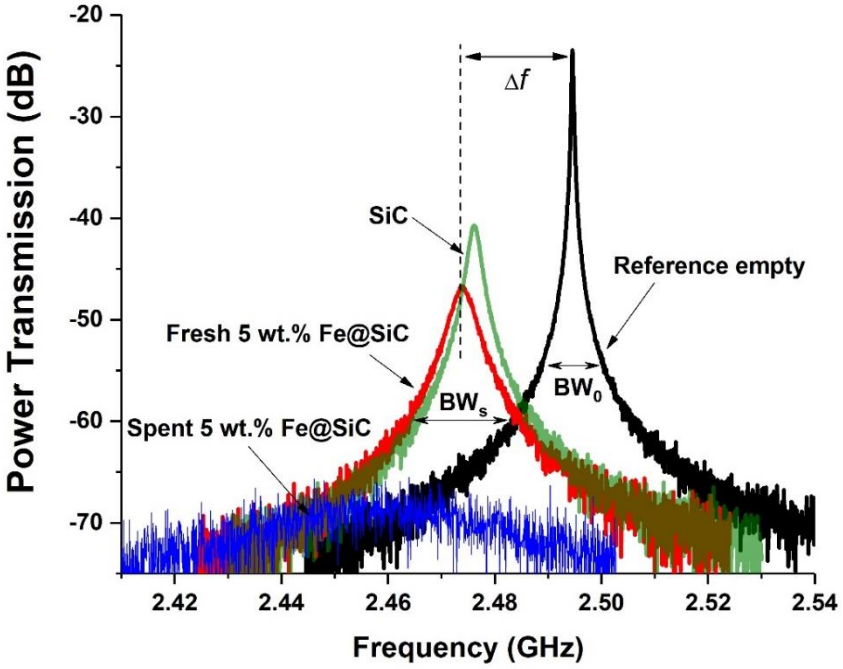


Figure 3.6. Microwave cavity perturbation measurement curve of pre- and post- reaction 5 wt.% Fe/SiC catalysts.

Table 3.1: Dielectric properties of catalysts. *: The number in parentheses after catalyst shows the metal content, wt. %. The values given show an average of at least 5 times individual tests.

Catalyst*	Dielectric constant (ε')	Dielectric loss (ε'')	Loss tangent (tan δ)
Fe/SiC (5)	12.86	1.47	0.11
Ni/SiC (5)	8.95	0.49	0.06
FeNi/SiC (5,5)	10.83	0.62	0.06
Spent-Fe/SiC (5)	17.34	7.99	0.46
Spent-Ni/SiC (5)	11.94	5.02	0.42
Spent-FeNi/SiC (5,5)	14.01	8.8	0.63

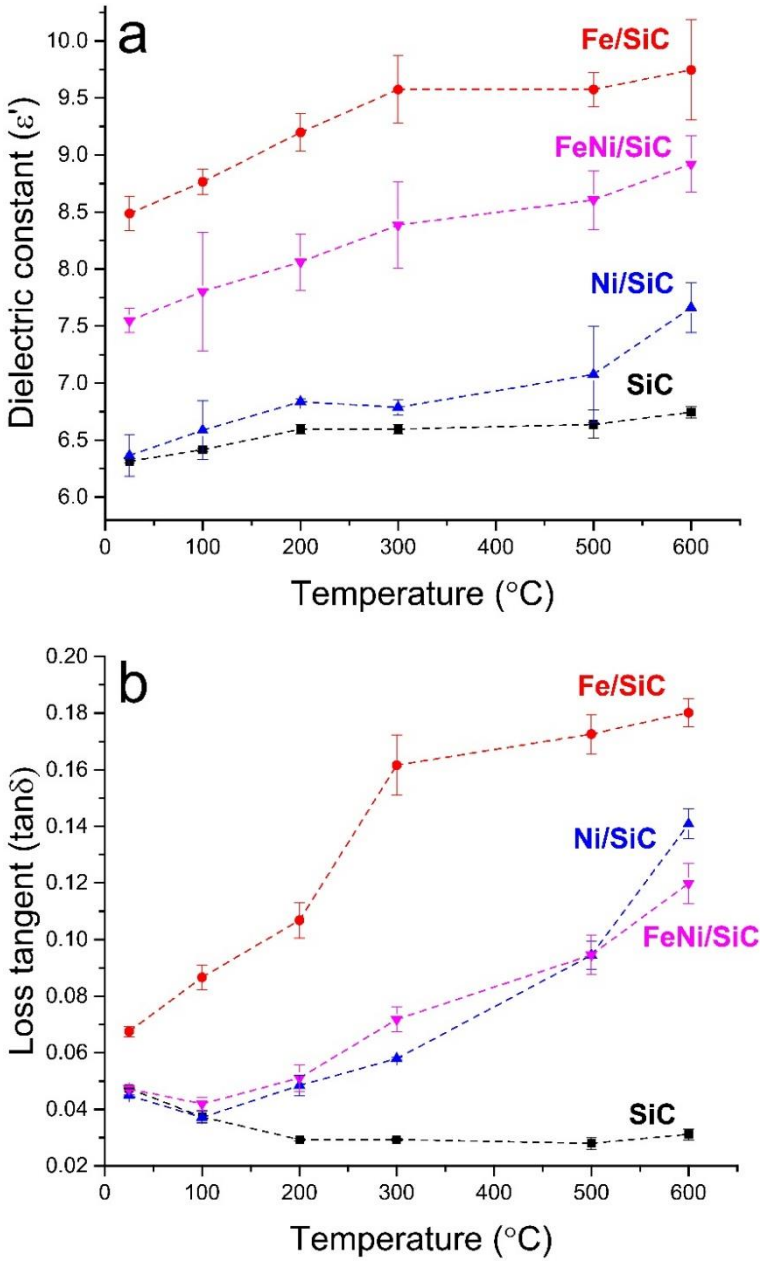


Figure 3.7. High-temperature microwave cavity perturbation measurement. (a) Delectric constant and (b) Loss tangent of representative 5 wt.% Fe/SiC, 5 wt.% Ni/SiC, 5 wt.%- 5 wt.% FeNi/SiC and SiC catalyst for the microwave cavity perturbation measurement at high temperature. The experiments were recorded every 100 °C and up to 600 °C. Error bars given show the standard deviations across different samples.

Although no simple dependency has been found between the so-called loss tangent and the product distributions, microwave irradiation clearly gives higher product selectivity as compared to conventional thermal reactions (Figure 3.5). However, the dielectric properties of the catalysts are also

temperature dependent, which could alter any trend observed at a single temperature. It was found that the dielectric property of metal catalysts showed a similar trend with increasing temperature. A higher loss tangent ($\tan\delta$) was obtained at higher temperatures, but no clear differences were observed for the dielectric constant (ε') (Figure 3.7). Unlike carbon based catalyst materials which can be highly efficient absorbers of electromagnetic energy, for metal/SiC catalysts, various polarisation and dissipation mechanisms clearly contribute to drive the reactions under microwave irradiation which lead to the high hydrogen selectivity[45].

3.3.4 Pre- and post- reaction analysis of catalysts

The catalyst particles were examined by X-ray Diffraction, scanning electron microscopy and high-resolution transmission electron microscopy both before and after microwave treatment. Metallic iron, nickel and iron-nickel alloy particles, having typical particle diameters less than 150 nm, have been identified in fresh samples (Figure 3.8, Figure 3.12 and Figure 3.13).

Following the microwave-initiated catalytic dehydrogenation of hexadecane, multi-walled carbon nanotubes that encapsulate some of the metal nanoparticles were found (Figure 3.12 and Figure 3.13). Iron carbide was observed in spent Fe/SiC catalyst but not in FeNi/SiC catalyst, which suggests -importantly- that the presence of Ni can suppress the formation of iron carbide. These results are consistent with data obtained from XRD (Figure 3.9).

3.3.4.1 X-ray diffraction (XRD)

The catalysts of Fe/SiC, Ni/SiC, and FeNi/SiC were examined by X-ray diffraction (XRD) before (Figure 3.8) and after (Figure 3.9) the dehydrogenation of hexadecane with the assistance of microwaves. The peaks for iron at 44.79° and 65.11° were detected and corresponds to the 110 and 200 lattice planes of iron metal, respectively. The XRD pattern of the catalysts, which the catalysts were obtained *via* the hydrogen-thermal reduction, indicates that the iron particles are pure α-Fe phase with a cubic structure (JCPDS No. 05-0696) [46]. The peaks at $2\theta = 45.50°, 53.05°$ corresponds to the Ni (111) and Ni (200) reflections [46, 47]. No characteristic peaks can be detected indicating metallic iron and nickel

separates on FeNi/SiC catalyst. The specific diffraction peaks of FeNi/SiC have shown a clear negative shift which indicates a formation of Fe-Ni alloy.

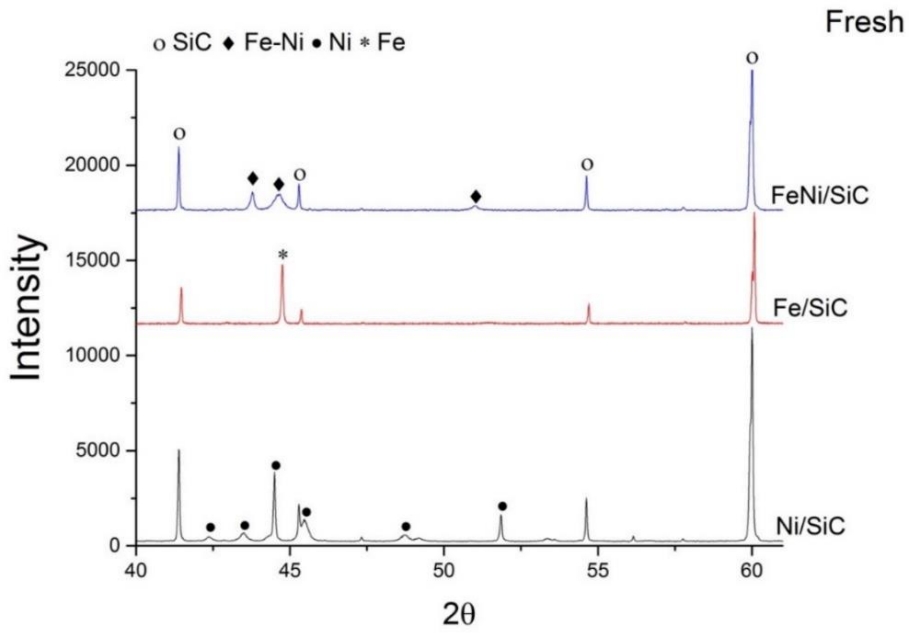


Figure 3.8. XRD pattern comparison of 5 wt.% Fe/SiC, 5 wt.% Ni/SiC, and 5 wt.%-Fe, 1 wt.%-Ni Fe-Ni/SiC catalysts before the microwave-initiated catalytic dehydrogenation of hexadecane, 2θ= 40°-50°.

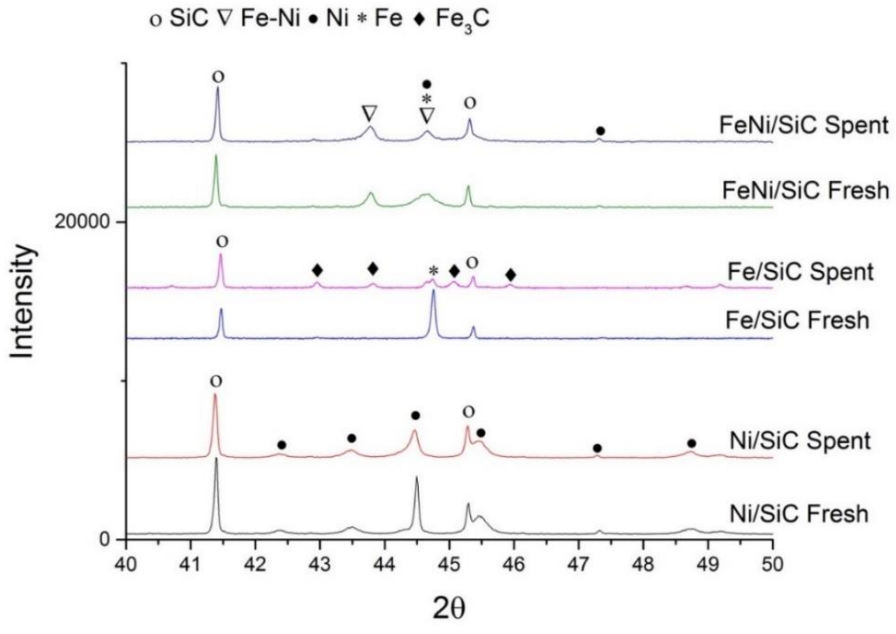


Figure 3.9. XRD pattern comparison of 5 wt.% Fe/SiC, 5 wt.% Ni/SiC, and 5 wt.%-Fe, 1 wt.%-Ni Fe-Ni/SiC catalysts before and after the microwave-promoted catalytic decomposition of hexadecane, 2θ= 40°-50°.

Figure 3.9 compared the pre- and post-reaction catalysts used for microwave-initiated catalytic dehydrogenation of hexadecane. The formation of Fe_3C was observed on Fe/SiC catalyst. The diffraction peak of iron carbide at $2\theta = 42.92°$, 43.82°, 44.72°, 45.04°, 45.9°, and 49.18° was detected. Meanwhile, no clear changes have been found on both Ni/SiC and FeNi/SiC catalyst.

3.3.4.2 Scanning electron microscopy (SEM)

The surface morphology of catalysts was pictured by scanning electron microscope (SEM). Figure 3.10 shows the SEM images comparing the Fe/SiC, Ni/SiC, and FeNi/SiC catalysts before and after the experiments. The metal particles were found uniformly dispersed on the SiC surface with a nano-scale particle size in the pre-reaction samples. The SiC is not a porous structure material and has a particle size of ca. 20-40 μm.

The images of spent catalysts show the carbon deposition on the catalysts' surface and a clear agglomeration can be observed in the spent samples. It should be noted that less agglomeration and few carbons were found in the FeNi/SiC catalysts which indicates the Fe-Ni alloy catalysts may play an important role in suppressing carbon formation as well as reducing the possibility of iron carbide formation. This has also been demonstrated in our XRD study (Figure 3.9).

In addition, the SEM images also shows the nano-scale metal particles were successfully synthesised on the SiC's surface when zoomed in to the metal particles (Figure 3.11). Moreover, Fe-Ni alloy catalysts presented a higher dispersion and smaller particle sizes than that of Fe particles observed on SiC's surface.

In the study of surface carbons obtained from hexadecane dehydrogenation, both spherical and filamentous carbons were observed in the clusters (Figure 3.11). The metal particle catalysts that were encapsulated in some multi-walled carbon nanotubes, were identified and further studied by high resolution transmission electron microscopy (HRTEM) (Figure 3.12).

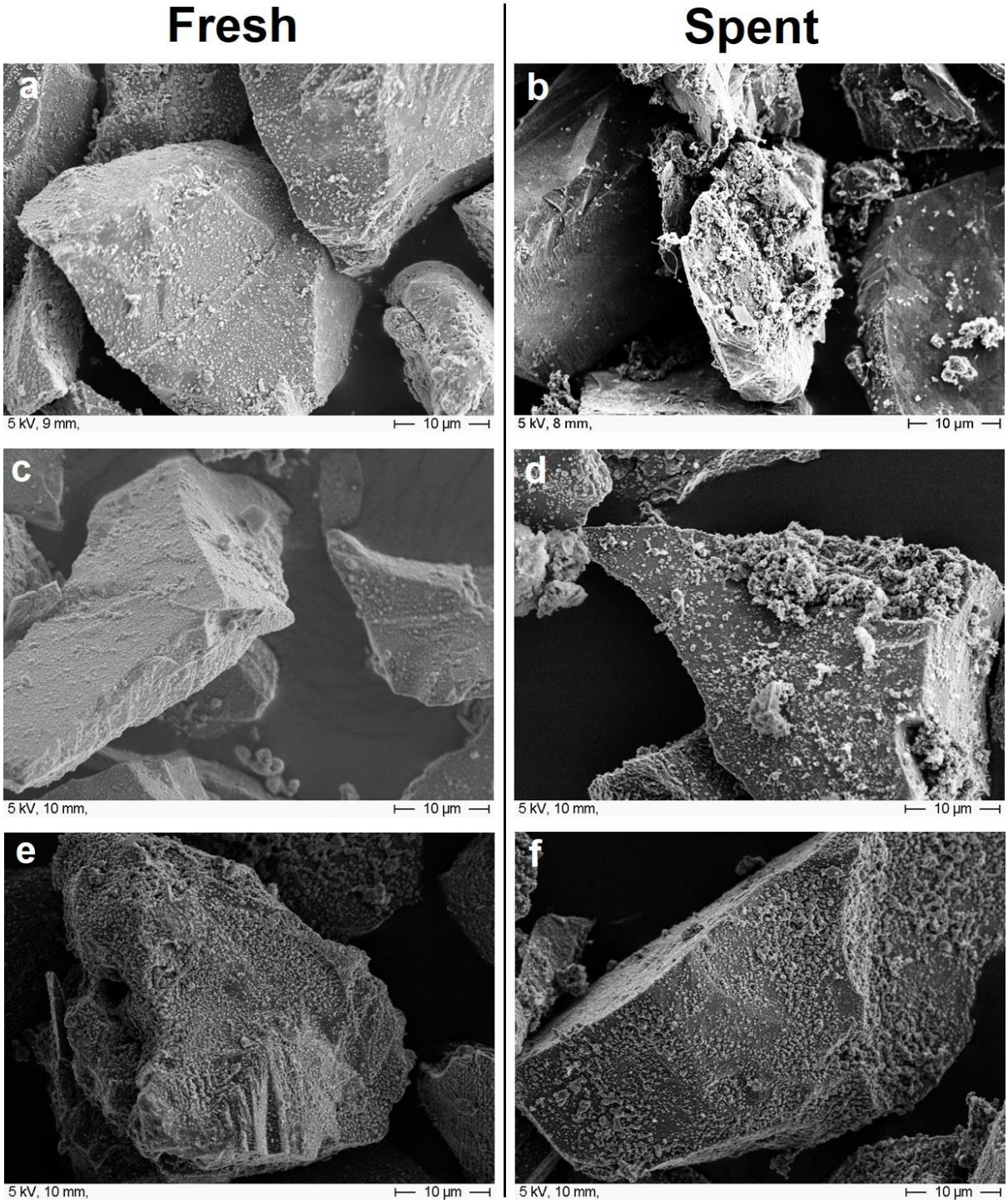


Figure 3.10. The scanning electron microscopy (SEM) images of **(a, b)** 5 wt.% Fe/SiC catalyst, **(c, d)** 5 wt.% Ni/SiC, **(e, f)** 5 wt.%-Fe, 5 wt.%-Ni Fe-Ni/SiC catalysts before and after the microwave-initiated catalytic dehydrogenation of hexadecane.

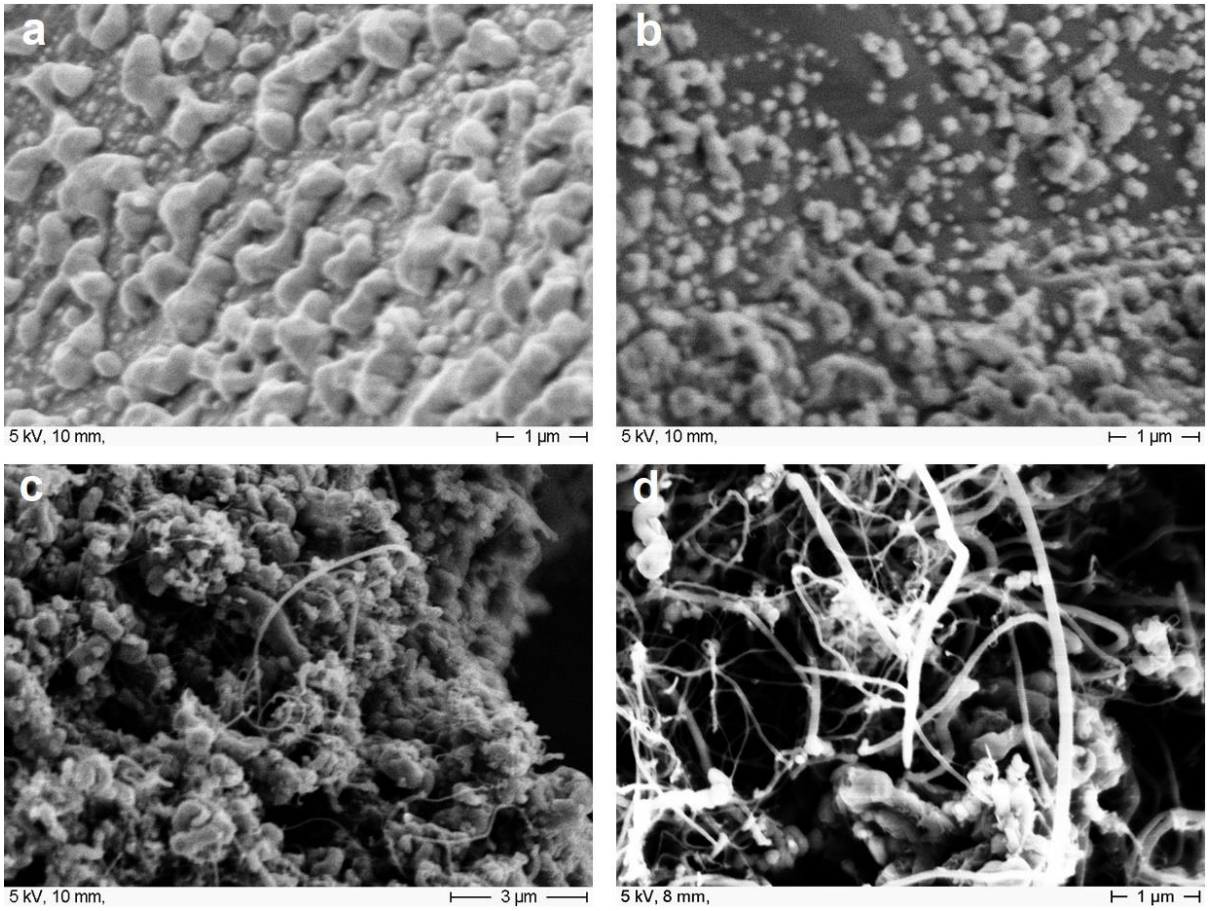


Figure 3.11. The scanning electron microscopy (SEM) images of **(a)** fresh Fe particle catalysts on SiC of 5 wt.% Fe/SiC catalyst; **(b)** fresh Fe-Ni alloy particle catalysts on SiC of 5 wt.%-Fe, 5 wt.%-Ni Fe-Ni/SiC catalysts; **(c, d)** resulting carbon residues observed after the dehydrogenation of hexadecane under microwave irradiation.

3.3.4.3 High resolution transmission electron microscopy (HRTEM)

Figure 3.12-3.14 presented the images of representative Fe/SiC, FeNi/SiC and Ni/SiC catalysts studied by high-resolution transmission electron microscope (HRTEM) before and after microwave treatment. As a result, metallic iron and iron-nickel alloy particles were identified in fresh samples, having particle diameters less than 150 nm. This is corresponding to the study of SEM and the XRD characterisation as which the crystalline size of metal particles was estimated by Sherrer Equation (Eq. 2.2).

The presence of Fe_3O_4 has also been detected by HRTEM (Figure 3.12b) in fresh Fe/SiC sample and is considered due to the aerial oxidation of iron. Energy-dispersive X-ray spectroscopy (EDS) mapping also detected the presence of oxygen on some of the iron particle surfaces which could be the source of

CO. However, importantly, adding nickel as a promoter reduced the amounts of CO found in the exit gases (Figure 3.1).

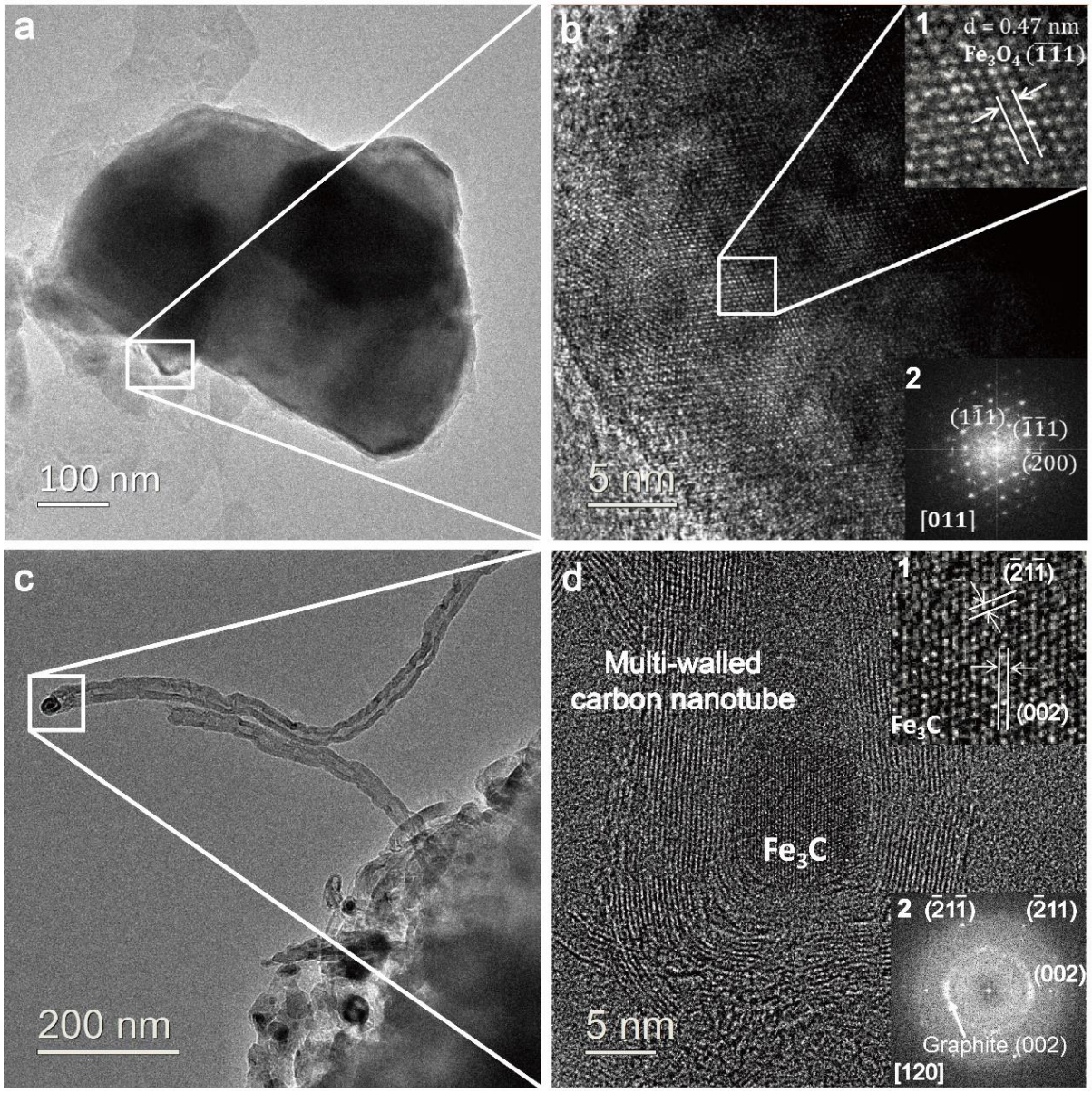


Figure 3.12. High Resolution Transmission Electron Microscopy (HRTEM) images of 5 wt.% Fe/SiC before (a, b) and after (c, d) microwave-initiated catalytic dehydrogenation of hexadecane. (a) Low magnification Transmission Electron Microscopy (TEM) images of unreacted Fe/SiC catalyst. (b) HRTEM images of unreacted catalyst recorded along a <011> zone axis of a Fe_3O_4 particle and In Figure 3.12a, the presence of Fe_3O_4 is due to the oxidation of Fe by exposure to air. (a2) Diffraction pattern calculated from images of Fe_3O_4 particles of 5 wt. % Fe/SiC, before microwave-initiated catalytic reactions. (c) Low magnification TEM images of 5 wt.% Fe/SiC after microwave treatment. (d) The HRTEM images of 5 wt.% Fe/SiC after microwave treatment. Magnified inset (f1) recorded along a <120> zone axis of a Fe_3C particle that is encapsulated in a multi-walled carbon nanotube. The power spectrum (f2) calculated from (f) shows characteristic reflections from graphite (002) plane and Fe_3C along <120> zone axis.

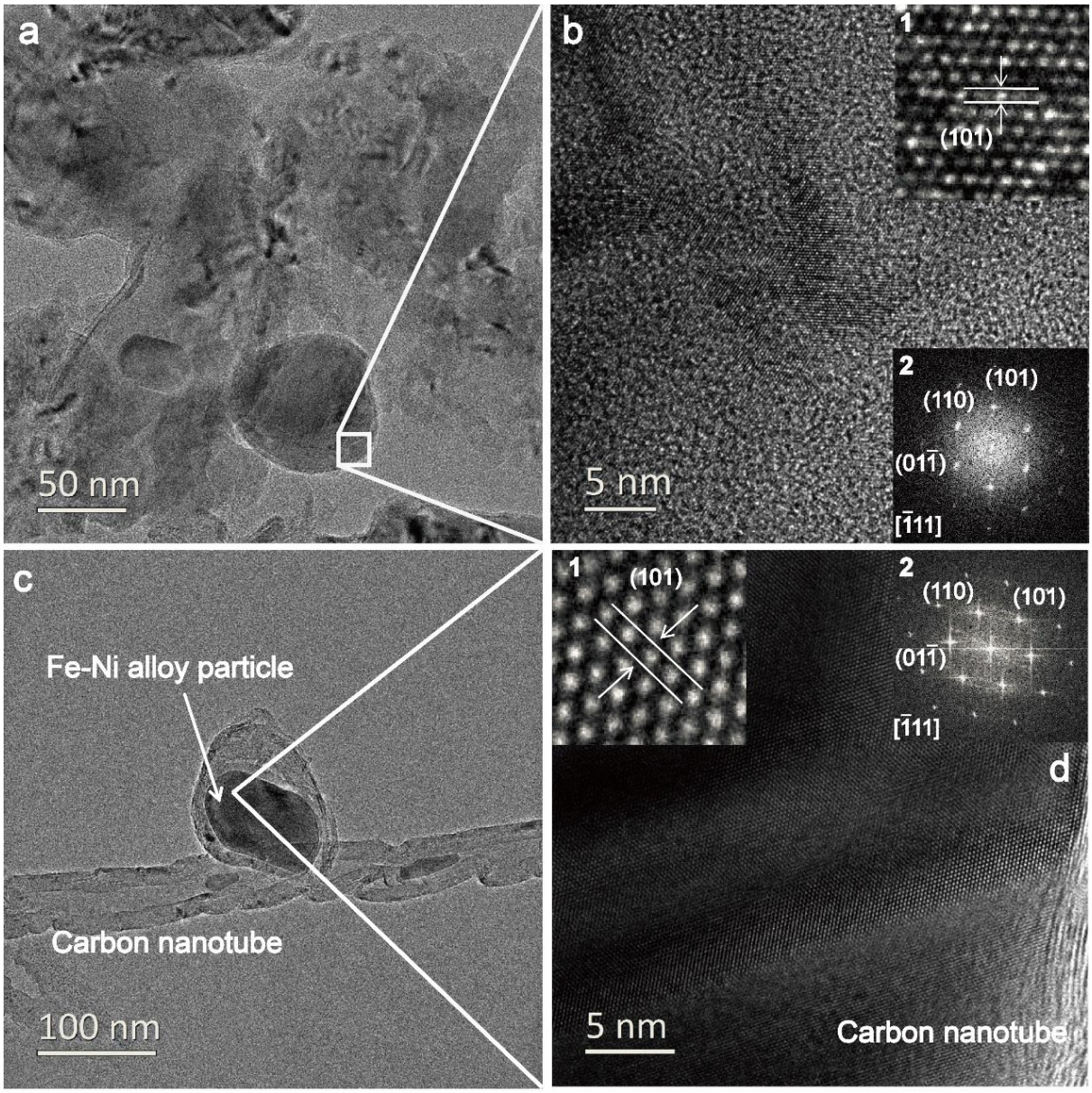


Figure 3.13. High Resolution Transmission Electron Microscopy (HRTEM) images of 5 wt.%-Fe, 1 wt.%-Ni FeNi/SiC before (a, b) and after (c, d) microwave-initiated catalytic dehydrogenation of hexadecane. (a, c) Low magnification Transmission Electron Microscopy (TEM) images of FeNi/SiC before and after microwave treatment, respectively. (b, d) HRTEM images and magnified insets (b1, d1) recorded along <$\bar{1}$11> zone axes of α-(Fe, Ni) alloy particles. The one in (d) is embedded in a carbon nanotube. The power spectra (b2, d2) calculated from (b, d) show characteristic reflections from α-(Fe, Ni) along <$\bar{1}$11> zone axes.

At the completion of microwave initiation experiments, HRTEM revealed turbostratic graphitic sheets and multi-walled carbon nanotubes (MWCNTs) that encapsulate both iron and iron carbide nanoparticles. The generation of iron carbide suggested that the supported iron particles react with the hydrocarbon during the catalytic reactions under microwave initiation (Figure 3.12d). In

comparison, there was no iron carbide was observed in spent FeNi/SiC catalyst (Figure 3.13). This importantly illustrate the effect of adding Ni can possibly avoid the formation of iron carbide and the alloy can stabilise the iron under this process.

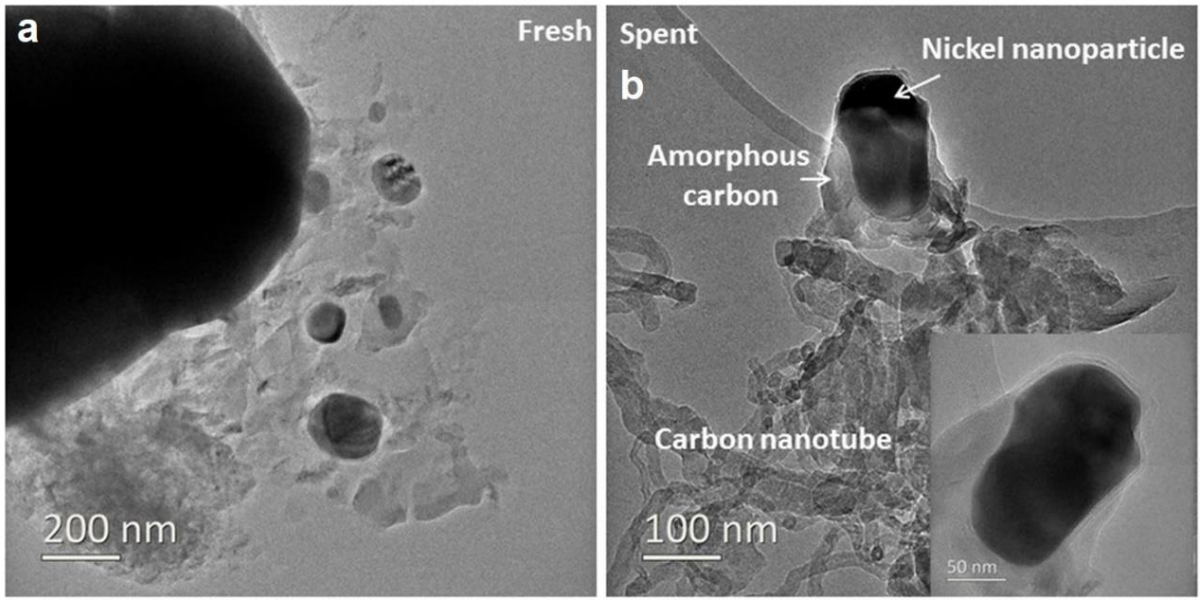


Figure 3.14. Low magnification Transmission Electron Microscopy (TEM) images of Ni/SiC (a) before and (b) after microwave treatment.

3.3.4.4 Energy-dispersive X-ray spectroscopy (EDS)

Figure 3.15 below presented the analysis of surface elemental for representative Fe/SiC catalyst by Energy-dispersive X-ray spectroscopy (EDS). As a general observation, some of the metallic iron particles were oxidised and the presence of oxygen on the surface of iron particles was detected. There is thus, providing oxygen source for CO formation that obtained through hexadecane dehydrogenation under microwave irradiation. It should be noted that the iron is very sensitive to oxygen and it is easy to be oxidised when exposed to the air. Therefore, the tiny amount of CO produced in the process cannot be avoid using metallic iron catalysts.

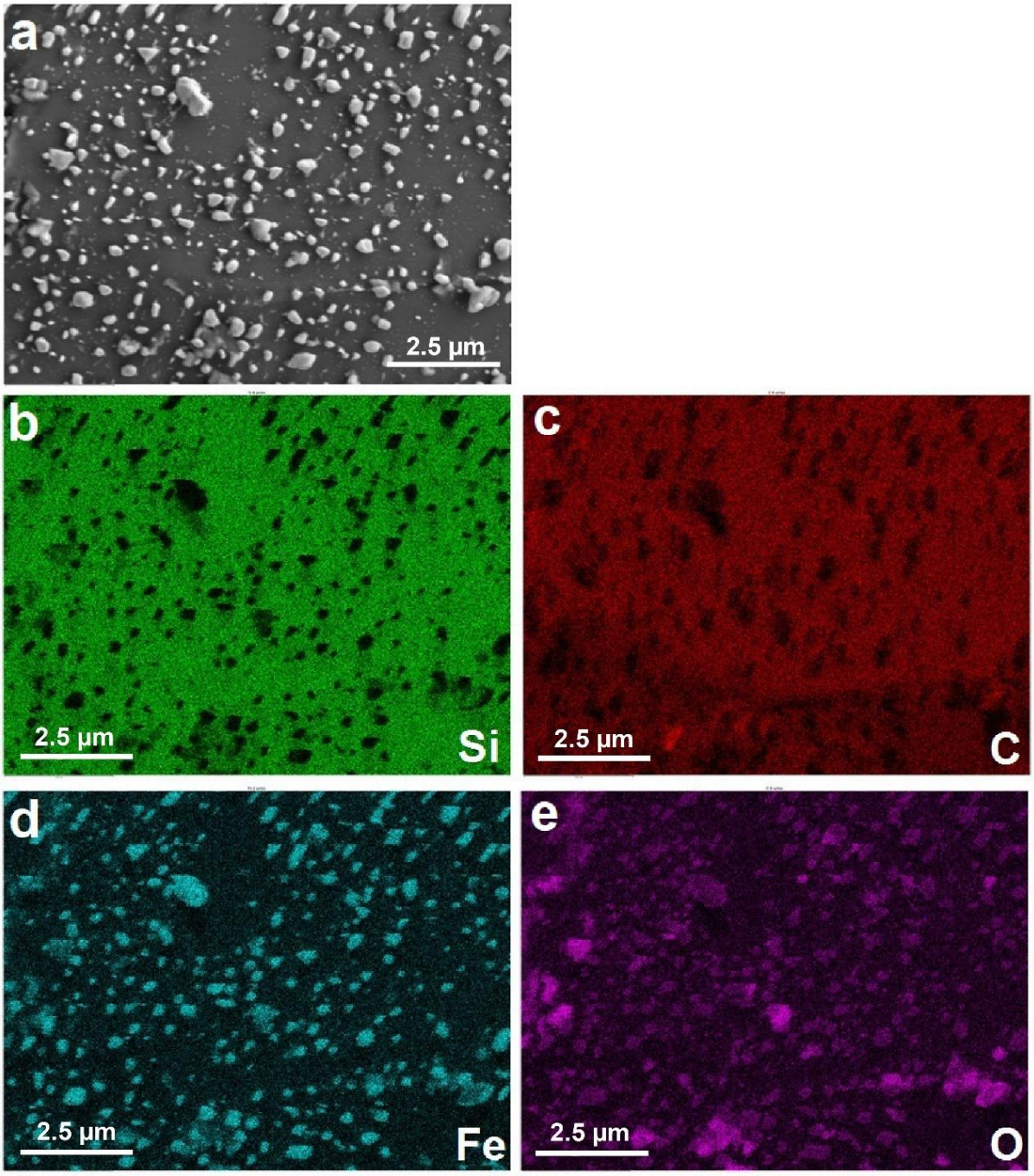


Figure 3.15. Scanning electron microscope (SEM) and Energy-dispersive X-ray spectroscopy (EDS) mapping of the elemental species on the surface of 5 wt.% Fe/SiC catalysts before microwave initiation. **(a)** SEM (backscattered electron) morphology, **(b)** Si map, **(c)** C map, **(d)** Fe map, and **(e)** O map.

3.3.5 Possible mechanisms for the microwave-initiated deep dehydrogenation using iron catalysts

A consecutive mechanism for the scission of the C-H bonds through deep dehydrogenation under microwave initiation is proposed in Figure 3.16. The applied microwave electric field induces highly

non-uniform field distributions both in the catalyst and the support material. This rapidly fluctuating incoming electric field creates an (induced) highly polar catalytic reaction within the iron particles that enhances the polarisation of, for example, a C-H bond and subsequently facilitate the cleavage of the C-H bond[34].

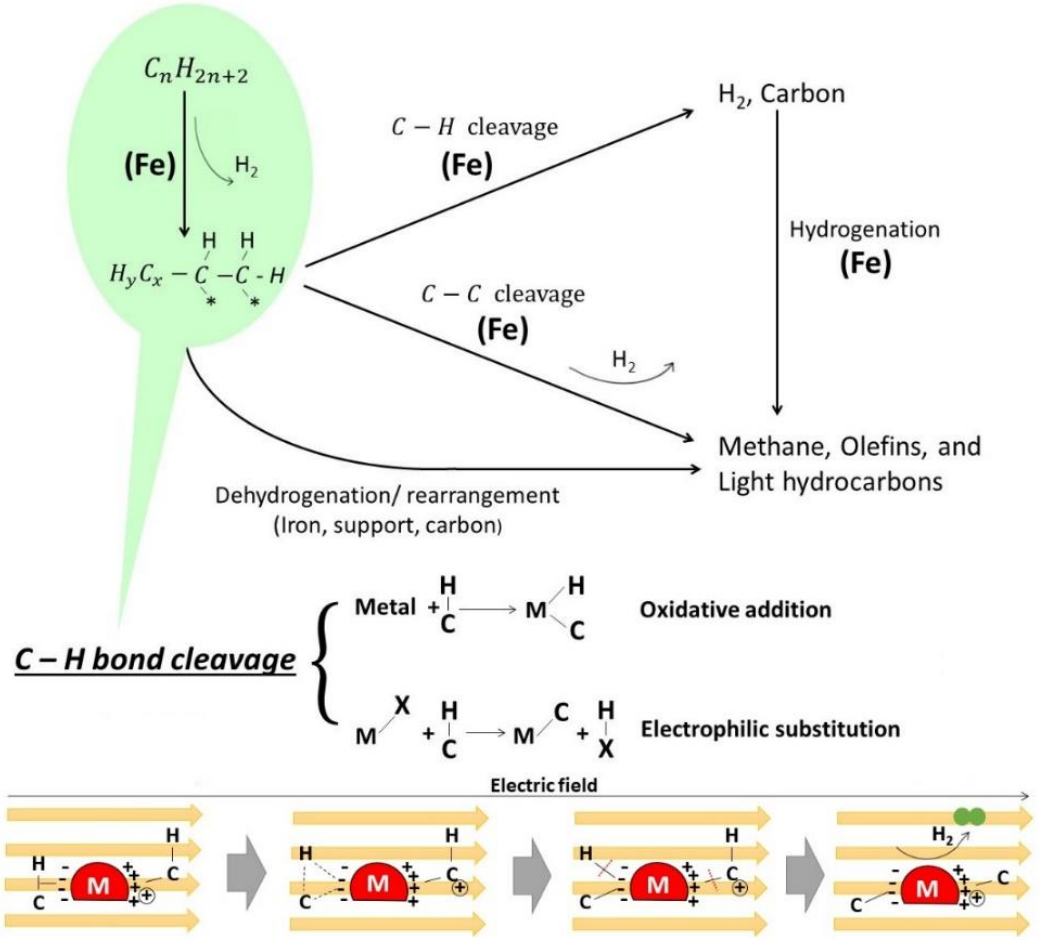


Figure 3.16. Proposed reaction pathways and selective C-H bond cleavage mechanisms for high-purity hydrogen production through microwave-initiated iron catalysed dehydrogenation of fossil fuels. (* corresponds to a surface active site of Fe).

The complete cleavage of C-H via two mechanisms of oxidative addition and electrophilic substitution are considered to be accelerated by microwave initiation which leads to the high hydrogen selectivity[34]. Oxidative addition is the most common mechanism which is typical for electron-rich, low-valent complexes of the late transition metals (Fe, Ru, Pt), by which a C – H bond cleaves and a M – C bond and a M – H bond are formed. The electrophilic substitution is usually observed for late- or post-transition metals, usually in a strongly polar medium where the hydrogen atom of the substrate has been

formally substituted by the metal centre acting as a Lewis acid[34]. Moreover, the high thermal conductivity and mechanical strength of SiC, together with a clearly reduced tendency to yield oxygenated products are also considered important. These factors contribute by restricting the formation of by-products under microwave irradiation by quickly achieving a thermal balance in the system[35], and avoiding any thermal degradation to the support during the reactions.

3.4 Conclusion

Thus, the key challenge of rapid production of, and high selectivity towards, H_2 production has been demonstrated using resonant microwave-electric field irradiation applied in a laboratory device, typically achieving >98% H_2 purity. Such a rapid and selective production of hydrogen from liquid hydrocarbon alkanes reveals a powerful new platform for hydrogen production. We believe these findings represent a new and attractive path towards a decarbonised fossil fuels economy: Thus, fluid hydrocarbon fuels are not consumed by aerial combustion as in the conventional use of fossil hydrocarbon fuel -with attendant problems of CO_2 emission. Rather these valuable hydrocarbon resources are utilised through microwave-promoted catalytic deep hydrogenation as an abundant, widespread source for the rapid production of high purity hydrogen for use in fuel cell vehicles. In this approach –suitably optimised - CO_2 would never enter the atmosphere- as in a conventional combustion process. The utilisation process yields elemental hydrogen and elemental carbon; the latter can then be readily subjected to recycling through a range of established chemical routes.

Bibliography:

1. X. Jie, S. Gonzalez-Cortes, T. Xiao, J. Wang, B. Yao, D. R. Slocombe, H. A. Al-Megren, J. R. Dilworth, J. M. Thomas and P. P. Edwards, *Angewandte Chemie International Edition*, 2017, 56, 10170-10173.
2. J. M. Thomas, *Nature Catalysis*, 2018, 1, 2.
3. J. M. Bockris, *Science*, 1972, 176, 1323-1323.
4. J. A. Turner, *Science*, 2004, 305, 972-974.
5. G. W. Crabtree, M. S. Dresselhaus and M. V. Buchanan, *Physics Today*, 2004, 57, 39-44.
6. J. Ogden, *Scientific American*, 2006, 295, 94-101.
7. P. P. Edwards, V. L. Kuznetsov, W. I. F. David and N. P. Brandon, *Energy Policy*, 2008, 36, 4356-4362.
8. K. Hirose, *Philosophical Transactions of the Royal Society of London A: Mathematical, Physical and Engineering Sciences*, 2010, 368, 3365-3377.
9. U. Eberle, B. Müller and R. Von Helmolt, *Energy & Environmental Science*, 2012, 5, 8780-8798.
10. J. Barber, *Sustainable Energy & Fuels*, 2018;2(5), 927-35.
11. S. A. Wells, A. Sartbaeva, V. L. Kuznetsov and P. P. Edwards, *Encyclopedia of Inorganic and Bioinorganic Chemistry*, 2010, 309-332.
12. L. Barreto, A. Makihira and K. Riahi, *International Journal of Hydrogen Energy*, 2003, 28, 267-284.
13. M. Steinberg and H. C. Cheng, *International Journal of Hydrogen Energy*, 1989, 14, 797-820.
14. M. Steinberg, *International Journal of Hydrogen Energy*, 1999, 24, 771-777.
15. N. Z. Muradov, *International Journal of Hydrogen Energy*, 1993, 18, 211-215.
16. N. Z. Muradov, *Energy Fuels*, 1998, 12, 41-48.
17. N. Z. Muradov, *International Journal of Hydrogen Energy*, 2017, *42*(20), 14058-14088.
18. H. Arakawa, M. Aresta, J. N. Armor, M. A. Barteau, E. J. Beckman, A. T. Bell, J. E. Bercaw, C. Creutz, E. Dinjus, D. A. Dixon, K. Domen, D. L. DuBois, J. Eckert, E. Fujita, D. H. Gibson,

W. A. Goddard, D. W. Goodman, J. Keller, G. J. Kubas, H. H. Kung, J. E. Lyons, L. E. Manzer, T. J. Marks, K. Morokuma, K. M. Nicholas, R. Periana, L. Que, J. Rostrup-Nielson, W. M. H. Sachtler, L. D. Schmidt, A. Sen, G. A. Somorjai, P. C. Stair, B. R. Stults and W. Tumas, *Chemical Reviews*, 2001, 101, 953-996.

19. H. B. Gray, *Nature Chemistry*, 2009, 1, 7-7.
20. D. G. Nocera, *Accounts of Chemical Research*, 2012, 45, 767-776.
21. C. Genovese, C. Ampelli, S. Perathoner and G. Centi, *Journal of Catalysis*, 2013, 308, 237-249.
22. J. M. Thomas, *ChemSusChem*, 2014, 7, 1801-1832.
23. A. Ursua, L. M. Gandia and P. Sanchis, *Proceedings of the IEEE*, 2012, 100, 410-426.
24. S. E. Hosseini and M. A. Wahid, *Renewable and Sustainable Energy Reviews*, 2016, 57, 850-866.
25. D. D. Tanner, P. Kandanarachchi, Q. Ding, H. Shao, D. Vizitiu and J. A. Franz, *Energy & Fuels*, 2001, 15, 197-204.
26. A. Domínguez, B. Fidalgo, Y. Fernández, J. Pis and J. Menéndez, *International Journal of Hydrogen Energy*, 2007, 32, 4792-4799.
27. Y. Suttisawat, S. Horikoshi, H. Sakai and M. Abe, *International Journal of Hydrogen Energy*, 2010, 35, 6179-6183.
28. O. Mutaf-yardimci, A. V. Saveliev, A. A. Fridman and L. A. Kennedy, *International Journal of Hydrogen Energy*, 1998, 23, 1109-1111.
29. H. L. Chen, H. M. Lee, S. H. Chen, Y. Chao and M. B. Chang, *Applied Catalysis B: Environmental*, 2008, 85, 1-9.
30. T. Geißler, A. Abánades, A. Heinzel, K. Mehravaran, G. Müller, R. K. Rathnam, C. Rubbia, D. Salmieri, L. Stoppel, S. Stückrad, A. Weisenburger, H. Wenninger and T. Wetzel, *Chemical Engineering Journal*, 2016, 299, 192-200.
31. D. C. Upham, V. Agarwal, A. Khechfe, Z. R. Snodgrass, M. J. Gordon, H. Metiu and E. W. McFarland, *Science*, 2017, 358, 917-921.
32. C. Antonio and R. T. Deam, *Physical Chemistry Chemical Physics*, 2007, 9, 2976-2982.

33. S. Horikoshi and N. Serpone, *Microwaves in Catalysis : Methodology and Applications*.

34. S. Gonzalez-Cortes, D. Slocombe, T. Xiao, A. Aldawsari, B. Yao, V. Kuznetsov, E. Liberti, A. Kirkland, M. Alkinani and H. Al-Megren, *Scientific Reports*, 2016, 6, 35315.

35. M. A. Vannice, *Journal of Catalysis*, 1977, 50, 228-236.

36. G. P. Van der Laan and A. A. C. M. Beenackers, *Catalysis Review*, 1999, 41, 255-318.

37. F. Langa, P. De La Cruz, A. De La Hoz, A. Diaz-Ortiz and E. Diez-Barra, *Contemporary Organic Synthesis*, 1997, 4, 373-386.

38. D. Balcells, E. Clot and O. Eisenstein, *Chemical Review*, 2010, 110, 749-823.

39. M. J. Ledoux and C. Pham-Huu, *Cattech*, 2001, 5, 226-246.

40. A. M. Aldawsari, *Dielectric measurements and catalytic cracking of heavy oils using advanced microwave technologies*, Thesis, 2017.

41. A. Porch, D. Slocombe, J. Beutler, P. Edwards, A. Aldawsari, T. Xiao, V. Kuznetsov, H. Almegren, S. Aldrees and N. Almaqati, *Applied Petrochem Research*, 2012, 2, 37-44.

42. S. Li, C. Akyel and R. G. Bosisio, *IEEE Trans. Microwave Theory Technology*, 1981, MTT-29, 1041-1048.

43. P. Lidstrom, J. Tierney, B. Wathey and J. Westman, *Tetrahedron*, 2001, 57, 10229.

44. S. A. Galema, *Chemical Sociaty Review*, 1997, 26, 233-238.

45. A. Porch, D. Slocombe and P. P. Edwards, *Physical Chemistry Chemical Physics*, 2013, 15, 2757-2763.

46. L.-S. Fu, J.-T. Jiang, C.-Y. Xu and L. Zhen, *CrystEngComm*, 2012, 14, 6827-6832.

47. J. Geng, D. A. Jefferson and B. F. G. Johnson, *Chemcal Communication*, 2007, 969-971.

Chapter 4

Optimisation of Catalyst Performance

Overview

In the previous chapter, the innovative microwave-initiated catalysis has been shown to offer unique advantages in the rapid production of hydrogen from hexadecane. This chapter [2] presents the investigation and optimisation of catalyst system for high-purity hydrogen production through microwave-initiated catalytic dehydrogenation of hexadecane ($C_{16}H_{34}$) [1, 2]. Various metal catalysts supported by SiC were prepared and their performance towards H_2 production from hexadecane dehydrogenation were evaluated using the same experimental set-up under same conditions. Furthermore, iron-based catalysts were synthesised using a series of support materials including activated carbon (AC), silica (SiO_2) and aluminium oxide (Al_2O_3) etc.; and SiC supported iron catalysts with different iron content was tested.

4.1 Introduction

In the previous chapter, it has been demonstrated that hydrogen can be rapidly and efficiently released from hexadecane and through microwave-initiated catalytic dehydrogenation[1, 3, 4]. However, the microwave is a rather complex system and is more challenging to understand when combined with heterogeneous catalysis.

[2] The work described in this chapter is reproduced and modified from my publications in 2018, in *Catalysis Today* entitled ‘‘On the performance optimisation of Fe catalysts in the microwave-initiated H_2 production by the dehydrogenation of hexadecane’’; and in 2017, in *Angewandte Chemie* entitled ‘‘Rapid Production of High-Purity Hydrogen Fuel through Microwave-Promoted Catalytic Dehydrogenation of Liquid Alkanes with Abundant Metals’’.

Dielectric heating by high-frequency electromagnetic radiation waves could interact with only charged particles (catalysts, reactants or solvent) and cause these compounds heat up in the electric field of electromagnetic radiation. In the dielectric heating, selective heating can lead to less by-products [5]. Two different mechanisms are associated to the resulting heating from the interaction between materials and electric field of electromagnetic radiation. Polarisation of the polar molecules such as water etc. results in these molecules are trying to align themselves under an alternating electric field. This movement and friction between the rotating molecules subsequently causes heat. For the solid materials, interfacial or Maxwell-Wagner polarisation effect causes the heat because of charged particles[6-8]. The microwave irradiating of dielectric materials, can efficiently convert electromagnetic energy into heat and offers many advantages over conventional heating, such as selective and rapid heating, quick start-up and stopping, non-contact heat, energy transfer of as opposed contact heat transfer and heating from the interior of the material with purely thermal methods.

Therefore, it is rather important to scan suitable catalysts and optimise the catalyst system for the hydrogen production process under microwave irradiation. The catalysts studied for hydrogen production system are generally transition metals. The catalysts containing group 8, 9 and 10 metals (Ni, Co, Ru, Pt, Pd, Rh, etc.) are reported preferred for the steam reforming of liquid hydrocarbons[31]. And the tetra- and pentavalent p metals (Ge, Sn, and Pb or As, Sb, and Bi) have been studied as promotors to suppress coke formation during steam reforming[9, 10]. In the steam methane process (SMR) for example, nickel catalysts are selected as the most effective and economic catalysts in industry. Moreover, in terms of the studies on support materials, the magnesia- and silica-supported nickel catalysts improved catalytic lifetime[11].

The catalyst for microwave-initiated catalytic hydrogen production process must be a good microwave absorber/receptor and able to retain its structure and properties under intense microwave irradiation[12, 13]. In general, metal- and carbon-based catalysts have been developed for microwave-initiated CO_2-free hydrogen production from hydrocarbons decomposition (mostly methane decomposition). The use of carbon-based catalysts offers certain advantages due to their excellent ability to efficiently convert the electromagnetic energy to heat [14]. Thus, in few prior works[15-19] using microwave for hydrogen production carbon-based catalysts were predominated.

In this chapter, the investigation of various metal catalysts including Fe, Ni, Co, Cu, Pt, Ru etc. were discussed for hydrogen production through microwave-initiated hexadecane dehydrogenation. Among all the metals examined, we found that Fe and Ni are the most effective catalysts for high-purity hydrogen production. In addition, the optimisation of catalysts system was achieved by varying the iron content of the Fe/SiC catalysts, and a variety of support materials were investigated. In summary, iron-based catalysts supported by SiC with low iron loading levels (<10 wt.%) are preferred for high-purity H_2 production from hydrocarbons (hexadecane) using microwave catalysis.

4.2 Experimental

4.2.1 Preparation of catalysts

The catalysts were prepared using the so-called incipient wetness impregnation method. Metal nitrates such as iron nitrate nonahydrate ($Fe(NO_3)_3 \cdot 9H_2O$) bought from Sigma-Aldrich, were used as catalyst precursors whilst SiC (silicon carbide, Fisher Scientific) was used as support. The support material was mixed with an aqueous solution of metal nitrate, the concentration of which was calculated to produce the desired metal loading. The mixture was then stirred at 150°C on a magnetic hot plate for 3h until it became a slurry, which was moved into the drying oven and left overnight. The resulting solid mixtures were calcined in a furnace at 350 °C for 3 h under air. Finally, the active catalysts were obtained by a reduction process in 10% H_2/Ar gases at 800 °C for 6h.

Using same preparation methods, iron-based catalysts on different supports including SiC (silicon carbide, Fisher Scientific), AC (activated carbon, Sigma-Aldrich), SiO_2 (silica mesoporous, Sigma-Aldrich) and Al_2O_3 (aluminium oxide, Sigma-Aldrich) were synthesised with the iron content of 5 wt.%. Furthermore, Fe/SiC catalysts with a different iron contents from 0 – 100 wt.% were prepared

4.2.2 Characterisation of catalysts

The catalysts were carefully characterised before and after experiments by powder X-ray diffraction (XRD, PANalytical X'Pert PRO diffractometer), thermogravimetric analysis (TGA, TA Instrument,

SDT Q-600), Laser-Raman spectroscopy (PerkinElmer RamanStationTM 400F spectrometer), and scanning electron microscope (SEM, ZEISS EVO).

The powder X-ray diffraction (XRD) used a Cu Kα X-ray source (45 kV, 40 mA). The scanning range (in 2θ) in this study was 20° to 80°. Thermogravimetric analysis (TGA) was used to characterise the feedstocks remaining and the resulting carbon residue in spent samples. The TGA of spent catalysts was first carried out in an N_2 atmosphere to measure the hexadecane remaining, the atmosphere was then changed to air to analyse the carbon residue. Moreover, the resulting carbon residues were also studied via Laser-Raman spectroscopy, with laser excitation is at 785nm. The scanning electron microscope (SEM, ZEISS EVO) was used to characterise the surface morphology of the Fe/SiC catalysts. The catalysts before and after microwave treatment were also examined by high-resolution transmission electron microscopy (HRTEM) using a JEM-3000F microscope (300 kV).

4.2.3 Evaluation of catalysts' performance

The experimental setup was outlined in detail in Chapter 2 (Figure 2.1) which consists of a microwave generation system, a purpose-built microwave cavity and a control system [3, 4]. The catalyst with a volume typically about 1.13 cm^3 was first placed in a quartz tube (inner diameter 6mm, outer diameter 9mm). The height of the catalyst bed exposed to the axially polarised (TM_{010}) uniform electric fields is 4cm. 0.5 mL hexadecane (about 30 wt.% of catalyst) was then injected into tube and after a time of 5-10 minutes to wait the liquid hexadecane was well dispersed throughout the catalyst bed. Then, the filled tube was placed axially in the centre of the TM_{010} microwave cavity to minimise depolarisation effects under microwave radiation. Before starting microwave activation, the samples were purged with an Ar flow rate of 1.67 $mL \cdot s^{-1}$ for a period of 15 minutes. Then, the sample was irradiated with microwaves for 30 min at 750 W. The generated gases were collected and analysed by gas chromatography (GC) using a Perkin-Elmer, Clarus 580 GC. The 'unreacted' hydrocarbon was also analysed by gas chromatograph mass spectrometer (GC-MS) using a SHIMADZU, GCMS-QP2010 SE.

All the experiments were carried out over a "Trickle-Bed" liquid-solid system, with a focus on the volume of gaseous products produced from the dehydrogenation process. The selectivity toward different gaseous products was evaluated in terms of the volume % of the product composition in the

exit gases**.** In terms of the conversion and yields, it should be noted that unlike gaseous feedstocks, the "Trickle-Bed" liquid-solid heterogenous catalyst system is a more challenging system to estimate the quantitative % of product yields when the catalytic system is exposed to microwaves, which itself is a super-fast heating process. Thus, it is difficult to precisely determine the total conversion and total product yields due to a large amount of hexadecane reactant which is rapidly volatised upon entry into the reaction chamber and subsequently collected in a cold trap. The "unreacted" hydrocarbons was confirmed by gas chromatograph - mass spectrometer (GC-MS) that the substances remain unreacted. Thus, for simplicity, the conversion and H_2 yields evaluated in this study are defined as follow (Eq. 4.1 and Eq. 4.2), where only the reacted hexadecane is considered.

$$Conversion\ (\%) = \frac{Fuel_{input} - Fuel_{re-collect}}{Fuel_{input}} \times 100\% \qquad (4.1)\ *$$

$$H_2\ Yields\ (\%) = \frac{Mole\ of\ H_2\ gas\ collected}{Calculated\ mole\ of\ H_2\ in\ hexadecane\ (reacted)} \times 100\% \qquad (4.2)\ **$$

* ***Fuel*** $_{input}$: is the weight of the aliquot of hexadecane injected into the catalyst bed before microwave activation.

Fuel $_{re\text{-}collected}$: represents the "escaped" (unreacted) hexadecane that is collected in the outlet by a cold trap. The resulting condensed liquid was analysed by GCMS and showed only unreacted hexadecane. No other liquid products had been detected.

** ***Moles of*** H_2 ***gas collected***: represents the moles of H_2 in the evolved gas products, suitably standardised from GC.

Calculated moles of H_2 ***in hexadecane (reacted)***: represents the theoretical moles of H_2 in hexadecane that had been dehydrogenated during the microwave activation.

4.3 Results and discussion

4.3.1 Studies on different metal catalysts supported by SiC

Different metals supported by SiC exhibited various levels of performance under microwave irradiation with somewhat different product distributions. However, elemental hydrogen always remained the dominant product (Figure 4.1). Iron or nickel catalysts showed extremely high hydrogen selectivity (ca. 93 vol. % and 96 vol. %, respectively), while other metals (Co, Cu, Pt and Ru) had noticeably reduced values. Lighter hydrocarbons (methane and olefins) were observed in the effluent gases over Co, Cu and Pt, whereas no reaction was produced through this microwave-initiated dehydrogenation of hexadecane on Ru. It should be noted that Fe/SiC catalysts produced more CO than Ni and Co which is attributed to the formation of FeO_x on the Fe surface. This could be significantly improved by adding Ni and Co etc. as promoters, and the Fe-based alloy catalysts will be described in detail in a later section.

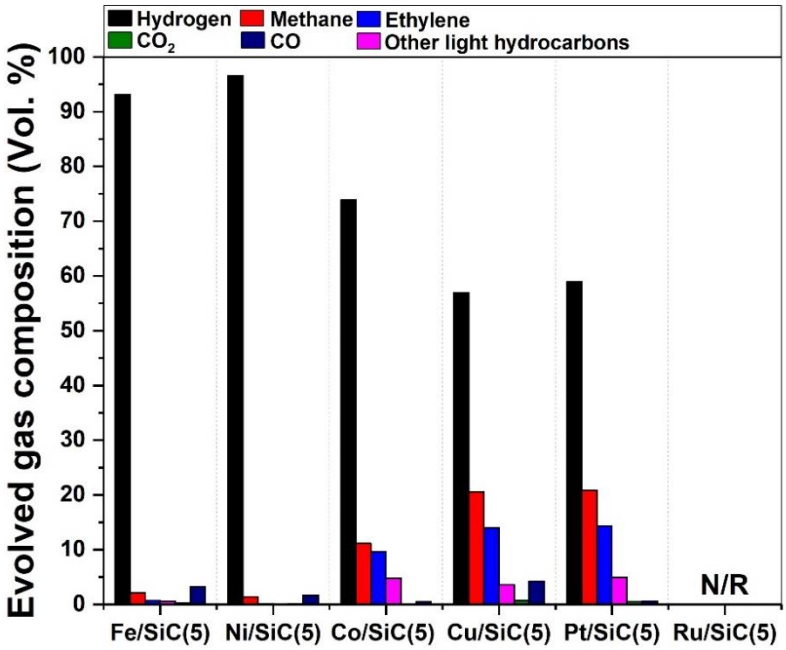


Figure 4.1. Comparison of different metals operating under same conditions of one cycle of substrate and products analysed after 10 minutes. 750W microwave power was used for each experiment and the gaseous products from hexadecane dehydrogenation were collected and analysed by GC. 'N/R' means no reaction was observed under these conditions. The number in parentheses after catalyst shows the metal content, wt. %.

In Table 4.1, the H_2 conversion and yields obtained over various metal catalysts is presented. The overall conversion obtained on each experiment was ca. 30 – 40%. This is because experiments were carried out over a batch liquid-solid system which caused the hexadecane to be rapidly volatised due to a super-fast heating process when exposed to microwaves. The unreacted hydrocarbon was subsequently collected in a cold trap. Both Fe and Ni gave a high H_2 yields of 61% and 50%, respectively while others only produced a H_2 yields at low levels (10-30%). In a brief summary, Fe and Ni presented a superb catalytic activity towards hydrogen production from hydrocarbons (hexadecane) dehydrogenation when interact with induced microwaves.

Table 4.1: Summary of H_2 conversion and yields of different metal catalysts supported by SiC through microwave-initiated dehydrogenation of hexadecane. Reactions were conducted at 750 W input power for 10 min with an aliquot of 5 mL (ca. 30 wt. % of catalysts) hexadecane impregnated. All the catalysts were synthesised with 5 wt.% metal loading.

Metals	Volume of H_2 gas [mL]	Conversion* [%]	H_2 Yields** [%]
Fe	158	39	61
Ni	150	43	50
Co	128	32	34
Cu	70	30	15
Pt	80	30	16
Ru	(-)	(-)	(-)

* Defined in Eq. 4.1. ** Defined in Eq. 4.2.

In addition, iron based bimetallic metal catalysts supported by SiC (Fe-X/SiC, X = Ni, Co, Cu and Ru) were investigated, aiming to optimise the iron catalysts for higher H_2 selectivity and suppress the formation of carbon monoxide (CO). As a general observation, all the bimetallic metal alloy catalysts gave an extremely high hydrogen selectivity of over 95 vol.%. Nearly 98% of hydrogen selectivity was observed over the Fe-Ni/SiC catalyst and less than 0.5 vol.% of CO was produced. Hence, the CO_2 emission is close to zero. It was found that the presence of nickel improves the dispersion of metal particles on the SiC surface and appears to suppress the formation of iron carbides, implicated in the

gradual reduction in catalytic activity (Further information is outlined in Chapter 3). Furthermore, the Fe-Ni/SiC catalysts were prepared by varying the Ni contents. Although, no obvious difference was noticed in terms of hydrogen selectivity among these catalysts; Ni contents below the weight ratio of 1 (w_{iron}/ w_{nickel} < 1) was preferred and gave higher hydrogen selectivity and less CO. This demonstrates the effects of nickel as a promoter can optimise the performance of Fe-based catalyst under microwave conditions for higher hydrogen production and suppress the formation of CO. Other metals like Co, Ru and Cu in combination with Fe also produced less CO_x in the effluent gases.

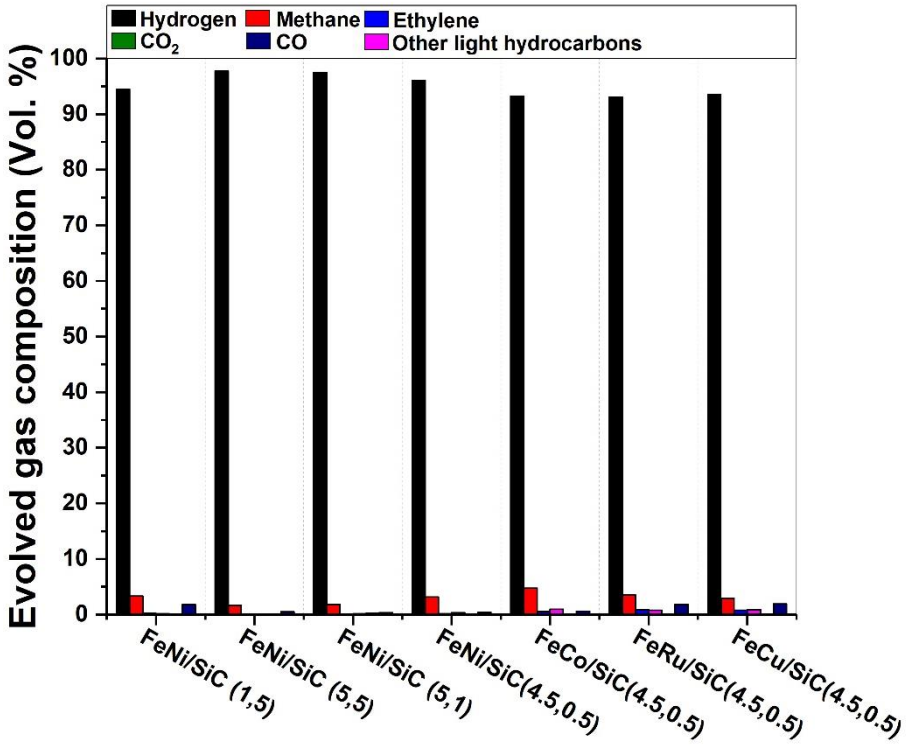


Figure 4.2. Evolved gas composition of iron based bimetallic metal (Fe-X/SiC, X = Ni, Co, Cu and Ru) through microwave-initiated dehydrogenation of hexadecane. Each experiment was carried out for 10 minutes with 750W input power and the gaseous products were collected and analysed by GC. The number in parentheses after catalyst shows the metal content, wt. %.

The H_2 conversion and yields of different iron-based alloy metal catalysts are summarised in Table 4.2. Like metallic iron catalysts, the conversion of hexadecane over these alloy catalysts was around 40% due to the volatilisation causing by the super-fast heating process under a batch system. However, importantly the H_2 yields were significantly increased and the Fe-5wt.%, Ni-1 wt.% Fe-Ni/SiC catalysts gave a very high H_2 yields of 87%. Other metal alloy catalysts were also showed a higher H_2 yields than

that of mono-metallic metal catalysts. Overall, H_2 yields of over 60% were achieved among these metal alloys. Therefore, it demonstrates that iron-based metal alloys supported by SiC can improve the catalytic activity in terms of hydrogen selectivity and yields when comparing with simple metallic iron catalysts system for hydrogen production using microwave.

Table 4.2. Summary of H_2 conversion and yields of various iron-based bimetallic metal alloy catalysts supported by SiC through microwave-initiated dehydrogenation of hexadecane. Reactions were conducted at 750 W input power for 10 min with an aliquot of 5 mL (ca. 30 wt. % of catalysts) hexadecane impregnated.

Metals┼	**Volume of H_2 gas [mL]**	**Conversion* [%]**	**H_2 Yields** [%]**
Fe-Ni/SiC (1, 5)	188	34	63
Fe-Ni/SiC (5, 5)	192	40	68
Fe-Ni/SiC (5, 1)	250	34	87
Fe-Ni/SiC (4.5, 0.5)	250	44	85
Fe-Co/SiC (4.5, 0.5)	232	38	77
Fe-Ru/SiC (4.5, 0.5)	110	32	36
Fe-Cu/SiC (4.5, 0.5)	150	41	50

┼ The number in parentheses after catalyst shows the metal content, wt. %; * Defined in Eq. 4.1; ** Defined in Eq. 4.2.

4.3.2 Study of the effect of support materials

The effect of the support materials was investigated by preparing 5 wt.% Fe catalysts on different supports. The supports used in the study included silicon carbide (SiC), activated carbon (AC), silica (SiO_2), and aluminium oxide (Al_2O_3). SiC is itself an excellent microwave absorber and has an exceptionally high thermal conductivity and is mechanically very strong. These properties appear to contribute significantly to the observed high selectivity to H_2 production. AC is well known as an efficient microwave absorber and receptor that has been widely used in microwave catalysis [9, 15, 20, 21]. Moreover, AC is a cheap material with porous structure and has a very high surface area. SiO_2 and Al_2O_3 in contrast, are not efficient microwave absorbers but have often been used as supports for

hydrocarbon decomposition via conventional thermal catalytic process [22-25]. Fe nano particles are also very good microwave absorbers. For comparison purposes, pure "free-standing" Fe nano particles were synthesised by hydrogen reduction of the iron precursor and subjected to the microwave activation towards hexadecane dehydrogenation.

It was found that hexadecane undergoes rapid, deep dehydrogenation to predominantly H_2, solid carbon and small alkanes (methane, ethylene and propylene etc.) for all the examined Fe catalysts on these support materials. However, differences in the evolved gas composition were observed over different support materials (Figure 4.3). Clearly, Fe on SiC performed the best among all the supports towards H_2 selectivity, and a remarkable hydrogen selectivity of ca. 93 vol. % was obtained in the effluent gas stream.

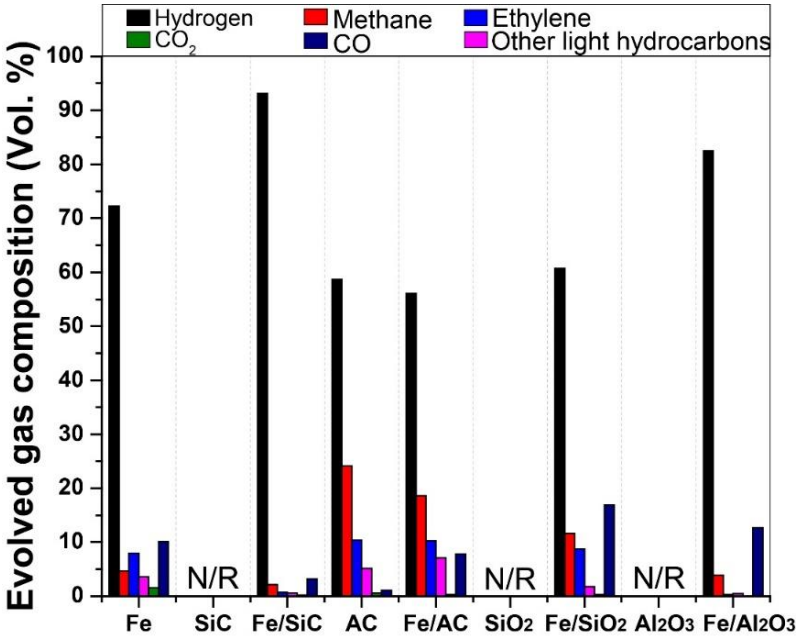


Figure 4.3. Evolved gas composition for catalysts on different support materials in the microwave–assisted dehydrogenation of hexadecane. 'N/R' indicates no observable reaction under microwave treatment.

In comparison, the H_2 selectivity of Fe/AC, Fe/SiO_2 and Fe/Al_2O_3 catalysts were 56, 60 and 83 vol.%, respectively. The Fe/AC catalysts for hexadecane dehydrogenation produced nearly19 vol.% of CH_4 and 10 vol.% of C_2H_4, while high levels of CO were obtained over Fe/SiO_2 and Fe/Al_2O_3 catalysts (17 and 13 vol.%, respectively). It should be noted that SiO_2 could react with any produced carbon residue which leads to the formation of CO and SiC. The Fe nano particles act as a catalyst for this reaction

under microwave irradiation [26]. In addition, differences were clearly found over pure supports i.e. without Fe, towards the catalytic hexadecane dehydrogenation under microwave activation. AC was the only support material that alone catalysed the reactions under the influence of microwaves. Importantly, the SiC, SiO_2, and Al_2O_3 supports only produced any measurable catalytic activity under microwave activation when the Fe particles were added.

In Table 4.3 the H_2 conversion and yields of Fe catalysts on various supports is given. Both Fe nano particles and Fe catalysts on SiC have a comparable low conversion of ca. 40%, but both gave a high H_2 yields (ca. 60%) compared to Fe containing catalysts. AC and Fe/SiC have conversions of over 55 %, only ca. 20% H_2 yields were obtained. Similarly, the H_2 yields of Fe/SiO_2 and Fe/Al_2O_3 are 43%.

Table 4.3: Summary of H_2 conversion and yields of Fe catalysts on different support materials under microwave-initiated dehydrogenation of hexadecane. Reactions were conducted at 750 W input power for 10 min with an aliquot of 5 mL (ca. 30 wt. %) hexadecane deposited on the various supported catalyst systems. All the catalysts were synthesised with 5 wt.% Fe loading.

Catalysts	**Volume of H_2 gas [mL]**	**Conversion* [%]**	**H_2 Yields** [%]**
Pure Fe	130	35	57
Fe/SiC	158	39	61
AC	78	56	21
Fe/AC	114	65	25
Fe/SiO_2	163	57	43
Fe/Al_2O_3	128	46	43

* Defined in Eq. 4.1. ** Defined in Eq. 4.2.

Many prior works have studied the effect of supports in hydrogen production systems. Like silica which has been demonstrated that the enhanced adsorption of surface hydroxyl groups on its surface can react with the CH_x fragments adsorbed on the nickel surface and subsequently improves performance of catalysts for SMR[11]. Other supports such as TiO_2[27], CeO_2[28] and Fe_2O_3[29] were also reported for optimising catalysts system for hydrogen production. Under microwave conditions however, it is essential that a support can retain its structure and properties under intense microwave

irradiation. Therefore, herein the SiC is selected as a superb support for this process due to its high mechanical strength and thermal conductivity. Moreover, the chemical inertness of SiC minimises the tendency to produce oxygenated products.

4.3.3 Fe/SiC catalysts with various Fe loading

A series of Fe/SiC catalysts were synthesised with increasing Fe loadings of 2, 5, 10, and 20 wt.% and a sample of "free-standing" Fe nano particles was also prepared. As a general observation, Fe loading at low levels (< 10 wt.%) is always preferred for high levels of hydrogen production. The Fe catalysts with 2, 5 and 10 wt.% Fe loading exhibited over 92 % selectivity for H_2 over other gases (Figure 4.4). The hydrogen amount decreased with increasing Fe contents above 10 % loading and only 85 % and 72 % selectivity are obtained over the sample with 20 wt.% Fe loading and pure Fe, respectively. It was found that more CO was produced at higher Fe contents and nearly 10 vol.% of CO was obtained with pure Fe. Presumably, this is because iron oxide is formed by the oxidation of iron through air present in the operating system and/or the insufficient reduction of the Fe precursor. Moreover, a clear increase in ethylene formation was found for pure Fe without a support material. As Fe is active in the C – C coupling reaction during CO hydrogenation, it is understandable that more minor products such as methane and ethylene etc. were produced at the higher Fe loading levels [30-32].

In terms of conversion and the H_2 yields (Table 4.4), no obvious difference was observed over Fe catalysts with various Fe loadings. The overall conversion of hexadecane to gaseous products over Fe/SiC catalyst is ca. 40%, and the H_2 yields is ca. 60%. We attribute the comparable low yield of H_2 to the very low surface area of SiC and the inevitable rapid vaporisation of hexadecane with the "Trickle-Bed" liquid-solid configuration used here under rapid microwave dielectric heating.

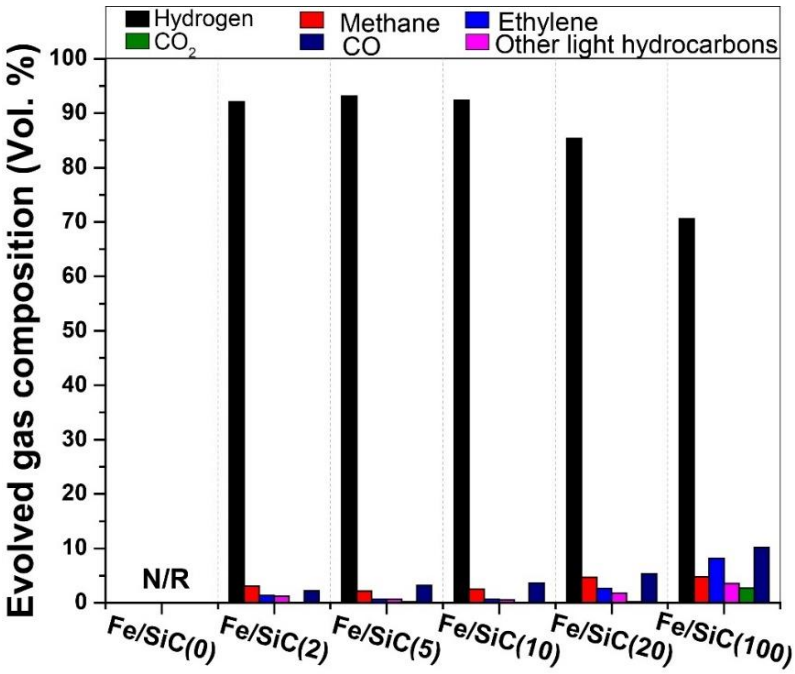


Figure 4.4. Evolved gas composition for Fe/SiC catalysts at different Fe loadings under microwave–initiated dehydrogenation of hexadecane. The number in parentheses for each catalyst shows the metal content, in wt. %. 'N/R' indicates no reaction was found under microwave treatment.

Table 4.4: Summary of H_2 conversion and yields of Fe catalysts with various Fe loadings in the microwave-initiated dehydrogenation of hexadecane. Reaction conducted at 750 W incident power for 10 min with 5 mL (ca. 30 wt. %) hexadecane deposited on catalyst.

Catalysts┼	**Volume of H_2 gas [mL]**	**Conversion* [%]**	**H_2 Yields** [%]**
Fe/SiC (2)	149	41	57
Fe/SiC (5)	158	39	61
Fe/SiC (10)	174	42	63
Fe/SiC (20)	162	38	62
Pure Fe	130	35	57

┼ The number in parentheses for each catalyst shows the metal content, wt. %; * Defined in Eq. 4.1; ** Defined in Eq. 4.2.

In addition, the Fe/SiC catalysts with various Fe contents were carefully examined by X-ray diffraction (XRD), scanning electron microscopy (SEM), thermogravimetric analysis (TGA) and Raman spectroscopy.

Figure 4.5 illustrates the XRD patterns of Fe/SiC catalysts with Fe contents of 2, 5, 10, and 20 wt.%. The characteristic peaks of Fe and SiC were observed. SiC peaks were detected at 2θ = 34.22°, 35.73°, 38.25°, 41.51°, 45.4°, 54.73°, 60.12°, 65.73°, 70.94°, 71.86°, 73.45° and 75.49°. The peaks for Fe metal at 44.79° and 65.11° were also detected. These last two peaks correspond to the 110 and 200 lattice planes of Fe, respectively. The diffraction pattern for the catalysts obtained *via* the hydrogen-thermal reduction indicate that the iron particles were pure α-Fe phase with a cubic structure (JCPDS No. 05-0696)[33]. No other Fe species were detected by XRD. Clearly, the peak intensity of metallic iron became stronger when the Fe loading increased from 2 to 20 wt.% (Figure 4.5a). After microwave treatment, the peak for Fe at 44.79° and 65.11° dramatically decreased or disappeared. Instead, the characteristic peaks of iron carbide at 2θ = 42.92°, 43.82°, 44.72°, 45.04°, 45.9°, and 49.18° were detected. No clear changes were observed for the diffraction peaks of SiC, which suggest that it was largely stable under the reaction conditions.

Although, no clear diffraction peaks for carbon were detected in the XRD, the presence of carbon residues has been confirmed through Raman scattering, thermogravimetric analysis (TGA) and scanning electron microscopy (SEM) studies. Figure 4.6 compares the Raman spectrum of Fe/SiC samples before and after the microwave treatment. Three prominent features in the Raman spectra of carbon were appeared in the spent sample. The so-called D-band, G-band and G'-band were observed at 1312 cm^{-1}, 1584 cm^{-1} and 2624 cm^{-1}, respectively. The higher intensity found in the D-band indicates the resulting carbon residues contain disordered sp^2-hybridized carbons. The presence of a G'-band suggests the formation of graphitic sp^2-hybridized carbon which is also confirmed by our high-resolution transmission electron microscopy (HRTEM) studies in the previous Chapter. Moreover, very small Raman peaks associated with SiC are observed in the spent samples with high Fe contents (i.e., 5, 10 and 20 wt. %) which is considered as being due to the surface coverage of SiC with coke. The thermogravimetric analysis (TGA) showed that the combustion temperatures of the carbon residues are similar, at about 593 °C (Figure 4.7), while the weight gain at lower temperatures is due to the oxidation of iron/iron carbide.

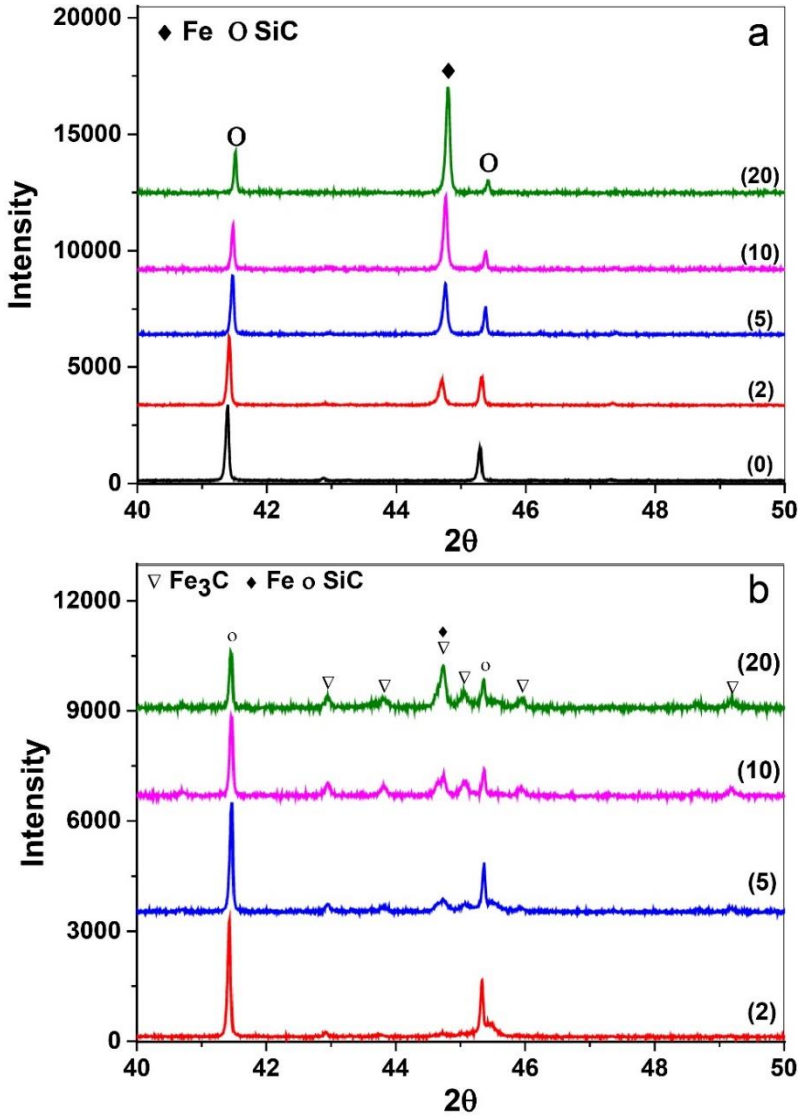


Figure 4.5. X-Ray Diffraction patterns of Fe/SiC with various Fe loadings. (a) Before; and (b) After microwave-initiated catalytic dehydrogenation of hexadecane. The number in parentheses shows the Fe loading, in wt. %.

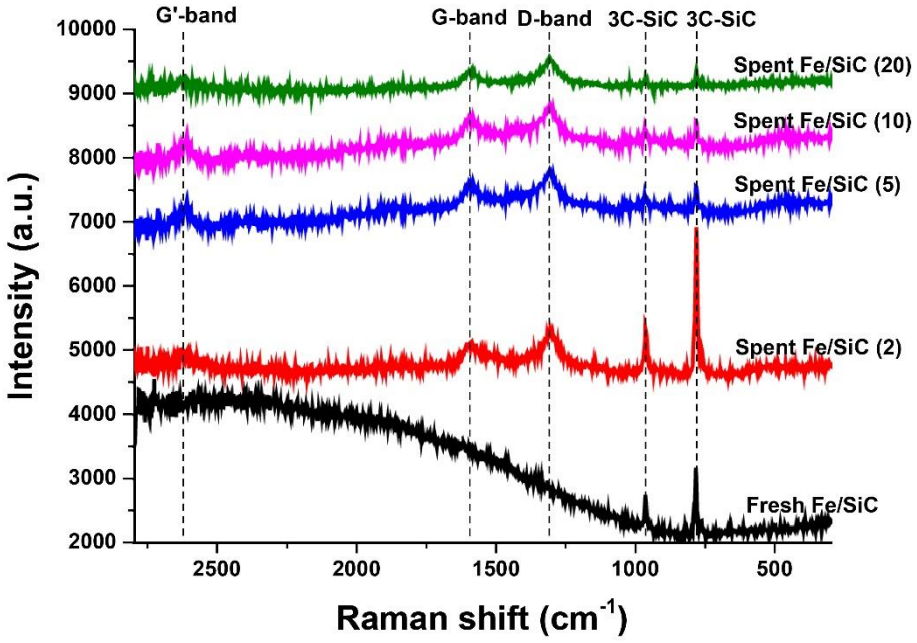


Figure 4.6. Raman spectra of Fe/SiC catalysts with various Fe loading after the microwave-initiated dehydrogenation of hexadecane. The number in parentheses shows the Fe loading, in wt. %.

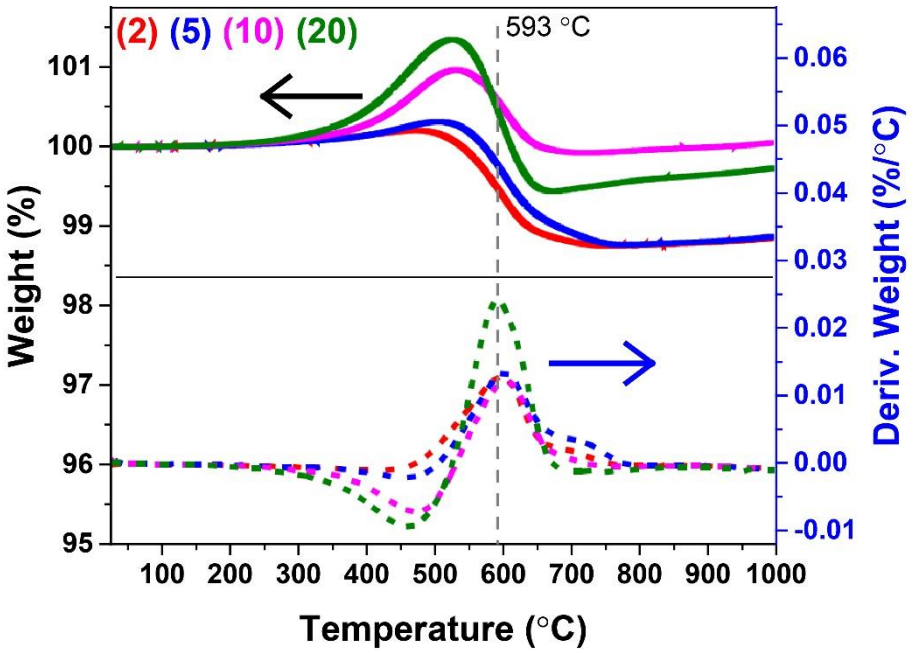


Figure 4.7. Thermogravimetric analysis (TGA) of Fe/SiC catalysts with various Fe loading through microwave-initiated dehydrogenation of hexadecane. The TGA was heated in air. The number in parentheses shows the Fe loading, in wt. %.

Figure 4.8 shows the SEM images of Fe/SiC catalysts with different Fe loading before and after microwave treatment. In the fresh samples, it was found that SiC particles are 20-40 μm and Fe particles

are ca. 10 – 100 nm, which corresponds to the XRD analysis. In addition, more Fe particles can be observed at higher Fe loading but have larger particle sizes. After the microwave treatment, some carbon clusters were found on the SiC surface with the size of 10 μm. Some filamentous carbon was also observed in these carbon clusters.

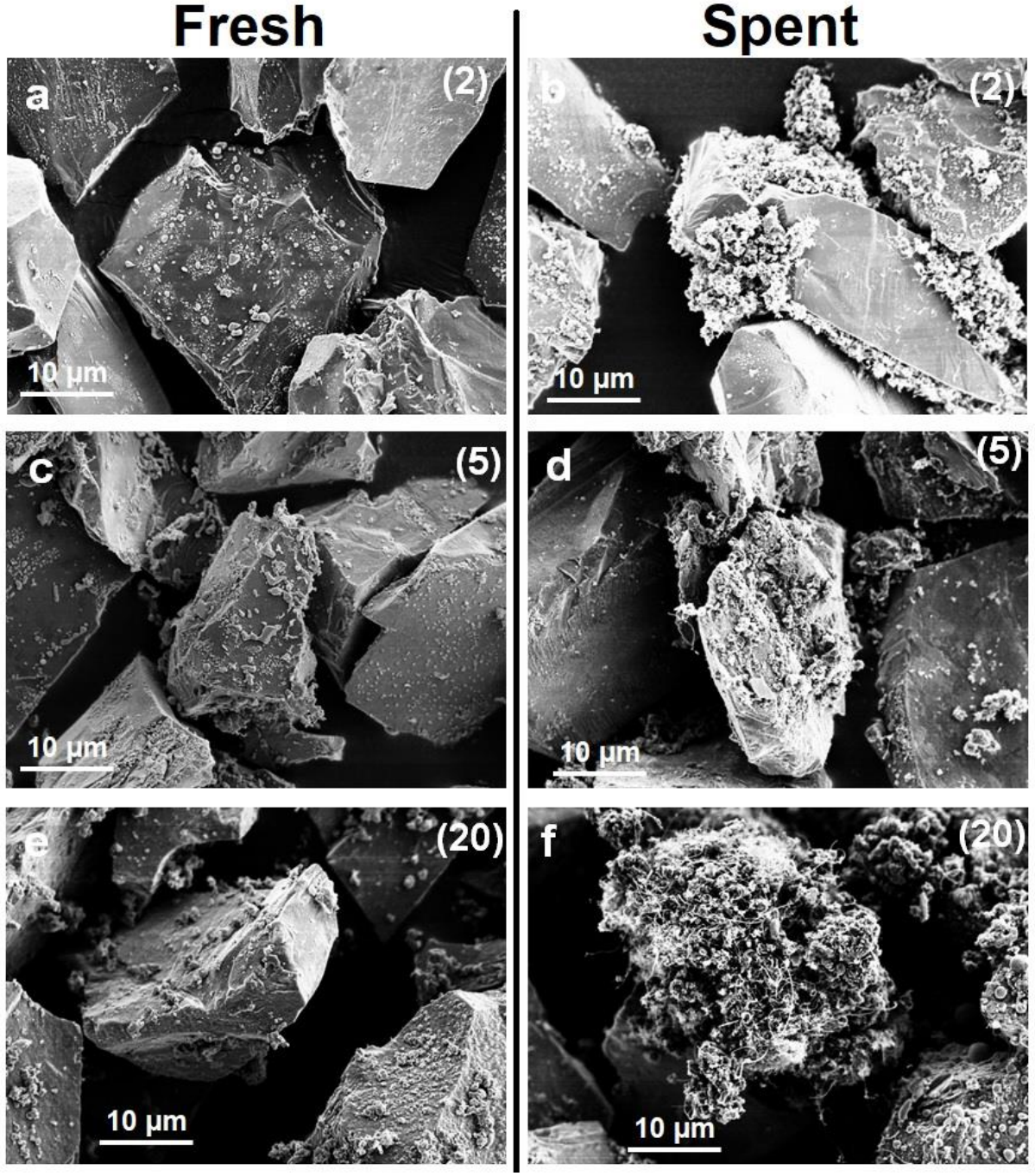


Figure 4.8. Scanning electron microscopy (SEM) of Fe/SiC catalysts with various Fe loading, (a, c and e) before and (b, d and f) after microwave-initiated catalytic hexadecane dehydrogenation. The number in parentheses shows the Fe loading, in wt. %.

4.3.4 Power absorption and temperature considerations

Changes of absorption power and the surface temperature of representative 5 wt.% Fe/SiC samples were carefully investigated via hexadecane (fuel) dehydrogenation. For reference, Fe/SiC catalytic systems both with, and without hexadecane are presented. Here, the changes of temperature (°C) and microwave absorption power (watts) as the functions of the reaction time (in seconds) are given in Figure 4.9.

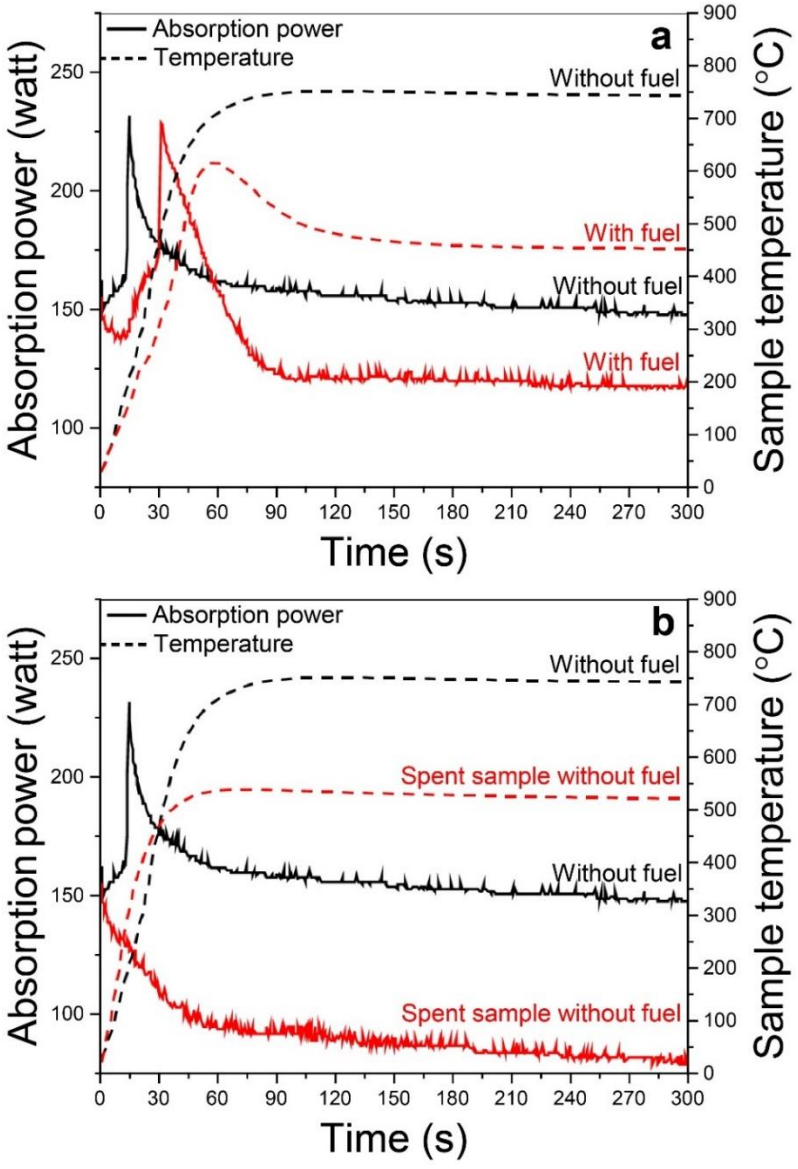


Figure 4.9. The changes of microwave absorption power (Watts) and temperature (°C) for 5 wt. % Fe/SiC catalyst under 750 W microwave power **(a)** with and without hexadecane fuel during exposure of the system to microwaves **(b)** Comparison of fresh and spent sample without fuel**.**

A noticeable *increase* in the absorption of microwave power was observed at the onset of microwave promotion or activation, but it rapidly decreased after the system attained the maximum absorption of about 230 watts. Meanwhile, the surface temperature rapidly increased during this short period of ca. 90 seconds. One notes that the behaviour of the temperature changes was noticeably different for samples with and without hexadecane. The temperature of the sample with hexadecane showed a noticeable decrease of temperature of nearly 150 °C from the maximum temperature (ca. 610 °C). For the sample without hexadecane, however, the temperature reached the maximum (ca. 740 °C) and remained at that value to the end of experiment. A temperature difference of nearly 280 °C is observed between samples with and without hexadecane. A similar difference was also observed on absorption power.

Considering both the microwave and temperature variations under microwave operating conditions, it was found that the sample with the hexadecane fuel exhibited a slower temperature increase. This behaviour is attributed to the major deep dehydrogenation reaction being highly endothermic and thus the heat is absorbed in these dehydrogenation reactions at the very onset of microwave activation.

In addition, the system temperature was found to decrease after reaching the maximum temperature of 610 °C. This is considered due to the developing deposition of carbon residues and the formation of iron carbide that affects the dielectric properties and thermal conductivities of the original Fe/SiC samples, which has been demonstrated by comparing the temperature profile and absorption power between the fresh and spent Fe/SiC sample without fuel (Figure 4.9b).

4.3.5 Dielectric properties of investigated catalysts

The dielectric properties of catalysts were measured via microwave cavity perturbation measurement at room temperature using a TM_{010} resonant cavity. It should be noted that the dielectric properties of the catalysts are temperature dependent, which could alter any trend observed at low temperature. The high temperature measurement of representative Fe/SiC, Ni/SiC and FeNi/SiC catalysts was outlined in detail in Chapter 3.

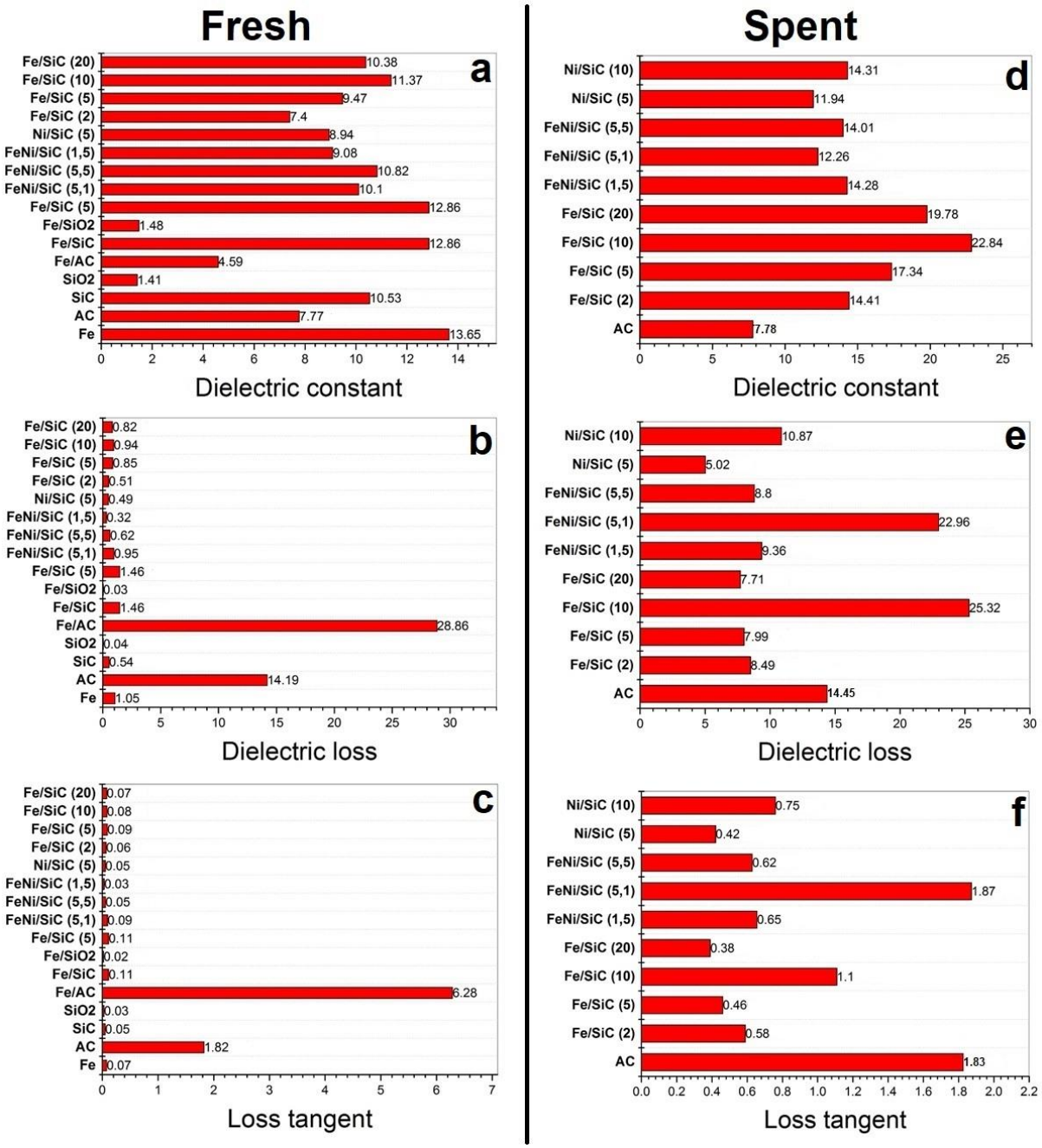


Figure 4.10. Dielectric properties of catalysts, (a, b and c) before and (d, e and f) after microwave-initiated catalytic dehydrogenation of hexadecane. The number in parentheses shows the metal loading, in wt. %. The values given show an average of at least 5 times individual tests.

Figure 4.10 summarised the dielectric constant, dielectric loss and loss tangent of catalysts before and after microwave treatment. The dielectric constant represents the ability of the material to store electrical potential energy under the microwave irradiation and the loss tangent defines the ability of the material to convert electromagnetic energy into heat energy at a given frequency and temperature [5,

[7]. As a general observation, the SiC, AC and Fe particles have a comparable dielectric constant while the loss tangent of AC is several times larger than that of SiC and Fe particles. The loss tangent of Fe, SiC, SiO_2 and metal/SiC catalysts is low at the range of 0.03 – 0.1. In comparison, the loss tangent of ca. 1.8 and 6.3 were measured for AC and Fe/AC sample respectively. Moreover, both dielectric loss and loss tangent of metal/SiC catalysts were significantly increased after the reactions as a result of carbon deposition. This is because the carbons are excellent microwave absorbers which can efficiently convert electromagnetic energy to heat. In contrast, there was nearly no change of AC before and after microwave treatment.

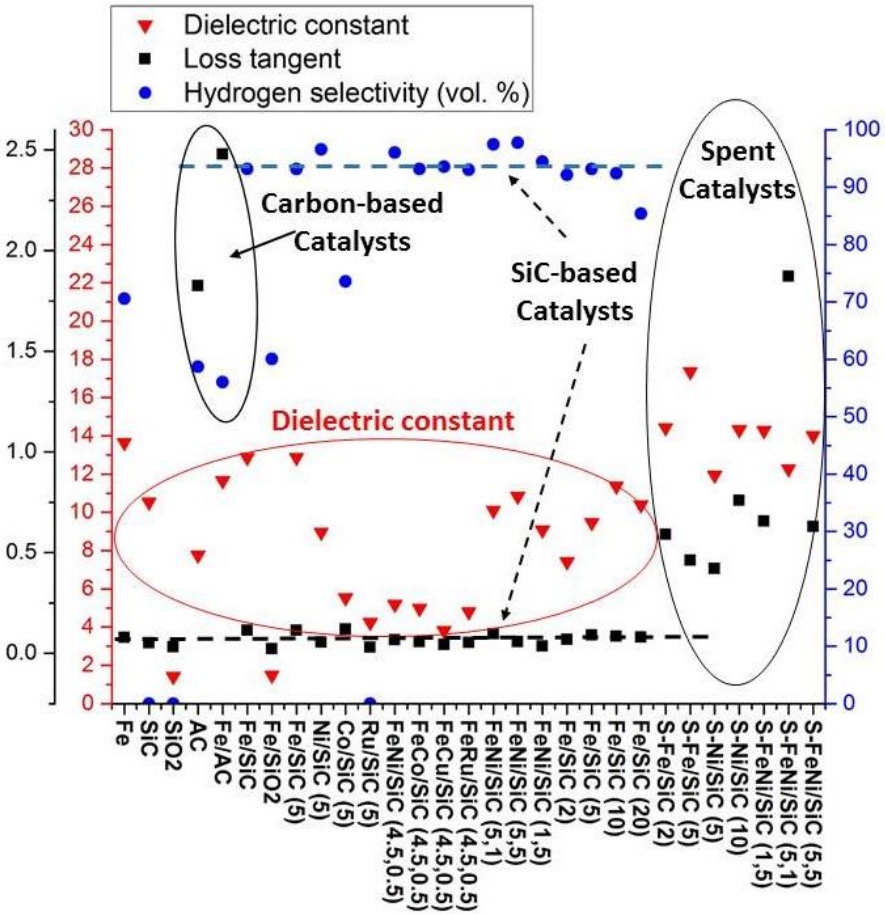


Figure 4.11. The plots summarised the relation between dielectric properties of catalysts and hydrogen selectivity. The number in parentheses shows the metal loading, in wt. %.

In relation to the hydrogen selectivity, no simple dependency has been found between the dielectric properties of catalysts and their product distributions (Figure 4.11). However, the catalytic activity of

different catalysts is still related to their dielectric properties. In the study of microwave-initiated dehydrogenation of hexadecane, materials with low loss tangent and dielectric constant such as SiO_2, have shown no catalytic activity under microwave irradiation because such catalysts are unable to achieve the required temperature for reactions. The metal/SiC catalysts by contrast, have a similar dielectric property to SiO_2, but showed a remarkable hydrogen selectivity under microwave irradiation. Unlike carbon-based catalysts which the driving force is considered to be dominanted by the heat that has been efficiently converted from electromagnetic energy, the SiC supported metal catalysts rely on various polarisation and dissipation mechanisms that contribute to drive the reactions under microwave irradiation which subsequently lead to the high hydrogen selectivity[34].

It is concluded that the dielectric property of a material is important for designing a catalyst for microwave catalysis; however, it is not a decisive parameter affecting the catalytic performance under microwave irradiation. The dielectric property of materials only reflects the efficiency in term of converting electromagnetic energy to heat; and the catalytic properties of a catalyst are rather important for specific reactions. Moreover, it is more complex in a heterogeneous catalyst system and various polarisation and dissipation mechanisms may enhanced under microwave irradiation.

4.3.6 Summary of catalyst characterisation

The pre- and post-reaction catalysts were carefully characterised via a variety of surface techniques including X-ray Diffraction (XRD), thermogravimetric analysis (TGA), Raman spectroscopy, and scanning electron microscopy (SEM). The selective Fe/SiC, Fe-Ni/SiC and Ni/SiC catalysts before and after microwave treatment has been detailed studied and discussed in Chapter 3, thus in this section a brief summary on characterisation of other catalysts is given.

4.3.6.1 X-ray diffraction (XRD)

Figure 4.12 summarised the XRD patterns of different metals and iron-based bimetallic alloys. The characteristic peaks of metals and SiC were observed. The diffraction peaks of SiC were detected at 2θ = 34.22°, 35.73°, 38.25°, 41.51°, 45.4°, 54.73°, 60.12°, 65.73°, 70.94°, 71.86°, 73.45° and 75.49°, and there are no obvious changes were found after microwave treatment which suggest the stable properties

of SiC under the intensive microwave irradiation. In contrast, the difference is always observed on metals after reactions; for example, the characteristic peaks of iron carbide were detected on iron catalysts.

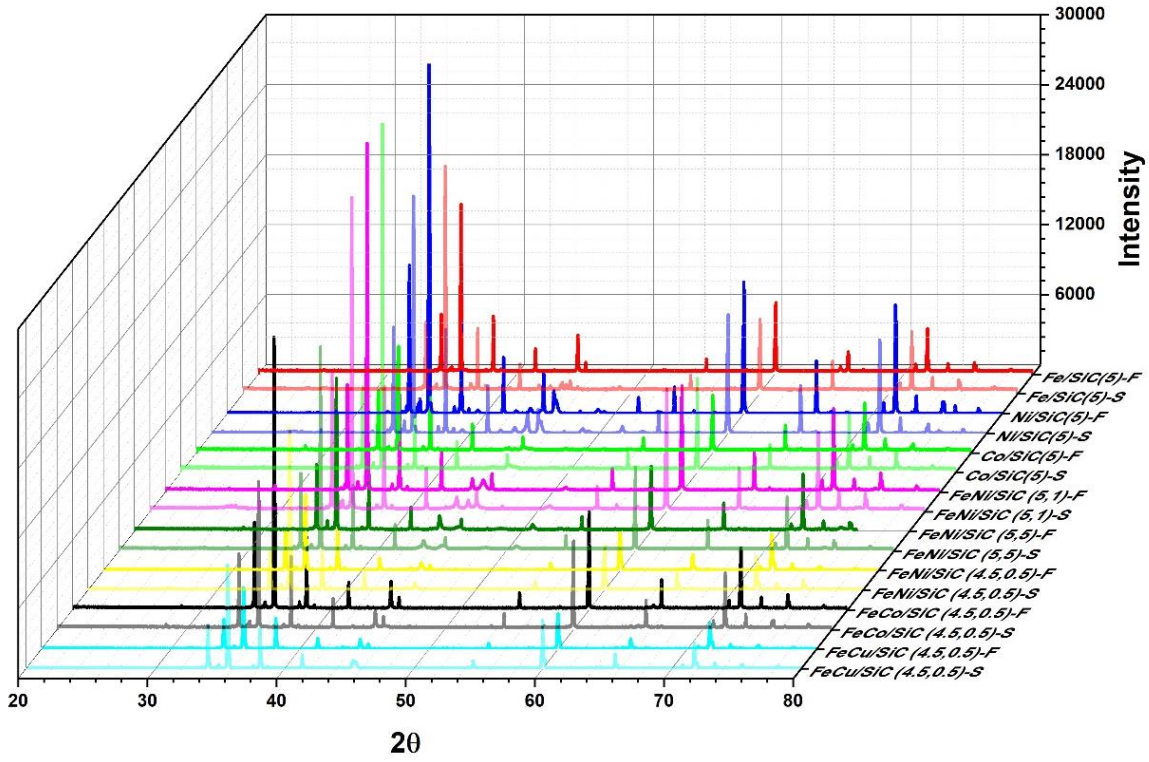


Figure 4.12. XRD patterns of various metal catalysts and metal alloys before and after the microwave-initiated catalytic dehydrogenation of hexadecane, 2θ= 20°-80°. The number in parentheses shows the metal loading, in wt. %. The ‘‘-F’’ and ‘‘-S’’ after the parentheses refer to the fresh and spent sample respectively.

4.3.6.2 Scanning electron microscopy (SEM)

Figure 4.13 and Figure 4.14 presented the SEM images of prepared catalysts with different supports and various metal catalysts supported by SiC, respectively. The different surface morphology has been observed among different catalysts. This may also relate to the various catalytic performance under microwaves.

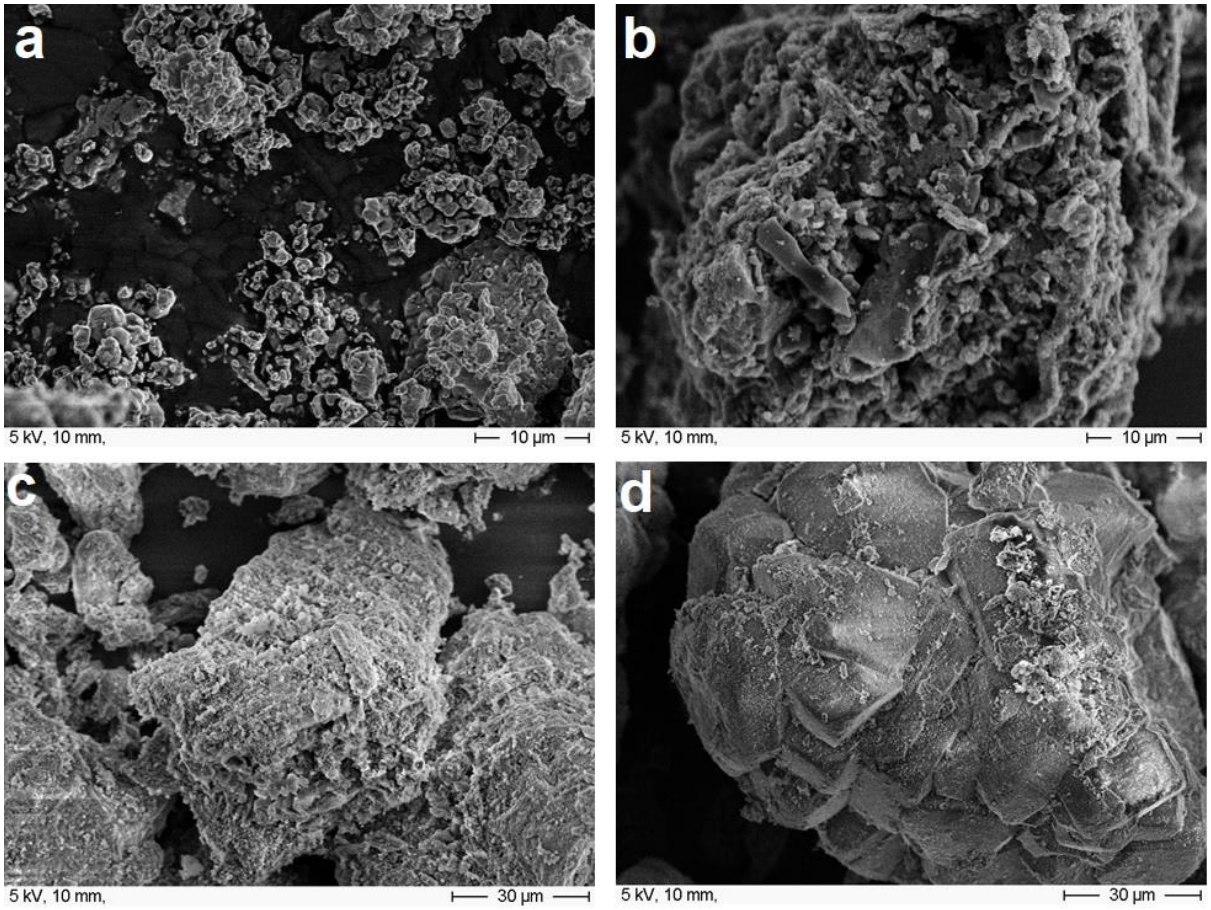


Figure 4.13. The scanning electron microscopy (SEM) images of (a) Fe particle obtained by hydro-reduction from iron nitrate, (b) 5 wt.% Fe/AC catalyst, (c) 5 wt.% Fe/SiO_2 catalyst, (c) 5 wt.% Fe/Al_2O_3 catalyst.

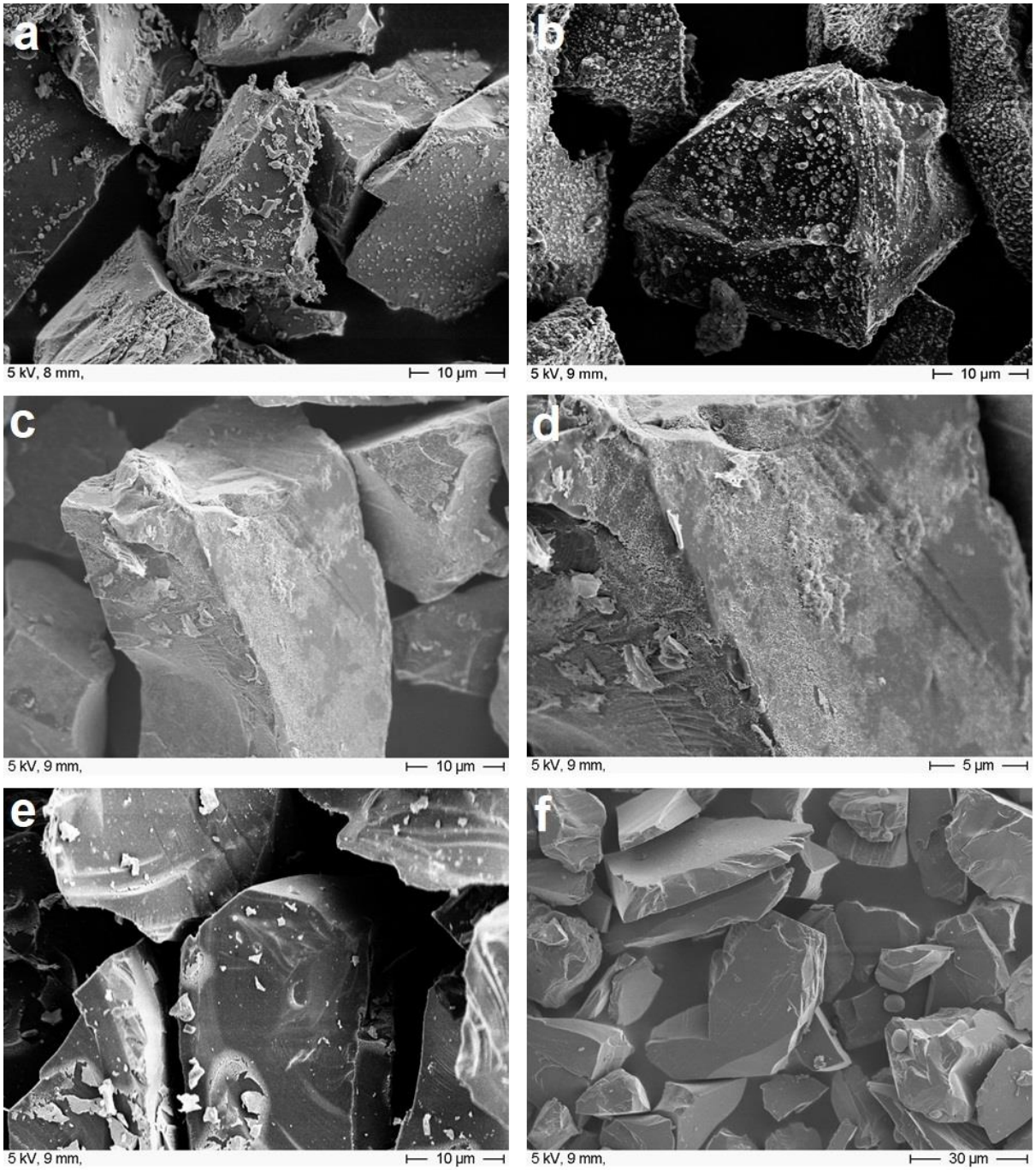


Figure 4.14. The scanning electron microscopy (SEM) images of (a) 5 wt.% Fe/SiC catalyst, (b) 5 wt.% Ni/SiC catalyst, (c, d) 5 wt.% Pt /SiC catalysts, (e) 5 wt.% Ru/SiC catalyst and (f) 5 wt.% Cu/SiC catalyst.

4.3.6.3 Raman spectroscopy

The resulting carbon residues are further confirmed and studied by Raman spectroscopy. The so-called D-band, G-band and G'-band were obviously appearted at about 1312 cm^{-1}, 1584 cm^{-1} and 2624 cm^{-1}, respectively in spent samples (Figure 4.16). There are thus, both disordered and graphitic sp^2-

hybridized carbons were formed during the process. And a more comprehensive study on these carbons will be given in Chapter 6.

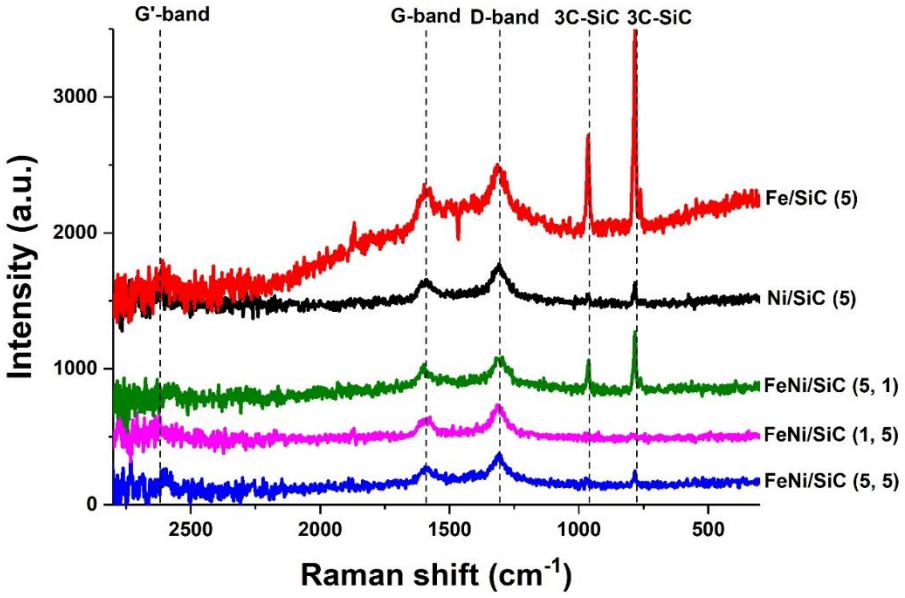


Figure 4.15. Raman spectra of spent catalysts from hexadecane dehydrogenation under microwave treatment. The number in parentheses shows the Fe loading, in wt. %.

4.4 Conclusion

The microwave process is a rather complex process and system when combined with heterogeneous catalysis. The catalyst system was investigated and optimised by scanning various metal catalysts, supports and varying the metal contents. The catalytic performance of prepared catalysts was studied through microwave-initiated catalytic dehydrogenation of hexadecane. In summary, Fe and Ni showed a superb catalytic activity among other metals (Co, Cu, Pt and Ru) for this catalytic process under microwaves and high hydrogen selectivities and yields were produced. Moreover, the study on iron-based metal alloy catalysts showed that all the bimetallic metal alloy catalysts gave an extremely high hydrogen selectivity and nearly 98% of hydrogen selectivity was obtained over the Fe-Ni/SiC catalyst with the production of CO_x close to zero. It is therefore concluded that the presence of a second metal (such as Ni and Co) in an iron-based metal alloy can improve the catalytic activity in terms of hydrogen selectivity and yields for high-purity hydrogen under microwave condition.

In the study of support material, SiC is selected for the process as it is an excellent microwave absorber/acceptor and is mechanically strength with exceptionally high thermal conductivity. These properties make SiC an excellent support for metal catalysts using under the intense microwave irradiation for high-purity hydrogen production. Furthermore, it has been demonstrated that Fe/SiC catalysts with low Fe loading level (< 10 wt.%) is preferred for high purity hydrogen production under microwave.

Bibliography:

1. X. Jie, S. Gonzalez-Cortes, T. Xiao, J. Wang, B. Yao, D. R. Slocombe, H. A. Al-Megren, J. R. Dilworth, J. M. Thomas and P. P. Edwards, *Angewandte Chemie International Edition*, 2017, 56, 10170-10173.
2. X. Jie, T. Xiao, B. Yao, S. Gonzalez-Cortes, J. Wang, Y. Fang, N. Miller, H. AlMegren, J. R. Dilworth and P. P. Edwards, *Catalysis Today*, 2018, 317, 29-35.
3. X. Jie, S. Gonzalez-Cortes, T. Xiao, B. Yao, J. Wang, D. R. Slocombe, Y. Fang, N. Miller, H. A. Al-Megren and J. R. Dilworth, J. M. Thomas and P. P. Edwards, *Energy & Environmental Science*, 2018, *12*(1), 238-249.
4. S. Gonzalez-Cortes, D. Slocombe, T. Xiao, A. Aldawsari, B. Yao, V. Kuznetsov, E. Liberti, A. Kirkland, M. Alkinani and H. Al-Megren, J. M. Thomas and P. P. Edwards, *Scientific Reports*, 2016, 6, 35315.
5. P. Lidstrom, J. Tierney, B. Wathey and J. Westman, *Tetrahedron*, 2001, 57, 10229.
6. S. Horikoshi and N. Serpone, *Catalysis Science & Technology*, 2014, 4, 1197-1210.
7. S. A. Galema, *Chemical Sociaty Review*, 1997, 26, 233-238.
8. F. Langa, P. De La Cruz, A. De La Hoz, A. Diaz-Ortiz and E. Diez-Barra, *Contemporary Organic Synthesis*, 1997, 4, 373-386.
9. R. M. Navarro, M. A. Pena and J. L. G. Fierro, *Chemical Review*, 2007, 107, 3952-3991.
10. D. L. Trimm, *Catalysis Today*, 1999, 49, 3-10.
11. M. C. J. Bradford and M. A. Vannice, *Applied Catalysis A: General*, 1996, 142, 97-122.
12. Y. Y. Tanashev, V. I. Fedoseev, Y. I. Aristov, V. V. Pushkarev, L. B. Avdeeva, V. I. Zaikovskii and V. N. Parmon, *Catalysis Today*, 1998, 42, 333-336.
13. H. F. Abbas and W. M. A. Wan Daud, *International Journal of Hydrogen Energy*, 2010, 35, 1160-1190.
14. N. Z. Muradov, F. Smith, G. Bockerman and K. Scammon, *Applied Catalysis A: General*, 2009, 365, 292-300.

15. A. Domínguez, B. Fidalgo, Y. Fernández, J. Pis and J. Menéndez, *International Journal of Hydrogen Energy*, 2007, 32, 4792-4799.

16. B. Fidalgo, Y. Fernández, A. Domínguez, J. Pis and J. Menéndez, *Journal of Analytical and Applied Pyrolysis*, 2008, 82, 158-162.

17. E. Udalov, V. Bolotov, Y. Y. Tanashev, Y. D. Chernousov and V. Parmon, *Theoretical and Experimental Chemistry*, 2011, 46, 384-392.

18. Y. Suttisawat, S. Horikoshi, H. Sakai and M. Abe, *International Journal of Hydrogen Energy*, 2010, 35, 6179-6183.

19. D. D. Tanner, P. Kandanarachchi, Q. Ding, H. Shao, D. Vizitiu and J. A. Franz, *Energy & Fuels*, 2001, 15, 197-204.

20. X. Zhang, C. S.-M. Lee, D. M. P. Mingos and D. O. Hayward, *Catalysis Letters*, 2003, 88, 129-139.

21. V. G. Gude, P. Patil, E. Martinez-Guerra, S. Deng and N. Nirmalakhandan, *Sustainable Chemical Processes*, 2013, 1, 1.

22. T. V. Reshetenko, L. B. Avdeeva, V. A. Ushakov, E. M. Moroz, A. N. Shmakov, V. V. Kriventsov, D. I. Kochubey, Y. T. Pavlyukhin, A. L. Chuvilin and Z. R. Ismagilov, *Applied Catalysis A: General*, 2004, 270, 87-99.

23. A. A. Ibrahim, A. H. Fakeeha, A. S. Al-Fatesh, A. E. Abasaeed and W. U. Khan, *International Journal of Hydrogen Energy*, 2015, 40, 7593-7600.

24. L. Zhou, L. R. Enakonda, Y. Saih, S. Loptain, D. Gary, P. Del-Gallo and J. M. Basset, *ChemSusChem*, 2016, 9, 1243-1248.

25. M. Pudukudy and Z. Yaakob, *Chemical Engineering Journal*, 2015, 262, 1009-1021.

26. J. D. Katz, *Annual Review Material Science*, 1992, 22, 153-170.

27. H. Iida, K. Tahara, H. Higashi and A. Igarashi, *Advances in Technlogy of Materials and Materials Processing Journal*, 2002, 4, 62-65.

28. D. Andreeva, V. Idakiev, T. Tabakova, L. Ilieva, P. Falaras, A. Bourlinos and A. Travlos, *Catalysis Today*, 2002, 72, 51-57.

29. D. Andreeva, T. Tabakova, V. Idakiev, P. Christov and R. Giovanoli, *Applied Catalysis A: General*, 1998, 169, 9-14.

30. T. Li, H. Wang, Y. Yang, H. Xiang and Y. Li, *Fuel Processing Technology*, 2014, 118, 117-124.

31. A. A. Mirzaei, R. M. Kiai, H. Atashi, M. Arsalanfar and S. Shahriari, *Journal of Industrial and Engineering Chemistry*, 2012, 18, 1242-1251.

32. G. P. Van der Laan and A. A. C. M. Beenackers, *Catalysis Review*, 1999, 41, 255-318.

33. L.-S. Fu, J.-T. Jiang, C.-Y. Xu and L. Zhen, *CrystEngComm*, 2012, 14, 6827-6832.

34. A. Porch, D. Slocombe and P. P. Edwards, *Physical Chemistry Chemical Physics*, 2013, 15, 2757-2763.

Chapter 5

The Decarbonisation of Petroleum and Other Fossil Hydrocarbon Fuels for the Facile Production and Safe Storage of Hydrogen

Overview

The process of microwave-initiated catalytic dehydrogenation has been described in the previous chapters where only one model fluid hydrocarbon – namely hexadecane – was studied. In this chapter[3], a variety of actual, real petroleum products, ranging from heavy crude oil, crude oil through diesel, petrol through to methane, was investigated through microwave-initiated catalytic dehydrogenation process for high-purity hydrogen production. The results have demonstrated that real hydrocarbon fossil fuels (even crude oil) can be the vehicle for high-purity hydrogen production. Based on these advances, we are of the view that this can set the scene for the natural bridge between the current fossil fuel economy and a decarbonised hydrogen economy.

5.1 Introduction

The importance of petroleum and extracted and refined fossil carbonaceous fuels (petroleum, diesel *etc.*) to the development of human society cannot be overestimated. These natural resources have improved billions of lives, worldwide, in providing accessible, relatively inexpensive energy at nearly every scale. Notwithstanding the credible advances in renewable energy production over the past decade

[3] The work described in this chapter is reproduced and modified from my publications in 2018, in *Energy & Environmental Science* entitled ‘‘The decarbonisation of petroleum and fossil hydrocarbon fuels for the production and storage of hydrogen’’.

or so, the aerial combustion of coal, natural gas and liquid fossil fuels, given humankinds' insatiable demand for power, will continue to be the ready source of more than 85% of the world's energy in the foreseeable and possibly the distant future.

The extracted and refined hydrocarbon fossil fuels, petrol and diesel are quite simply unrivalled in terms of their energy density and widespread ease of use and storage. These hydrocarbon energy sources are easily be burned in air to produce copious amounts of easily-controlled heat[1]. Indeed, our whole industrial society is based upon their oxidation/ combustion reactions These naturally occurring carbonaceous fuels have increased our comfort, longevity, and affluence. However, it is now recognised that their usage may come at a cost; the aerial combustion of these fuels leads to significant emissions of CO_2 to the atmosphere, estimated at 32.5 giga-tons (Gt) of CO_2 in 2017 alone[2]. Therefore, it is perhaps unnecessary to remark that there may be a clear need to shift to alternative fuels, which provide energy without adding CO_2 to the atmosphere[3-5]. One of the principal reasons why progress has been so slow towards what is recognised as the ultimate of such an sustainable energy transition – the hydrogen economy[6-13]- devolves to the fact that there is no readily available, massive source of "natural" hydrogen. Furthermore, to date, no reliable means exists for storing hydrogen so that it can be rapidly released – safely, and on demand- for fuel cell and other applications[6, 14-16]**.**

Paradoxically, we report here the required production of high volumes of high-purity hydrogen through the catalytic dehydrogenation of a range of fossil fuel sources including petroleum, crude and heavy crude oil, petrol, diesel and methane through microwave -initiated catalysis, using microwave-receptive fine iron particles. The co-product of this dehydrogenation process, solid carbon, can be safely stored underground in perpetuity or converted in future to valuable hydrocarbons and other materials. Through their catalytic dehydrogenation to yield carbon-free hydrogen - rather than through their aerial combustion to produce carbon dioxide - petroleum and other fossil fuels can now serve as an energy pathway to stabilising global mean temperatures.

5.2 Experimental

The complete experimental process is outlined in Chapter 2 in details. Briefly, the experimental methods are summarised below by sections.

5.2.1 Preparation of catalysts

The catalysts used in this study were iron based catalysts and prepared by an incipient wetness impregnation method. Iron nitrates, $Fe(NO_3)_3 \cdot 9H_2O$ (Iron (III) nitrate nonahydrate, Sigma-Aldrich), was used as catalyst precursors whilst SiC (silicon carbide, Fisher Scientific) and AC (activated carbon, Sigma-Aldrich) were used as supports. The supports were mixed with an aqueous solution of iron nitrate, the concentration of which was calculated to produce a desired Fe loading. The mixture was then stirred at 150°C on a magnetic hot plate for 3h until it became a slurry, which was moved into the drying oven and left overnight. The resulting solid mixtures were calcined in a furnace at 350 °C for 3 h. Finally, the active catalysts were obtained by a reduction process in a 10% H_2/Ar gas mixture at 800 °C for 6h.

5.2.2 Characterisation of catalysts

The pre- and post- reaction catalysts were carefully characterised by x-ray diffraction (XRD), thermogravimetric analysis (TGA), Laser-Raman spectroscopy, scanning electron microscopy (SEM), Energy-dispersive X-ray spectroscopy (EDS) and high-resolution transmission electron microscopy (HRTEM). The operating procedure and full details related to these techniques were given previously in Chapter 2.

5.2.3 Microwave initiated dehydrogenation process

The experimental setup is shown in Figure 2.1. The microwave system consists of a microwave generation system, a purpose-built microwave cavity and a control system.

Typically, the catalyst filled quartz tube was impregnated with aqueous hydrocarbon fuels, then the tube was exposed to microwave irradiation. Before starting microwave irradiation, the samples were purged with an Ar flow rate of 1.67 $mL \cdot s^{-1}$ for a period of 15 minutes. Then, the sample was irradiated

with microwaves for 10-30 min at a microwave input power of 750 W. The generated gases were collected and analysed by gas chromatography (GC). And the liquid products or unreacted hydrocarbons were analysed with a gas chromatograph mass spectrometer (GC-MS).

The sample temperature was measured using an infrared (IR) pyrometer, which was also used to control the power to the generator. The reflected power was measured by a crystal detector, from which the power absorbed by the sample is determined. During the microwave experiment a temperature (T) and power dissipation (W) versus time (t) of reaction profile was recorded[17, 18]. It should be noted that the microwave system is not impedance matched, thus the energy delivered to the sample cavity and the microwave power to which the sample was exposed was less than this value.

5.2.4 Conventional thermal dehydrogenation process

The conventional thermal experiments for diesel dehydrogenation were carried out in an electric furnace for comparison purpose with microwave-initiated experiments. The experimental setup is shown in Figure 2.4. The heating rate of electric furnace used in these experiments were 10 °C/min.

The conventional thermal dehydrogenation of diesel was investigated through two different procedures. For one thermal procedure, a diesel pre-loaded Fe/SiC sample was subjected to a pre-heated furnace (550 °C), while in another procedure, the Fe/SiC catalyst (without fuel) was pre-heated in the furnace to 550 °C and the diesel was then carefully introduced to the hot catalyst bed via a syringe

5.2.5 Compositional analysis of petroleum samples

The detailed composition of extra-heavy crude oil and crude oil were determined via elemental analysis. The composition of petroleum samples including diesel and petrol were analysed by a GC-MS. All the petroleum samples used in this study were supplied by Saudi Aramco.

The GC-MS analysis on these petroleum samples are given in Figure 5.1. The detailed chemical compositions for diesel, petrol, extra-heavy crude oil and crude oil are given in Appendix Table A1-A4, respectively.

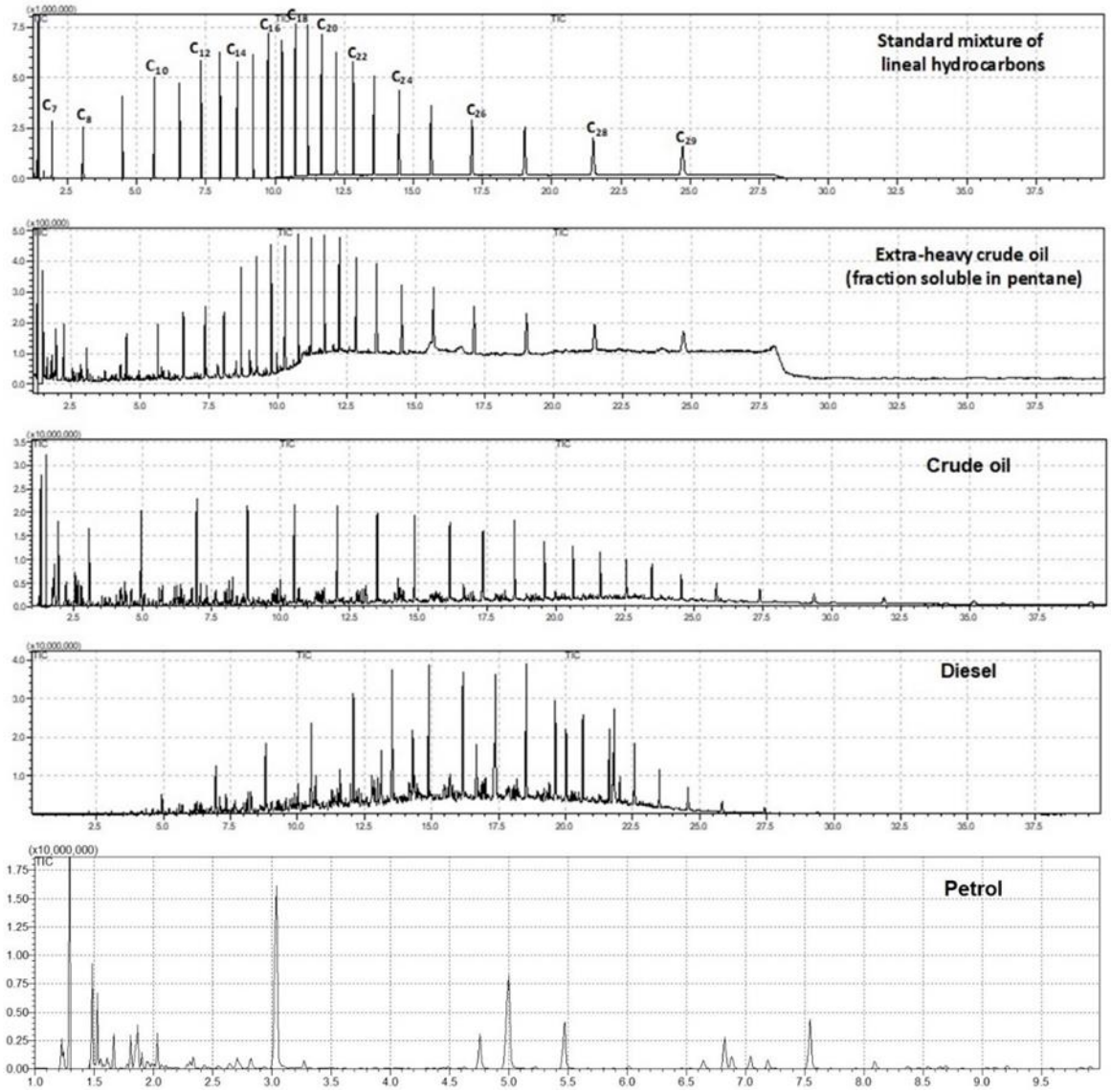


Figure 5.1. Gas chromatography-mass spectrometry (GCMS) analysis on extra-heavy crude oil, crude oil and diesel.

5.3 Results and discussion

5.3.1 Model fluid *n*-alkanes and aromatics

In addition to hexadecane ($C_{16}H_{34}$), liquid saturated alkanes (C_nH_{2n+2}) from C_7 to C_{17} were also investigated over 5 wt.% Fe/SiC catalysts and 5 wt.%-Fe, 5 wt.%-Ni FeNi/SiC catalysts respectively. It was demonstrated on Fe/SiC catalyst that hydrogen selectivity of over or close to 90% were produced from these saturated hydrocarbons (Figure 5.2a). Similarly, FeNi/SiC catalysts gave higher hydrogen selectivity than that of Fe/SiC catalysts.

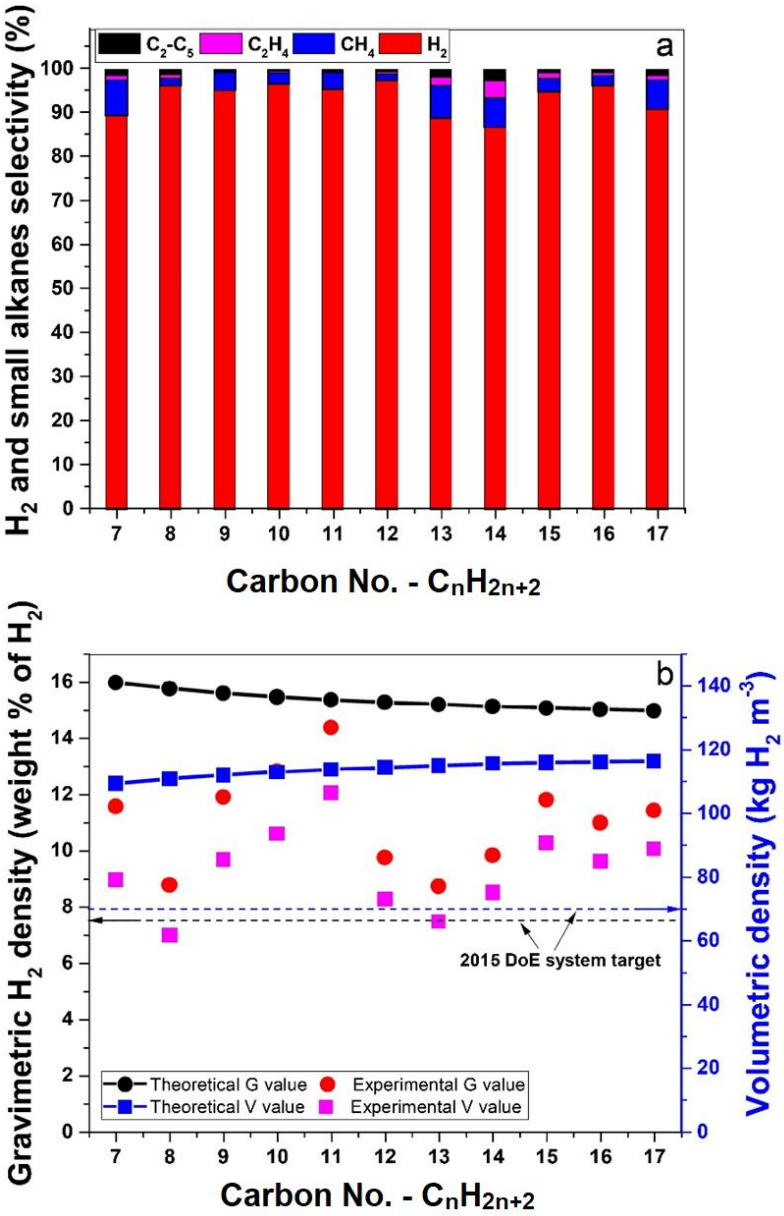


Figure 5.2. Microwave initiated dehydrogenation of saturated alkanes (C_7 to C_{17}) and aromatics over 5 wt.% Fe/SiC catalysts under 750W microwave irradiation. (a) Selectivity of H_2 and small alkanes; (b) Comparison on theoretical and experimental H_2 density of these aliphatics via microwave initiated heterogenous catalysis.

It should be noted that at current experimental set-up, only 10- 40 % of feedstocks were converted during this rapid catalytic process and the rest of the feedstock was vaporised and remained unreacted but can be recycled and again decomposed via this system. Although, the experimental gravimetric H_2 density and volumetric H_2 density of these alkanes were lower than their theoretical values due to the low conversion (Figure 5.2b), but these experimental H_2 density obtained was still higher than the target of hydrogen storage techniques set by U.S. DoE.

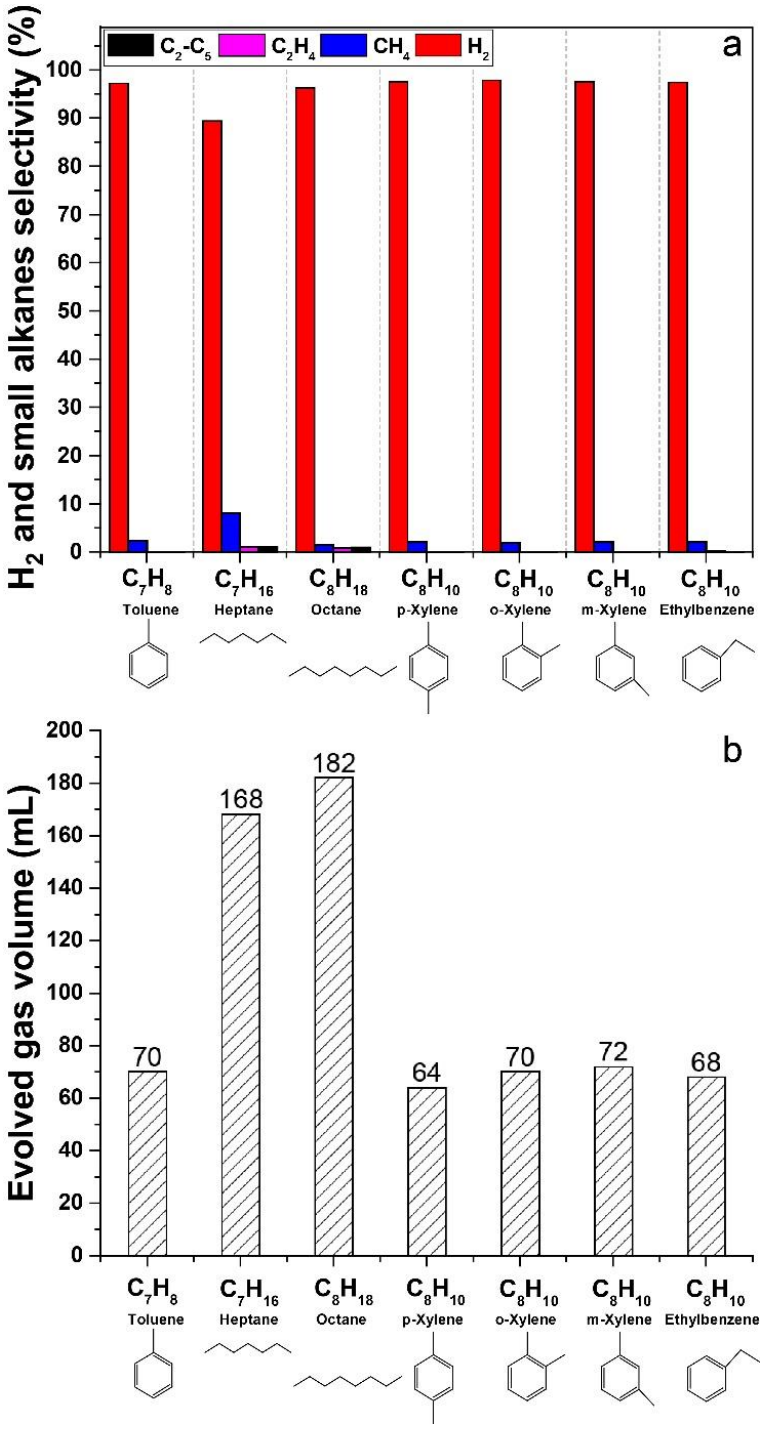


Figure 5.3. Comparison of microwave-initiated dehydrogenation of selective aliphatics and aromatics using a 5 wt.% Fe/SiC catalyst. (a) Selectivity of H_2 and small alkanes; (b) Evolved gas volume obtained through aromatics dehydrogenation.

The heptane and octane were compared with toluene and 3 isomers of dimethylbenzene and ethylbenzene to study on the difference between aliphatics and aromatics via microwave-initiated catalytic dehydrogenation (Figure 5.3). Each of the toluene, m, p, o- xylene and ethylbenzene produced

a hydrogen selectivity of over 95 % over Fe/SiC catalysts. The hydrogen selectivity obtained among aromatics dehydrogenation was higher than that of aliphatics (heptane and octane). This is ascribed to more stable C-C bond in aromatics [19] which is more difficult to break than a C-C bond in aliphatics. As a result, less light hydrocarbons such as methane, ethane and ethylene etc. were produced from aromatics.

Furthermore, when compared of aliphatics, less hydrogen was produced from aromatics, but higher H_2 selectivity was observed (Figure 5.3). This is considered due to the presence of benzene rings in aromatics are rather stable, thus causing lower H_2 yields whilst prohibiting the side reactions for small alkanes production (methane etc.).

5.3.2 Hydrogen production characteristics from petroleum and fossil hydrocarbons

Figure 5.4 shows the time-dependent hydrogen evolution arising from the microwave-initiated dehydrogenation of both crude and heavy crude oils and various fossil fuels using fine iron catalyst particles (typically 100 nm diameter) on the support materials of either activated carbon (AC) or silicon carbide (SiC). For the simplest comparisons, comparable weight % loading levels of the liquid fossil feedstocks on the same support was used.

Activated carbon is established as an excellent microwave absorber or receptor whilst silicon carbide is characterised by its superior mechanical thermal and dielectric properties which, coupled to exceptional chemical inertness, avoids any complicating issues that may arise with activated carbon support materials.

Immediately at the very initiation of microwave irradiation of the samples, a considerable volume of high-purity hydrogen was readily extracted from the petroleum and heavy liquid feedstocks, and that typically in periods of about 3 minutes. A selectivity of over 90 % for hydrogen in the exiting gas stream following this dehydrogenation of methane, petrol and diesel was obtained (Figure 5.5). The selectivity is defined here as the volume % of the particular product within the total volume of gaseous products.

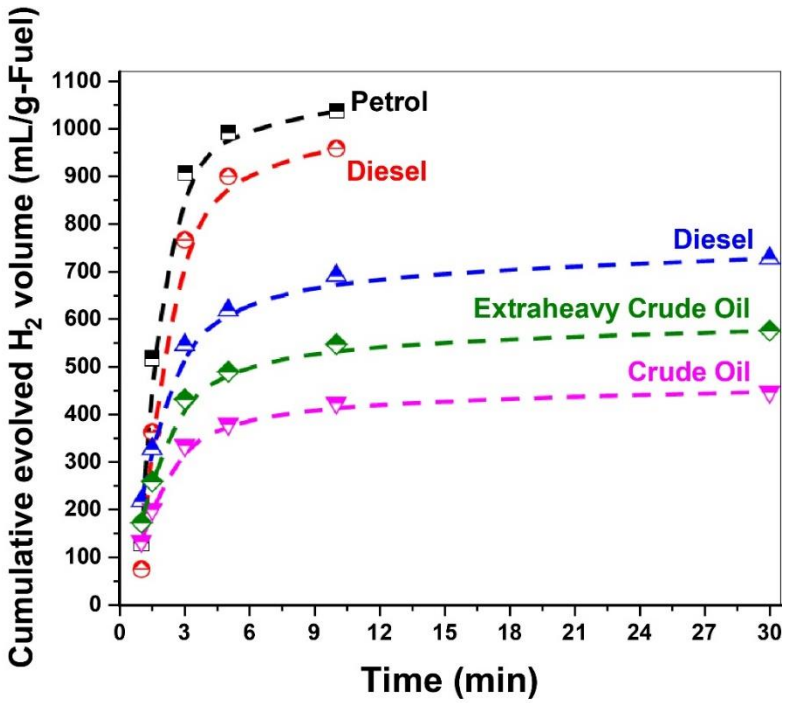


Figure 5.4. Cumulative evolved H_2 volume through the microwave-initiated iron catalysed dehydrogenation of fossil fuels. Samples are, black: 30 wt.% petrol @ Fe/SiC, red: 30 wt.% diesel @ Fe/SiC, blue: 40 wt.% diesel @ Fe/AC, magenta: 40 wt.% crude oil @ Fe/AC, olive: 40 wt.% extra-heavy crude oil @ Fe/AC

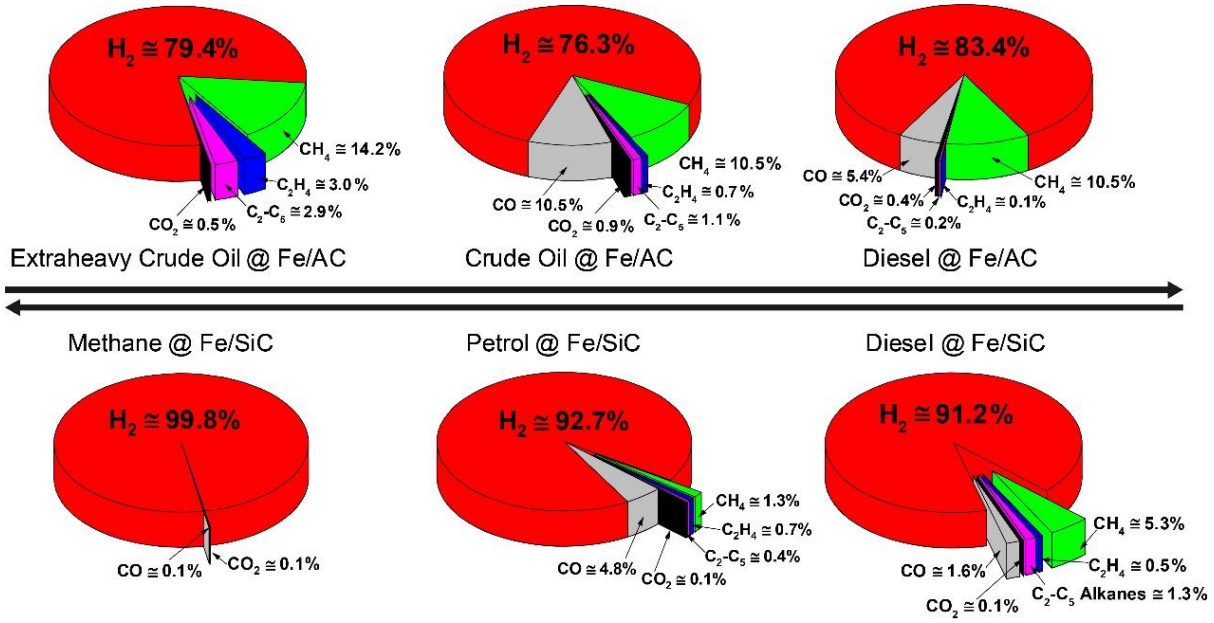


Figure 5.5. Evolved gas composition of various fossil fuel feedstocks over iron catalysts on silicon carbide (SiC) and activated carbon (AC) under microwave initiation.

For the heavier, and obviously inherently more complex crude and heavy crude oil, the selectivity of evolved hydrogen is decreased to ca. 75-85 %. Although less hydrogen is produced from these heavy feedstocks, microwave-initiated catalytic dehydrogenation is clearly still highly effective. Due to the inevitable extraneous or residual oxygen contained in the fuel feedstocks (see below), the catalysts and also their supports, the production of CO and CO_2 in very low concentrations cannot be avoided under our present experimental conditions[17, 18].

The dehydrogenation of methane to hydrogen and solid elemental carbon reached values of 90% conversion through this microwave-initiated catalytic dehydrogenation process (Figure 5.6). Corresponding quantitative conversion estimates for petroleum or crude oils are obviously more difficult since they are complex, multicomponent mixtures[20]. For example, petroleum (or crude oil) is a naturally occurring liquid mixture containing mostly hydrocarbons, but also containing some compounds of oxygen, nitrogen and sulphur.

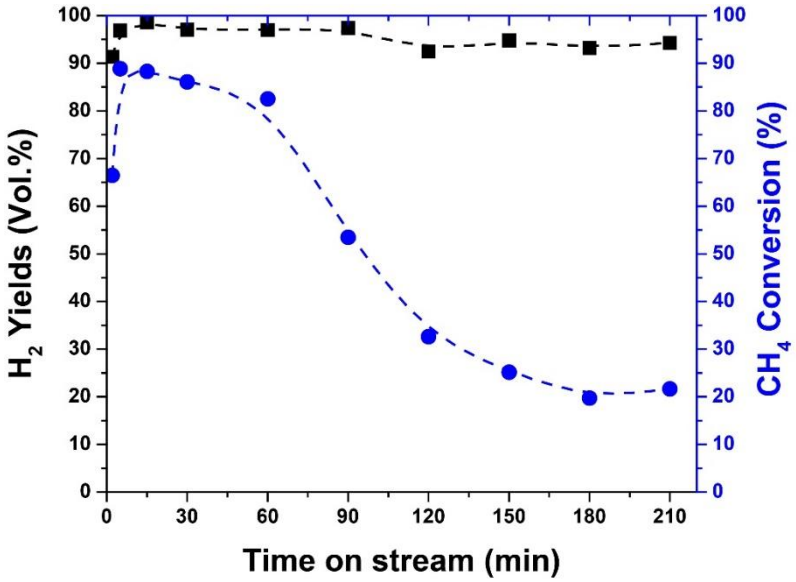


Figure 5.6. Methane conversion and hydrogen selectivity over 5 wt.% Fe/SiC catalysts under microwave. Reaction conditions; the reaction was conducted at microwave power of 750 W. Pure methane (>99.99%) was fed in a flow rate of 8.5 mL/min. The space velocity (SV) was 5.7 L/g_{cat}·h.

Notwithstanding, we report that hydrogen masses of 0.04, 0.051, and 0.065 kg were extracted from 1 kg of crude oil, extra-heavy crude oil and diesel, respectively, over Fe/AC catalysts (Figure 5.7), illustrating the efficacy of the microwave-initiated catalytic dehydrogenation process. Higher levels of hydrogen production, 0.086 and 0.093 kg of hydrogen were liberated from 1 kg of diesel and petrol,

respectively, over Fe/SiC catalysts, thus these hydrocarbons are themselves natural hydrogen storage materials.

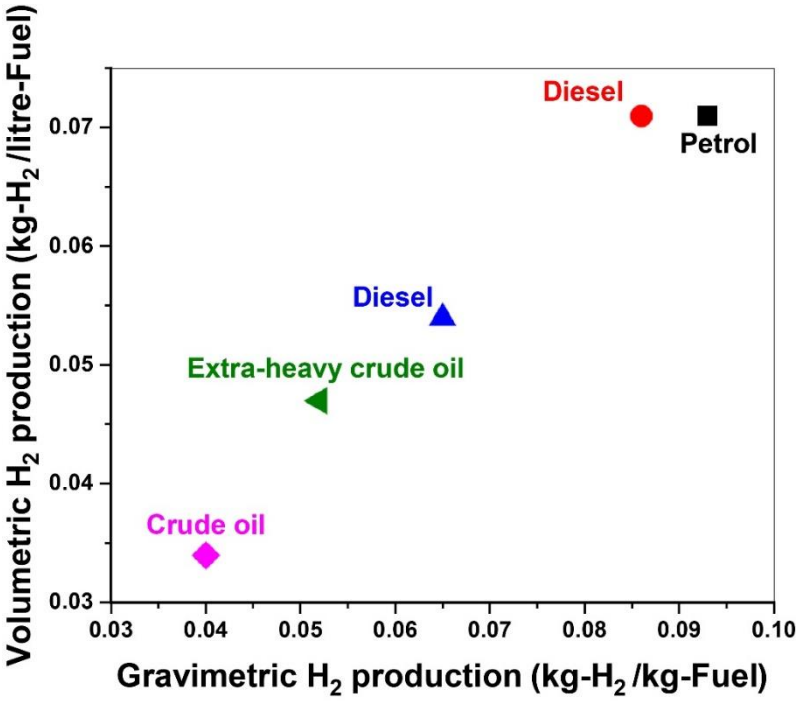


Figure 5.7. H_2 production per volumetric and gravimetric fuel consumption. Samples are, black: 30 wt.% petrol @ Fe/SiC, red: 30 wt.% diesel @ Fe/SiC, blue: 40 wt.% diesel @ Fe/AC, magenta: 40 wt.% crude oil @ Fe/AC, olive: 40 wt.% extra-heavy crude oil @ Fe/AC.

5.3.3 Parametric studies of the microwave-initiated dehydrogenation of diesel fuel

For detailed studies, the diesel was chosen as a well- characterised hydrocarbon fuel product derived from petroleum. The fuel consisted of mainly n-alkanes from C_{12} to C_{21} (89%) with some oxygen containing compounds (11%) such as dodecanol and methyl octadecenoate etc.; all constituents identified by gas chromatography-mass spectrometry (GCMS).

Under the microwave-initiated process, diesel fuel was rapidly dehydrogenated over the Fe/SiC catalyst. Hydrogen selectivity exceeded 91% in the evolved gases with less than a fraction of a percent of adventitious CO_2. Small alkanes, mainly methane, comprised ca. 7 vol. % of the remainder of the exit gases (Figure 5.5).

In Figure 5.8a, b and c, it shows data for “time-on-stream” experiments for diesel fuel on a Fe/SiC catalyst initiated under various microwave absorbed powers. It can be seen that whilst hydrogen

production rates are strongly dependent upon the incident microwave power levels, hydrogen selectivity itself is not significantly affected by the levels of incident and absorbed microwave power.

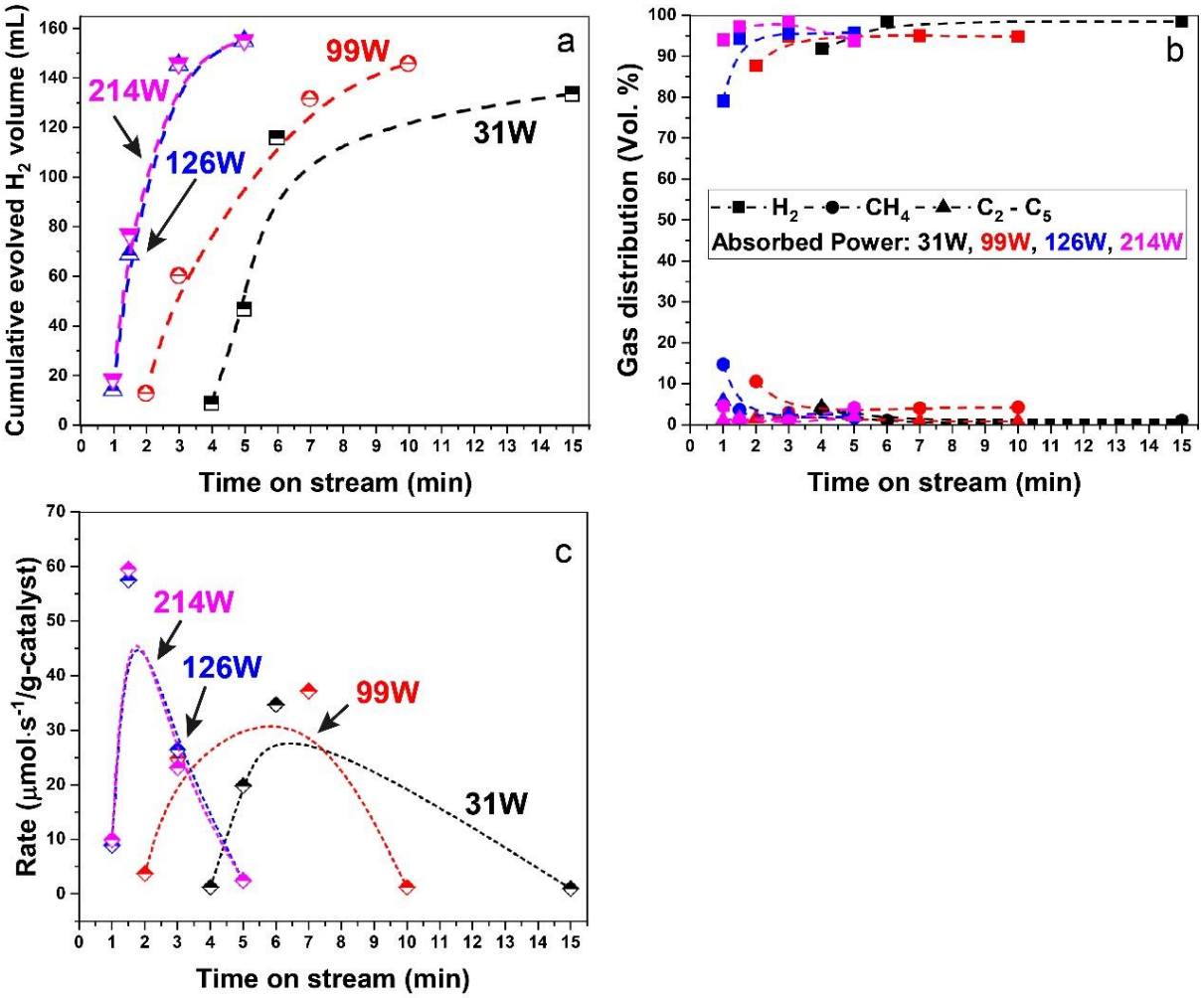


Figure 5.8. Study of hydrogen production from diesel over 5 wt.% Fe/SiC catalyst under microwave initiation. (a) Cumulative evolved H_2 volume determined by 'time on stream' with different absorbed power. (b) The effect of absorbed power on the gas distribution and (c) reaction rate of hydrogen production with different absorbed power.

Importantly, as with our earlier studies on wax[17], it should be noted that hydrogen evolution also ceases *instantly* upon the cessation of microwave irradiation. This is in direct contrast to any conventional thermal heating process, where hydrogen evolution continues to proceed even upon the loss of input (external) heat, as both the catalyst particle and the surrounding "bath" of hydrocarbons slowly cool. Further studies are underway to investigate this important aspect relating to the electromagnetic microwave energy – induced catalyst metal particle- host hydrocarbon ''bath'' interaction. This is a clear illustration that electromagnetic energy from the incident microwaves is

being directly – and highly effectively- transmitted to the metal catalyst particles themselves to catalyse hydrogen production from the fossil fuels.

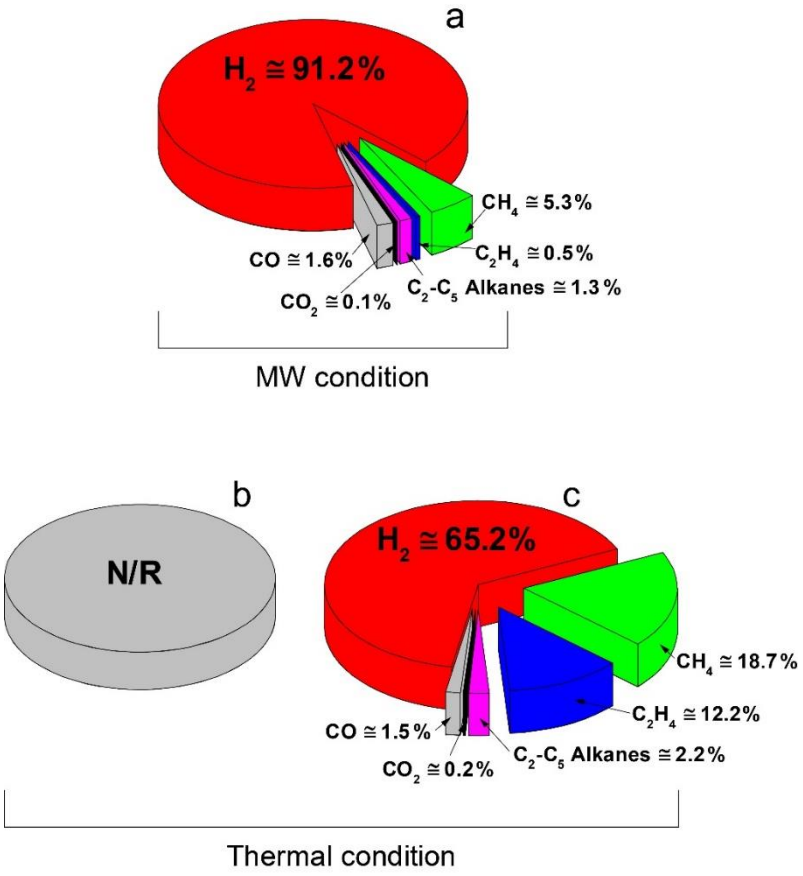


Figure 5.9. Comparison of product distribution from diesel @ 5 wt.% Fe/SiC sample under (a) microwave initiation and (b, c) thermal reactions. (b), a diesel pre-loaded Fe/SiC sample was subjected to a pre-heated furnace (550 °C), while in the (c), the Fe/SiC catalyst (without fuel) was pre-heated in the furnace to 550 °C and the diesel was then carefully introduced to the hot catalyst bed by a syringe. The average and the highest temperature recorded under microwave initiation were 416 °C and 568 °C, respectively. 'N/R' indicates no reaction was observed.

As shown in Figure 5.9, the microwave-initiated catalytic dehydrogenation of diesel produced different levels both of catalytic activity and the (resulting) product selectivities, as compared to the conventional thermal catalytic processes. A stand-out observation, actually common to all the various hydrocarbon feedstocks, is the recurring high selectivity to hydrogen formation under the microwave-initiated catalytic process, as compared to the conventional thermal catalytic dehydrogenation process. We attribute this behaviour once again to the incident microwave electromagnetic energy being selectively, effectively and preferentially absorbed by the iron fine particles as the active catalytic centre, with only modest heating of the surrounding bulk hydrocarbon fuel by the incoming microwaves. Thus,

pure hydrogen is rapidly extracted from the reactant hydrocarbon fuel through the microwave-initiated catalytic reaction at the iron particle surface; this process occurring faster than either the vaporisation of fuel from the heated particle (in our trickle-feed catalyst bed configuration) or the alternative catalytic- cracking to various hydrocarbons. In contrast, for the corresponding thermal process (Figure 5.9b), rapid vaporisation of the fuel at elevated temperatures predominates before significant catalytic dehydrogenation can occur, with attendant changes also in the resulting product distribution.

In the absence of microwave-initiation of the catalytic process, the hydrogen concentration was significantly decreased when the catalyst bed was preheated (using an electrical furnace) before carefully introducing the diesel fuel (Figure 5.9c); under these conditions, higher concentrations of light alkane products were obtained in the evolved gases, suggesting that (conventional) thermal cracking was dominant[21, 22].

In contrast, under microwave initiation, the iron particles themselves are rapidly heated to initiate the catalytic dehydrogenation process. This probably arises since a conventional thermally -heated catalytic process produces a multitude of active constituents at the high temperatures of the catalytic process – these active constituents would include the metal catalyst particles, the support material itself and the hydrocarbon bath.

In view of the complex nature of the microwave-initiated heterogeneous catalytic processes involved in this process, at present it is not possible to formulate a complete detailed mechanism for the highly selective dehydrogenation we observe. Further detailed studies that take into account the nature, and amount, of selective microwave absorption during catalytic turnover are now planned. However, what is clear is that this heterogeneous system - hydrocarbon fuel + catalyst - under microwave initiation can lead to non-equilibrium conditions at the catalyst that appear to accelerate specific endothermic reactions. In particular, the primary products of the catalytic transformation on the (microwave) heated metal particle surface are quenched rapidly as they diffuse away from the metal particle and move into the bulk of the colder hydrocarbon reaction mixture surrounding the catalyst, (of course, that hydrocarbon fluid does not itself significantly absorb the microwave energy). It may be the case that products such as hydrogen, an atypical product for the conventional (uniform) heating of the catalytic system, can be formed and stabilised. Furthermore, hydrogen corresponds to the stabilised product that

very high “local” temperatures – i.e. at the catalyst particle itself - can be rapidly generated under non-equilibrium pyrolytic conditions.

5.3.4 Post- reaction analysis of catalysts

5.3.4.1 High resolution transmission electron microscopy (HRTEM)

At the completion of microwave initiation experiments, high-resolution transmission electron microscopy (HRTEM) revealed turbostratic graphitic sheets and multi-walled carbon nanotubes (MWCNTs) that encapsulate both iron and iron carbide nanoparticles. The generation of iron carbide suggested that the supported iron particles react with the hydrocarbon during the catalytic reactions under microwave initiation (Figure 5.10b, c).

The presence of Fe_3O_4 has also been detected by HRTEM (Figure 5.10a) in the unreacted catalyst and is considered to form due to the aerial oxidation of nanoparticulate iron. Energy-dispersive X-ray spectroscopy (EDS) mapping also detected the presence of oxygen on some of the iron particle surfaces which could be the source of CO (Figure 3.15).

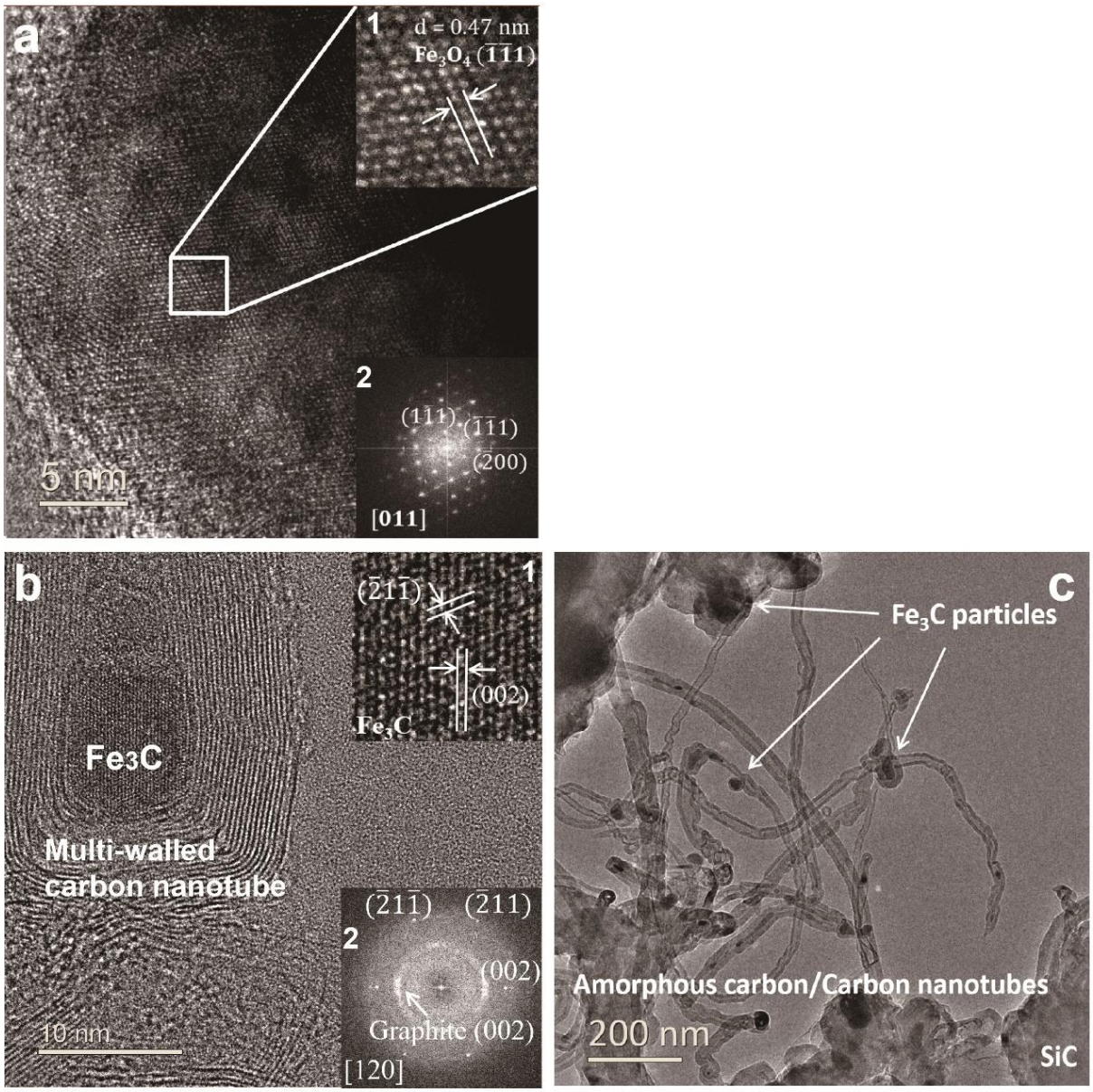


Figure 5.10. Characterisation of 5 wt.% Fe/SiC catalyst before and after microwave-initiated dehydrogenation of diesel. HRTEM images of (a) unreacted catalyst recorded along a <011> zone axis of a Fe_3O_4 particle and (b) spent catalyst recorded along a <120> zone axis of a Fe_3C particle. In Figure 5.10a, the presence of Fe_3O_4 is due to the oxidation of Fe by exposure to air. (a2) Diffraction pattern calculated from images of Fe_3O_4 particles of 5 wt. % Fe/SiC, before; and (b2) after microwave-initiated catalytic reactions, showing characteristic reflections from graphite (002) plane and Fe_3C along <120> zone axis. (c) Low magnification TEM images of produced carbon nanotubes and iron carbide particles in a spent sample.

5.3.4.2 X-ray diffraction (XRD), Raman spectroscopy, thermogravimetric analysis (TGA) and scanning electron microscopy (SEM)

The formation of iron carbide was also confirmed by X-ray diffraction (XRD) (Figure 5.11a). The peak of iron at 44.79° was detected in the fresh sample but disappeared after microwave reaction after

which the diffraction peaks of Fe_3C detected in spent samples at the angles (2θ) of 42.92°, 43.82°, 44.72°, 45.04°, 45.9°, and 49.18° [23]. Although no single diffraction peak of carbon was observed in the spent samples, the formation of graphitic carbon and MWCNTs were evident in our HRTEM studies, as well as the Raman spectra, thermogravimetric analysis (TGA) and scanning electron microscope (SEM) (Figure 5.12).

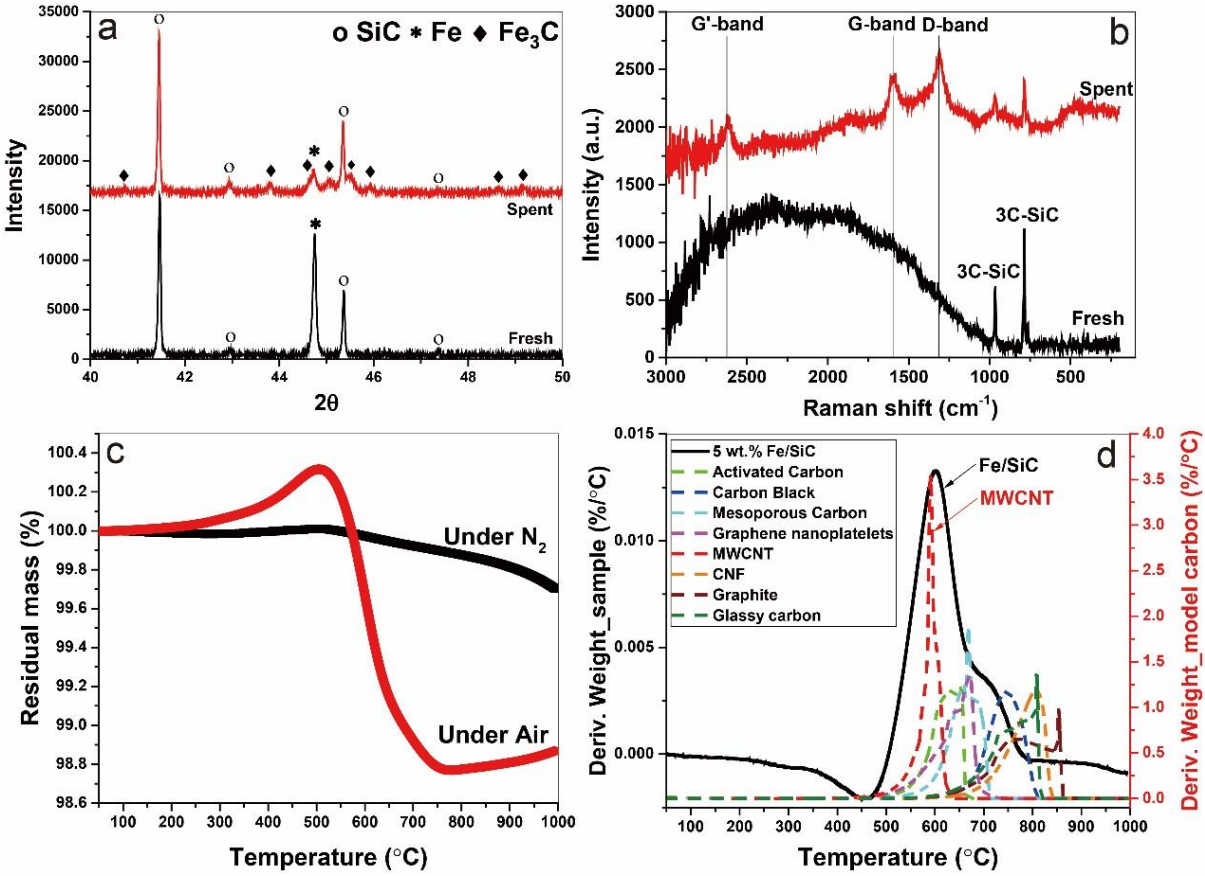


Figure 5.11. Pre- and Post- reaction characterisation of 5 wt.% Fe/SiC catalyst. (a) X-ray diffraction (XRD) patterns and (b) Raman spectra of 5 wt.% Fe/SiC catalyst. before and after microwave-initiated dehydrogenation of diesel; (c) Thermogravimetric analysis (TGA) of spent sample after microwave treatment, the sample was first characterised under nitrogen, and followed by a temperature programmed oxidation; (d) Derivative plots of temperature programmed oxidation of spent sample reference to the model carbons.

Raman spectroscopy reveals characteristic D-band, G-band and G'-band of solid carbon (Figure 5.11b) in the spent samples. The D-band observed at around wavelength of 1350 cm^{-1} is characteristic of amorphous or disordered carbon, while the peak at about 1580 cm^{-1} (G-band) is ascribed to the vibration of sp^2-bonded carbon atoms in a graphite layer corresponding to ordered graphite carbons.

The G'-band peak at around 2700 cm^{-1} is associated with the process of two-photon elastic scattering. The peak intensity ratio of I_G/I_D and $I_{G'}/I_G$ of the spent samples are 0.9 and 0.79, respectively, which suggests the deposited carbon has high carbon nanotubes content[24]. This is also evident in our thermogravimetric analysis (TGA) when compared to various model carbons.

The TGA study under N_2 atmosphere shows that no intermediates and/or unreacted feedstock were stored in the spent catalysts (Figure 5.11c). The following temperature programmed oxidation (TPO) illustrated the yield of carbon after single batch test, which is about 2 wt.%. The catalysts can be effectively used for several catalytic cycles through successive additions of fresh feedstock to the reactor system with the growing carbon instantly accumulated on the metal catalyst particle. The oxidation temperature of resulting carbon was referenced to a range of selected model sp^2-bonded carbons (Figure 5.11d), including activated carbons (ACs), carbon black (CB), graphite, carbon nanofibers (CNFs) and MWCNTs etc. Among these 8 different carbons, the resulting carbon in the spent catalyst has a similar oxidation temperature to MWCNTs at about 593 °C, which also strongly suggests that the majority of carbon produced through this catalytic dehydrogenation is carbon nanotubes. A secondary peak at ca. 700 °C is considered caused by the oxidation of other types of carbon with high content of structural defects.

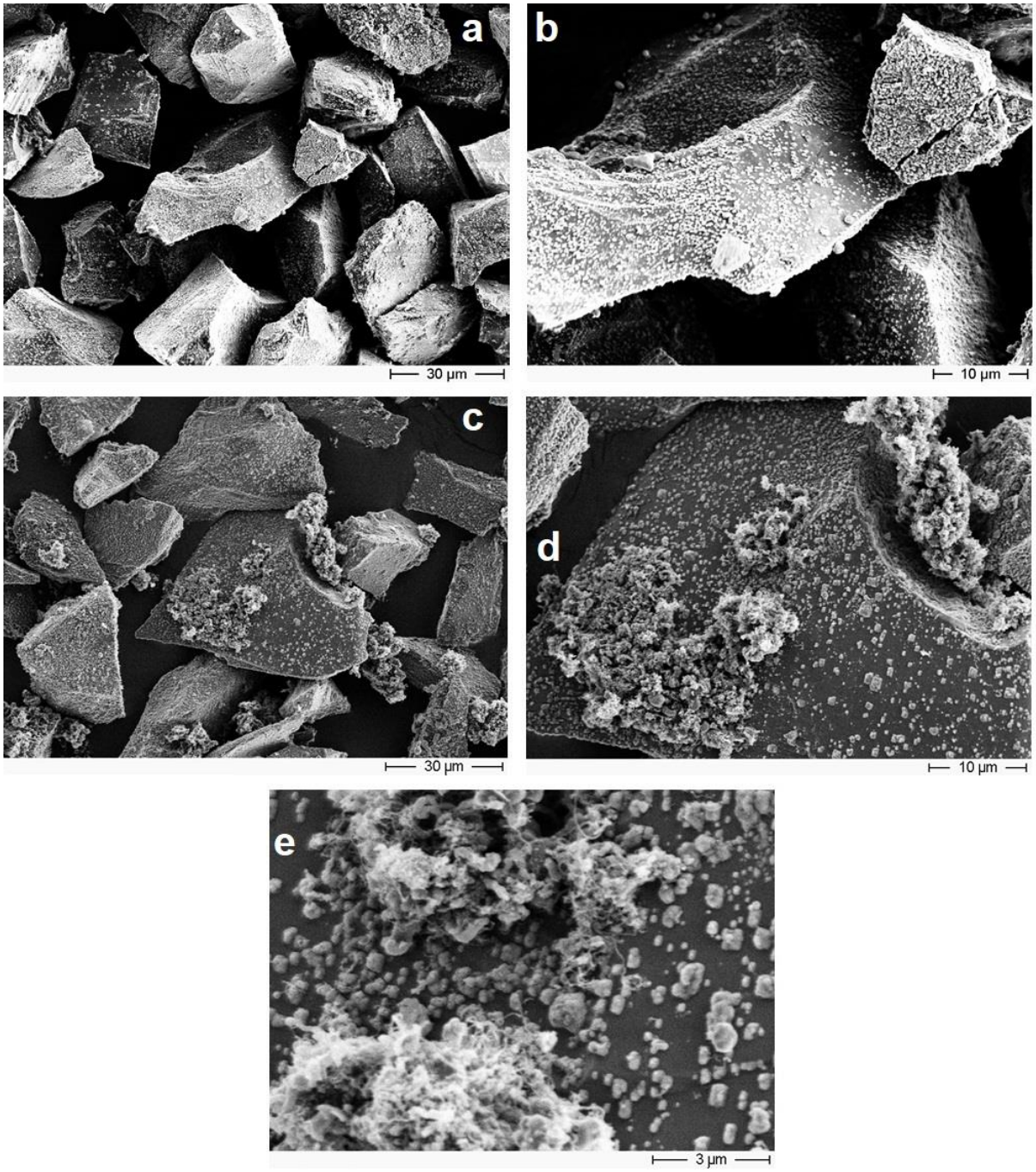


Figure 5.12. The scanning electron microscope (SEM) of 5 wt.% Fe/SiC catalyst, (a), (b) before and (c), (d) and (e) after microwave-initiated dehydrogenation of diesel.

5.3.5 Fossil fuels as hydrogen storage materials

Fossil hydrocarbon fuels are themselves excellent natural hydrogen storage materials since they potentially exceed the targets of H_2 gravimetric and volumetric densities set by the U.S DoE[15, 25]. Through the microwave-initiated catalytic dehydrogenation of various fossil fuels over Fe catalysts, the

fuels were rapidly and deeply decomposed to hydrogen and solid carbon. The experimental hydrogen density of gravimetric value and volumetric value was then calculated by the equations showing below:

$$Gravimetric\ H_2\ density = \frac{Mass\ of\ H_2\ obtained}{Fuel_{input} - Fuel_{re-collect}} \times 100\% \quad (5.1)$$

$$Volumetric\ H_2\ density = \frac{Mass\ of\ H_2\ obtained}{(Fuel_{input} - Fuel_{re-collect}) \times D_{fuel}} \quad (5.2)$$

where, the mass of H_2 is calculated from the collected gas volume and the H_2 selectivity obtained by GC. D_{fuel} refers to the density of fuel.

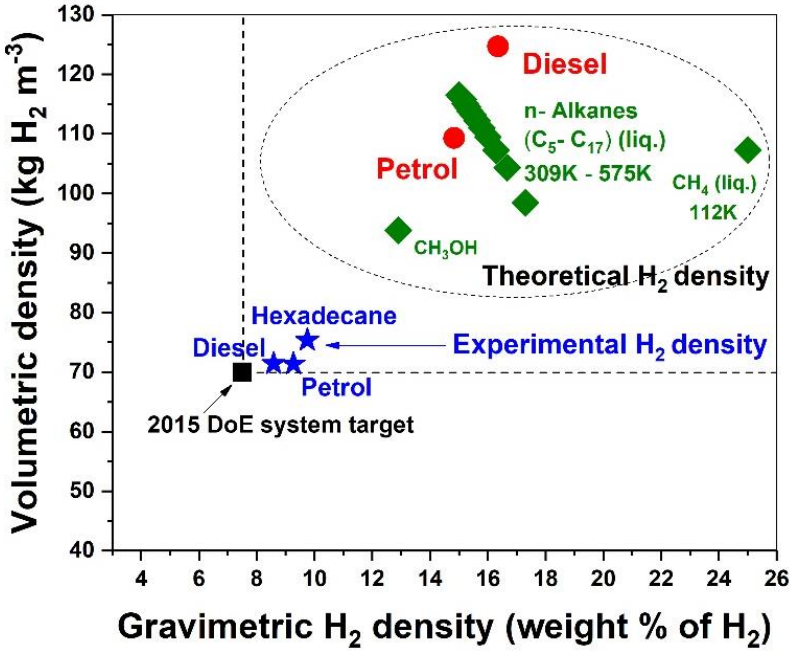


Figure 5.13. Comparison of theoretical hydrogen density of fossil hydrocarbons with the experimental hydrogen density obtained via microwave-initiated catalytic dehydrogenation of diesel and petrol over 5 wt.% Fe/SiC catalyst.

The results for the microwave-initiated iron -catalysed dehydrogenation of diesel, has shown H_2 gravimetric and volumetric densities of 8.6 kg-H_2/ kg and 71 kg-H_2/ m^3, respectively, exceeding the target of 7.5 kg-H_2/ kg and 70 kg-H_2/ m^3 set by the U.S DoE (Figure 5.13). Microwave-initiated catalytic dehydrogenation of fossil fuels could therefore become potentially viable for fuel cell vehicles because of three attractive features: *First*; the rapid production of high-purity hydrogen, highlighted in this study; *Second;* the necessity for only a small – scale microwave source and reactor system easily attainable for modern high power, small microwave devices for either localized or distributed distribution; and

Third; the well-established distribution infrastructure for fossil fuels. Clearly, further scale-up and other studies are needed in both engineering aspects and the optimisation of the entire catalytic process for future applications. Nevertheless, this work clearly highlights the possible advantages of microwave to assist in the instant generation of high purity hydrogen, not only from untreated petroleum products (crude oil etc.) but also from a variety of fossil-derived liquid fuels.

5.3.6 Net Energy Balance (NEB) considerations

Turning to the important consideration of energy balance, the microwave system is a rather complex system, particularly when combined with absorption of a dispersed heterogeneous catalysis in a host hydrocarbon medium. Thus, it is difficult to evaluate accurately the efficiency, particularly in a general-use laboratory microwave cavity device without, for example, impedance matching. Notwithstanding, this section attempts to look at the ultimate effectiveness of these hydrogen production processes through evaluation of the "Net Energy Balance (NEB)" [17, 26].

In its simplest and most transparent form, the NEB simply reflects the ratio of energy derived (i.e. the *Energy Out*) from the exiting chemical feedstock (here taken solely as hydrogen and neglecting the chemical energy of co-product solid carbon) to the energy invested (i.e. the *Energy In*) for the particular process.

Therefore, it takes the NEB here to be the ratio of chemical energy (*Energy Out*) as the enthalpy of combustion of only the hydrogen produced from the fossil fuels, to the energy invested (*Energy In*) as the electricity power consumption in both the microwave system or the electric furnace.

$$NEB = \frac{Energy\ Out}{Energy\ In} = \frac{Enthalpy\ of\ combustion\ of\ produced\ hydrogen}{Electricity\ consumption} \times 100\%$$

5.3.6.1 Thermodynamic analysis

As a preliminary investigation, a detailed thermodynamic analysis was also carried out on the process of the complete dehydrogenation of diesel as a representative hydrocarbon fuel, via Eq. 5.3.

$$C_nH_m \xrightarrow{catalyst} nC + \frac{m}{2}H_2 \qquad (5.3)$$

Petroleum-derived diesel is usually composed of about 75% of saturated hydrocarbons (primarily paraffin, including *n*, *iso*, and cycloparaffin) and 25% aromatic hydrocarbons (including naphthalene and alkyl benzene). However, different contents for diesel are found in the literature [27-29]. For simplicity, a specific diesel content was chosen for the calculation as follow:

Normal paraffin (60%): n-pentadecane (n-$C_{15}H_{32}$, 20%), n-hexadecane (n-$C_{16}H_{34}$, 20%) and n-heptadecane (n-$C_{17}H_{36}$, 20%)

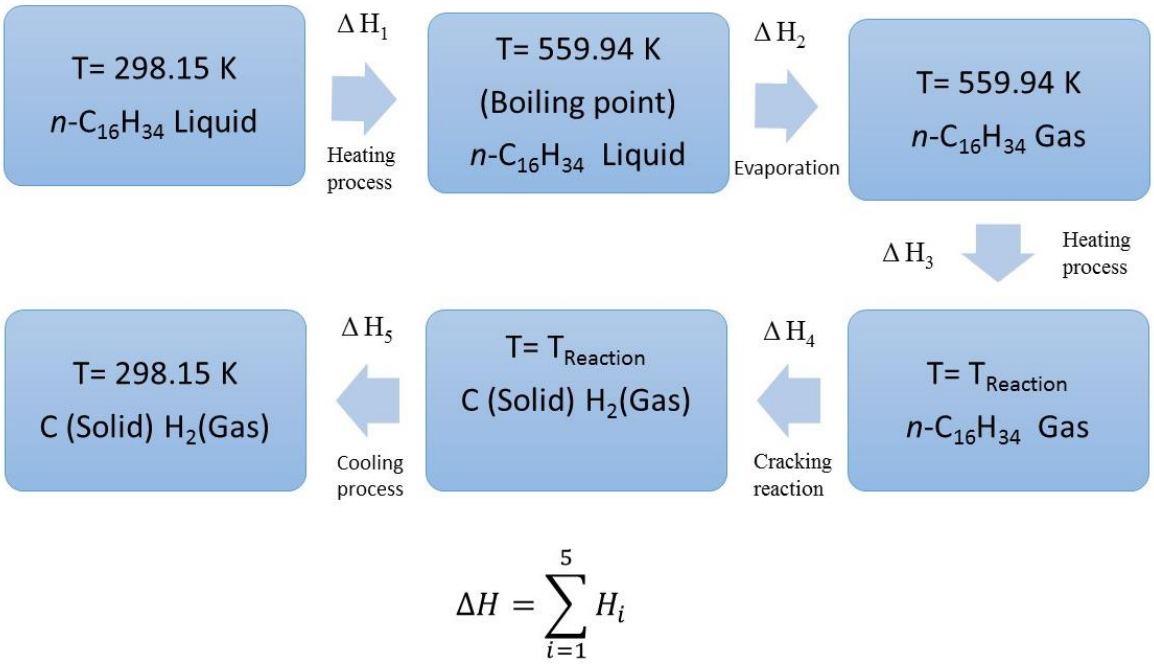
Cyclo-paraffin (15%): Decylcyclopentane (c-$C_{15}H_{30}$, 5%), Decylcyclohexane (c-$C_{16}H_{32}$, 5%) and Undecylcyclohexane (c-$C_{17}H_{34}$, 5%)

Alkylbenzeners (15%): 1,3,5-trimethyl benzene (C_9H_{12}, 7%), and Diphenyl ($C_{12}H_{10}$, 8%)

Indane: indane (C_9H_{10}, 5%)

Naphthalenes: Naphthalene ($C_{10}H_8$, 5%)

Below in Figure 5.14, the *n*-hexadecane is taken as an example to show the calculation of energy required for the cracking process. The energy requirement for the deep dehydrogenation of diesel was then calculated separately among different compounds following the various proportions shown above. As a result, the energy requirement for the complete dehydrogenation of the diesel described above is 1.40 MJ/kg, whilst 1.43 Nm^3 H_2 gas can be obtained per kg diesel. The energy output is then calculated as the enthalpy of combustion of the hydrogen produced, and thus for the 1.43 Nm^3 H_2 gas/ kg the energy out is 18.25 MJ/kg. In addition, same thermodynamics analysis on tested diesel (based on its constitution obtained by GCMS) showed that the energy requirement of complete dehydrogenation is 2.04 MJ/kg and with the amount of H_2 gas produced the energy output is 20.97 MJ/kg.



$$\Delta H = \sum_{i=1}^{5} H_i$$

Figure 5.14. Energy input of *n*-hexadecane cracking in atmospheric pressure.

Therefore, it concludes that the theoretical minimum energy required for complete dehydrogenation of diesel to elemental hydrogen and solid carbon is ~1.4 MJ/kg-Diesel and the produced hydrogen has an enthalpy of combustion of ~18.25 MJ/kg-Diesel. Thus, a very large positive net energy balance can, in principle, be obtained, given a high selectivity in the dehydrogenation process.

5.3.6.2 NEB comparison of microwave and conventional thermal methods in lab scale

However, the NEB ratio is of course critically dependent on the absorbed microwave power (i.e. the delivered power), Thus, the delivery of microwave power to the entire catalytic system and the subsequent conversion need to be further optimised and integrated in order to achieve these theoretical values.

Unfortunately, at present nearly 75 – 90% of the microwave energy used in our small-scale experimental laboratory configuration is lost (Figure 5.15), quite simply because the high-power microwave device is presently configured only for our very small sample volume (ca. 1.13 cm^3). However, future larger-scale microwave systems would be designed to achieve 99.9% efficient absorbed power and, most important, renewable sources of primary electricity can be used for the

generation of microwaves[30-32]. Such technology optimisation can lead to significant energy savings towards this process.

Notwithstanding these present laboratory limitations, it can be seen that the microwave –initiated process is energy efficient, as compared to conventional thermal catalytic processes (Table 5.1 and Figure 5.16). In this comparison, the corresponding conventional thermal catalytic dehydrogenation process was carried out in an electric furnace. Both processes (microwave + thermal) were controlled at a comparable reaction temperature with close to identical amounts of diesel input.

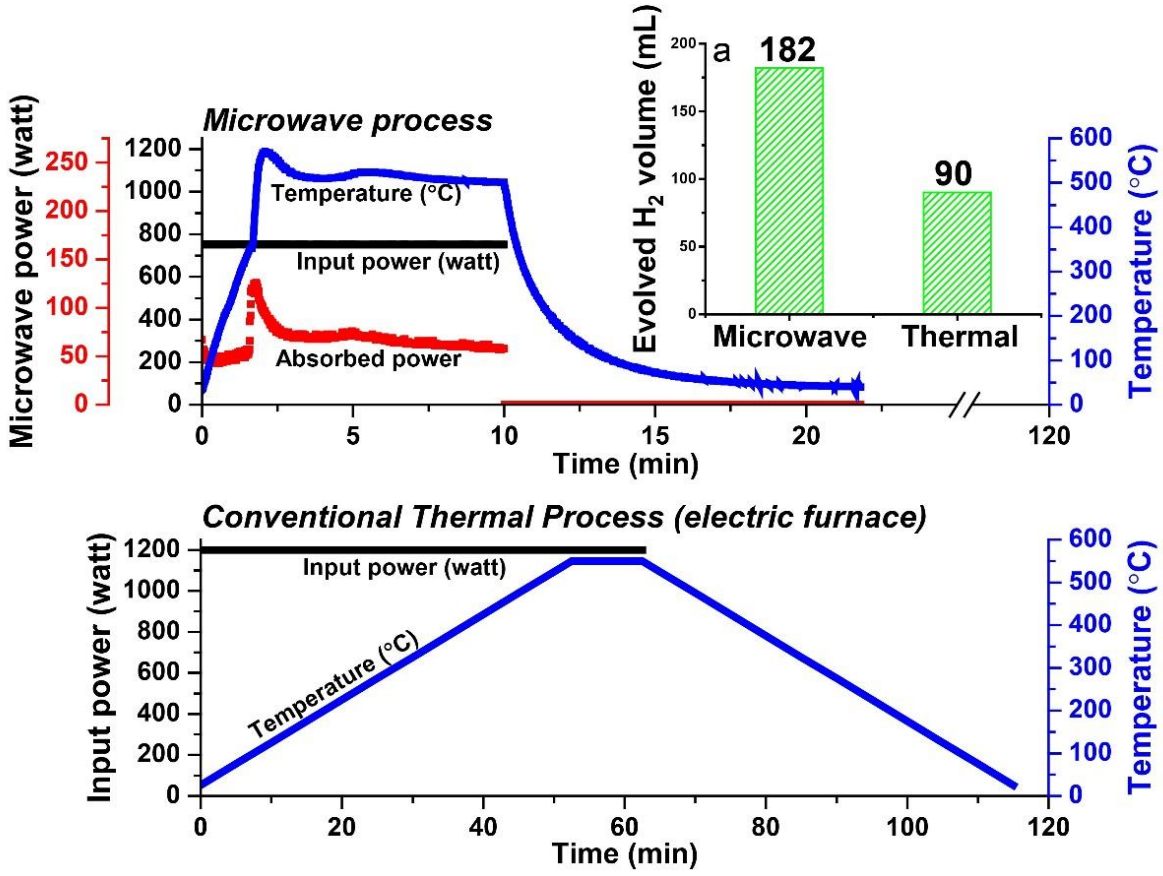


Figure 5.15. Comparison of microwave process and conventional thermal process for diesel dehydrogenation over 5 wt.% Fe/SiC catalyst. Note the differences in time for the two processes with the maximum yield of H_2 in the microwave process occurring after ca. 10min as compared to ca. 60 min for the conventional thermal process (a1).

Table 5.1: Comparison of the energy balance of microwave and conventional thermal methods.

	Microwave method*	**Thermal method**
Input power (W)	750 (126)	1200
Pre-heating (min)**	0	52.5
Experimental time (min)	10	10
Energy In (J)	450000 (75600)	4500000
Produced H_2 (mL)	182	90
Energy Out (J)***	2323	1149
Net Energy Balance (NEB)	0.516 (3.072)	0.026

* The number in parentheses shows the absorbed microwave power with corresponding NEB. ** The furnace used in the thermal method are pre-heated from room temperature (25 °C) to 550 °C by the heating rate of 10 °C /min. *** The energy out is calculated as the enthalpy of combustion of the produced hydrogen.

Figure 5.15 presents the profile of the two processes in terms of the electric input power and temperature. We note again the very short times for hydrogen evolution under microwave-initiation[17], and this highly effective energy transfer process in comparison to the conventional thermal process for heating catalyst particles and the subsequent dehydrogenation process is at the very heart of the enhanced efficiencies.

In relation to the Net Energy Balance (NEB) considerations, the *Energy Out* is taken as the enthalpy of combustion of the produced hydrogen from the two dehydrogenation processes, whereas, the *Energy In* refers to the electricity power consumption of the two different systems, which are calculated from their tabulated electric power rating and the experiment time of two processes. In the microwave-initiated process, the delivered (absorbed) microwave power has also been presented to give an outlook for a future optimised microwave system (Figure 5.16).

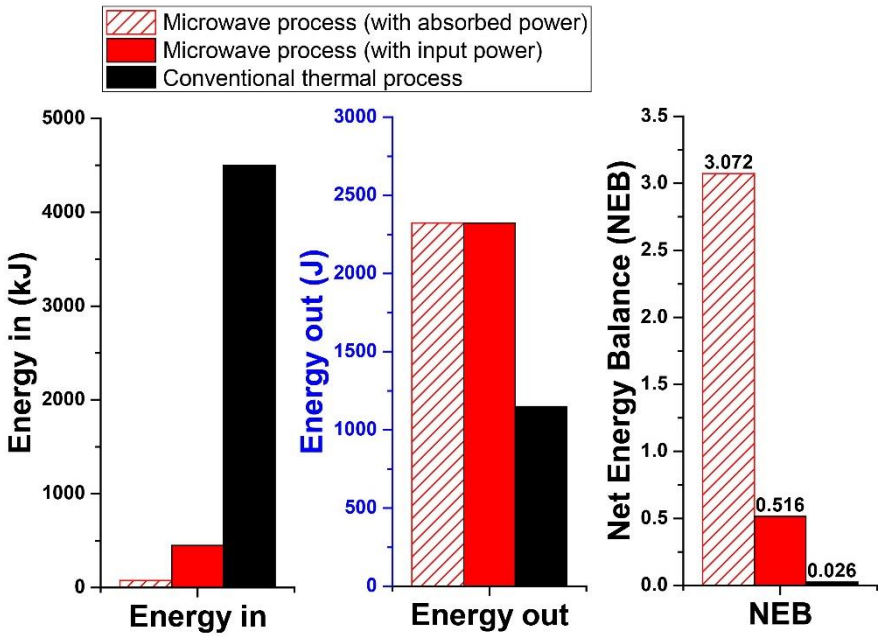


Figure 5.16. Energy balance evaluation between microwave process and conventional thermal processes. * The *Energy Out* is calculated as the enthalpy of combustion of the produced hydrogen.

It was found that the energy balance of *both* microwave and thermal processes were very low at the laboratory scale set-up, typically, less than 3%. However, the microwave initiation points to about 20 times higher NEB values as compared to values obtained under conventional thermal process, when one takes into account the time axis of both processes (Figure 5.16).

The superior Net Energy Balance of using microwaves for hydrogen production is due primarily to the rapid heating and the high activity and selectivity of the fine iron catalyst. Again, it should be noted that in our laboratory configuration, only about 17% of microwave input power was absorbed at the catalyst system used for the dehydrogenation process. The energy balance of the microwave could reach nearly 120 times higher than the thermal process if one considers only the level of directly absorbed microwave power.

5.3.7 The regeneration of metal catalysts and carbon by-product conversion

The Figure 5.17 below presents the results of a study to regenerate the iron catalyst activity by removing, through combustion, the build-up of carbon residues following a successive of 10 catalytic cycles. The high initial dehydrogenation rate in catalytic activity gradually diminished and

finally transitioned to at a low quasi-steady reaction rate. Following removal of elemental carbon on the catalyst particle by simple combustion after 10 cycles, the catalyst's activity was recovered and remained for several cycles of dehydrogenation. It should be noted that the activity of the catalyst was not fully recovered because of iron oxide presented after the combustion process.

Furthermore, the metal catalysts and indeed the carbon co-product could also be regenerated through gasification with steam to produce H_2 and CO. Then the syngas can be either separated or used directly as a Fischer- Tropsch feedstock and subsequently recycled back to high-value hydrocarbons. In this process, more H_2 can be produced and importantly, the carbon product itself could now also act as a "microwave receptor" catalyst under microwave irradiation.

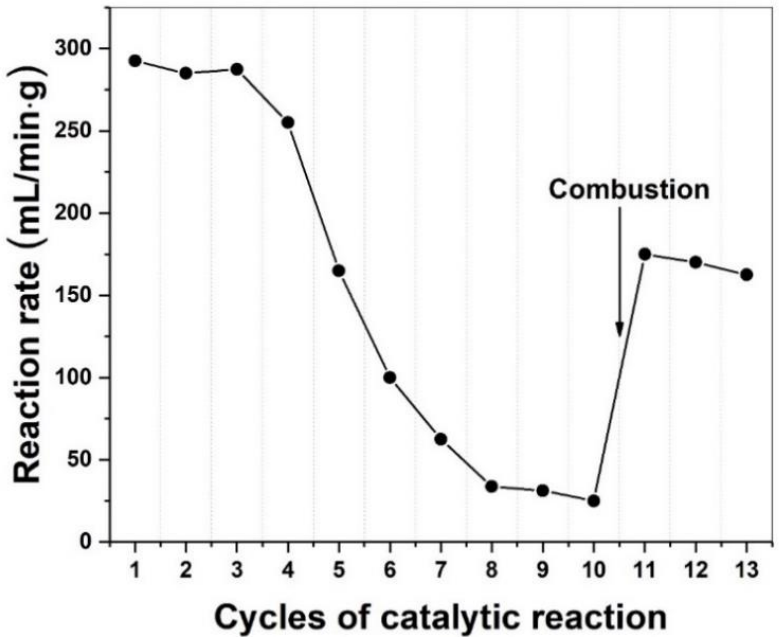


Figure 5.17. Successive tests on diesel dehydrogenation under microwave irradiation over 5 wt.% Fe/SiC catalysts. 0.5 mL of diesel was refuelled between each cycle and every cycle of tests were run for 10 minutes. The catalyst was recovered by combustion at 550 °C between cycle 10 and 11 in order to remove resulting carbon residues; the catalyst didn't reduce further, and the iron retained as oxides after cycle 11.

5.3.8 The storage and possible utilisation of carbon by-product residues

It is important to compare the present approach with conventional carbon capture and storage (CCS) to prevent the increasing CO_2 level in atmosphere by capturing and storing gaseous CO_2 under the ocean or into geologic formations (e.g. depleted oil and gas reservoirs, etc.)[33-35]. CCS remains an expensive

and ecologically uncertain solution; the capture, transportation and disposal of CO_2 remain costly and the potential hazards associated with underground and oceanic CO_2 sequestration are still uncertain[33, 36, 37]. Thus, an alternative route for CCS, could be achieved by extracting and storing *solid carbon* itself from our microwave-initiated catalytic dehydrogenation of fossil fuels, whilst also providing the formed hydrogen to be utilised as clean fuel. As Muradov[33] has noted, it is more attractive -from both a technical and indeed an ecological (and societal) viewpoint to store *elemental* carbon underground rather than *gaseous* CO_2. To contrast and reflect on the levels of both capture processes; taking diesel as an example, the complete dehydrogenation of 1 kg diesel to hydrogen and carbon would generate around 0.861 kg of elemental carbon. The complete aerial combustion of this same 1 kg of diesel will lead to 3.155 kg of CO_2 emission, corresponding to 1.606 m^3 of CO_2 released to the atmosphere.

Efficient catalytic dehydrogenation of the various hydrocarbon sources and fuels clearly leads to the production of pure by-product, elemental, solid carbon. It should be noted also that the resulting carbon nanotubes produced from this process potentially have high value whilst the iron catalysts are both inexpensive and abundant. The recycling of the pure co-product carbon for other applications is attractive and a key point that has been outlined elsewhere by Muradov, Steinberg and co-workers[33, 38, 39]. In Figure 5.18, potential utilisation routes were listed for the solid carbon product generated by microwave-initiated fossil fuels dehydrogenation. One possible application is that the carbon can be used as catalysts for other processes (e.g. electrochemistry) and carbon electrodes for industrial scale electrolyisis. In addition, given the fact that the majority of carbon produced during the process are CNTs. Deng *et al.* previously synthesised a catalyst with iron nanoparticles inside the CNTs[40], that exhibits a high activity and stability towards oxygen reduction reaction (ORR) in polymer electrolyte membrane fuel cells (PEMFC). Moreover, it has been estimated that the direct carbon utilisation by other areas (e.g. building construction materials and soil amendment) could potentially consume very considerable amounts of the solid carbon by-product[33]. Besides, it should be importantly noted that the carbon has a great host of uses such as manufacturing graphite anodes for the isolation of metals like aluminium, as well as producing syngas for valuable chemicals' synthesis.

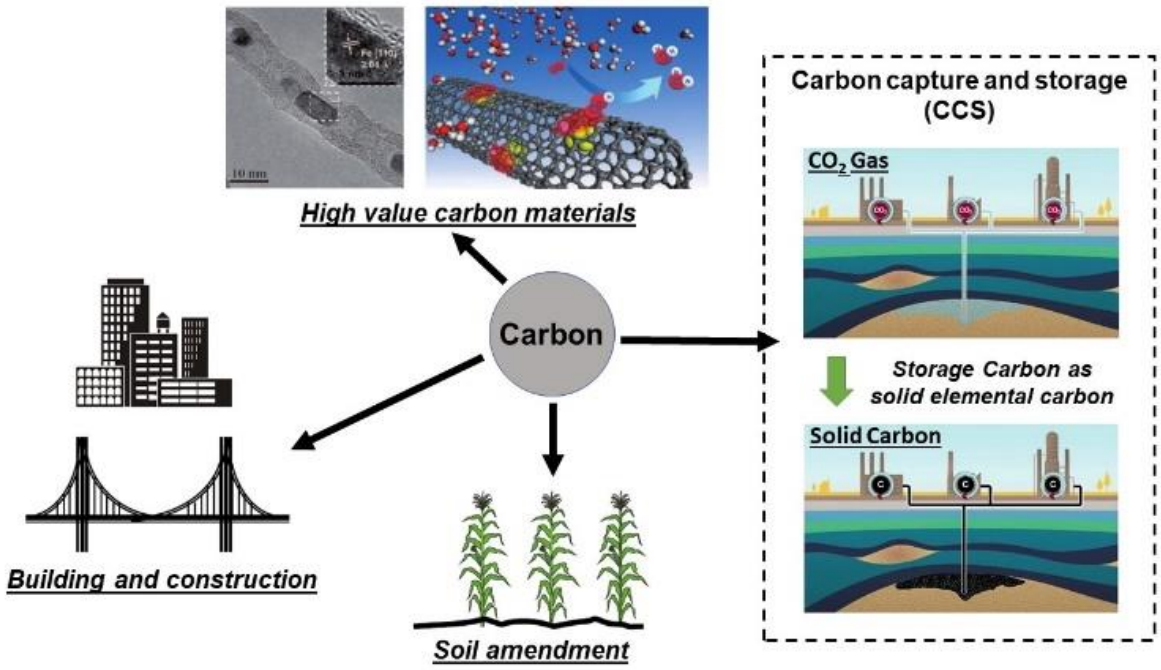


Figure 5.18. Representative storage and various utilisation routes for elemental carbon produced from fossil fuel dehydrogenation, where the hydrogen component of fossil fuels is used as a clean fuel and the remaining solid carbon ends up as either stored underground or other uses.

In the following chapter, the further investigation on carbons will be reported.

5.4 Conclusions

The work described in this chapter illustrates that the microwave-initiated catalytic dehydrogenation of naturally - occurring, crude oils, and the resulting hydrocarbon fossil fuels allows for the rapid production of large volumes of hydrogen using inexpensive and abundant fine iron catalysts.

Through their aerial combustion fossil fuels produce potentially climate – damaging CO_2. Alternatively, these same fossil fuels could be used to rapidly produce clean, carbon-free hydrogen through microwave –initiated catalytic dehydrogenation. Based on the advances reported here, it is our belief that the undoubted attributes of fossil fuels, being relatively inexpensive, widely available and readily adaptable to applications large and small, simple and complex, can significantly catalyse the staged transition to a hydrogen-based, sustainable energy economy.

Bibliography:

1. J. C. Macrae, *An Introduction to the Study of Fuel*, Elsevier, 1966.
2. International Energy Agency, *Global Energy & CO_2 Status Report*, 2017.
3. J. M. Thomas, *Nature Catalysis*, 2018, 1, 2.
4. A. Sartbaeva, V. Kuznetsov, S. Wells and P. Edwards, *Energy & Environmental Science*, 2008, 1, 79-85.
5. S. J. Davis, N. S. Lewis, M. Shaner, S. Aggarwal, D. Arent, I. L. Azevedo, S. M. Benson, T. Bradley, J. Brouwer and Y.-M. Chiang, *Science*, 2018, 360, eaas9793.
6. P. P. Edwards, V. L. Kuznetsov, W. I. F. David and N. P. Brandon, *Energy Policy*, 2008, 36, 4356-4362.
7. S. A. Wells, A. Sartbaeva, V. L. Kuznetsov and P. P. Edwards, *Encyclopedia of Inorganic and Bioinorganic Chemistry*, 2010, 309-332.
8. J. M. Bockris, *Science*, 1972, 176, 1323-1323.
9. J. A. Turner, *Science*, 2004, 305, 972-974.
10. U. Eberle, B. Müller and R. Von Helmolt, *Energy & Environmental Science*, 2012, 5, 8780-8798.
11. K. Hirose, *Philosophical Transactions of the Royal Society of London A: Mathematical, Physical and Engineering Sciences*, 2010, 368, 3365-3377.
12. L. Barreto, A. Makihira and K. Riahi, *International Journal of Hydrogen Energy*, 2003, 28, 267-284.
13. J. Barber, *Sustainable Energy & Fuels*, 2018.
14. R. H. Crabtree, *Energy & Environmental Science*, 2008, 1, 134-138.
15. S. Satyapal, J. Petrovic, C. Read, G. Thomas and G. Ordaz, *Catalysis Today*, 2007, 120, 246-256.
16. M. L. Wald, *Scientific American*, 2004, 290, 66-73.

17. S. Gonzalez-Cortes, D. Slocombe, T. Xiao, A. Aldawsari, B. Yao, V. Kuznetsov, E. Liberti, A. Kirkland, M. Alkinani and H. Al-Megren, J. M. Thomas and P. P. Edwards, *Scientific Reports*, 2016, 6, 35315.

18. X. Jie, S. Gonzalez-Cortes, T. Xiao, J. Wang, B. Yao, D. R. Slocombe, H. A. Al-Megren, J. R. Dilworth, J. M. Thomas and P. P. Edwards, *Angewandte Chemie International Edition*, 2017, 56, 10170-10173.

19. H. Bernstein, *Transactions of the Faraday Society*, 1962, 58, 2285-2306.

20. L. R. Radovic and H. H. Schobert, *Energy and Fuels in Society*, McGraw-Hill, 1992.

21. B. Greensfelder, H. Voge and G. Good, *Industrial & Engineering Chemistry*, 1949, 41, 2573-2584.

22. R. O. Idem, S. P. Katikaneni and N. N. Bakhshi, *Energy & Fuels*, 1996, 10, 1150-1162.

23. L.-S. Fu, J.-T. Jiang, C.-Y. Xu and L. Zhen, *CrystEngComm*, 2012, 14, 6827-6832.

24. D. Yao, Y. Zhang, P. T. Williams, H. Yang and H. Chen, *Applied Catalysis B: Environmental*, 2018, 221, 584-597.

25. W. Grochala and P. P. Edwards, *Chemical Review*, 2004, 104, 1283-1315.

26. V. G. Gude, P. Patil, E. Martinez-Guerra, S. Deng and N. Nirmalakhandan, *Sustainable Chemical Processes*, 2013, 1, 1.

27. X. Xu, P. Li and Y. Shen, *Applied Energy*, 2013, 108, 202-217.

28. J. Farrell, N. Cernansky, F. Dryer, C. Law, D. Friend, C. Hergart, R. McDavid, A. Patel, C. J. Mueller and H. Pitsch, *Development of an experimental database and kinetic models for surrogate diesel fuels*, Report 0148-7191, SAE Technical Paper, 2007.

29. A. Tsolakis, A. Megaritis and M. L. Wyszynski, *Fuel*, 2004, 83, 1837-1845.

30. D. M. Pozar, *Microwave Engineering*, John Wiley & Sons, 2009.

31. A. Porch, D. Slocombe, J. Beutler, P. Edwards, A. Aldawsari, T. Xiao, V. Kuznetsov, H. Almegren, S. Aldrees and N. Almaqati, *Applied Petrochem Research*, 2012, 2, 37-44.

32. J. Benford, J. A. Swegle and E. Schamiloglu, *High Power Microwaves*, CRC Press, 2015.

33. N. Z. Muradov and T. N. Veziroğlu, *International Journal of Hydrogen Energy*, 2005, 30, 225-237.

34. M. Bui, C. S. Adjiman, A. Bardow, E. J. Anthony, A. Boston, S. Brown, P. S. Fennell, S. Fuss, A. Galindo and L. A. Hackett, *Energy & Environmental Science*, 2018, 11, 1062-1176.

35. M. E. Boot-Handford, J. C. Abanades, E. J. Anthony, M. J. Blunt, S. Brandani, N. Mac Dowell, J. R. Fernández, M.-C. Ferrari, R. Gross and J. P. Hallett, *Energy & Environmental Science*, 2014, 7, 130-189.

36. M. Steinberg, *International Journal of Hydrogen Energy*, 1999, 24, 771-777.

37. Zero Emission Platform, The Hard Facts behind Carbon Capture and Storage, available at https://environmentaljusticetv.wordpress.com/2014/10/22/zep-the-hard-facts-behind-carbon-capture-and-storage/.

38. M. Steinberg and H. C. Cheng, *International Journal of Hydrogen Energy*, 1989, 14, 797-820.

39. N. Z. Muradov, *International Journal of Hydrogen Energy*, 1993, 18, 211-215.

40. D. Deng, L. Yu, X. Chen, G. Wang, L. Jin, X. Pan, J. Deng, G. Sun and X. Bao, *Angewandte Chemie International Edition*, 2013, 52, 371-375.

Chapter 6

Study of Carbonaceous Materials for Their Catalytic Performance under Microwave Irradiation

Overview

The catalytic hydrocarbons dehydrogenation over Fe catalysts is a green and economic route to produce H_2 without CO_2 emission. However, these processes have a rather short running period compare to reforming process due to the catalyst's deactivation by carbon deposition. The carbon has been widely used as microwave acceptor for transforming electromagnetic energy to heat. Thus, the resulting carbons may catalytic active towards hydrocarbons dehydrogenation under microwave irradiation. Following the end section of last Chapter which has briefly made a discussion on resulting carbons, an important by-product produced through this microwave-initiated dehydrogenation of hydrocarbons, this chapter will continually display the further study on these carbon residues as well as a variety of carbon nano-materials for their properties and catalytic activity under microwaves.

6.1 Introduction

Hydrogen is a promising vector for clean energy, but most of it is currently obtained from the steam reforming of fossil fuels which emits a huge amount of CO_2 [1]. In comparison, catalytic hydrocarbons dehydrogenation is an ideal process to produce pure hydrogen without CO_2 contamination [2-11]. Moreover, the energy input requirements for catalytic hydrocarbons dehydrogenation to produce same amount of H_2 is significantly less than that of steam reforming. This makes catalytic hydrocarbons dehydrogenation an more economic route than steam reforming to produce H_2 [9, 12].

However, the carbon deposition is the major challenge for catalytic hydrocarbons dehydrogenation that will quickly deactivate catalysts by block the catalyst pores and the reactor and/or completely

encapsulated the metal catalysts[13, 14]. Carbon materials have been widely used in microwave catalysis due to their highly efficient ability to absorb microwaves. Dielectric heating by high-frequency electromagnetic radiation waves could interact with only carbon particles (catalysts) and cause them heat up in the electric field of electromagnetic radiation [15]. Thus, the life time of catalytic hydrocarbons dehydrogenation may be extented with the assistance of microwave initiation.

In terms of the dielectric heating, two different mechanisms are associated to the resulting heating from the interaction between materials and electric field of electromagnetic radiation [16-18]. Dipolar polarisation effect responds to the polar molecules such as water etc. which these molecules are trying to align themselves under an alternating electric field. This movement and friction between the rotating molecules subsequently causes heat. For the solid materials, interfacial or Maxwell-Wagner polarisation effect causes the heat because of charged particles[16-18]. For the dehydrogenation of hydrocarbons, unfortunately, hydrocarbons are not able to absorb microwave and turn it into heat. Thus, dielectric materials are required for the energy converting and importantly drive the hydrocarbons dehydrogenation as a catalyst. Among many of the dielectric materials, carbon materials are, in general, excellent microwave absorbers which can be used as microwave receptors to indirectly heat for non-polar materials and/ or act as direct catalysts. Thus, carbon based catalysts have been investigated for microwave-initiated catalytic reactions such as the decomposition of methane [19, 20], carbon dioxide reforming [21] and the pyrolysis of biomass and organic wastes etc [22, 23].

Domínguez *et al.* reported microwave-initiated decomposition of methane on activated carbon and illustrated a higher selectivity to H_2 with higher conversions compared to electric heating [19]. Through the reactions of hydrocarbon dehydrogenation, carbon-forming processes involve chemisorption of different kinds of carbons or condensed hydrocarbons of which some may active towards the catalytic reactions and others may act as catalyst poisons. Muradov *et al.* previously investigated the catalytic decomposition of methane over element carbon by thermal cracking, which suggested the disordered forms of carbon (e.g. activated carbon and carbon black) are more catalytically active than the ordered carbon of graphite and diamond powder [2, 11, 24]. Moliner *et al.* later studied the deactivation mechanism of carbon blacks for methane dehydrogenation which reported the carbon crystallites formed from methane dehydrogenation may create new active sites[13].

In relation to our microwave-initiated dehydrogenation, the resulting carbon residues as well as the selective model sp^2 bonded carbons were carefully studied in this chapter, in terms of their catalytic activity for hydrogen production and their response to microwave irradiation. This will not only present a broader view of this microwave-initiated dehydrogenation process but also give a fundamental study of the behaviour of different carbon materials under microwave irradiation, and their catalytic properties.

6.2 Experimental

6.2.1 Preparation of catalysts

Iron catalyst supported by silicon carbide was prepared by an incipient wetness impregnation method. Iron nitrate, $Fe(NO_3)_3 \cdot 9H_2O$ (Iron (III) nitrate nonahydrate, Sigma-Aldrich), was used as the metal precursor and SiC (silicon carbide, Fisher Scientific) is used as the support material. All the model carbon materials were used as purchased without further purification. Activated carbon, carbon nanofiber and carbon nanotubes (multi-walled) were purchased from Sigama Aldrich and the carbon black was purchased from Alfa Aesar. The details of catalyst preparation have been described in Chapter 2.

6.2.2 Apparatus and method used for catalytic activity evaluation

In accordance with previous study, the process of dehydrogenation of hexadecane over Fe/SiC catalyst was chosen as a prototype for the study of carbons under microwave irradiation. The experiments were conducted for a successive cycle of tests using a purpose-built microwave cavity and a control system (Please refer to Chapter 2 for more details)[25, 26]. A quartz tube (inner diameter 6mm, outer diameter 9mm) was filled with about 1.13 cm^3 catalyst and 4cm high, to allow the sample was fully exposed to the axially polarised (TM_{010}) electric fields. 0.5 mL hexadecane was then injected into the tube at each cycle of tests. The sample was hold for 5-10 minutes in order to get a fully dispersion of the hexadecane in catalysts bed. All experiments were conducted at atmospheric pressure and the samples were purged with an Ar flow rate of 1.67 mL · s−1 for a period of 15 minutes before the starting

of microwave activation. Typically, the sample was irradiated under microwave for 10 minutes at 750 W in each cycle. And a fresh 0.5 mL of hexadecane was refuelled between each cycle of test. The generated gases were collected and analysed by gas chromatography (GC) using a Perkin-Elmer, Clarus 580 GC. The catalytic performance of model carbon samples was tested following the same methods.

All references to the catalytic activity of catalysts relate to the gas generation rate per unit of catalyst weight (in mL/min-g). The selectivity to different gaseous products was described in terms of the volume % of the product composition in the exit gases

6.2.3 Characterisation of catalysts

The Fe/SiC catalysts as well as a variety of model carbons were carefully studied before and after reactions by several characterisation techniques including x-ray diffraction (XRD), Raman spectroscopy, thermogravimetric analysis (TGA), scanning electron microscopy (SEM) and high-resolution transmission electron microscopy (HRTEM). In addition, the changes of dielectric properties of Fe/SiC catalysts and some model carbons through the successive cycles of dehydrogenation test were measured via microwave cavity perturbation measurement (Transverse Magnetic TM_{010} mode).

6.3 Results and discussion

6.3.1 Successive cycles of hexadecane dehydrogenation using Fe/SiC catalysts

At the outset, the Fe/SiC catalysts were tested based on a successive cycle of dehydrogenation of hexadecane. As a general observation, hexadecane was rapidly and dehydrogenated to mainly H_2 and solid carbon with the minor small alkanes (methane, ethylene and C_2-C_5 alkanes) were produced. However, it has been found that the Fe/SiC catalysts were gradually deactivated after 10 cycles of successive tests under microwave (Figure 6.1). The 5 wt. % Fe/SiC catalyst started to deactivate after 3 cycles and nearly lost the catalytic activity fully after 10 cycles (Figure 6.1a).

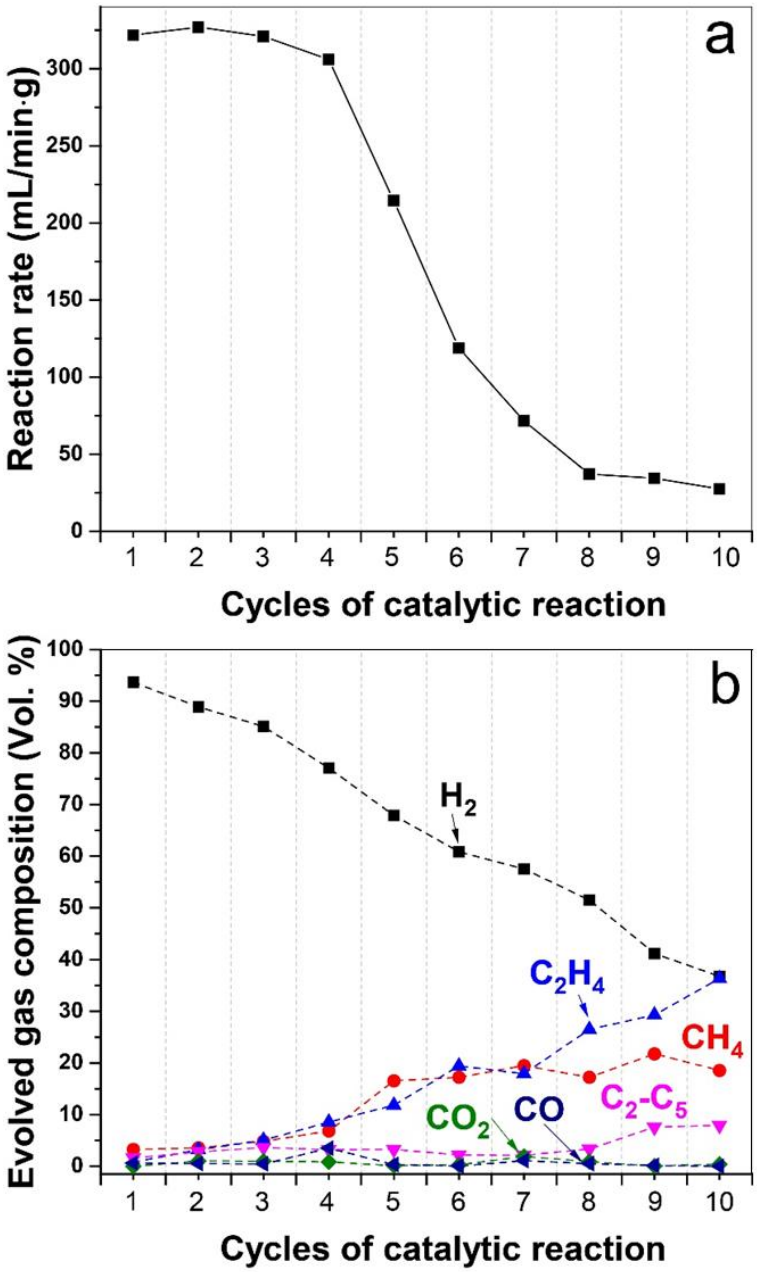


Figure 6.1. Successive 10 cycles of hexadecane dehydrogenation over 5 wt. % Fe/SiC catalyst. (a) $C_{16}H_{34}$ dehydrogenation rate; (b) evolved gas composition in the exit gas. 0.5 mL hexadecane (only) was additionally added into the sample between every cycles of test.

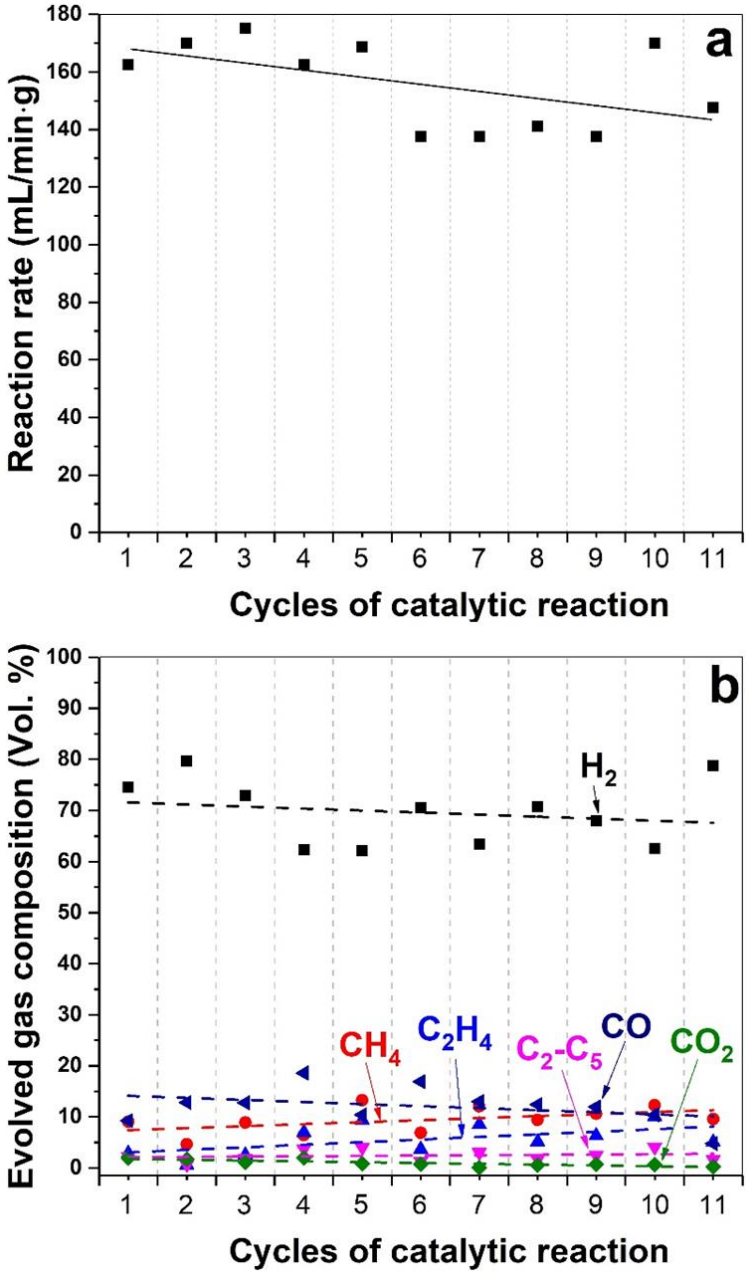


Figure 6.2. The effect of carbon residue removal and regeneration of Fe_2O_3/SiC sample for hexadecane dehydrogenation. (a) $C_{16}H_{34}$ dehydrogenation rate; (b) evolved gas composition in the exit gas. The carbon residues were removed by calcination between each cycle.

In these successive cycles of test, we refuelled the sample with 0.5 mL of hexadecane between each cycle and every cycle of tests were run for 10 minutes. High initial dehydrogenation rate in catalytic activity was gradually dropped and finally kept at a quasi-steady reaction rate. Evolved gas selectivity to hydrogen gradually decreased, whilst corresponding methane and ethylene concentrations gradually increased (Figure 6.1b). This decrease of both reaction rate and the hydrogen selectivity is considered

due to the formation of carbon that deposited on the iron catalyst active sites, as will be evident in our recovery test and the electron microscopy studies.

Figure 6.2 shows a recovery test of spent Fe/SiC catalysts after 10 cycles of test described above. Here, the carbon residues were removed simply by calcination at a temperature of 550 °C. Then, Fe_2O_3/SiC samples, without further hydro-reduction, were tested for dehydrogenation of hexadecane under microwave irradiation. For the successive 10 cycles of test, the Fe_2O_3/SiC samples were refuelled with 0.5 mL of fresh hexadecane and repeatedly calcined between each cycle in order to remove the resulting carbons.

In general, the recovered Fe_2O_3/SiC samples were highly effective for hexadecane dehydrogenation. Although, both the reaction rate and hydrogen selectivity were lower than original Fe/SiC catalyst, but this clearly depicts the effect of resulting carbon residues which obviously responsible for the catalyst deactivation. Furthermore, it can be seen that both the reaction rate and the products distribution were retained at a quasi-steady level throughout the 10 cycles of test when the carbons were removed.

It should be also noted that the gradually decreased hydrogen selectivity on Fe/SiC catalysts (Figure 6.1a) could imply that some of the resulting carbons were catalytically active and participated in the reactions under microwave irradiation. And the loss of catalytic activity is considered due to the formation of non-active carbon species (presumably carbon nanotubes etc.) that covered the active sites on the iron and active carbon species.

6.3.2 Catalytic activity of model carbons for microwave-initiated dehydrogenation of hexadecane

In comparison, a variety of model carbon materials with different origin and structure was investigated under same conditions. The model carbons studied here are mainly consisted of sp^2 bonded carbon, such as activated carbons (ACs), carbon black (CB), graphite, and multi-wall carbon nanotubes (MWCNTs) etc. Among 9 different kinds of model carbon, only activated carbons (ACs) and graphene nanoplatelets showed the catalytic activity for the hexadecane dehydrogenation under microwave irradiation (Figure 6.3a).

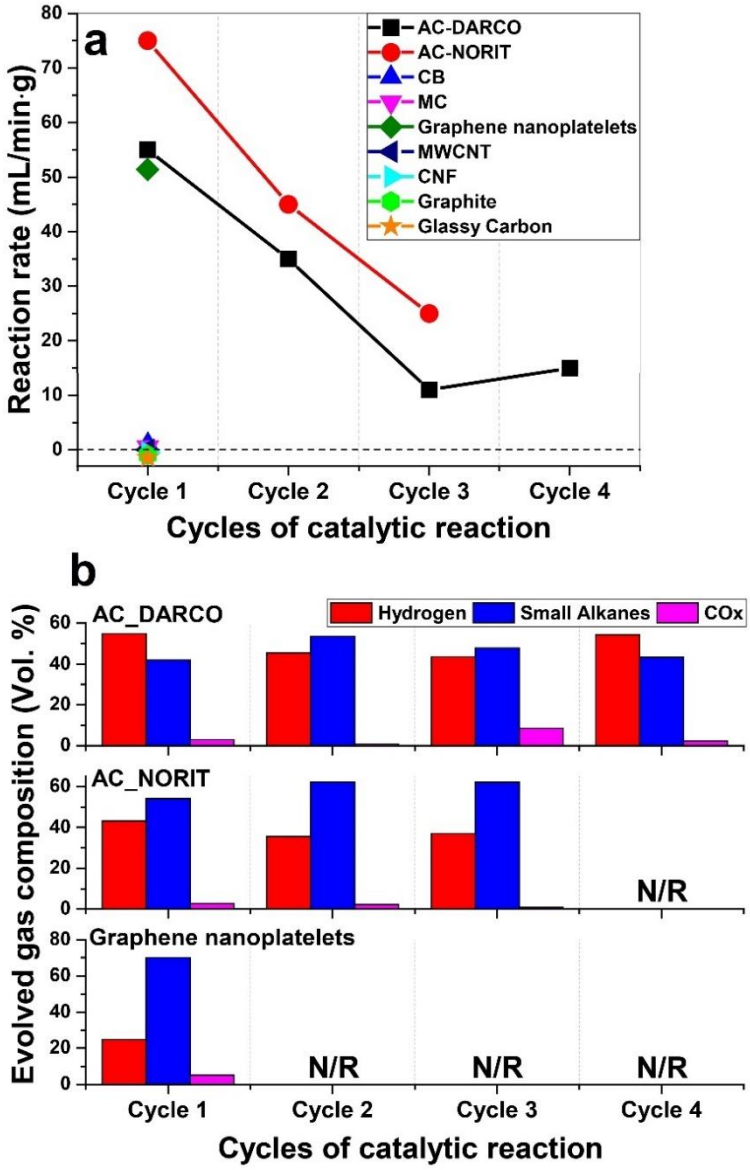


Figure 6.3. Hexadecane dehydrogenation over model carbon materials, of activated carbons (ACs), carbon black (CB), mesoporous carbon (MC), graphene nanoplatelets, multi-wall carbon nanotubes (MWCNT), carbon nanofibers (CNF), graphite, and glassy carbon. (a) $C_{16}H_{34}$ dehydrogenation rate; (b) evolved gas composition in the exit gas.

Different products distribution was also observed between these two kinds of carbon materials. For carbon nanoplatelets, small alkanes consisted of nearly 70 vol.% of the produced gases, while only ca. 50 vol.% small alkanes were obtained over activated carbons. Moreover, the hydrogen selectivity of activated carbons was nearly twice as that of carbon nanoplatelets (Figure 6.3b). Interestingly, although these carbon materials are excellent microwave absorbers/acceptors and can catalyse the dehydrogenation reactions under microwave irradiation [19, 26, 27], the carbons were quickly deactivated

after only few cycles of test when compared to Fe/SiC catalyst. There is thus, the special properties or structure are required for carbons when they perform as a catalyst. Another hypothesis is that the active sites on carbon were covered by deposited carbons which do not have any catalytic activity under microwave irradiation.

6.3.3 Reaction temperature and absorption power

Figure 6.4 and Figure 6.5 compared the microwave (MW) absorption power and the reaction temperature respectively, recorded during hexadecane dehydrogenation under microwave irradiation. In terms of model carbon materials, higher temperature was observed on those carbons who displayed catalytic activity under microwaves and ACs were found to be able absorb more microwave power than other carbon materials. Moreover, it was found that absorption power was very high on carbons just when the microwave was turned on, but the power rapidly dropped over a period of ca. 10s, and then stablised at a quasi-steady level. It assumes that a thermal balance was quickly built over a short period of 10s on these carbons. Interestingly, the Fe/SiC and Fe_2O_3/SiC catalysts which have exceptional catalytic activity and produced a high-purity hydrogen from hexadecane dehydrogenation, absorbed less microwave power than that of Fe and SiC particles and model carbons (Figure 6.4b).

In relation to the reaction temperature, the highly active Fe/SiC and Fe_2O_3/SiC samples showed a temperature of about 450 °C, whereas a higher reaction temperature of about 500 – 600 °C was observed on ACs and graphene nanoplates, the carbons who showed the catalytic activity. Other carbons such as carbon black, carbon nanotubes and fibres etc. which were found inactive under microwave irradiation, were heated to only 350 °C or below. It thus concluded that a temperature of over 500 °C may required for carbons in order to drive the dehydrogenation under microwaves. Furthermore, the active Fe particles are obviously essential for high-purity hydrogen production under microwave by providing effective active sites which can efficiently extract H from -CH_3 groups by dissociating C-H bonds.

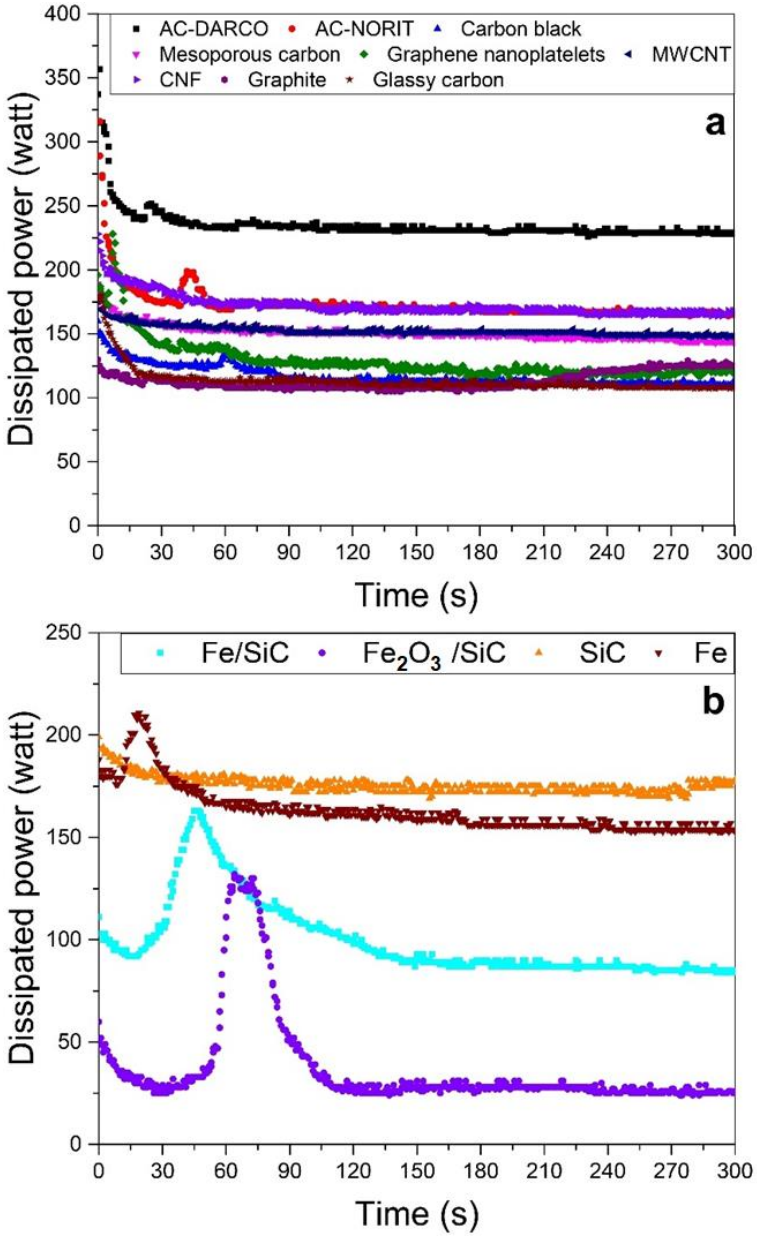


Figure 6.4. Absorbed (dissipated) power as a function of time. (a) model carbon materials. (b) Fe/SiC, Fe_2O_3/SiC, SiC, and Fe.

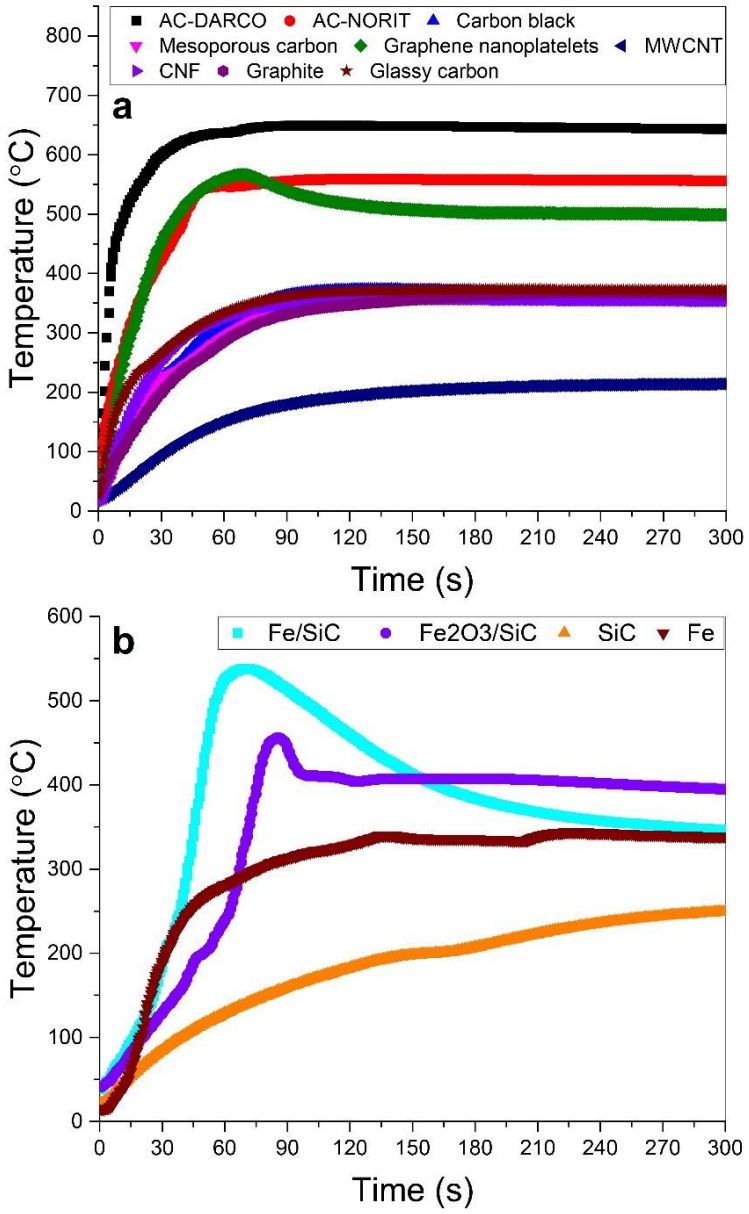


Figure 6.5. Reaction temperature recorded as a function of time. (a) model carbon materials. (b) Fe/SiC, Fe_2O_3/SiC, SiC, and Fe.

6.3.4 Characterisation of carbon residues and comparison with model carbon materials

6.3.4.1 Thermogravimetric analysis (TGA)

The spent Fe/SiC samples and model carbons were studied by thermogravimetric analysis (TGA). Through successive cycles of catalytic reactions, carbon residues were constantly accumulated (Figure 6.6), and the oxidation temperatures of resulting carbons from each cycle are similar at about 600 °C. However, the oxidation temperatures were found shifted to the lower temperature at later cycles (Table

6.1). In comparison, various oxidation temperatures were observed on model carbons from 590 °C to 800 °C (Figure 6.7). Interestingly, in Figure 6.7 where the spent Fe/SiC catalyst was compared with the selected model carbons in temperature programmed oxidation (TPO), the carbon produced at early cycles had a similar oxidation temperature to activated carbons (ACs) at 650 °C; whereas after 10 cycles, the oxidation temperature of carbon residues in spent catalysts shifted to about 590 °C, which is corresponding to the model multi-walled carbon nanotubes (MWCNTs). Moreover, a secondary peak at ca. 810 °C was also observed and this was ascribed to the formation of carbon nanofibers (CNF) and/or graphite.

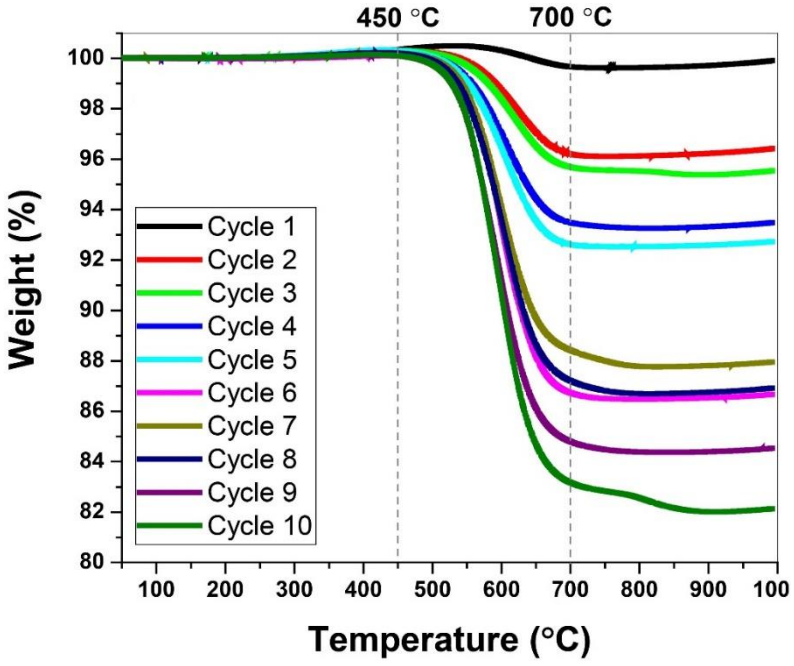


Figure 6.6. Thermogravimetric analysis (TGA).

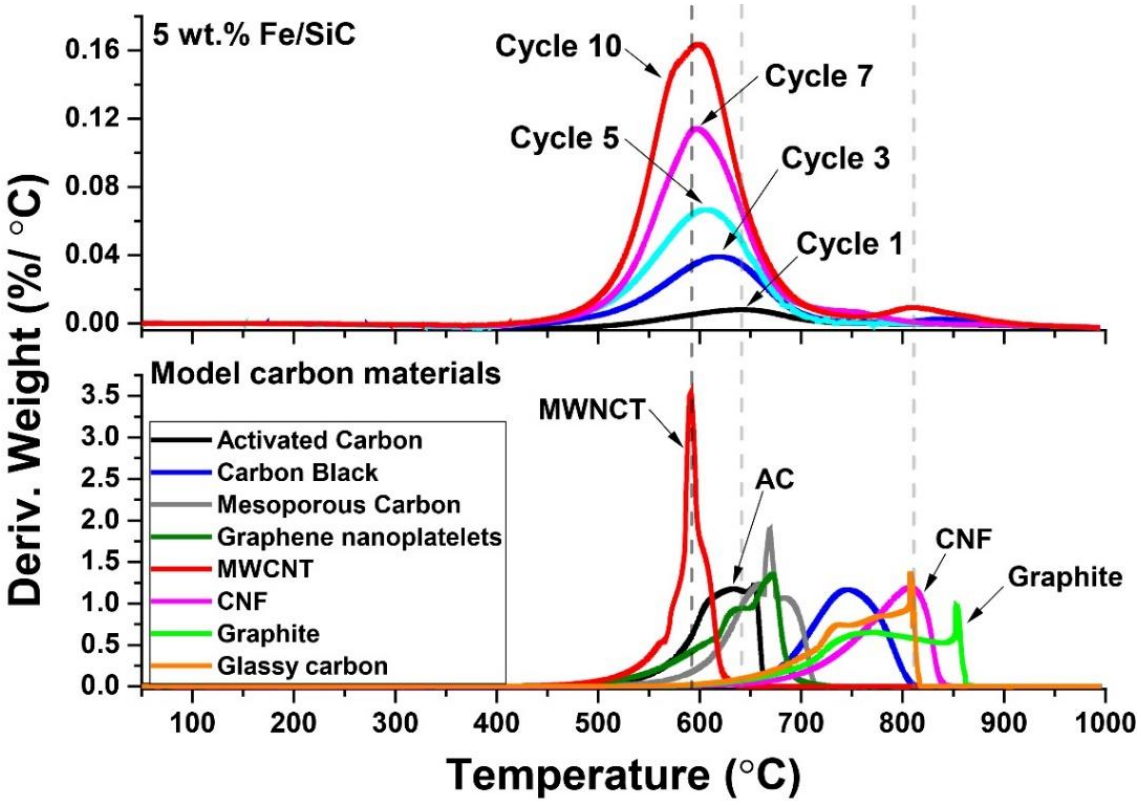


Figure 6.7. Derivative plots of temperature programmed oxidation (TPO) of spent Fe/SiC sample reference to the model carbons.

Table 6.1: Oxidation temperatures of Model Carbon Materials and Fe/SiC sample.

Fe/SiC catalyst	Temperature (°C)	Model carbon Materials	Temperature (°C)
Cycle1	640	Activated carbon	653
Cycle2	625	Carbon black	745
Cycle3	619	Mesoporous Carbon	668
Cycle4	608	Graphene nanoplatelets	671
Cycle5	605	MWCNT	591
Cycle6	599	CNF	807
Cycle7	596	Graphite	853
Cycle8	603	Glassy carbon	808
Cycle9	596		
Cycle10	598		

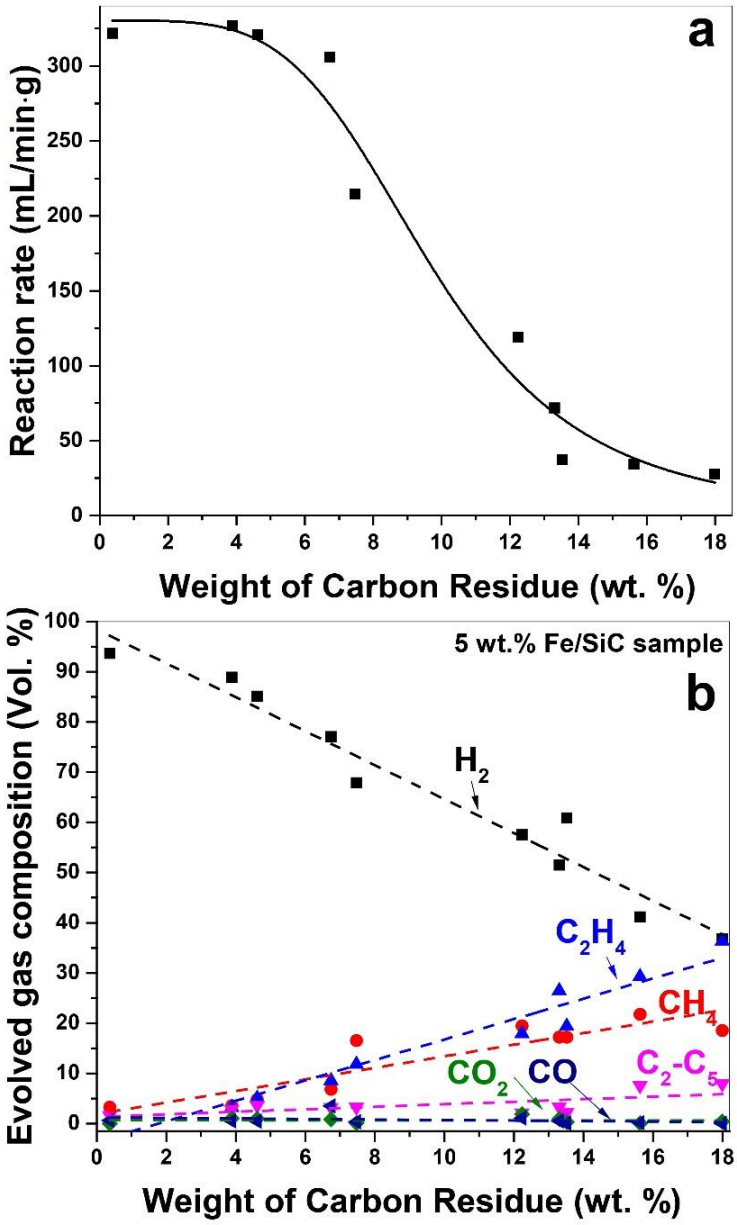


Figure 6.8. Reaction rate (a) and Evolved gas composition (b) as a function of the weight of carbon deposition

Finally, Figure 6.8 illustrated the reaction rate and products distribution as a function of carbon contents in the spent Fe/SiC samples. As a general observation, the carbon produced was not only cause the blockage of active sites on iron surface, but also catalysed the hexadecane dehydrogenation under the influence of microwave-electric fields. This is evident in the decreased H_2 concentration in the evolved gases, whilst the concentration of methane, ethylene and other small alkanes increased; otherwise, the products distribution should remain same if the carbon produce was fully inactive. After

several cycles of test that the samples were continually reacted with freshly added hexadecane, the catalysts were deactivated finally by the accumulation of inactive carbons. This therefore suggests that not only the active sites on iron surface were covered by inactive carbons, the original active carbons were also transformed into or covered by these inactive carbons. The changes of carbon morphology on the catalyst's surface are also evident in our scanning electron microscope (SEM) studies.

6.3.4.2 Scanning electron microscopy (SEM), Transmission electron microscopy (TEM) and Energy-dispersive x-ray spectroscopy (EDS)

Figure 6.9 shows the scanning electron microscopy (SEM) studies on spent Fe/SiC catalysts throughout the cycles of hexadecane dehydrogenation under microwave initiation. The obvious changes over Fe/SiC catalysts were observed with the carbon residues that being transformed/produced from dis-ordered carbon clusters to the filamentous carbons throughout the successive cycles of test. It can be seen that only very few clusters of carbon residues were found after cycle 1 (Figure 6.9a), and these carbon clusters were significantly grown and accumulated on the catalyst's surface after 5 cycles. Some filamentous carbon was also observed in these carbon clusters. Interestingly, after 10 cycles of tests, these large clusters of carbon residues were "disappeared", instead the needle-liked fibres were observed on the SiC surface.

In addition, Figure 6.10 summarised the SEM images of model carbons, showing the different morphologies and structures of these various kinds of sp^2 bonded carbons.

Further studies on spent Fe/SiC samples by transmission electron microscopy (TEM) and energy-dispersive X-ray spectroscopy (EDS) were shown in Figure 6.11. Similarly, little carbons was observed deposited on iron nanoparticles after cycle 1, and therefore, many fresh Fe active sites were exposed and remained active for new added hexadecane. Following the continued reactions, more carbons were deposited, and the carbon nanotubes were formed. Similarly, it was found that iron/ iron carbide nanoparticles were encapsulated by multi-walled carbon nanotubes and as discussed in the previous chapters, the formation of iron carbides suggests the iron particles reacted with produced carbon during the reactions[25]. Moreover, it concluded that not only more carbons were accumulated on the catalysts'

surface, the carbons were transformed/ produced into other kinds of carbons which were catalytically inactive. These changes and transformation are assumed responsible to the deactivation of catalysts.

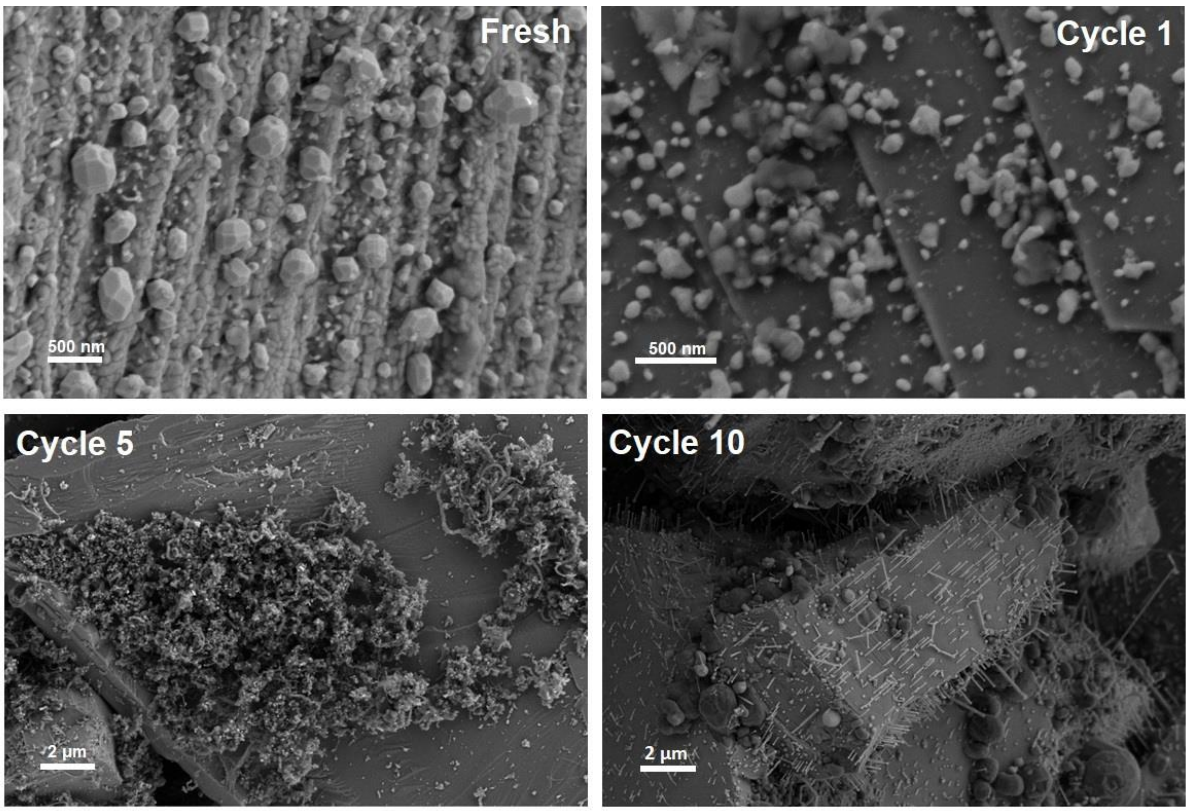


Figure 6.9. The Scanning Electron Microscope (SEM) of Fe/SiC samples through successive cycles of hexadecane dehydrogenation under microwave.

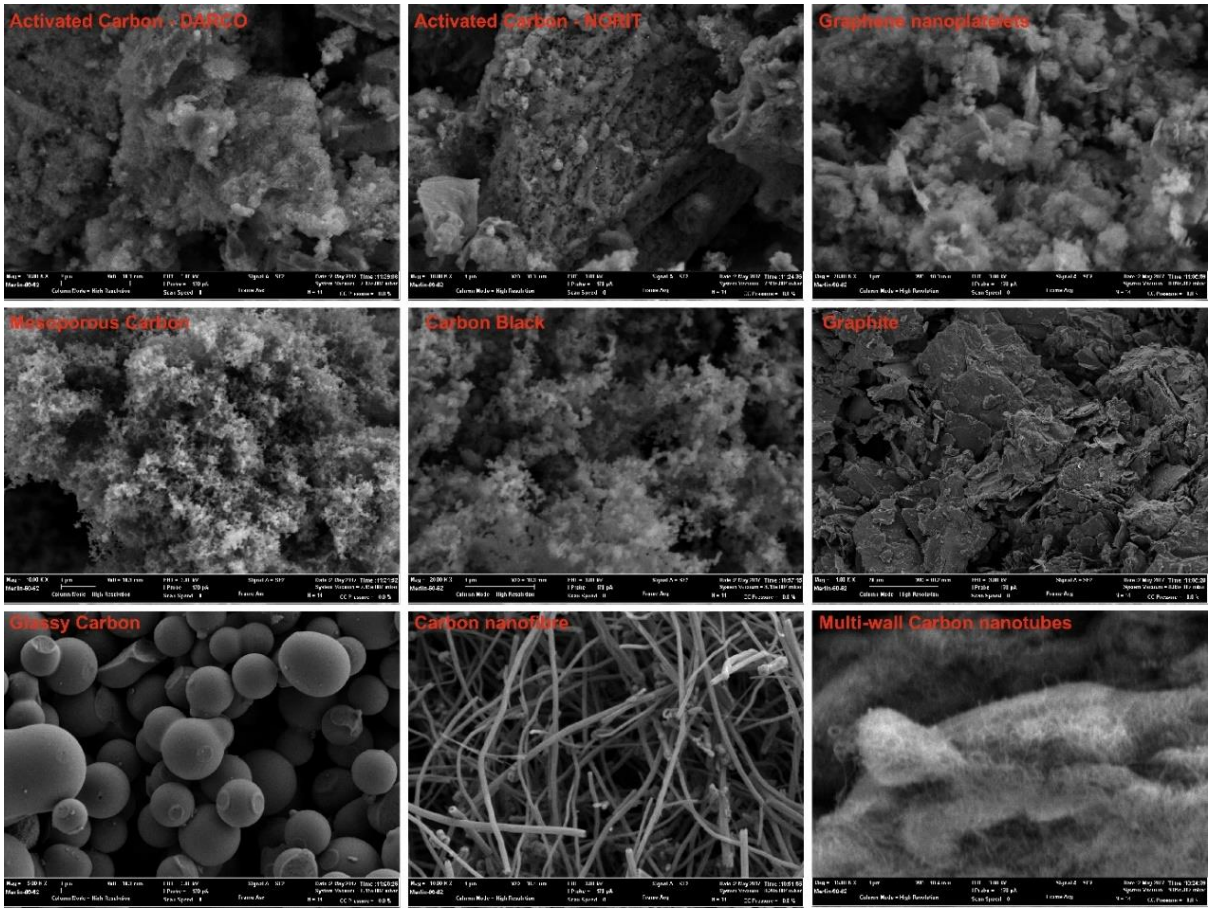


Figure 6.10. The Scanning Electron Microscope (SEM) of model carbon materials.

The energy-dispersive X-ray spectroscopy (EDS) mapping has illustrated the presence of oxygen on Fe nanoparticles, which is considered originally from the oxidation of Fe on exposure in the air (Figure 6.11). However, throughout the successive cycles of dehydrogenation of hexadecane under microwaves, the presence of these oxygen compounds may lead the formation of various materials (such as the needle-liked fibres on SiC).

Figure 6.12 shows the EDS mapping of needle-like fibres on the surface of SiC after 10 cycles. The fibres have a core-shell like structure. The top head was consisted of mainly Fe, and the Si was detected in the core. The O and C were observed throughout the whole filaments and the C formed the shell of the fibres. Like the formation of carbon whiskers, it was considered that this core-shell structure was form by Si and C diffusion. Both C and Si were diffused and/or dissolved into Fe nanoparticles due to the temperature and concentration gradient between Fe nanoparticles and SiC supports [28-30]. Clearly,

further studies are needed to ascertain these compounds and their formation mechanism under microwave irradiation.

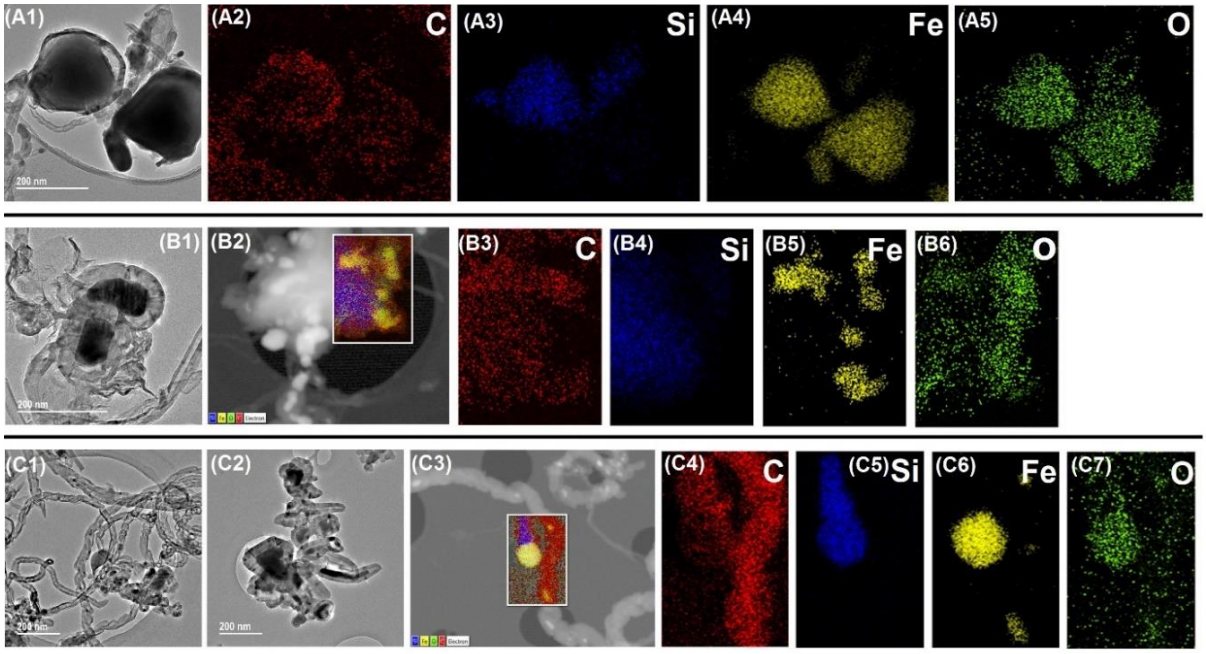


Figure 6.11. Transmission electron microscopy (TEM) and Energy-dispersive X-ray spectroscopy (EDS) mapping on spent Fe/SiC samples. (a) Cycle 1, (b) Cycle 5 and (c) Cycle 10. (a1, b1, b2, c1, c2, c3) TEM (backscattered electron) morphology. (a2, b3, c4) C map, (a3, b4, c5) Si map, (a4, b5, c6) Fe map, and (a5, b6, c7) O map.

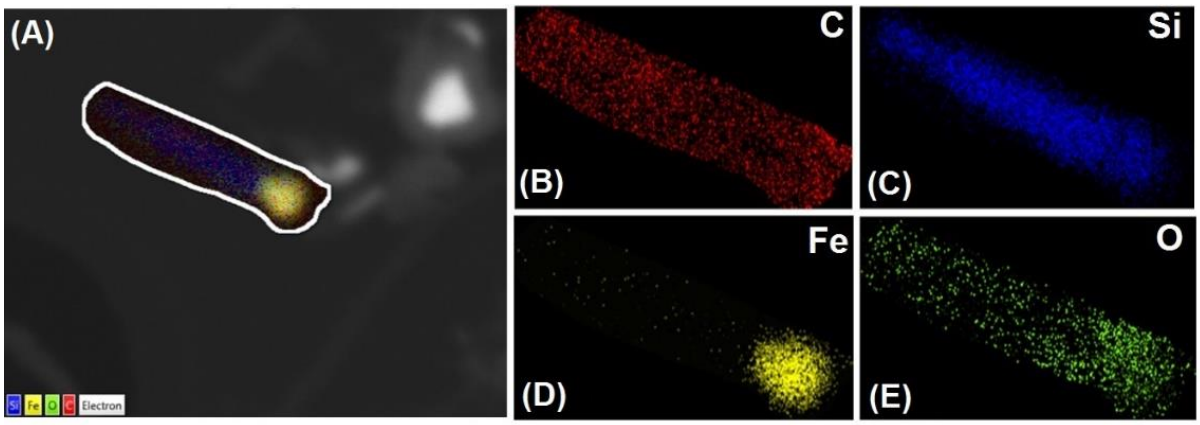


Figure 6.12. EDS mapping of needle-liked fibres that observed on the surface of SiC. (a) backscattered electron morphology (b) C map, (c) Si map, (d) Fe map, and (e) O map

6.3.4.3 Raman spectroscopy, x-ray diffraction (XRD) and BET analysis

The Raman Spectrum illustrated that the G-band and D-band of carbon residues at each cycle were at nearly same position of 1598 cm^{-1} and 1313 cm^{-1}, respectively (Figure 6.13a). The intensities of G-

band and D-band were observed to be stronger at the later cycles, but no clear shift can be found for the identification of carbon species. When reference to the Raman spectrum of model carbons (Figure 6.13b), the MWCNTs has the G-band and D-band at the position of 1600 cm^{-1} and 1312 cm^{-1}, respectively which are close to the carbons observed over spent Fe/SiC samples.

In addition, The XRD studies on spent Fe/SiC catalyst and the model carbons are given in Figure 6.14. Through the successive cycles of hexadecane dehydrogenation, an increasing intensity of the reflexion was observed at 11.7° and 28° on Fe/SiC catalysts, typical of amorphous and crystalline silicon (Figure 6.14c). No peaks were found for carbon at spent Fe/SiC samples. Additionally, the peak for iron at 44.79° was detected in the fresh sample and disappeared in spent samples where the diffraction peaks of Fe_3C were detected at the angles (2θ) of 42.92°, 43.82°, 44.72°, 45.04°, 45.9°, and 49.18° (Figure 6.14d) [31].

The XRD patterns of model carbon materials were presented in Figure 6.14b. The strongest diffraction peak at the angle (2θ) of 26.7° can be indexed as the C (002) reflection of the hexagonal graphite structure [32]. The sharpness of the peak at the angle (2θ) of 26.7° indicates that in the model carbon materials are highly crystalline. The XRD peak of MWCNTs at 2θ = 26.7° is broader and shifted towards lower angles which indicates the decrease in the order of crystallinity. The other characteristic diffraction peaks of graphite at 2θ of about 43° and 53° are associated with C (100) and C (004) diffractions of graphite, respectively[32].

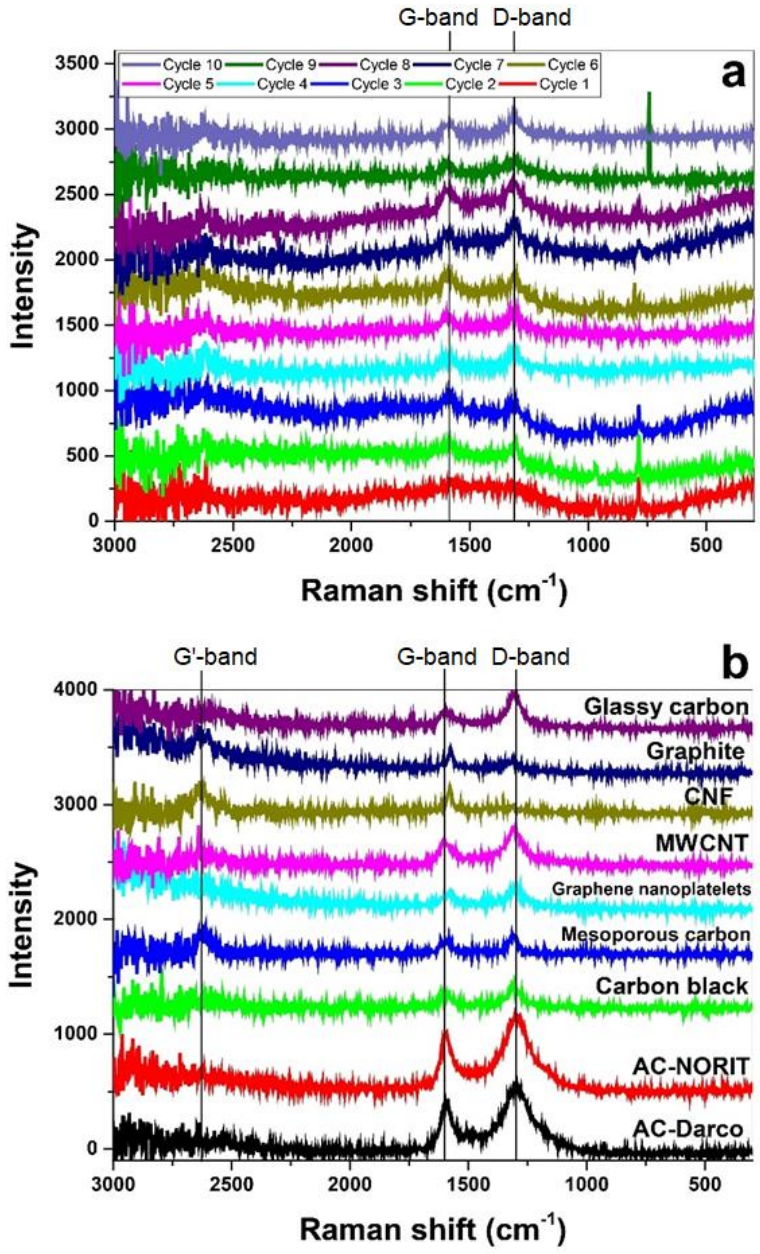


Figure 6.13. Raman Spectrum. (a) samples of Fe/SiC through 10 successive cycles of catalytic reaction. (b) samples of different model carbon materials.

There are two reasons hypothesised for not detecting carbons in XRD; one could be the carbon residues in spent Fe/SiC catalysts were dominated by amorphous carbon, and another is the carbons were not highly crystallised like MWCNTs and such diffraction peaks overlapped with other peaks. Although, the Raman and XRD analysis did not show the clear evidence of the producing/transforming of resulting carbons during the experiments, and no single diffraction peak of carbons was detected in

spent Fe/SiC samples, but the change of both Fe particles and the constantly accumulated carbon residues are clearly observed.

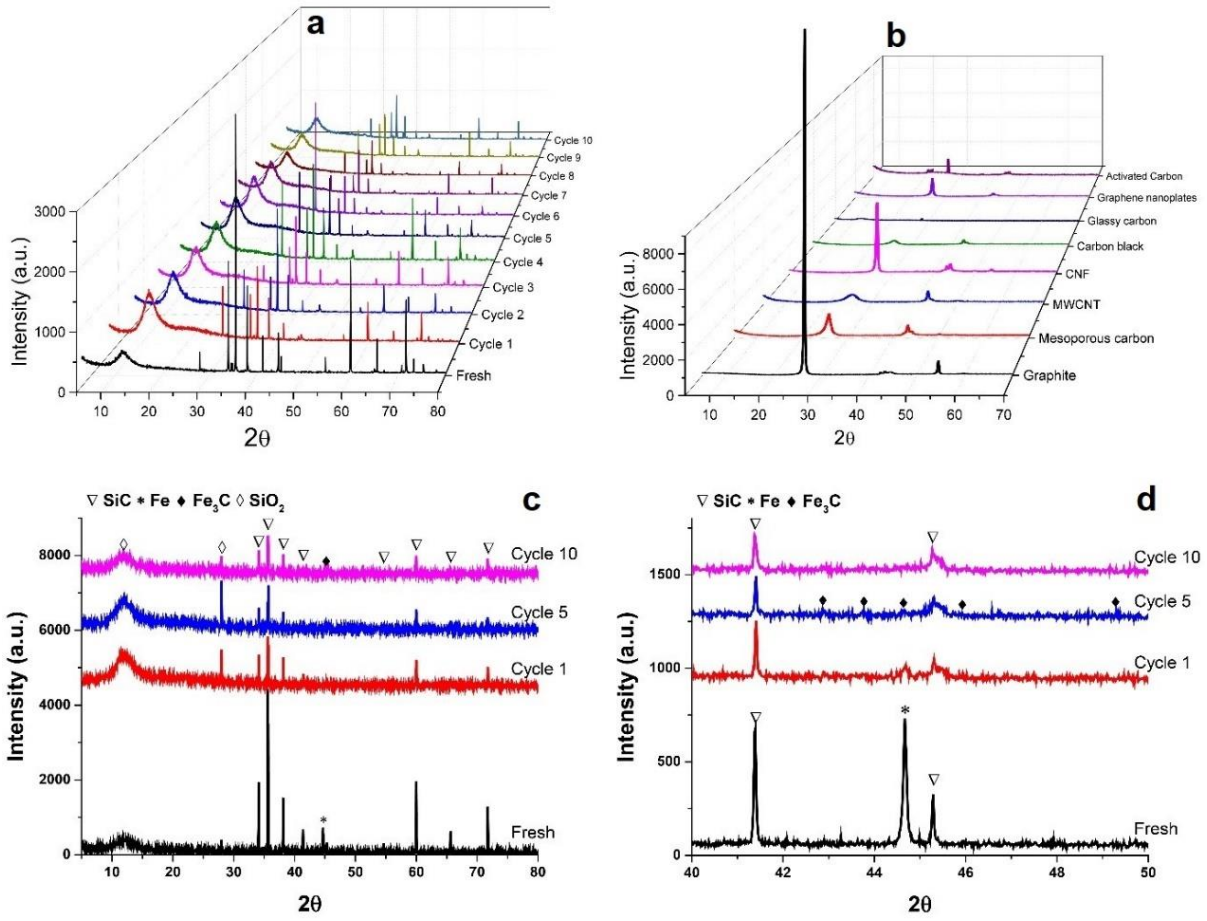


Figure 6.14. XRD patterns. (a) The change of the XRD pattern of 5 wt.% Fe/SiC sample during the successive cycles of hexadecane dehydrogenation under microwaves. (b) The XRD pattern of model carbon materials. (c) XRD pattern comparison of fresh Fe/SiC sample and after 1, 5, and 10 cycles, 2θ= 5°-80°, and (d) 2θ= 40°-50°.

Table 6.2 summarised the physical properties of surface area and porosity of model carbons and Fe/SiC catalysts before and after reactions. It can be seen that the active carbon species of ACs and graphene nanoplatelets, have very high surface area together with comparable small pore sizes. The AC has nearly 870 m^2/g surface area with average pore size of 4 nm and the graphene nanoplatelets has the surface area and pore size of 460 m^2/g and 7 nm, respectively. Other carbon materials, however, have less than 80 m^2/g surface area (excluding MWCNTs, 255 m^2/g) with the pore size of nearly 17 nm. Thus, the carbons with higher surface area and small pore size are considered preferred for this process

under microwaves. However, Muradov reported that there is no apparent correlation between the surface area of carbons and their catalytic activity for methane decomposition via conventional thermal process[2]. The studies by Moliner *et al.* also showed despite of the decreased surface area and the porosity of carbon black, a quasi-steady state in the activity towards methane dehydrogenation was observed [13].

Table 6.2: BET Surface and Porosity of Model Carbon Materials and Fe/SiC sample.

Materials*	BET Surface Area [m^2/g]	Micropore Area [m^2/g]	External Surface Area [m^2/g]	Pore Volume [m^3/g]	Pore Size [nm]
Activated Charcoal	875	418	457	0.841	3.8
AC (Norit)	864	424	440.1	0.831	3.8
Graphene Nanoplatelets	460	79.3	381	0.775	6.7
Mesoporous Carbon	734	12.0	61.3	0.321	17.5
Glassy Carbon	1.8	0	2.2	0.003	7.6
Carbon Black	65.1	6.5	58.6	0.269	16.5
CNF	14.7	0.6	14.1	0.066	17.8
MWCNT	255	32.4	223.1	1.310	20.5
SiC	0.3	0.1	0.2	0	6.2
5 wt.% Fe/SiC (Fresh)	0.9	0.2	0.6	0.003	11.9
5 wt.% Fe/SiC (Spent)	1.3	0	1.4	0.006	17.2

The Fe/SiC samples, on the other hand, have very low surface area (i.e., 0.9 m^2/g) but are highly active for hexadecane dehydrogenation under microwaves. The surface area of Fe/SiC samples was increased after reactions to 1.3 m^2/g which is ascribed to the carbon deposition.

6.3.4.4 Microwave cavity perturbation measurements

A prior work by Cuenca *et al.*[33] reported using microwave cavity perturbation technique to determine sp^2 carbon fraction in nanodiamond powders. And previous work in the group has also shown the microwave cavity perturbation analysis is an effective method to examine the cokes formed over zeolite catalysts[34]. This technique can offer a rapid and non-intrusive measurement of catalytically coked catalysts based on the detection of the changes of their dielectric properties. Here, the cavity perturbation measurements were carried out to monitor the change of Fe/SiC samples under microwave irradiation through the successive cycles of dehydrogenation of hexadecane. The dielectric properties of various model carbons were also measured.

The dielectric properties of model carbon materials have been found various (Figure 6.15). Although few changes have been found in the dielectric properties with increasing temperature among all the tested carbons, the different carbons still present various values on both dielectric constant (ε') and loss tangent (ε''). The dielectric constant of graphite at 300 °C is about 89, which is nearly 16 times higher than that of graphene nanoplatelets at the same temperature. Similarly, the loss tangent of MWCNTs is about 6 times higher than ACs at room temperature. Interestingly, the active carbon species of ACs and graphene nanoplatelets have comparable low dielectric constant. Moreover, the AC displayed the lowest value of loss tangent but their recorded reaction temperature was higher than other inactive carbons.

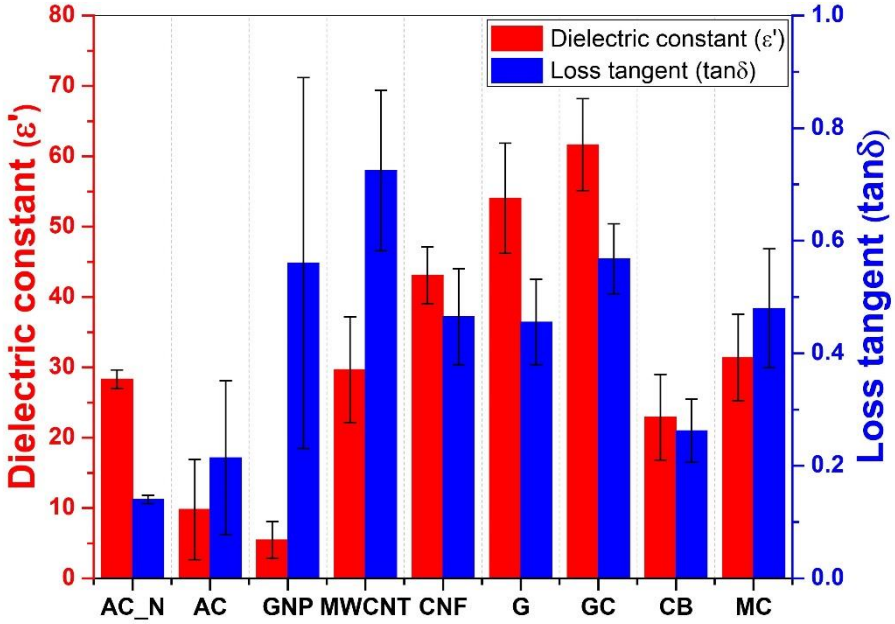


Figure 6.15. Dielectric constant and Loss tangent of 9 different kinds of model carbon materials. Error bars indicate the standard deviations across different samples.

Figure 6.16 compared the ACs and graphene nanoplatelets before and after reactions. The dielectric constant of deactivated ACs decreased slightly after the microwave treatment, while the value of deactivated graphene nanoplatelets has a clear increase. The loss tangent of spent graphene nanoplatelets was decreased and the spent ACs has a nearly same loss tangent as the fresh samples. It therefore suggested that no simple dependency on dielectric properties of carbon materials for the deactivation.

Figure 6.17 presents the changes of dielectric properties of Fe/SiC samples through the successive cycles of test under microwaves. Both dielectric constant and the loss tangent were increased significantly after reactions due to the deposition of resulting carbon residues. Compared to model carbon materials, the dielectric constant (ε') and the loss tangent (ε'') of Fe/SiC sample was more sensitive with increasing temperature. This may be attributed to the mixtures of carbon, iron carbide and silicon carbide that enhanced the polarisation between each particle. It should be noted that the loss tangent ($\tan\delta$) given in Figure 6.17 defines the ability of the catalysts to convert electromagnetic energy into heat energy that expressed as $\tan\delta = \varepsilon'/\varepsilon''$. Thus, the change of loss (ε'') can be more apparent than that of loss tangent ($\tan\delta$).

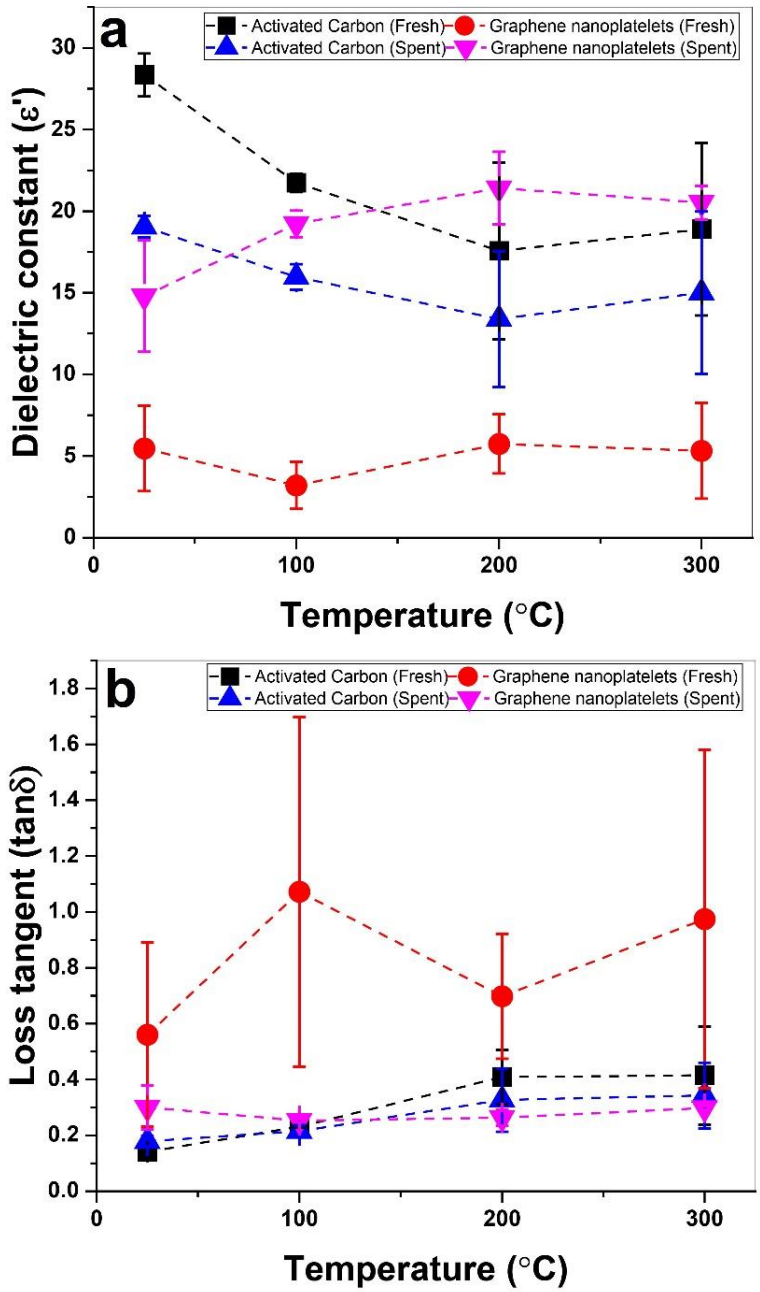


Figure 6.16. Microwave cavity perturbation measurement of activated carbon and graphene nanoplatelets, before and after catalytic reactions under microwave irradiation. (a) Dielectric constant and (b) Loss tangent. Error bars indicate the standard deviations across different samples.

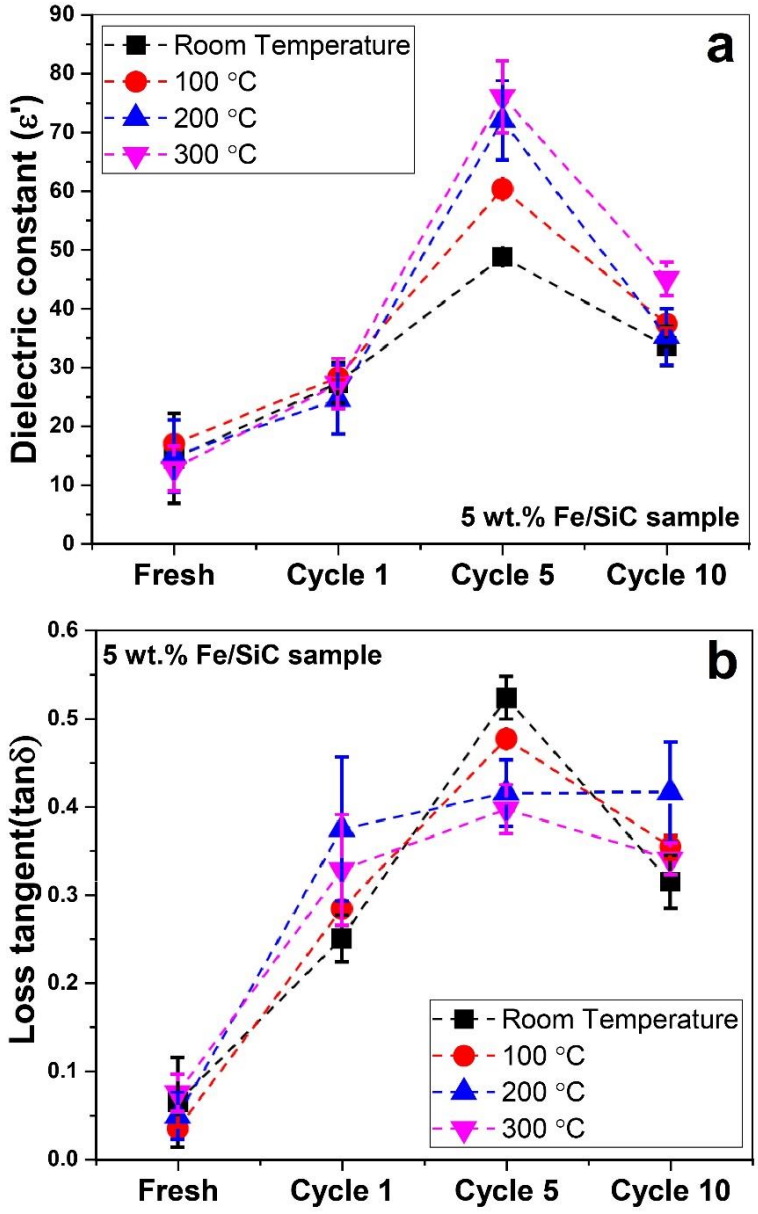


Figure 6.17. (a) Dielectric constant and (b) Loss tangent of 5 wt.% Fe/SiC sample measured at different temperature, before and after successive cycles of catalytic reactions. Error bars indicate the standard deviations across different samples.

Figure 6.18 displays the changes in dielectric properties of Fe/SiC samples throughout the successive cycles of test that has been detected by cavity perturbation measurements[33]. Obviously, 3 steps of noticeable changes of dielectric properties of Fe/SiC sample were measured during the reactions. Both the dielectric constant and loss tangent of Fe/SiC samples were significantly increased between the cycle 1 to cycle 4 (1st step), which ascribed to the deposition of carbons. Then, both values were fluctuated during the experiments of cycle 4 to cycle 7 (2nd step) followed by a decrease to half of the

maximum values after 10 cycles of test (3rd step). This is hypothesised be due to the formation/ transformation of inactive carbons which were deposited on both iron and active carbon surface. The changes of dielectric properties during the tests were also presented as a function of amount of carbons in spent samples (Figure 6.18b).

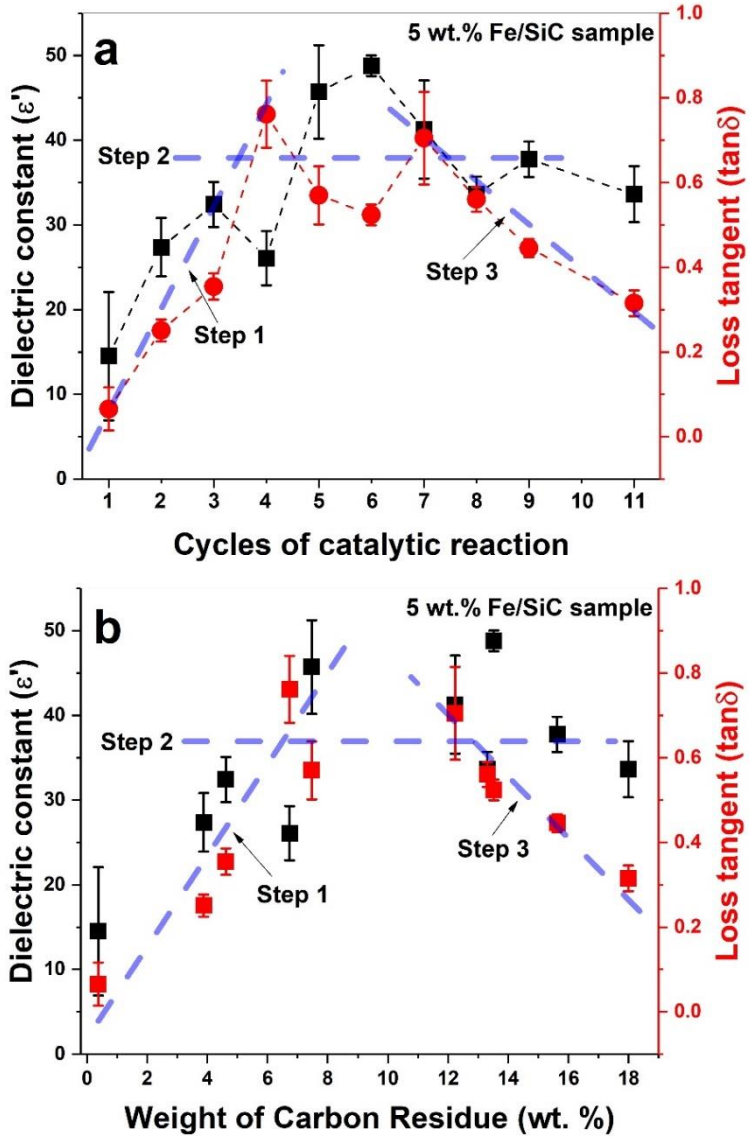


Figure 6.18. (a) The change of dielectric constant and loss tangent of 5 wt.% Fe/SiC samples through successive cycles of catalytic reactions under microwave activation. (b) Dielectric constant and Loss tangent of 5 wt.% Fe/SiC samples as a function of the weight of carbon residues. The results shown above were measured at room temperature. Error bars indicate the standard deviations across different samples.

In a brief summary, the dielectric properties of model carbons varied considerably; and the dielectric properties of model carbons and the Fe/SiC samples are negligibly affected by increased temperature.

However, based on the cavity perturbation measurements of evolved Fe/SiC samples, there is no single kind of carbon can be adapted to the produced carbon residues. This suggests the produced carbons are a mixture of different kinds of carbons.

6.3.5 Evolved carbon deposition and the proposed deactivation Mechanisms

Figure 6.19 depicts a proposed representative diagram of carbon formation/ transformation on iron particle surface during the microwave-initiated dehydrogenation of hexadecane. At the beginning, catalysts remained active at an initial level despite of some carbons being deposited on the surface of iron. The iron remained active and the active sites on iron were still dominant. However, the continuous accumulation of carbons on iron led to the C atom from the C-H bonds dissociation is chemisorbed strongly as a monolayer or physically adsorb in multilayers on the iron metals to form C_α, where the C_α is an adsorbed atomic carbon or surface carbide (Eq. 6.1)[14]. The C_α can either react with following C atoms to form C_β (Eq. 6.2), a polymeric carbon film, or penetrate into Fe to form iron carbides. Moreover, some of the C atoms could be dissolved in Fe as vermicular carbon[14]. Obviously, the active amorphous α-carbon and β-carbon were formed at the early cycles of test.

At the 2nd step, the iron reacted with produced carbons to form iron carbides (Eq. 6.4) and more carbons were produced and deposited on the catalysts' surface. These carbons were assumed to be catalytically active and dominant in the reactions later stages of the cycles whilst the iron lost most of its active sites. This was reflected by the decreased reaction rates and the changed products distribution of the catalysts observed between cycle 4 and cycle 7.

Finally, these active carbons were also deactivated as a result of the active sites or the so-called defects on the active carbons were blocked/covered by C produced later. Therefore, the active amorphous α-carbon and β-carbon that formed at the early cycles are converted to inactive polymeric platelets, films or filaments (Eq. 6.3). Consequently, the iron particles as well as the active carbons were encapsulated/ covered by the inactive polymeric carbons and thereby deactivated.

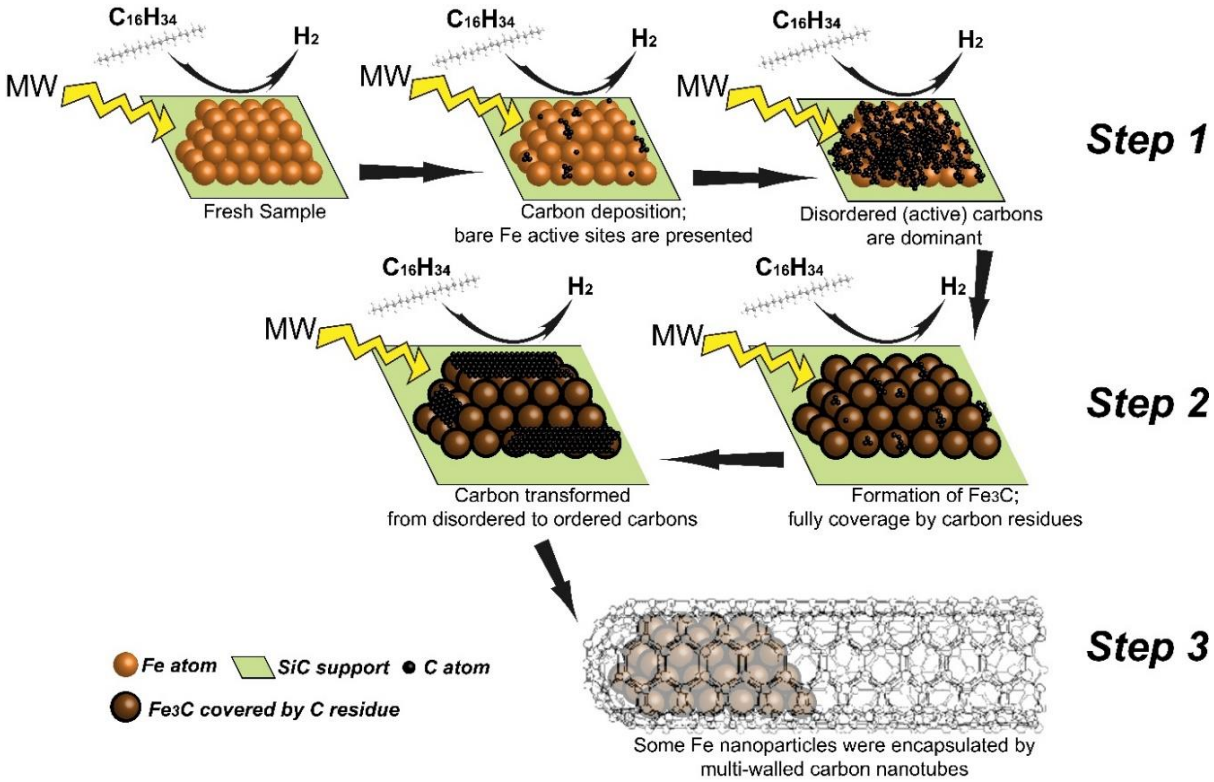


Figure 6.19. A representative diagram of carbon deposition and transformation through microwave-initiated hexadecane dehydrogenation over Fe/SiC catalysts.

$$C_nH_{2n+2}\ (a)^* \rightarrow nC_\alpha\ (a) + (2n+2)\ H\ (a) \quad (6.1)$$

$$C_\alpha\ (a) + C_\alpha\ (a) \rightarrow C_\beta\ (a) \rightarrow \text{Carbon}\ (s)^*\ \text{(amorphous and graphitic carbons)} \quad (6.2)$$

$$C_\beta\ (a) + C_\beta\ (a) \rightarrow \text{Carbon}\ (s)\ \text{(Polymeric, graphitic platelets, films or filaments)} \quad (6.3)$$

$$C_\alpha\ (a) + Fe \rightarrow \text{Iron Carbides}\ (s) \quad (6.4)$$

$$C_\alpha\ (a) + 4H\ (a) \rightarrow CH_4\ (g) \quad (6.5)$$

$$2H\ (a) + H_2\ (a) \rightarrow H_2\ (g)^* \quad (6.6)$$

* (a), (g) and (s) refer to adsorbed, gaseous and solid states, respectively.

6.4 Conclusion

Catalytic hydrocarbon dehydrogenation is an ideal process to produce pure hydrogen without CO_2 contamination. The challenge of carbon produced during the process can be instigated potentially by their action as catalysts for further dehydrogenation in an applied microwave-electric field due to its highly efficient ability for microwave absorption. Among the many carbon allotropes studied, only some types of carbon are catalytically active for hydrocarbon dehydrogenation in a microwave-electric field. It has been demonstrated that activated carbon and graphene nanoplatelets are catalytically active while the filamentous carbon (MWCNTs and CNFs), graphite and glassy carbon were inactive.

The Fe/SiC catalysts can effectively catalyse the dehydrogenation of hexadecane under microwave irradiation for several cycles. The deactivation of catalysts was attributed to the carbon residues. However, it has been found that some types of carbons produced in the early cycles of test were themselves catalytically active for the reactions. An obvious change of morphology and the properties of catalysts were observed by SEM and the cavity perturbation measurements throughout the successive cycles of hexadecane dehydrogenation. It was found that the formation of inactive polymeric carbons such as MWCNTs, CNFs and graphite etc. can finally deactivate the catalysts.

Thus, the active carbon materials for hydrocarbons dehydrogenation in the microwave-electric field have been distinguished by the specific structure and properties. Theoretically, control of the types of carbon produced during the process could potentially extend the lifetime of catalysts or make the catalysts remain active longer in an induced microwave-electric field. Based upon their unique origin and structures, the carbon-based catalysts could be used as a variety of catalyst with different selectivities in microwave-initiated catalysis.

Bibliography:

1. D. M. D'Alessandro, B. Smit and J. R. Long, *Angewandte Chemie International Edition*, 2010, 49, 6058-6082.
2. N. Z. Muradov, *Catalysis Communications*, 2001, 2, 89-94.
3. S. Ahmed, A. Aitani, F. Rahman, A. Al-Dawood and F. Al-Muhaish, *Applied Catalysis A: General*, 2009, 359, 1-24.
4. J. Ashok, M. Subrahmanyam and A. Venugopal, *Catalysis Surveys from Asia*, 2008, 12, 229.
5. T. V. Choudhary, C. Sivadinarayana, C. C. Chusuei, A. Klinghoffer and D. W. Goodman, *Journal of Catalysis*, 2001, 199, 9-18.
6. E. K. Lee, S. Y. Lee, G. Y. Han, B. K. Lee, T.-J. Lee, J. H. Jun and K. J. Yoon, *Carbon*, 2004, 42, 2641-2648.
7. N. Z. Muradov, Z. Chen and F. Smith, *International Journal of Hydrogen Energy*, 2005, 30, 1149-1158.
8. M. Steinberg and H. C. Cheng, *International Journal of Hydrogen Energy*, 1989, 14, 797-820.
9. M. Steinberg, *International Journal of Hydrogen Energy*, 1999, 24, 771-777.
10. N. Z. Muradov, *International Journal of Hydrogen Energy*, 2017, 42(20), 14058-14088.
11. N. Z. Muradov, *International Journal of Hydrogen Energy*, 1993, 18, 211-215.
12. L. Zhou, L. R. Enakonda, M. Harb, Y. Saih, A. Aguilar-Tapia, S. Ould-Chikh, J.-l. Hazemann, J. Li, N. Wei and D. Gary, *Applied Catalysis B: Environmental*, 2017, 208, 44-59.
13. M. Lázaro, J. Pinilla, I. Suelves and R. Moliner, *International Journal of Hydrogen Energy*, 2008, 33, 4104-4111.
14. C. H. Bartholomew, *Applied Catalysis A: General*, 2001, 212, 17-60.
15. P. Lidstrom, J. Tierney, B. Wathey and J. Westman, *Tetrahedron*, 2001, 57, 10229.
16. S. Horikoshi and N. Serpone, *Catalysis Science & Technology*, 2014, 4, 1197-1210.
17. S. A. Galema, *Chemical Sociaty Review*, 1997, 26, 233-238.
18. F. Langa, P. De La Cruz, A. De La Hoz, A. Diaz-Ortiz and E. Diez-Barra, *Contemporary Organic Synthesis*, 1997, 4, 373-386.

19. A. Domínguez, B. Fidalgo, Y. Fernández, J. Pis and J. Menéndez, *International Journal of Hydrogen Energy*, 2007, 32, 4792-4799.

20. M. Jasiński, M. Dors and J. Mizeraczyk, *Journal of Power Sources*, 2008, 181, 41-45.

21. X. Zhang, C. S.-M. Lee, D. M. P. Mingos and D. O. Hayward, *Catalysis Letters*, 2003, 88, 129-139.

22. R. M. Navarro, M. A. Pena and J. L. G. Fierro, *Chemical Review*, 2007, 107, 3952-3991.

23. V. G. Gude, P. Patil, E. Martinez-Guerra, S. Deng and N. Nirmalakhandan, *Sustainable Chemical Processes*, 2013, 1, 1.

24. N. Z. Muradov, F. Smith, C. Huang and T. Ali, *Catalysis Today*, 2006, 116, 281-288.

25. X. Jie, S. Gonzalez-Cortes, T. Xiao, J. Wang, B. Yao, D. R. Slocombe, H. A. Al-Megren, J. R. Dilworth, J. M. Thomas and P. P. Edwards, *Angewandte Chemie International Edition*, 2017, 56, 10170-10173.

26. S. Gonzalez-Cortes, D. Slocombe, T. Xiao, A. Aldawsari, B. Yao, V. Kuznetsov, E. Liberti, A. Kirkland, M. Alkinani and H. Al-Megren, J. M. Thomas and P. P. Edwards, *Scientific Reports*, 2016, 6, 35315.

27. X. Zhang, D. O. Hayward and D. M. P. Mingos, *Catalysis Letters*, 2003, 88, 33-38.

28. J. Rostrup-Nielsen and D. L. Trimm, *Journal of Catalysis*, 1977, 48, 155-165.

29. R. Yang and K. Yang, *Journal of Catalysis*, 1985, 93, 182-185.

30. R. Baker, *Carbon*, 1989, 27, 315-323.

31. L.-S. Fu, J.-T. Jiang, C.-Y. Xu and L. Zhen, *CrystEngComm*, 2012, 14, 6827-6832.

32. T. A. Saleh, *The role of carbon nanotubes in enhancement of photocatalysis. Syntheses and applications of carbon nanotubes and their composites*, Synthesis and Applications of Carbon Nanotubes and Their Composites, 2013, 479-493.

33. J. A. Cuenca, E. Thomas, S. Mandal, O. Williams and A. Porch, *Carbon*, 2015, 81, 174-178.

34. B. Liu, D. Slocombe, J. Wang, A. Aldawsari, S. Gonzalez-Cortes, J. Arden, V. Kuznetsov, H. AlMegren, M. AlKinany and T. Xiao, *Nature Communications*, 2017, 8, 514.

Chapter 7

Conclusion, Challenges and Perspectives

7.1 Concluding remarks

My doctoral work aimed at further developing a new, innovative catalytic process for carbon emission-free hydrogen production from fossil fuels. It is based on a novel catalyst system initiated by microwave energy, achieving the rapid release of high-purity hydrogen directly from hydrocarbon fuels, with the co-product of solid carbon being recycled into value-added materials or otherwise sequestered in perpetuity.

Hydrogen has long been acknowledged as a promising vector for future clean energy. However, the large-scale production of hydrogen is predominantly through the steam reforming of fossil fuels (methane), a process which emits large quantities of CO_2. The vision of CO_2-free hydrogen production from hydrocarbons via thermal, catalytic decomposition was developed in pioneering work and also achieved more recently through the use of microwave pyrolysis, plasma processing and molten metals. However, these approaches still face significant technological challenges, often operate at very high temperatures/require high energy input and scale up/down poorly across applications.

My doctoral research, which has generated a patent and three scientific articles in internationally leading journals, has demonstrated that high purity hydrogen can be rapidly produced through microwave-initiated catalytic dehydrogenation using earth abundant iron and nickel particle catalysts. Remarkably, this process can be directly applied to all natural occruing fossil fuels, ranging from extra-heavy crude oil and crude oil through diesel, and finally to methane. This advance offers the possibility of extracting clean hydrogen at large scale and at a relatively low energy input directly from fossil fuels through distributed or dispersed production units, with the concept of CCS now being applied by storing carbon as a solid form instead of as aerial CO_2. In addition, the co-product solid carbon, can be

converted for numerous high-value applications (graphite, carbon black, carbon nanotubes, high surface area carbon, etc.).

Fossil hydrocarbon fuels are themselves excellent natural hydrogen storage materials since they potentially exceed the targets of H_2 gravimetric and volumetric densities set by the U.S Department of Energy (DoE). The results for the microwave-initiated dehydrogenation of diesel, for example, have shown higher H_2 gravimetric and volumetric densities than those targets. Microwave-initiated catalytic dehydrogenation of fossil fuels could therefore become transformative for hydrogen production applications (refuelling station, methane reforming alternative, fuel cells in stationary and automotive sectors, etc.) because of three attractive features: *First*; the rapid production of high-purity hydrogen; *Second;* the requirement of only a small–scale microwave source and reactor system for either localized or distributed applications; and *Third;* the well-established infrastructure for fossil fuels, leading to distributed or dispersed hydrogen production units – effectively negating the need for a dedicated hydrogen pipeline system.

In summary, we offer here a solution for carbon free hydrogen production and hydrogen storage for fuel cells application. There is thus, a new scientific and technological era of "*Fossil fuel decarbonisation*'' can arise where we would not destroy naturally-occurring fossil fuels by combustion with attendant CO_2 emissions, but rather utilise them to produce clean hydrogen. Thus, through this process, carbonaceous fossil fuels are thereby transformed from carbon-rich to hydrogen-rich fuels for our future energy needs.

7.2 The challenges and future works

The technique must now be upgraded in order to provide the economic impetus for its uptake. There are several necessary steps of research needed to integrate chemistry with engineering design in order to scale-up the technology:

i. Pilot-scale device

   Typical benchtop devices (lab-scale devices) are relatively inefficient and magnetron-based; in particular the power transfer to the sample is often only a fraction of the microwave power

generated. Therefore, to upgrade the devices to meet pilot scale requirements, the devices need to have correct impedance matching and efficient solid-state microwave sources. Currently, the magnetron-based device operates at <20% efficiency for power transfer and a solid-state microwave sources-based device can theoretically bring the power transfer efficient up to >99%. This will significantly reduce the energy consumption of process.

ii. The catalyst system optimisation for a pilot-scale device

The important engineering questions of microwave field penetration and uniformity dictate the electromagnetic conditions in the catalyst bed. Therefore, it is essential to optimise the whole catalyst system to integrate with a larger scale device for any given input energy and consequently to produce the desirable conversion and selectivity. The effective use of microwave energy and balance of plant will be the key tasks to improve the efficiency and also the hydrogen purity.

iii. Continuous flow study for methane decomposition and liquid fuels (diesel and petrol etc.).

Methane has the highest hydrogen-to carbon (H/C) ratio and is the simplest aliphatic among all hydrocarbons. Importantly, the infrastructure for methane transportation and distribution is well-developed. Therefore, it will be key to further investigate methane decomposition to hydrogen in various flow feed scenarios. This would demonstrate the possibility to replace the current SMR process for hydrogen production. Like the methane, the investigation on liquid fuels dehydrogenation at various flow feed scenarios would provide an important step forwards towards the end user in transportation and stationary hydrogen production using microwave.

iv. The catalytic sites

Perhaps most importantly, knowledge of the required local environment at catalytic sites in operation and a better understanding of the dehydrogenation process under microwave irradiation will lead to further optimisation of the technique. In situ probes for simultaneous

microwave heating and measurement using neutrons, x-rays and electron paramagnetic resonance studies are under development in order to elucidate the processes

v. Kinetics/ Artificial neural network study and system optimisation

It will be important to study the kinetics such as temperature, pressure and flow feed, etc. of the whole system and make it optimised to meet the requirements of operation at large scale. Due to the complexities of the microwave systems, it will involve applying an artificial neural network to help optimise the whole system before the process is fully commercialised.

vi. Carbon separation technology and catalysts regeneration

A high volume of carbon, in general carbon nano-tubes (CNT) are produced during this process. The separation of these carbon materials can produce high quality carbons with significant commercial value depending on their characteristics. This would consequently reduce the overall cost of hydrogen production. Regeneration of catalysts is highly dependent on the size capacity of the system and the end user. The in-situ regeneration of catalysts is currently a significant challenge, but catalysts may be regenerated on a centralised basis. Solutions to both will be explored and developed.

vii. High value CNTs applications

The harvesting of CNTs for use in applications, such as lithium-ion batteries offers a separate unique opportunity. Initial development on the best means of downstream processing to recover these, whilst producing industrial-grade high-purity hydrogen.

In summary, the applicability and sustainability credentials of this approach for scale up will obviously be the next step for any practical utilisation. The challenges listed above summarised the key points in both chemistry and engineering aspects that need to be studied towards potential industrial application.

7.3 Perspectives

It is a clichéd and overused remark that there is now a presumed need to phase out fossil-derived fuels due to increasingly CO_2 emission and equally to phase-in hydrogen and hydrogen-containing materials so as to accelerate the arrival of the so-called hydrogen economy. Indeed, one of the principal reasons why progress towards the most advocated hydrogen economy has been so slow devolves to the fact that there is no readily available large-scale source of "natural" hydrogen. Another is the fact that, to date, no reliable means exists for storing hydrogen in such a manner that it can be rapidly released - on demand- for the appropriate fuel cell application.

Almost all the hydrogen that is nowadays used, worldwide, for industrial purposes comes from the steam reforming of natural gas and, to a lesser degree, from the gasification of coal. These processes, however, generate a vast amount of carbon dioxide[1-4]. Although, extensive work involving principally solar radiation (as well as wind and other natural renewable energy sources) has been done to produce hydrogen by splitting water either via photo-assisted manner or by electrolysis, these technologies suffer from low efficiency, durability and safety – and require further research and development. Another related question is how to utilise fossil–based fuel resources so as not to liberate CO_2 and associated unwanted products.

The intrinsically high hydrogen content of hydrocarbons offers a potential route to CO_2-free hydrogen production through their catalytic deep dehydrogenation. The proposed hydrogen supply demonstration centres on a method of rapidly liberating high-purity hydrogen from hydrocarbons without CO_2 emissions. There is thus an innovative system combining microwave technology and heterogeneous catalysis has been developed. Laboratory demonstration has shown high-purity hydrogen production through *microwave-initiated catalytic dehydrogenation* of liquid alkanes using cheap and abundant iron (Fe) and nickel (Ni) catalysts. The results show nearly pure hydrogen with selectivity from all evolved gases of some 98%, achieved with less than a fraction of a percent of adventitious CO and CO_2. The major co-product is solid, elemental carbon. The advantages of this technology are the following:

a. High H_2 selectivity of some 98% (efficiency)/ extremely low concentration of by-products (i.e., light hydrocarbons) and less than 1% CO and CO_2.

b. Processing of hydrogen production with Fe and Ni catalysts will significantly reduce the cost; in addition, ability to construct SiC monoliths as support with decorated non-noble-metal catalysts is technologically and commercially attractive.
c. Rapid heating and high heat conductivity (high-energy efficiency) of the process.
d. Close-to zero CO_2 emission (environmental-friendly)
e. Rapid reaction system allows it to be applied to diverse applications.
f. Scalability of the system components offers the potential to design a portable device for use in transportation or scaled up for industrial applications.
g. Solid carbon produced has further potential high value applications

Based on these key advantages, this technology has potential to be applied to centralised hydrogen production such as in hydrogen refuelling stations as well as on-board hydrogen production for larger vehicles (trucks, maritime vessels, etc.). There is thus, a model of microwave-initiated fuel cell vehicle for which a microwave system is accommodated on board to produce high purity hydrogen for fuel cell was proposed based on our experimental demonstration (Figure 7.1). Here, we compared the CO_2 emission as well as the mileage of this microwave-initiated fuel cell vehicle to the conventional diesel and petrol vehicles. The result shows that the microwave-initiated fuel cell vehicle could possibly achieve 80% and 65% mileages of conventional petrol and diesel vehicles, respectively. Importantly, no CO_2 emission and hot air are generated and no after treatment is required as the only product is pure water. It should be noted that the microwave-initiated fuel cell vehicle could achieve longer mileages with the improvement of efficiency of electric motor, fuel cell and microwave system. All the matrices used in the calculation is based on current efficiency of electric motor and fuel cell [5-8], and a comparable low efficiency of microwave system (19%) that estimated based on our experiments [9, 10]. Clearly, the model of microwave-initiated fuel cell vehicle is highly attractive for the future application. But further studies are needed in many aspects such as catalyst optimisation and the engineering problem, etc., for its application.

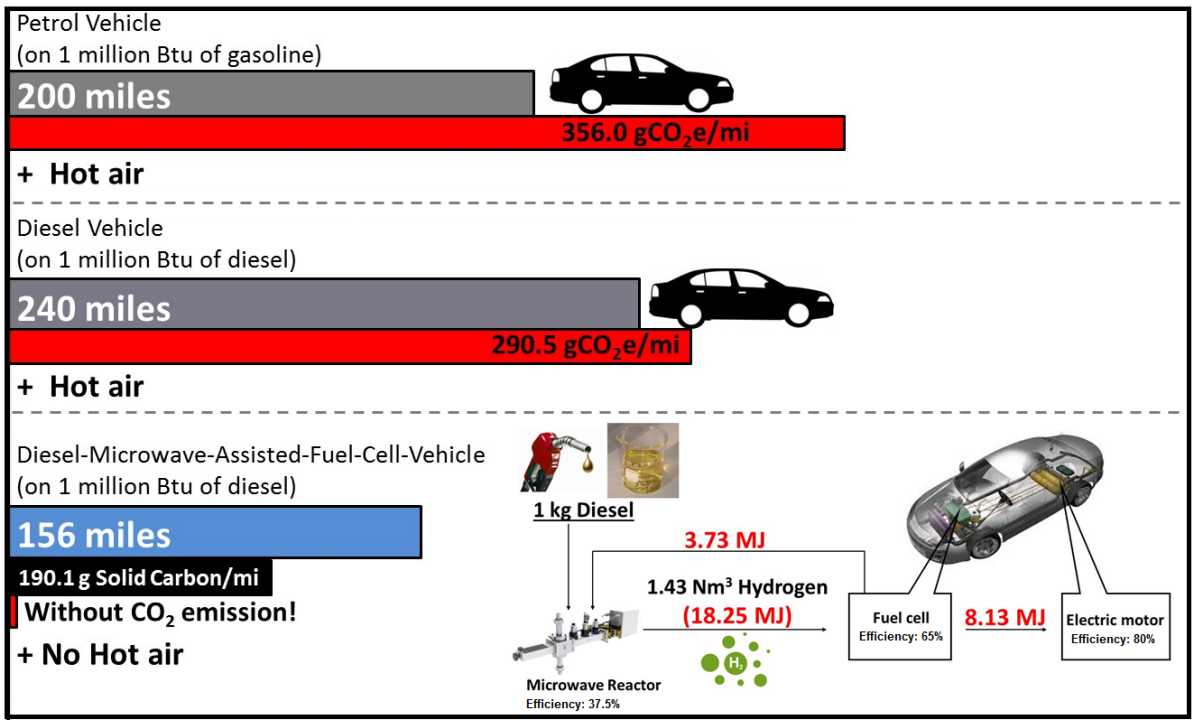


Figure 7.1. Schematic representation of one approach to mitigate CO_2 emission in transportation. Comparison of the mileage and CO_2 emission for a microwave-initiated fuel cell with conventional diesel and gasoline propelled vehicles assuming each consumes fuel equivalent to 1 million Btu.

Similarly, it could provide centralised hydrogen production into the natural gas grid, or decentralised units as part of industrial processes and power generation or even in domestic combined heat and power units. Obviously, the various applications would require further development in terms of engineering design and system optimisation, but the microwave reactors themselves can be designed from the portable to industrial scale. Moreover, the cheap and abundant nature of the catalysts employed allows this to be a commercially scalable solution.

Furthermore, this proposed hydrogen supply solution provides a new method for safe hydrogen production and hydrogen storage whilst also offering a solution for decarbonising fossil fuels. Moreover, the well-established distribution infrastructure for fossil fuels would significantly reduce any initial capital investment for hydrogen transportation and distribution and thus catalyse and accelerate the smooth transition to a hydrogen economy.

Bibliography:

1. M. Steinberg and H. C. Cheng, *International Journal of Hydrogen Energy*, 1989, 14, 797-820.
2. M. Steinberg, *International Journal of Hydrogen Energy*, 1999, 24, 771-777.
3. N. Z. Muradov, *International Journal of Hydrogen Energy*, 2017, *42*(20), 14058-14088.
4. H. Arakawa, M. Aresta, J. N. Armor, M. A. Barteau, E. J. Beckman, A. T. Bell, J. E. Bercaw, C. Creutz, E. Dinjus, D. A. Dixon, K. Domen, D. L. DuBois, J. Eckert, E. Fujita, D. H. Gibson, W. A. Goddard, D. W. Goodman, J. Keller, G. J. Kubas, H. H. Kung, J. E. Lyons, L. E. Manzer, T. J. Marks, K. Morokuma, K. M. Nicholas, R. Periana, L. Que, J. Rostrup-Nielson, W. M. H. Sachtler, L. D. Schmidt, A. Sen, G. A. Somorjai, P. C. Stair, B. R. Stults and W. Tumas, *Chemical Reviews*, 2001, 101, 953-996.
5. P. Waide and C. Brunner, *Energy-Efficiency Policy Opportunities for Electric Motor-Driven Systems*, OECD Publishing, 2011.
6. U.S. department of Energy, Determining electric motor load and efficiency, available at https://www.energy.gov/sites/prod/files/2014/04/f15/10097517.pdf.
7. J. Larminie, A. Dicks and M. S. McDonald, *Fuel Cell Systems Explained*, J. Wiley Chichester, UK, 2003.
8. A. B. Stambouli and E. Traversa, *Renewable and Sustainable Energy Reviews*, 2002, 6, 433-455.
9. C. L. Brace, *Current Problems in Diagnostic Radiology*, 2009, 38, 61-67.
10. J. Benford, J. A. Swegle and E. Schamiloglu, *High Power Microwaves*, CRC Press, 2015.

Appendix A

The detailed composition analysis of petroleum samples

Table A1: The composition of diesel determined by GCMS. (The percentage is the area% obtained from GCMS)

Compounds	Formula	Percentage (%)
Nonane	C_9H_{20}	0.97
1-Octanol, 2-butyl-	$C_{12}H_{26}O$	1.43
Decane	$C_{10}H_{22}$	2.39
Benzene, 1,2,3-trimethyl-	C_9H_{12}	1.00
Decane, 4-methyl-	$C_{11}H_{24}$	0.82
1-Iodo-2-methylnonane	$C_{10}H_{21}$	1.15
Undecane	$C_{11}H_{24}$	3.48
Octane, 2,3,6,7-tetramethyl-	$C_{12}H_{26}$	1.81
Undecane, 2-methyl-	$C_{12}H_{26}$	0.95
Dodecane	$C_{12}H_{26}$	4.49
Tridecane	$C_{13}H_{28}$	5.92
Tetradecane	$C_{14}H_{30}$	7.22
Hexadecane	$C_{16}H_{34}$	17.56
Octadecane	$C_{18}H_{38}$	13.06
Heptadecane	$C_{17}H_{36}$	6.75
Nonadecane	$C_{19}H_{40}$	5.26

9-Octadecenoic acid, methyl ester, (E)-	$C_{19}H_{36}O_2$	8.01
Octadecanoic acid, methyl ester	$C_{19}H_{38}O_2$	1.84
Heneicosane	$C_{21}H_{44}$	12.30
Eicosane	$C_{20}H_{42}$	2.26
Tetracosane	$C_{24}H_{50}$	1.32
Sum	**(-)**	**100**

Table A2: The composition of petrol determined by GCMS. (The percentage is the area% obtained from GCMS)

Compounds	**Percentage (%)**
Isobutane	2.14
Butane, 2-methyl-	13.22
Pentane, 3-methyl-	4.55
Hexane	4.11
(2,2-Dimethylcyclopropyl)-methanol	1.15
Cyclopentane, methyl-	2.16
Hexane, 2-methyl-	2.1
Hexane, 3-methyl-	3.7
Benzene	0.87
Pentane, 2,2,3,4-tetramethyl-	1.15
Heptane	2
Cyclohexane, methyl-	1.69
Cyclopentane, propyl-	0.39
1-Heptene, 4-methyl-	0.47

Heptane, 3-ethyl-5-methylene-	0.56
Heptane, 2-methyl-	1.31
Heptane, 3-methyl-	1.1
Toluene	19.86
Octane	0.93
Ethylbenzene	3.35
o-Xylene	13.12
o-Xylene	4.83
Benzene, propyl-	0.88
Benzene, 1-ethyl-3-methyl-	2.99
Benzene, 1-ethyl-2-methyl-	1.18
Benzene, 1,2,4-trimethyl-	1.21
Benzene, 1-ethyl-2-methyl-	0.86
Benzene, 1,2,3-trimethyl-	4.92
Benzene, 1,2,4-trimethyl-	0.69
2,4-Dimethylstyrene	0.18
Azulene	0.13
n-Hexadecanoic acid	0.43
Octadecanoic acid	0.12
Sum	**98.35**

Table A3: The chemical compounds analysis on extra-heavy crude oil.

Analysis of light fractions wt.%	
C	84.020
H	11.220
S	4.750
S/C	0.04
H/C	1.60
Density	0.913

Table A 4: The chemical compounds analysis on crude oil.

Analysis of light fractions wt.%	
C	84.160
H	12.700
S	3.140
S/C	0.03
H/C	1.81
Density	0.86

Appendix B

The detailed composition analysis of product distribution by GC

Table B1: Evolved gas composition of the prepared catalysts assessed by GC analysis. Conditions: hexadecane (ca. 0.5ml) was well mixed with catalysts. The samples were irradiated under 750 W power microwave for 30 min. The error for GC is $\pm$0.01 – 0.1%.

Sample*	H_2 [Vol%]	Methane [Vol%]	Ethylene [Vol%]	Small Alkanes (C_2-C_5) [Vol%]	CO_2 [Vol%]	CO [Vol%]
Fe	72.21	4.66	7.99	3.54	1.51	10.10
SiC	N/R					
Fe/SiC (5)	93.13	2.16	0.68	0.61	0.2	3.2
Ni/SiC (5)	96.60	1.39	0.13	0.07	0.1	1.7
Co/SiC (5)	73.85	11.15	9.67	4.81	0.0	0.5
Cu/SiC (5)	58.94	20.78	14.32	4.89	0.48	0.58
Pt/SiC (5)	56.97	20.56	13.98	3.59	0.70	4.20
Ru/SiC (5)	N/R					
Fe/SiC (2)	92.14	3.07	1.37	1.16	0.07	2.21
Fe/SiC (10)	92.41	2.56	0.67	0.56	0.14	3.66
Fe/SiC (20)	85.35	4.69	2.64	1.79	0.19	5.34
Ni/SiC (10)	94.52	4.32	0.28	0.57	0.1	0.2
Fe-Ni/SiC (4.5,0.5)	96.00	3.15	0.14	0.31	0.0	0.4

Fe-Co/SiC (4.5,0.5)	93.18	4.72	0.54	0.97	0.0	0.6
Fe-Ru/SiC (4.5,0.5)	93.02	3.48	0.81	0.80	0.1	1.8
Fe-Cu/SiC (4.5,0.5)	93.53	2.95	0.76	0.87	0.0	1.9
Fe/SiC (10)	92.41	2.56	0.67	0.56	0.1	3.7
Fe-Ni/SiC (5,1)	97.47	1.80	0.10	0.15	0.2	0.3
Fe-Ni/SiC (5,5)	97.72	1.63	0.05	0.05	0.0	0.5
Fe-Ni/SiC (1,5)	94.45	3.34	0.22	0.13	0.1	1.8
Activated carbon	58.66	24.14	10.37	5.17	0.58	1.09
Fe/AC (5)	56.03	18.62	10.25	7.05	0.26	7.80
SiO_2	N/R					
Fe/SiO_2 (5)	60.70	11.58	8.75	1.74	0.30	16.93
Al_2O_3	N/R					
Fe/Al_2O_3 (5)	82.55	3.91	0.31	0.48	0.00	12.75
Graphene nanoplatelet	24.78	24.97	23.79	21.31	3.50	1.66

*: The number in parentheses after catalyst shows the metal content, wt. %. 'N/R' means no reaction was found on pointed catalyst during the experiment.

Table B2: Evolved gas composition of 5 wt.% Fe/SiC assessed by GC analysis from various liquid alkanes and aromatics. Conditions: feedstock (ca. 0.5ml) was first well mixed with catalyst. The sample was then irradiated under 750 W power microwave for 30 min. The error for GC is ±0.01 – 0.1%.

Sample	H_2 [Vol%]	Methane [Vol%]	Ethylene [Vol%]	Small Alkanes (C_2-C_5) [Vol%]	CO_2 [Vol%]	CO [Vol%]
$C_{17}H_{36}$	87.35	6.37	0.90	1.41	0.10	3.87
$C_{16}H_{34}$	93.13	2.16	0.68	0.61	0.18	3.24
$C_{15}H_{32}$	91.66	2.87	1.29	0.71	0.08	3.39
$C_{14}H_{30}$	85.03	6.50	3.96	2.40	0.07	2.03
$C_{13}H_{28}$	86.46	7.13	1.84	1.74	0.05	2.79
$C_{12}H_{26}$	92.66	1.31	0.68	0.41	0.11	4.82
$C_{11}H_{24}$	91.40	3.61	0.27	0.29	0.06	4.37
$C_{10}H_{22}$	94.11	2.57	0.39	0.37	0.07	2.49
C_9H_{20}	92.79	4.00	0.17	0.41	0.05	2.57
C_8H_{18}	88.25	1.45	0.84	1.02	0.42	8.02
C_7H_{16}	86.17	7.82	1.10	1.17	0.26	3.47
Toluene	91.78	2.31	0.04	0.08	0.10	5.70
p-Xylene	84.39	1.84	0.07	0.12	0.64	12.93
o-Xylene	87.48	1.78	0.03	0.04	0.61	10.07
m-Xylene	92.85	2.05	0.10	0.03	0.36	4.60
Ethyl-benzene	83.64	1.83	0.17	0.05	0.46	13.86

Table B3: Evolved gas composition of 5 wt.%-Fe, 5 wt.%-Ni FeNi/SiC assessed by GC analysis from various liquid alkanes and aromatics. Conditions: feedstock (ca. 0.5ml) was first well mixed with catalyst. The sample was then irradiated under 750 W power microwave for 30 min. The error for GC is $\pm$0.01 – 0.1%.

Sample	H_2 [Vol%]	Methane [Vol%]	Ethylene [Vol%]	Small Alkanes (C_2-C_5) [Vol%]	CO_2 [Vol%]	CO [Vol%]
$C_{17}H_{36}$	85.00	6.37	4.65	3.43	0.07	0.49
$C_{16}H_{34}$	97.72	1.63	0.05	0.05	0.00	0.50
$C_{15}H_{32}$	93.96	3.59	0.69	0.40	0.05	1.31
$C_{14}H_{30}$	95.95	3.10	0.25	0.27	0.05	0.38
$C_{13}H_{28}$	95.29	3.20	0.26	0.53	0.05	0.66
$C_{12}H_{26}$	90.85	5.25	1.54	1.73	0.04	0.61
$C_{11}H_{24}$	96.37	2.59	0.14	0.47	0.04	0.39
$C_{10}H_{22}$	93.46	2.62	0.88	0.32	0.14	2.58
C_9H_{20}	94.80	2.00	0.31	0.19	0.07	2.63
C_8H_{18}	83.27	1.52	1.17	0.45	3.46	10.13
C_7H_{16}	96.41	1.85	0.06	0.03	0.07	1.59
Toluene	95.59	1.21	0.03	0.01	0.08	3.09
p-Xylene	94.04	0.74	0.15	0.18	0.10	4.79
o-Xylene	84.01	0.79	0.58	0.24	0.59	13.79
m-Xylene	96.87	1.22	0.05	0.02	0.06	1.78
Ethyl-benzene	93.89	1.12	0.06	0.03	0.06	4.84
Propyl-cyclohexane	88.50	0.95	0.15	0.14	0.09	10.17

Appendix C

Theoretical and Experimental Hydrogen Density of Hydrocarbons

Table C1: Theoretical hydrogen densities of various hydrogen storage materials.

Materials	Gravimetric Density (kg-H_2/kg)	Volumetric Density (kg-H_2/m^3)
DoE target	7.5	70
Petrol	14.84	109.29
diesel	16.35	124.69
CH_4 (liq.)	25	107.30
C_4H_{10} (liq.)	17.3	98.40
CH_4	25	0.179
C_2H_6	20	0.268
C_3H_8	18.18	0.357
C_4H_{10}	17.24	0.446
C_5H_{12}	16.67	104.33
C_6H_{14}	16.28	107.28
C_7H_{16}	16	109.44
C_8H_{18}	15.79	111.00
C_9H_{20}	15.63	112.19
$C_{10}H_{22}$	15.49	113.10
$C_{11}H_{24}$	15.38	113.85
$C_{12}H_{26}$	15.29	114.55
$C_{13}H_{28}$	15.22	115.04

$C_{14}H_{30}$	15.15	115.76
$C_{15}H_{32}$	15.09	116.08
$C_{16}H_{34}$	15.04	116.29
$C_{17}H_{36}$	15	116.55
CH_3OH	12.9	93.80
$NaBH_4$	10.7	114

Table C2: Experimental hydrogen densities of diesel, petrol and hexadecane obtained over 5 wt.% Fe/SiC catalysts.

Materials	**Gravimetric Density (kg-H_2/kg)**	**Volumetric Density (kg-H_2/m^3)**
DoE target	7.5	70
Diesel	8.57	71.28
Petrol	9.27	71.39
Hexadecane	9.75	75.36

Appendix D

Theoretical and Experimental Hydrogen Density of Hydrocarbons

Table D1: The energy requirement and energy output for the combustion of H_2 produced via the diesel cracking

Compounds	Formula	Percentage (%)	Energy requirement MJ/kg	H_2 product* Nm^3/kg	Energy output MJ/kg
Pentadecane	$C_{15}H_{32}$	20	2.02	1.69	21.53
Hexadecane	$C_{16}H_{34}$	20	2.01	1.68	21.46
Heptadecane	$C_{17}H_{36}$	20	2.00	1.49	19.02
Decylcyclopentane	$C_{15}H_{30}$	5	1.73	1.60	20.38
Decylcyclohexane	$C_{16}H_{32}$	5	1.85	1.60	20.38
Undecylcyclohexane	$C_{17}H_{34}$	5	1.74	1.60	20.38
1,3,5-trimethyl benzene	C_9H_{12}	7	0.51	1.12	14.27
Diphenyl	$C_{12}H_{10}$	8	-0.76	0.73	9.27
Indane	C_9H_{10}	5	-0.09	0.95	12.09
Naphthalene	$C_{10}H_8$	5	-0.76	0.70	8.92
Sum	**(-)**	**100**	**1.40**	**1.43**	**18.25**

Table D2: The energy requirement and energy output for the combustion of H_2 produced via the diesel cracking

Compounds	Formula	Percentage (%)	Energy requirement MJ/kg	H_2 product* Nm^3/kg	Energy output MJ/kg
Nonane	C_9H_{20}	0.97	2.15	1.75	22.24
1-Octanol, 2-butyl-**	$C_{12}H_{26}O$	1.43	2.86	1.56	19.90
Decane	$C_{10}H_{22}$	2.39	2.12	1.73	22.06
Benzene, 1,2,3-trimethyl-	C_9H_{12}	1	0.46	1.14	14.48
Decane, 4-methyl-	$C_{11}H_{24}$	0.82	2.11	1.72	21.90
1-Iodo-2-methylnonane***	$C_{10}H_{21}$	1.15	2.12	1.73	22.06
Undecane	$C_{11}H_{24}$	3.48	2.09	1.72	21.90
Octane, 2,3,6,7-tetramethyl-	$C_{12}H_{26}$	1.81	2.12	1.71	21.77
Undecane, 2-methyl-	$C_{12}H_{26}$	0.95	2.10	1.71	21.77
Dodecane	$C_{12}H_{26}$	4.49	2.07	1.71	21.77
Tridecane	$C_{13}H_{28}$	5.92	2.05	1.70	21.67
Tetradecane	$C_{14}H_{30}$	7.22	2.04	1.69	21.57

Hexadecane	$C_{16}H_{34}$	17.56	2.01	1.68	21.42
Octadecane	$C_{18}H_{38}$	13.06	1.99	1.67	21.30
Heptadecane	$C_{17}H_{36}$	6.75	2.00	1.68	21.36
Nonadecane	$C_{19}H_{40}$	5.26	1.98	1.67	21.25
9-Octadecenoic acid, methyl ester, (E)- ****	$C_{19}H_{36}O_2$	8.01	2.11	1.36	17.32
Octadecanoic acid, methyl ester	$C_{19}H_{38}O_2$	1.84	2.83	1.43	18.16
Heneicosane*****	$C_{21}H_{44}$	12.3	2.02	1.66	21.16
Eicosane	$C_{20}H_{42}$	2.26	1.98	1.66	21.20
Tetracosane	$C_{24}H_{50}$	1.32	1.95	1.65	21.06
Sum	**(-)**	**99.99**	**2.04**	**1.65**	**20.97**

Notes: * Assumption that there is no water formation during the diesel cracking; ** data of 1-dodecanol; *** data of n-decane; **** data of gas state; ***** data of 2,6,10,14-Tetramethylheptadecane

Appendix E

Representative Profiles of Microwave Absorption and Temperature during the Reactions

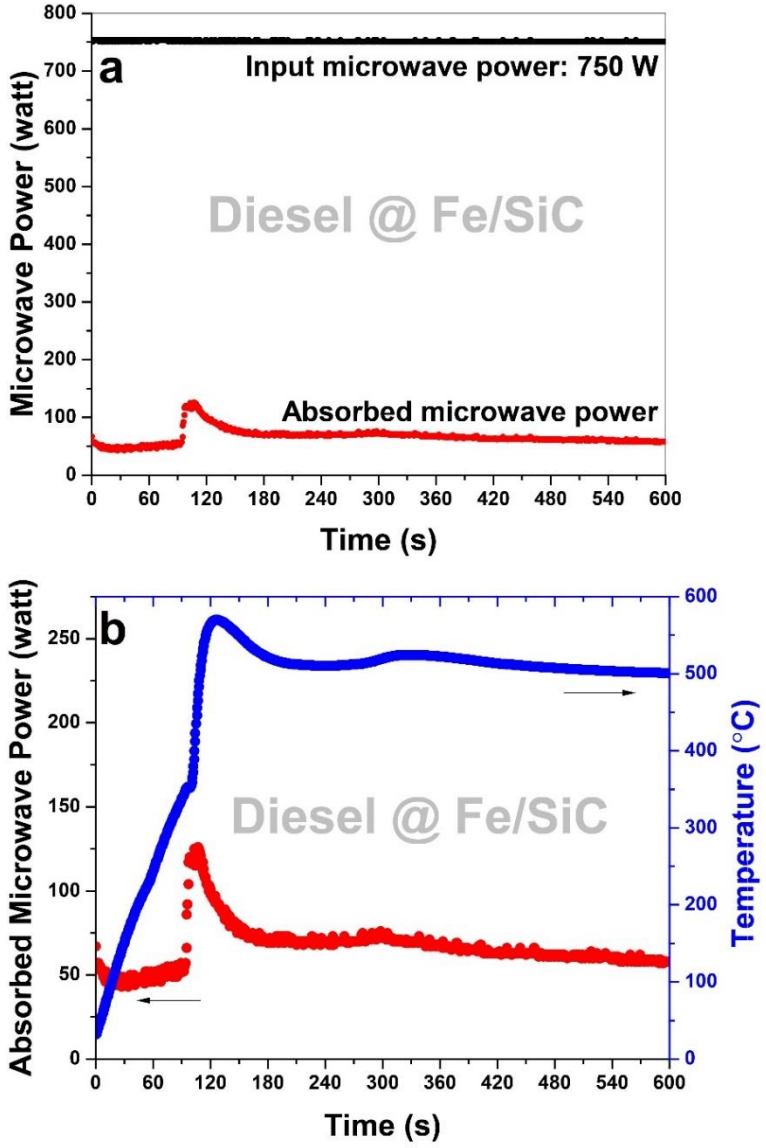


Figure E1. Microwave-initiated dehydrogenation of diesel on 5 wt.% Fe/SiC catalysts. (a) Original microwave input power and absorbed power (delivery power); (b) Record reaction temperature and absorbed power (delivery power). Conditions: fuels (ca. 0.5ml) was first well mixed with catalyst. The sample was then irradiated under 750 W power microwave for 10 min.

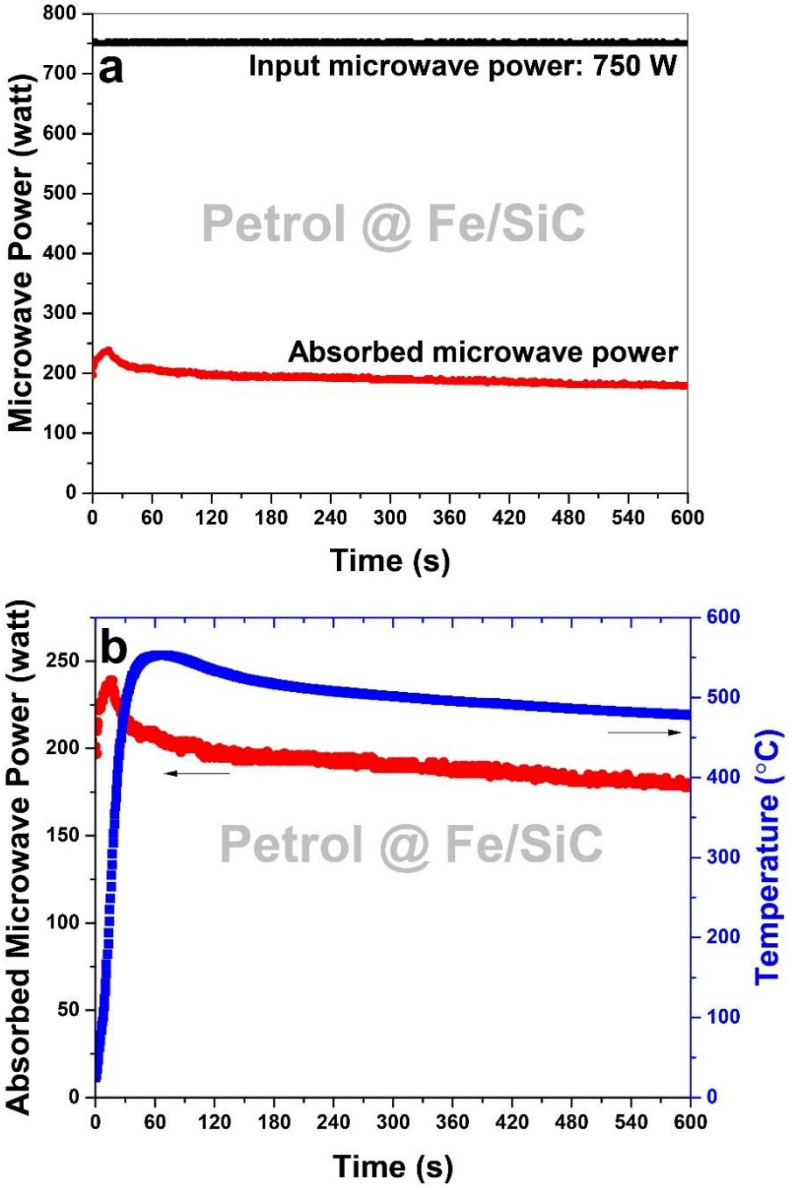


Figure E2. Microwave-initiated dehydrogenation of petrol on 5 wt.% Fe/SiC catalysts. (a) Original microwave input power and absorbed power (delivery power); (b) Record reaction temperature and absorbed power (delivery power). Conditions: fuels (ca. 0.5ml) was first well mixed with catalyst. The sample was then irradiated under 750 W power microwave for 10 min.

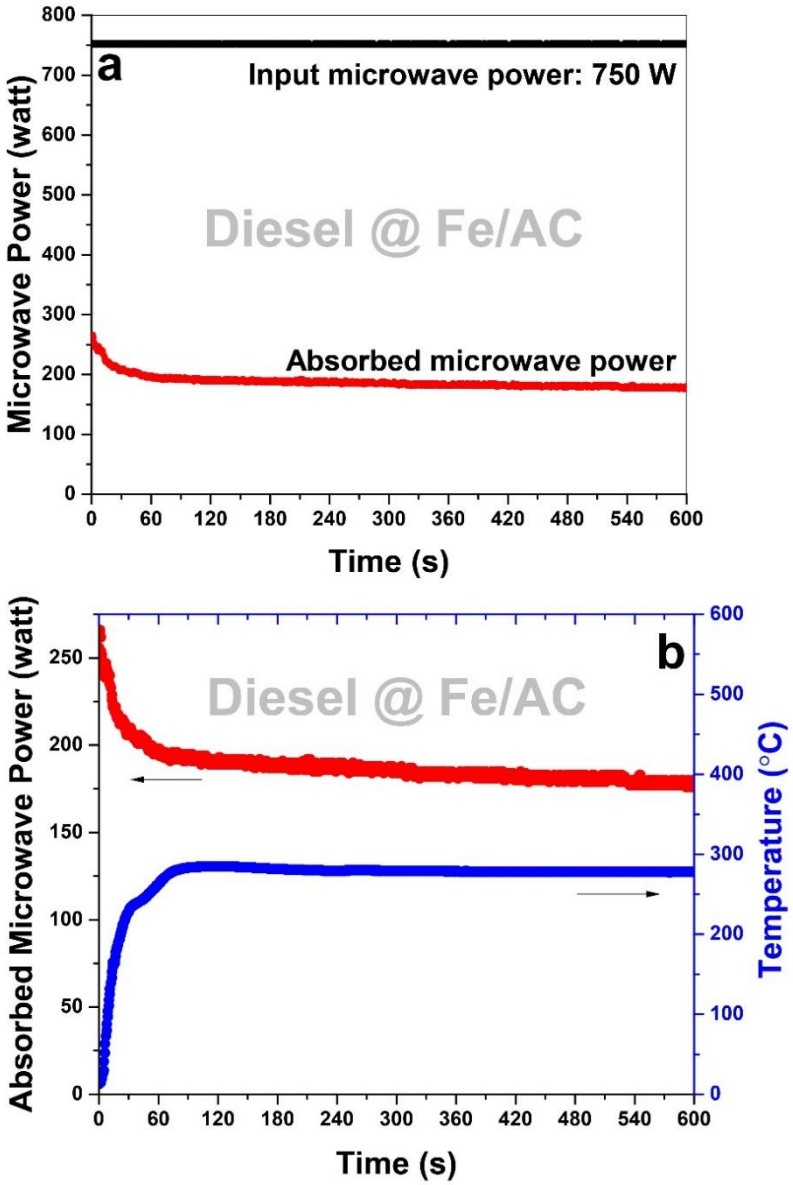


Figure E3. Microwave-initiated dehydrogenation of diesel on 5 wt.% Fe/AC catalysts. (a) Original microwave input power and absorbed power (delivery power); (b) Record reaction temperature and absorbed power (delivery power). Conditions: fuels (ca. 0.5ml) was first well mixed with catalyst. The sample was then irradiated under 750 W power microwave for 10 min.

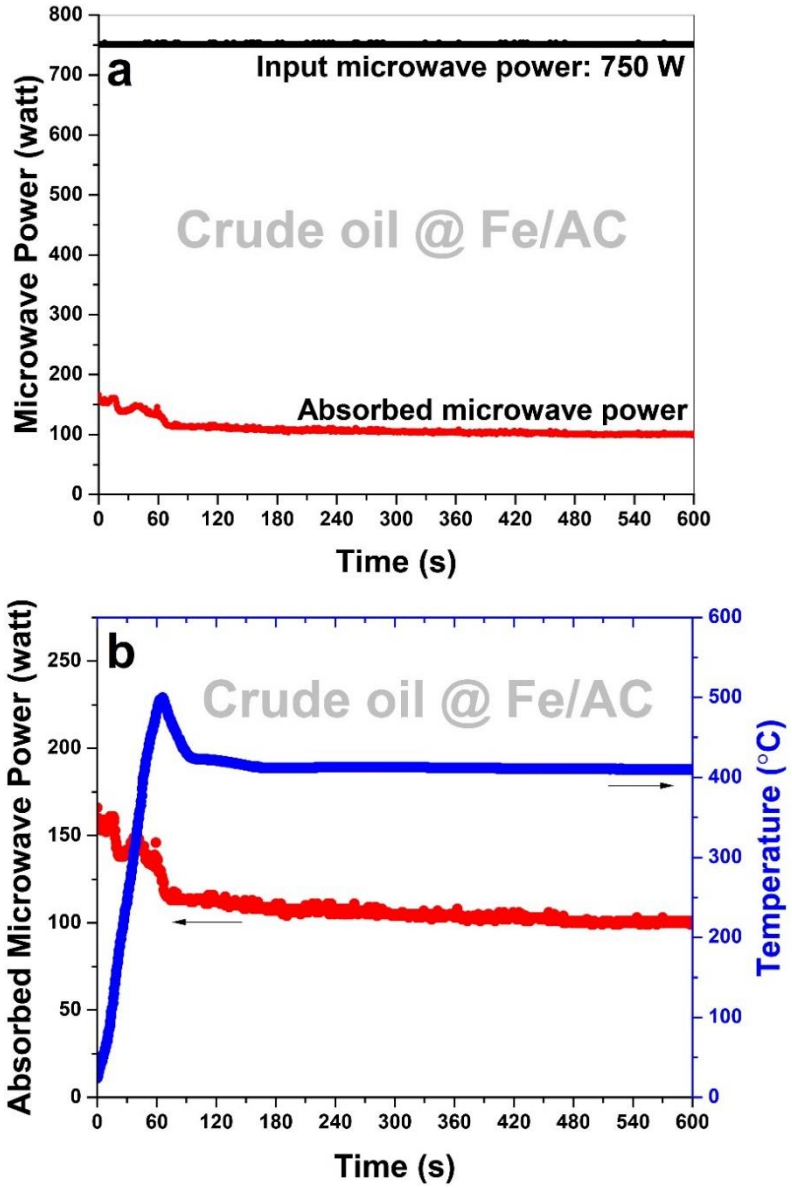


Figure E4. Microwave-initiated dehydrogenation of crude oil on 5 wt.% Fe/AC catalysts. (a) Original microwave input power and absorbed power (delivery power); (b) Record reaction temperature and absorbed power (delivery power). Conditions: fuels (ca. 0.5ml) was first well mixed with catalyst. The sample was then irradiated under 750 W power microwave for 10 min.

Appendix F

Acknowledgement and copyright

Three prior publications (listed below) are reproduced and reused in this thesis. I acknowledge that these publications were published based on my DPhil work carried out at Inorganic Chemistry Laboratory, University of Oxford under the supervision of Professor Peter P. Edwards. My contributions to the publications are conceived and designed the project; designed and developed the experiments and completed all the experiments myself; analysed and interpreted the results and drafted the original manuscript. All co-authors have been acknowledged for the reuse of these publications in this thesis.

1. Xiangyu Jie, Sergio Gonzalez-Cortes, Tiancun Xiao, Benzhen Yao, Jiale Wang, Daniel R. Slocombe, Yiwen Fang, Noah Miller, Hamid A. Al-Megren, Jonathan R. Dilworth, John M. Thomas, and Peter P. Edwards. *"The decarbonization of petroleum and other fossil hydrocarbon fuels for the facile production and safe storage of hydrogen."* Energy & Environmental Science (2019), 12(1), 238-249.
2. Xiangyu Jie, Tiancun Xiao, Benzhen Yao, Sergio Gonzalez-Cortes, Jiale Wang, Yiwen Fang, Hamid A. Al-Megren, Jonathan R. Dilworth, and Peter P. Edwards. *"On the performance optimization of Fe catalysts in the microwave – assisted H_2 production by the dehydrogenation of hexadecane"* Catalysis Today (2018), 317, 29-35.
3. Xiangyu Jie, Sergio Gonzalez-Cortes, Tiancun Xiao, Jiale Wang, Benzhen Yao, Daniel R. Slocombe, Hamid A. Al-Megren, Jonathan R. Dilworth, John M. Thomas, and Peter P. Edwards. *"Rapid Production of High-Purity Hydrogen Fuel through Microwave-Promoted Deep Catalytic Dehydrogenation of Liquid Alkanes with Abundant Metals."* Angewandte Chemie International Edition (2017), 56(34), 10170-10173.

The permission to reproduce or reuse the publications were granted from the publishers. A License and Terms and Conditions from John Wiley and Sons are attached below. Information about Licenses, copyright & permissions from ROYAL SOCIETY OF CHEMISTRY is available at: https://www.rsc.org/journals-books-databases/journal-authors-reviewers/licences-copyright-permissions/. Information about copyright from ELSEVIER is available at: https://www.elsevier.com/about/policies/copyright.

JOHN WILEY AND SONS LICENSE TERMS AND CONDITIONS

Aug 25, 2019

This Agreement between Xiangyu Jie ("You") and John Wiley and Sons ("John Wiley and Sons") consists of your license details and the terms and conditions provided by John Wiley and Sons and Copyright Clearance Center.

License Number	4655610465902
License date	Aug 24, 2019
Licensed Content Publisher	John Wiley and Sons
Licensed Content Publication	Angewandte Chemie International Edition
Licensed Content Title	Rapid Production of High-Purity Hydrogen Fuel through Microwave-Promoted Deep Catalytic Dehydrogenation of Liquid Alkanes with Abundant Metals
Licensed Content Author	Peter P. Edwards, John M. Thomas, Jonathan R. Dilworth, et al
Licensed Content Date	May 23, 2017
Licensed Content Volume	56
Licensed Content Issue	34
Licensed Content Pages	4
Type of use	Dissertation/Thesis
Requestor type	Author of this Wiley article
Format	Print and electronic

Portion	Full article
Will you be translating?	No
Title of your thesis / dissertation	Microwave-initiated Catalytic Dehydrogenation of Fossil Fuels for the Facile Production and Safe Storage of Hydrogen
Expected completion date	Aug 2019
Expected size (number of pages)	240
Requestor Location	Xiangyu Jie Inorganic Chemistry Laboratory University of Oxford South Parks Road Oxford, Oxford OX1 3QR United Kingdom Attn: Xiangyu Jie
Publisher Tax ID	EU826007151
Total	0.00 GBP
Terms and Conditions	

TERMS AND CONDITIONS

This copyrighted material is owned by or exclusively licensed to John Wiley & Sons, Inc. or one of its group companies (each a"Wiley Company") or handled on behalf of a society with which a Wiley Company has exclusive publishing rights in relation to a particular work (collectively "WILEY"). By clicking "accept" in connection with completing this licensing transaction, you agree that the following terms and conditions apply to this transaction (along with the billing and payment terms and conditions established by the Copyright Clearance Center Inc., ("CCC's Billing and Payment terms and conditions"), at the time that you opened your RightsLink account (these are available at any time at http://myaccount.copyright.com).

Terms and Conditions

- The materials you have requested permission to reproduce or reuse (the "Wiley Materials") are protected by copyright.
- You are hereby granted a personal, non-exclusive, non-sub licensable (on a stand-alone basis), non-transferable, worldwide, limited license to reproduce the Wiley Materials for the purpose specified in the licensing process. This license, **and any CONTENT (PDF or image file) purchased as part of your order,** is for a one-time use only and limited to any maximum distribution number specified in the license. The first instance of republication or reuse granted by this license must be completed within two years of the date of the grant of this license (although copies prepared before the end date may be distributed thereafter). The Wiley Materials shall not be used in any other manner or for any other purpose, beyond what is granted in the license. Permission is granted subject to an appropriate acknowledgement given to the author, title of the material/book/journal and the publisher. You shall also duplicate the copyright notice that appears in the Wiley publication in your use of the Wiley Material. Permission is also granted on the understanding that nowhere in the text is a previously published source acknowledged for all or part of this Wiley Material. Any third party content is expressly excluded from this permission.
- With respect to the Wiley Materials, all rights are reserved. Except as expressly granted by the terms of the license, no part of the Wiley Materials may be copied, modified, adapted

(except for minor reformatting required by the new Publication), translated, reproduced, transferred or distributed, in any form or by any means, and no derivative works may be made based on the Wiley Materials without the prior permission of the respective copyright owner.**For STM Signatory Publishers clearing permission under the terms of the STM Permissions Guidelines only, the terms of the license are extended to include subsequent editions and for editions in other languages, provided such editions are for the work as a whole in situ and does not involve the separate exploitation of the permitted figures or extracts,**You may not alter, remove or suppress in any manner any copyright, trademark or other notices displayed by the Wiley Materials. You may not license, rent, sell, loan, lease, pledge, offer as security, transfer or assign the Wiley Materials on a stand-alone basis, or any of the rights granted to you hereunder to any other person.

- The Wiley Materials and all of the intellectual property rights therein shall at all times remain the exclusive property of John Wiley & Sons Inc, the Wiley Companies, or their respective licensors, and your interest therein is only that of having possession of and the right to reproduce the Wiley Materials pursuant to Section 2 herein during the continuance of this Agreement. You agree that you own no right, title or interest in or to the Wiley Materials or any of the intellectual property rights therein. You shall have no rights hereunder other than the license as provided for above in Section 2. No right, license or interest to any trademark, trade name, service mark or other branding ("Marks") of WILEY or its licensors is granted hereunder, and you agree that you shall not assert any such right, license or interest with respect thereto

- NEITHER WILEY NOR ITS LICENSORS MAKES ANY WARRANTY OR REPRESENTATION OF ANY KIND TO YOU OR ANY THIRD PARTY, EXPRESS, IMPLIED OR STATUTORY, WITH RESPECT TO THE MATERIALS OR THE ACCURACY OF ANY INFORMATION CONTAINED IN THE MATERIALS, INCLUDING, WITHOUT LIMITATION, ANY IMPLIED WARRANTY OF MERCHANTABILITY, ACCURACY, SATISFACTORY QUALITY, FITNESS FOR A PARTICULAR PURPOSE, USABILITY, INTEGRATION OR NON-INFRINGEMENT AND ALL SUCH WARRANTIES ARE HEREBY EXCLUDED BY WILEY AND ITS LICENSORS AND WAIVED BY YOU.

- WILEY shall have the right to terminate this Agreement immediately upon breach of this Agreement by you.

- You shall indemnify, defend and hold harmless WILEY, its Licensors and their respective directors, officers, agents and employees, from and against any actual or threatened claims, demands, causes of action or proceedings arising from any breach of this Agreement by you.

- IN NO EVENT SHALL WILEY OR ITS LICENSORS BE LIABLE TO YOU OR ANY OTHER PARTY OR ANY OTHER PERSON OR ENTITY FOR ANY SPECIAL, CONSEQUENTIAL, INCIDENTAL, INDIRECT, EXEMPLARY OR PUNITIVE DAMAGES, HOWEVER CAUSED, ARISING OUT OF OR IN CONNECTION WITH THE DOWNLOADING, PROVISIONING, VIEWING OR USE OF THE MATERIALS REGARDLESS OF THE FORM OF ACTION, WHETHER FOR BREACH OF CONTRACT, BREACH OF WARRANTY, TORT, NEGLIGENCE, INFRINGEMENT OR OTHERWISE (INCLUDING, WITHOUT LIMITATION, DAMAGES BASED ON LOSS OF PROFITS, DATA, FILES, USE, BUSINESS OPPORTUNITY OR CLAIMS OF THIRD PARTIES), AND WHETHER OR NOT THE PARTY HAS BEEN ADVISED OF THE POSSIBILITY OF SUCH DAMAGES. THIS LIMITATION SHALL

APPLY NOTWITHSTANDING ANY FAILURE OF ESSENTIAL PURPOSE OF ANY LIMITED REMEDY PROVIDED HEREIN.

- Should any provision of this Agreement be held by a court of competent jurisdiction to be illegal, invalid, or unenforceable, that provision shall be deemed amended to achieve as nearly as possible the same economic effect as the original provision, and the legality, validity and enforceability of the remaining provisions of this Agreement shall not be affected or impaired thereby.

- The failure of either party to enforce any term or condition of this Agreement shall not constitute a waiver of either party's right to enforce each and every term and condition of this Agreement. No breach under this agreement shall be deemed waived or excused by either party unless such waiver or consent is in writing signed by the party granting such waiver or consent. The waiver by or consent of a party to a breach of any provision of this Agreement shall not operate or be construed as a waiver of or consent to any other or subsequent breach by such other party.

- This Agreement may not be assigned (including by operation of law or otherwise) by you without WILEY's prior written consent.

- Any fee required for this permission shall be non-refundable after thirty (30) days from receipt by the CCC.

- These terms and conditions together with CCC's Billing and Payment terms and conditions (which are incorporated herein) form the entire agreement between you and WILEY concerning this licensing transaction and (in the absence of fraud) supersedes all prior agreements and representations of the parties, oral or written. This Agreement may not be amended except in writing signed by both parties. This Agreement shall be binding upon and inure to the benefit of the parties' successors, legal representatives, and authorized assigns.

- In the event of any conflict between your obligations established by these terms and conditions and those established by CCC's Billing and Payment terms and conditions, these terms and conditions shall prevail.

- WILEY expressly reserves all rights not specifically granted in the combination of (i) the license details provided by you and accepted in the course of this licensing transaction, (ii) these terms and conditions and (iii) CCC's Billing and Payment terms and conditions.

- This Agreement will be void if the Type of Use, Format, Circulation, or Requestor Type was misrepresented during the licensing process.

- This Agreement shall be governed by and construed in accordance with the laws of the State of New York, USA, without regards to such state's conflict of law rules. Any legal action, suit or proceeding arising out of or relating to these Terms and Conditions or the breach thereof shall be instituted in a court of competent jurisdiction in New York County in the State of New York in the United States of America and each party hereby consents and submits to the personal jurisdiction of such court, waives any objection to venue in such court and consents to service of process by registered or certified mail, return receipt requested, at the last known address of such party.

WILEY OPEN ACCESS TERMS AND CONDITIONS

Wiley Publishes Open Access Articles in fully Open Access Journals and in Subscription journals offering Online Open. Although most of the fully Open Access journals publish open access articles under the terms of the Creative Commons Attribution (CC BY) License only, the

subscription journals and a few of the Open Access Journals offer a choice of Creative Commons Licenses. The license type is clearly identified on the article.

The Creative Commons Attribution License

The Creative Commons Attribution License (CC-BY) allows users to copy, distribute and transmit an article, adapt the article and make commercial use of the article. The CC-BY license permits commercial and non-

Creative Commons Attribution Non-Commercial License

The Creative Commons Attribution Non-Commercial (CC-BY-NC)License permits use, distribution and reproduction in any medium, provided the original work is properly cited and is not used for commercial purposes.(see below)

Creative Commons Attribution-Non-Commercial-NoDerivs License

The Creative Commons Attribution Non-Commercial-NoDerivs License (CC-BY-NC-ND) permits use, distribution and reproduction in any medium, provided the original work is properly cited, is not used for commercial purposes and no modifications or adaptations are made. (see below)

Use by commercial "for-profit" organizations

Use of Wiley Open Access articles for commercial, promotional, or marketing purposes requires further explicit permission from Wiley and will be subject to a fee.

Further details can be found on Wiley Online Library http://olabout.wiley.com/WileyCDA/Section/id-410895.html

Other Terms and Conditions:

v1.10 Last updated September 2015

Questions? customercare@copyright.com or +1-855-239-3415 (toll free in the US) or +1-978-646-2777.